



COP28UAE



جائزة خليفة الدولية لنخيل التمر والابتكار الزراعي  
KHALIFA INTERNATIONAL AWARD FOR DATE PALM  
AND AGRICULTURAL INNOVATION

# Date Palm & Carbon Footprint

A Geospatial Approach to Understanding the Desert Ecosystems,  
A case study from the Emirate of Abu Dhabi, UAE.



Authored by:  
**Dr. Basam S. Dahy, Ph.D.**

Edited and coordinated by:  
**Dr. Abdelouahhab Zaid, Prof.,**









# Contents

## **Preface / 10**

H.E. Sheikh Nahayan Mabarak Al Nahayan,

## **Editorial Statement / 12**

Dr. Abdelouahhab Zaid, Prof.,

## **Author's Note / 14**

Dr. Basam S. Dahy, Ph.D.

## **Summary / 16**

## **Chapter 1 / 18**

### **Introduction**

1.1. World Date Production, With a Special Emphasis on the UAE / 22

1.2. Overview / 24

1.3. Literature Review / 28

1.4. Structure of the Book / 58

## **Chapter 2 / 60**

### **Calculation of Carbon Stock in Date Palm Trees for Biomass and Soil**

2.1. Overview / 64

2.2. Phoenix dactylifera L., Date Palm / 65

2.3. Structural Field Variables of Date Palm / 68

2.4. Ratios of Date Palm Biomass Components (Crown, Trunk, and Roots) / 76

2.5. Biomass Allometric Equations of Date Palm / 78

2.6. Carbon Stock in Date Palm Trees at Different Age-Stages / 82

2.7. Summary / 85

## **Chapter 3 / 88**

### **Mapping & Counting of Date Palm Trees in Abu Dhabi Emirate Using Satellite Imageries**

- 3.1. Overview / 92
- 3.2. Land Use/Land Cover Classification of the Emirate of Abu Dhabi / 96
- 3.3. Mapping Vegetation and Date Palm Using Landsat-8 OLI Sensor / 99
- 3.4. Accurate Mapping of Date Palm at Different Age-Stages Using WorldView-2 Sensor / 102
- 3.5. Maps Validation / 104
- 3.6. Counting Date Palms in the Emirate of Abu Dhabi / 106
- 3.7. Summary / 107

## **Chapter 4 / 108**

### **Remote Sensing Based Models for Assessing Date Palm Biomass and Carbon Stock**

- 4.1. Overview / 112
- 4.2. Descriptive Statistics of the Structural Field Variables Assessed / 120
- 4.3. The Field Based Biomass Estimation Model of Date Palm and Estimating its Carbon / 121
- 4.4. The Remote Sensing Based Biomass Estimation Models / 122

- 4.5. Models Validation / 124

- 4.6. Creation of the Aboveground Carbon Map of Date Palm Trees / 126

- 4.7. Estimating the Total Carbon Stock of Date Palm Trees / 128

- 4.8. Summary / 129

## **Chapter 5 / 130**

### **Discussion**

- 5.1. Biomass Allometric Equations & Carbon Stock of Date Palm / 134
- 5.2. Mapping of Date Palm Trees at Three Age-Stages / 138
- 5.3. Estimating the Total Carbon Stock in Date Palm Trees / 142

## **Chapter 6 / 146**

### **Conclusions & Recommendations**

### **References / 152**

### **List of Publications / 168**

### **List of Figures / 170**

### **List of Tables / 172**

### **List of Infographics / 174**

### **Appendices / 176**

### **List of Abbreviations / 186**

### **Biographies / 188**

## Celebrating the UN Decade on Ecosystem Restoration (2021- 2030)

### **Date Palm and Carbon Footprint:**

A Geospatial Approach to Understanding the Desert Ecosystems, A case study from the Emirate of Abu Dhabi, UAE.

### **Published by**

© Khalifa International Award for Date Palm and Agricultural Innovation, 2023.

The idea of this book is by Dr. Basam S. Dahy, Ph.D.

### **Preface**

#### **H.E. Sheikh Nahayan Mabarak Al Nahayan,**

Cabinet Member, Minister of Tolerance and Coexistence, Chairman of Khalifa International Award for Date Palm and Agricultural Innovation Board of Trustees.

### **Author**

#### **Dr. Basam S. Dahy, Ph.D.**

### **Edited and coordinated by**

#### **Dr. Abdelouahhab Zaid, Prof.,**

Secretary General of Khalifa Int'l Award for Date Palm and Agricultural Innovation.

### **Designed by**

© Khalifa International Award for Date Palm and Agricultural Innovation, 2023.

### **Infographics by**

© Khalifa International Award for Date Palm and Agricultural Innovation, 2023 and Dr. Basam S. Dahy, Ph.D.

### **Typeface Euro-Arabic by**

Khalifa International Award for Date Palm and Agricultural Innovation, Abu Dhabi, United Arab Emirates.

### **Project management**

Khalifa International Award for Date Palm and Agricultural Innovation, Abu Dhabi, UAE.

### **Copyrights**

Text copyrights belong to Dr. Basam S. Dahy, Ph.D.

© Khalifa International Award for Date Palm and Agricultural Innovation, 2023.

### **Photography by**

This book contains photographs from the Khalifa Award Annual Photography Competition, from the own archive of the editors and author, and from Shutterstock.com and freepik.com.

A complete list of images with source is in the back of the book. All Copyrights reserved.

All rights reserved. No part of this publication may be reproduced or transmitted in any form or by any means, electronic or mechanical, including photography or any storage and retrieval system, without permission in writing from the co-editors.

**Respect copyrights, encourage creativity!**

### **Printed by**

Abu Dhabi Printing & Publishing Co.

Made in United Arab Emirates.

First printing, 2023.

NMC Printing Permit: MC-03-01-0785671

ISBN (Printed Book): 978-9948-777-86-1

ISBN (E-Book): 978-9948-777-87-8

For more information, please visit

[www.ekiaai.com](http://www.ekiaai.com)

[www.kiaai.ae](http://www.kiaai.ae)

This book was printed on paper certified by the FSC®



With a special thanks to all who contributed to the production of Date Palm and Carbon Footprint: A Geospatial Approach to Understanding the Desert Ecosystems - A case study from the Emirate of Abu Dhabi, UAE.

## Disclaimer

Please note that while reasonable efforts have been made to ensure the information contained in this report is accurate, complete, and current, circumstances change, so this document may not reflect recent developments. The Khalifa International Award for Date Palm and Agricultural Innovation does not assume responsibility or liability for any errors, omissions, or discrepancies in the information in this report, and does not assume responsibility or liability with respect to the use of or reliance on any information, methods, processes, conclusions, or judgements contained herein.

### Maps and political boundaries

The designations employed and the presentation of the material on the maps of this report do not imply the expression of any opinion whatsoever on the part of the Khalifa International Award for Date Palm and Agricultural Innovation concerning the legal status of any country, territory, city or area or of its authorities, or concerning the delimitation of its frontiers or boundaries.

Every effort is made to ensure that maps are free of errors but there is no warrant the map or its features are either spatially or temporally accurate or fit for a particular use. This map is provided without any warranty of any kind whatsoever, either express or implied.

We dedicate this book: "Date Palm and Carbon Footprint: A Geospatial Approach to Understanding the Desert Ecosystems -A case study from the Emirate of Abu Dhabi, UAE.", to H.H. Sheikh Mohamed bin Zayed Al Nahyan, President of the United Arab Emirates, "May God protect him", and H.H. Sheikh Mansour bin Zayed Al Nahyan, UAE Vice President and Deputy Prime Minister, Minister of the Presidential Court, the first supporter of date palm cultivation. The author and editor also extend their thanks and appreciation to H.E. Sheikh Nahayan Mabarak Al Nahayan, Minister of Tolerance and Coexistence, Chairman of the Award's Board of Trustees.



**H.E. Sheikh Nahayan Mabarak Al Nahayan,**

Cabinet Member, Minister of Tolerance and Coexistence,  
Chairman of Khalifa International Award for Date Palm and  
Agricultural Innovation Board of Trustees.

## **Preface**

# **The Blessed Tree,** and its role in **reducing** climate change

**T**he UAE is a pioneer in the region and the world in addressing climate change, as it is making great efforts to reduce gas emissions and switch to clean energy. The UAE has a large number of environmentally friendly projects, initiatives, and ambitious plans to increase the total use of renewable energy, by 2050. It also has a national green economy transformation plan, which aims to become a global center for green technology and sustainable economy. This includes investment in peaceful nuclear technologies for electricity generation, research on solar energy, and other clean energy sources. In addition to investing in scientific research to find innovative solutions that contribute to promoting smart agriculture and reducing the repercussions of climate change, environmental rehabilitation, and preserving biological diversity, and which includes programs to protect endangered species and rehabilitate natural areas.

In general, the UAE continues to strive towards sustainability and limiting climate change, through multiple and comprehensive strategies. However, climate change has been one of the main issues faced by the, as the country is working hard to achieve its ambitious goals. This interest was proofed through the UAE's Vision, 2021, which affirmed the UAE's commitment to be part of the global journey, and to participate in the development and implementation of innovative solutions to protect the environment and ensure its sustainability. The vision also affirmed the UAE's commitment to mitigating the impact of climate change in order to protect our environment for

future generations. We preserve our rich natural from dangers resulting from human activities globally and locally, through preventive measures such as reducing carbon emissions, and regulatory measures that protects environmental systems.

For its side, the United Nations confirmed several times, that the UAE is a global and effective partner in facing climate challenges, as hosting the Climate Change Conference (COP28), represents an opportunity to enhance international cooperation to find a balanced solution that guarantees the continuous economic growth of countries, while taking into account the protection and development of the environment, for future generations. Where it represents the strategic initiative to achieve climate neutrality, launched by H.H. Sheikh Mohamed bin Zayed Al Nahyan, President of the UAE, "May God protect him", in October 2021, a national engine, aimed at reducing emissions and climate neutrality, by the year 2050, This makes the UAE the first country in the Near East and North Africa (NENA) region, to announce its goal of achieving climate neutrality. This announcement comes as a milestone in the country's five-decade journey, in climate action and strategic vision for the next three decades.

Hence, the arising of the Award's initiative to measure the date palm tree carbon print, in line with the UAE initiative for climate neutrality, 2050. This works in providing new opportunities for workers in the agricultural sector in general, and the date palm cultivation and production sector in particular, to reduce greenhouse gas emissions, carbon print of this sector, and achieve sustainable development. This initiative also contributes to establishing the position of the date palm tree, as an essential element for absorbing CO<sub>2</sub> and mitigating the consequences of climate change.



**Editorial Statement**

# **Date palm trees**

are an essential component  
of carbon absorption  
**and storage**

Dr. Abdelouahhab Zaid, Prof.,

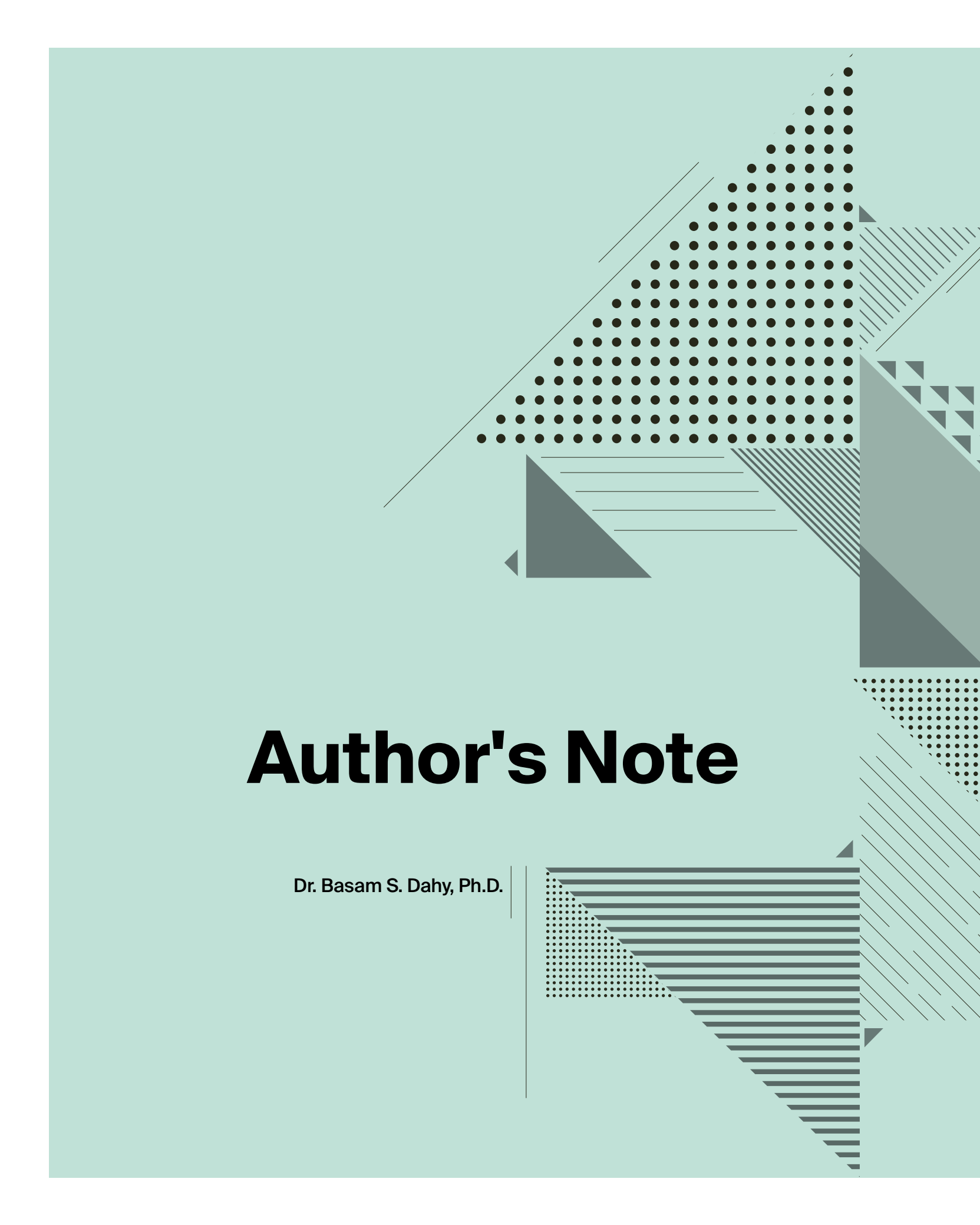
**T**he agricultural sector in general has a crucial role in reducing the effect of global warming, by absorbing greenhouse gases, the most important of which is Carbon Dioxide (CO<sub>2</sub>) from the atmosphere, as plants and trees absorb CO<sub>2</sub> during photosynthesis. Where sunlight is converted into chemical energy. The carbon dioxide and water are then used to produce sugar and oxygen. Therefore, the larger the agricultural area, the more CO<sub>2</sub> that can be absorbed from the atmosphere.

Furthermore, sustainable farming systems can improve soil health and enhance biodiversity, where this can contribute to storing carbon, reducing emissions, and enhancing resilience to climate change. Soil is one of the largest stores of carbon on the planet, as it contains about three times the amount of carbon in the atmosphere. Sustainable agriculture and other soil health measures, such as field rotation and organic farming, can also preserve the amount of carbon stored in the soil. Agroforestry, which combines agriculture and forestry, can also play an important role in storing carbon. Trees in general, including the date palm tree (*Phoenix dactylifera* L.), store a significant amount of carbon, and provide several other benefits, including improving soil quality, as well as providing shade to other crops.

It should be noted that the main challenge to make the most of agriculture as a carbon absorber, is to balance carbon storage with the nutritional needs of humans. As we are obliged to plant trees and crops to sustain our livelihood, but how we do it, determines how much CO<sub>2</sub> the agricultural system can absorb.

The use of farming methods that are harmonious or that take advantage of nature, such as organic farming, communal farming (growing multiple types of crops in the same field) and forestry, can help promote soil health, biodiversity, and carbon Long-term storage, and which includes applying techniques such as biological carbon neutralization and soil carbon neutralization, and which in return increases the amount of carbon that can be stored in the soil over the long term.

Making the most of agriculture as a carbon absorbent, requires balance between sustainable practices and nutritional needs. Hence the importance of the date palm tree, as it is one of the most important trees in its ability to absorb CO<sub>2</sub> from the atmosphere, and store it within its dry mass. Since the capture of CO<sub>2</sub> by a single tree depends on the size and area of its green parts. The date palm tree is characterized by the large size and density of its fronds, and therefore the volume of carbon stored by the date palm tree is considered huge. Highlighting the fact that the Near East and North Africa (NENA) region, includes more than one hundred million date palm trees, and which reflects the importance of the Award's interest in measuring the date palm trees' carbon print, according to a documented scientific method, because of its strategic importance in mitigating the effects of climate change.



# Author's Note

Dr. Basam S. Dahy, Ph.D.

I am immensely grateful and filled with joy for the opportunity to publish this book in collaboration with the esteemed “Khalifa International Award for Date Palm and Agricultural Innovation” (KIADPAI), represented by Prof. Abdelouahhab Zaid, Award’s Secretary-General, and Agricultural Advisor at the UAE Presidential Court.

As a scientific researcher who has dedicated a significant amount of time and efforts to conducting research, collecting and analyzing data, it is truly gratifying to have a KIADPAI as a platform that offers new avenues for expanding the reach of my research and facilitating its practical implementation. This book is based on a series of research studies that have been published in peer-reviewed journals and presented at international conferences. Furthermore, it is based on my doctoral dissertation titled “GEO-SPATIAL MODELING OF CARBON SEQUESTRATION ASSESSMENT IN DATE PALM, ABU DHABI: AN INTEGRATED APPROACH OF FIELDWORK, REMOTE SENSING, AND GIS”. The original Ph.D. dissertation was submitted in partial fulfillment of the requirements for the degree of Doctor of Philosophy in Ecology & Environmental Sciences from UAE University in the summer of 2021.

I would like to express my sincere gratitude to UAE University for funding my research and to all the members of the College of Science, particularly Professor Salem Issa from the Geosciences department, Professor Taoufik Ksiksi from the Biology department, and Dr. Nazmi Saleous from the Geography and Urban Sustainability department, for their invaluable assistance throughout my studies and research.

Special thanks are extended to my beloved wife, family, and my brother, Yasser Dahy, for their unwavering encouragement and support throughout this journey. I would also like to express my deep appreciation to Dr. Mohamed T. Moussa for his assistance in the UAE University’ Ecology Lab, as well as to Al Foah Farm Company for providing free access to their premises, equipment, and logistic support. My heartfelt thanks go to the workers and farmers who shared unforgettable memories with me during field visits in Abu Dhabi Emirate.

The background is a solid teal color. On the right side, there are several overlapping geometric shapes. A large triangle is filled with a grid of black dots. Below it, there are horizontal lines. To the right of the dot triangle, there are diagonal lines. At the bottom right, there is a triangle filled with horizontal lines, and a smaller triangle filled with a grid of black dots. The word "Summary" is centered in the lower half of the page.

# Summary

The United Arab Emirates (UAE) has undertaken huge efforts to green the desert and afforestation projects (planted mainly with date palms) hence, reducing its carbon footprint, which have never been accounted for, because of lack of implemented mechanisms and tools to assess the amount of biomass and carbon stock (CS) sequestered by plants in the country. The purpose of this book is to implement a new approach towards assessing the carbon sequestered by date palm (*Phoenix dactylifera* L.) trees, in both their biomass compartment as well as the soils underneath, using geospatial technologies (RS and GIS) assessed by field measurements. The methodology proposed in this book relied on both field and lab work, besides the intensive use of geospatial technology including, digital image processing of multi-scale, multi-resolution satellite imagery as well as Geographical Information Systems (GIS) modelling.

The current study was the development of new and unprecedented allometric equations for date palm trees in arid land. Such equations allow the development and calibration of a RS-based model for estimating biomass and CS of date palms with high accuracy. Results showed that the crown area (CA) best estimated both crown biomass (CB) and soil organic carbon (SOC). Likewise, the trunk height (Ht) was the best estimator of trunk biomass (TB). Using these variables, allometric equations were developed for date palms at different age stages and were used to estimate CB, TB and SOC with coefficients of determination ( $R^2$ ) of: 0.884, 0.835 and 0.952, respectively. Furthermore, the average ratios of below ground biomass (BGB) to above ground biomass (AGB) varied with palm maturity stages averaging 0.332, 0.925 and 0.496 for young, medium and mature date palms, respectively. Moreover, the present study demonstrated that the amounts of organic carbon stored in date palm trees were considerable with values of: 15.88 kg/palm for young, 96.62 kg/palm for medium, and 225.58 kg/palm for mature palm trees. Substantially higher amounts of SOC were measured compared to other local plants with values of: 18.092 kg/palm, 62.594 kg/palm, and 92.908 kg/palm under young, medium and mature palm trees, respectively.

For detecting and mapping the date palm trees, the research proposes a framework based on using mul-

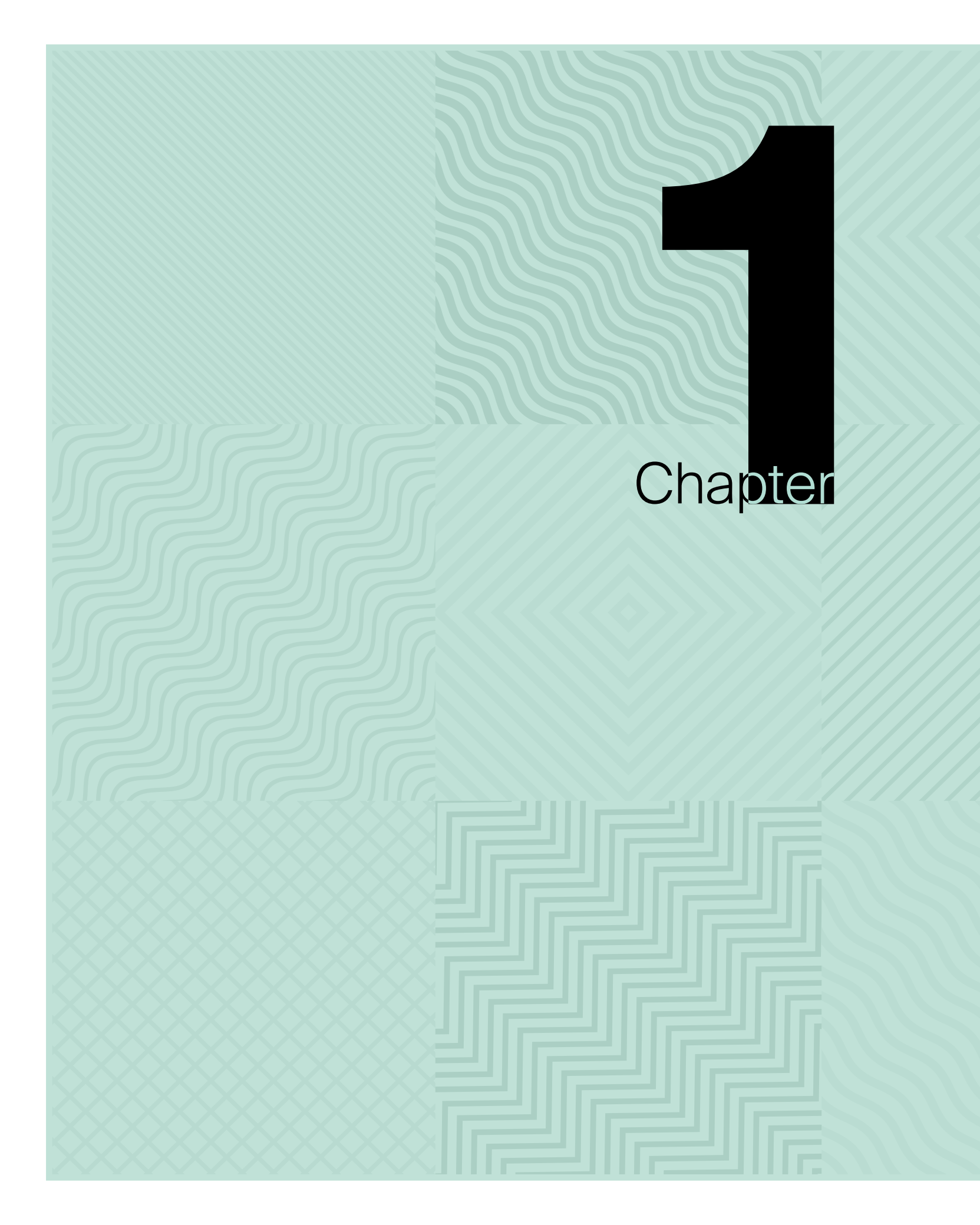
ti-source/ multi-sensor data in a hierarchical integrated approach (HIA) to map date palm trees at different age stages: young, medium, and mature. The outcomes of the implemented approach were the creation of detailed and accurate maps of DP at three age stages. The overall accuracies of date palm maps were 86.8%, 88%, and 90.7% for young, medium, and mature date palm, respectively. The area of each category was calculated and found to be 4,193.86 ha, 1,672.14 ha, and 1,722.05 ha, for mature, medium, and young date palm trees, respectively. The overall accuracies for mixed-ages date palm the value reached up to 94.5%, with an overall Kappa statistic estimated at 0.888 with a total area of date palm equal to 7,588.04 ha and the total number of date palm planted in the study area (Abu Dhabi Emirate) counted an estimated number of 8,966,826 palm trees.

The study showed that the correlation of mature date palm class alone (>10 years) with single bands was significant with shortwave infrared 1 (SWIR1) and shortwave infrared 2 (SWIR2), while the correlation was significant with all tested vegetation indices (VI), except for tasseled cap transformation index for brightness (TCB) and for greenness (TCG). By using different types of regression equations, tasseled cap transformation index for wetness (TCW) showed the strongest correlation using a second-order polynomial equation to estimate the biomass of mature date palm with  $R^2$  equal to 0.7643 and P value equal to 0.007. The exponential regression equation that uses renormalized difference vegetation index (RDVI) as RS predictor was the best single VI and had the strongest correlation among all RS variables of Landsat 8 OLI for AGB of non-mature DP, with an  $R^2$  value of 0.4987 and P value equal 0.00002. The total in date palm trees was estimated as the sum of the estimated CS in the five components: aboveground biomass, belowground biomass, litter, debris, and soil organic carbon. The overall CS by date palm trees in Abu Dhabi Emirate predicted from this map amounted to 2,447,856.87 tons.

The findings of the research work are promising and can be used to estimate the amount of biomass and carbon stock in DP trees in the country as well as in arid land in general. Therefore, it can be applied to enhance the decision-making process on sustainable monitoring and management of carbon sequestration by date palms in other similar ecosystems. The research's approach has never been developed elsewhere for date palms in arid areas.

---

**Keywords:** Date Palm, *Phoenix dactylifera* L., Carbon Sequestration, Arid Lands, Remote Sensing, Biomass, UAE.



# 1

Chapter



# Introduction





## 1.1.

# World Date Production, With a Special Emphasis on the UAE

## الكربونية

**D**ate palm is a crop that plays a central role in the agricultural systems across the world. The reason is its high nutritional value, resilience, and suitability to the arid and semi-arid areas that represent 90% of the Arab world. It is characterized by its tolerance to various environmental stresses (drought, low or high temperatures and salinity), but this may be reflected in flowering and fruiting. A single date palm can produce 70-100kg of good dates and 45kg of by-products (pruning residues, slippers, harvesting and fallen fruits). Dates are considered a nutritional prize that is easy to store, transport and handle, and one that is available throughout the year. It is consumed fresh in three main stages of maturity (Al-Khalal/Al-Bisr for some Cultivars, the Rutab stage, and Tamar), and used in many value-added industries.

Date palm cultivation and production sector has become a subject of concern and care because of its agricultural, economical and nutritional unique value across the world. Global date production is estimated about 8 million tons, of which Arab countries production constitutes more than 75%, distributed mostly in Asia and North Africa. In addition to several other regions such as Australia, America, Namibia and South Africa. The MENA region countries have been taking accelerated steps towards the development of this sector, whether in terms of investing in modern date palm cultivation, manufacture and marketing of dates.

On the other hand, the date palm and dates residues in most of the date producing countries, is of a great burden on date growers and dates processing factories, and which could reach average of 23 Kg of waste per tree annually. This resulted in accelerated steps and a remarkable shift towards adopting the Bio-Circular economy model, as a system that aims to reduce waste and make the most out of resources by reducing waste and emissions to the maximum extent. This in return brought to light several products that are trending in regional and international markets.

As the global demand for date palm fruit grows at 6%, countries of the region should focus on maximizing value and minimizing waste. The economy of a country will grow if the resources are used efficiently and sustainably. We have witnessed this in the expansion of the product range from the fruit and its derivatives to include all parts of the tree including to derive drinks, bars, bio fuel, seed oil and furniture. Latest biotechnological advancements have found use for the fruit and its byproducts to induce microbial growth for fermentation to be sold as bioactive compounds.

For centuries, the date palm has served as a source of nutrition, innumerable craftsmanship and folklore which build over millennia formed some learned unique traditions, cultural practices, customs and festivities. This acquired knowledge united and strengthened the connection between people from all across the Arab region, with date palm representing a

symbolism of shared challenges faced in the desert environment. Till date, the life skills acquired from the date palm is in one form or another preserved, where technology allowed the expansion of its uses.

The human skills factor is considered as an important element in preserving the date palm cultural heritage. The region faces the risk of youngsters preferring more white-collar vocations to traditional palm date cottage industries. Regional Governments and authorities need to work on understanding and adopting global market trends and facilitate technology, product design for innovation, marketing and building value chain linkages. Where a regional platform should be created for product innovation, creative solutions between the date growers, stakeholders, designers, artisans, organizations, entrepreneurs, and business community to remain connected to the latest innovations in the date palm industry and encourage the use of modern technologies in all fields and explore new niche markets.

As one of the world's largest producers of dates, with millions of trees, the United Arab Emirates recognizes the importance of preserving date-palm production systems and the rich traditions surrounding the fruit. Date palm production contributes immensely to economic revenue in the country through export, which supports the government's goal of utilizing other available resources to diversify away from oil. The date palm's wide range of uses for nutrition and raw materials also makes it important for food security in the region. Additionally, being a labor-intensive industry, date palm production contributes to job creation and income generation for farmers.

The UAE extends special care and importance to the date palm tree, which is considered a national wealth of great economic, environmental, nutritional and social value. From an economic point of view, the country has been able to be among the top ten date producing countries. Date palm trees also constitute as a source of income for many workers in this sector, whether producers or marketers, as well as owners of related industries.

From an environmental perspective, the date tree is distinguished by its ability to live in the desert environment, forming an ecological habitat for many organisms, such as soil organisms to birds and several other, which contribute to creating a kind of ecological balance. From a social aspect, the date palm tree constitutes a social heritage, in all segments of the society, as it is involved in many traditional and commercial industries.

The interest in the date palm tree in the UAE, is linked to the beginning of the UAE's establishment in the early seventies, where many national projects were implemented to increase the cultivated areas and adopt modern farming techniques such as irrigation, fertilization, pest control and others.



الكربونية

للنخيل

## 1.2. Overview

In 1990, the United Arab Emirates (UAE) was ranked at the 5th place as one of the top, per capita, CO<sub>2</sub> emitting countries (EU EDGAR, 2021). It has remained amongst the top, per capita, CO<sub>2</sub> emitting countries during the period 1990 – 2021 (last published statistics), when it was ranked the 7th at 19.58 tons per capita CO<sub>2</sub> emission in 2021 (EU EDGAR, 2021). Furthermore, the UAE became one of the first major oil-producing countries to ratify the Kyoto Protocol when it entered into force in 2005. In contrast, the country has undertaken huge efforts to green the desert hence, reducing its carbon footprint, which have never been accounted for, because of lack of implemented mechanisms and tools to assess the amount of biomass and carbon stock sequestered by plants in the country.

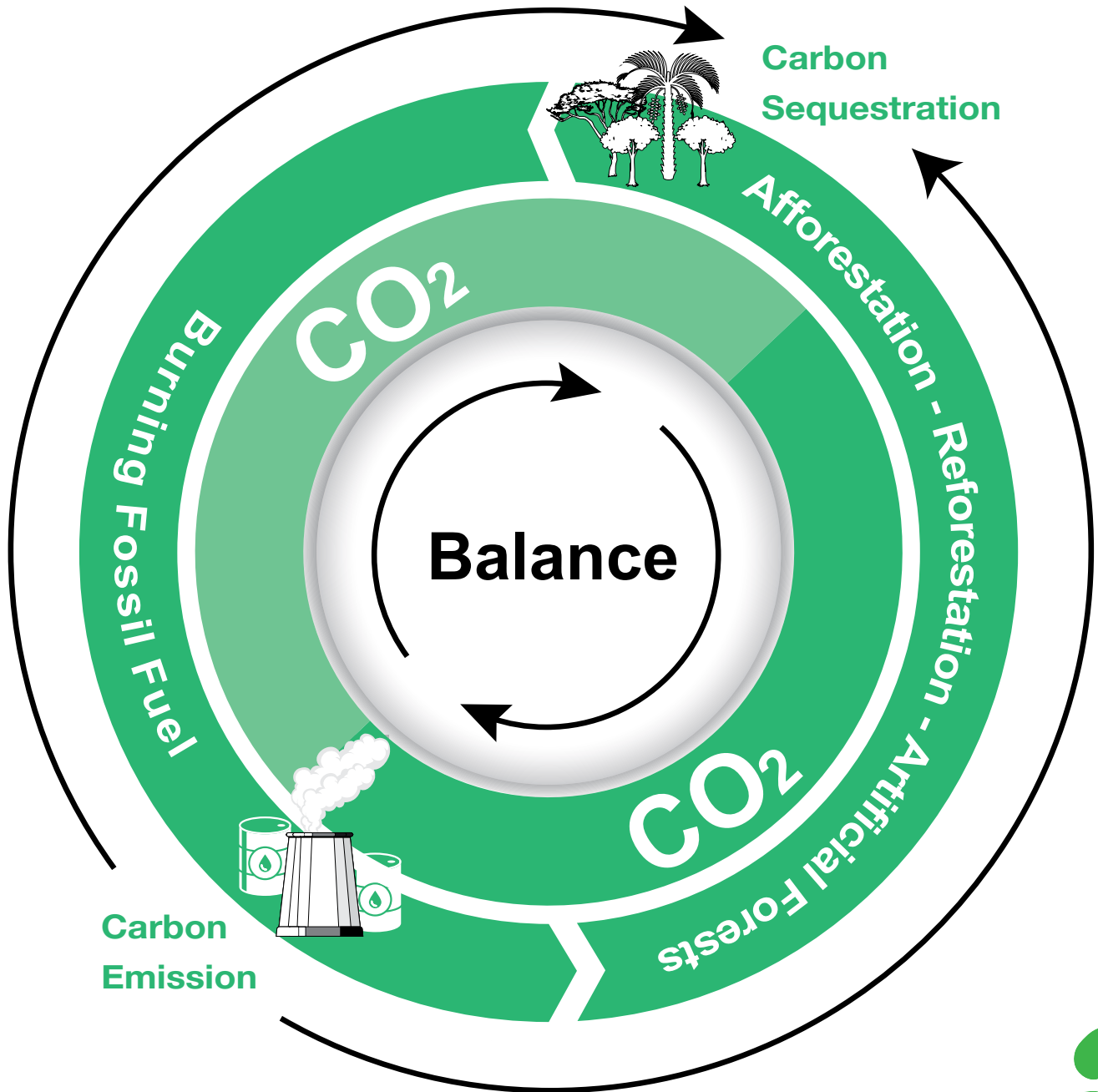
There is a common consent that afforestation and land-use conversion to a forest (reforestation) can be used to earn carbon credits and reduce the carbon footprint. This attitude has a growing interest among policymakers and governments (Baral & Guha, 2004). Estimation of carbon stock (CS) in forests and trees is important to assess their mitigation effects and hence balancing the carbon footprint (Ebuy *et al.*, 2011). Many techniques exist to estimate sequestered carbon (Gibbs *et al.*, 2007). Most existing techniques ultimately rely on the ground measurement of plant biomass

which is time-consuming, tedious, and destructive (Ebuy *et al.*, 2011). Alternatively, most of the existing non-destructive methods using developed biomass estimation equations have been developed for tropical rainforests ecosystems because of their importance to the global carbon cycle (Basuki *et al.*, 2009; Brown, 1997; Chave *et al.*, 2005; Cole & Ewel, 2006; Makinde *et al.*, 2017).

Unfortunately, very few plant species biomass estimation equations are available for desert ecosystems. Moreover, none of these equations were developed and used to fit one of the most important fruit crops in these arid regions, Phoenix dactylifera L. (Date Palm). Indeed, the only indigenous wild desert plant domesticated in its native harsh environments appears to be the date palm (Zohary & Hopf, 2000). Date palm is considered a renewable natural resource because it can be replaced in a relatively short period of time or used through conservation efforts without depletion (El-Juhany, 2010). Date palm has a vital component of the agricultural system.

The records show that the number of DP in the Near East and North Africa (NENA) region exceeds 100 million, distributed across 30 different countries (FA-OSTAT, 2013). They produce about 7.5 million tons of dates annually. Particularly, UAE has a minimum of 200 cultivars, 68 of which are commercially considered to be the most important (El-Juhany, 2010). Consequently, date palm, with its various cultivars, possesses the potential capacity to store carbon and hence be considered as a good means of carbon sequestration in such an arid ecosystem.

Nevertheless, the estimation of forest biomass raises scientific challenges to identify feasible approaches to assess carbon at the national-level (Gibbs *et al.*, 2007). Effective management requires repetitive monitoring and accurate measuring of biomass which is a classical subject in plant population ecology (Joshi & Ghose, 2014; Avery & Burkhart, 2015; Elzinga *et al.*, 1998; Husch *et al.*, 1982; Schreuder *et al.*, 1993; Shiver & Borders, 1996). Traditional biomass assessment methods (both destructive and allometric), based on



الكربونية

**Infographic 1:** Afforestation and land-use conversion to a forest (reforestation) can be used to earn carbon credits and balance carbon emissions.



field measurements are the most accurate methods; however, they are difficult to conduct over large areas besides, they are not a practical approach for broad-scale assessments (Kumar & Mutanga, 2017; Yuen *et al.*, 2016). These difficulties make monitoring activities more costly, time-consuming, and labour-intensive (Attarchi & Gloaguen, 2014; Khalid & Hamid, 2017). Furthermore, field-based resource inventories, are carried out for economic reasons and not environmental ones. They provide good historical data on patterns and trends but are not accurate enough to estimate fluxes for the entire landscape and all carbon pools therein (Cihlar *et al.*, 2002).

Recently, remote sensing (RS) procedures have been applied to natural resources management and biomass assessment (Kankare *et al.*, 2013; Maynard *et al.*, 2007; Salem Issa *et al.*, 2019; Wannasiri *et al.*, 2013). RS can obtain forest information over large areas with repetitive coverages, at a reasonable cost and with acceptable accuracy (Lu, 2006). Moreover, the integration of RS data into geographic information systems (GIS) models will benefit from the tools of both technologies; allowing for adding ancillary and field data to the analysis and increasing reliability in estimating the biomass, hence CS. Building GIS-based models to predict future scenarios for forest management and the implementation of afforestation plans is another more valuable product.

The purpose of this book is to implement a new approach towards assessing the carbon sequestered by date palm trees in Abu Dhabi Emirate, in both their biomass compartment as well as the soils under beneath, using geospatial technologies (RS and GIS) assessed by field measurements. Therefore, the main questions of the book are the following:

- Are geospatial technologies (RS and GIS), as an innovative method, capable of estimating biomass and CS in forests (date palm trees in the current case) with minimum cost and time while keeping high levels of accuracies?
- How can the geospatial technologies be con-

sidered as a reliable and feasible solution towards forest management in the arid regions and hence be adopted as a long-term strategy that can be integrated into the decision-making process at the national level?

- On the other hand, the UAE country's huge efforts undertaken to green the desert and hence, reduce its carbon footprint, have not been accounted for, because of the lack of implemented mechanisms and tools to assess the amount of biomass and CS sequestered by plants within its territories.
- Thus, Estimating CS in forests and trees by using a simple, practical, and an eco-friendly mechanism is an accompanying objective to assess decision makers and planners in their efforts for climate change mitigation and hence balancing the carbon footprint.

Several specific objectives of the current study have been defined and specified, with the corresponding chapter in which they are treated, as follows:

To calculate the biomass ratios in date palm including aboveground biomass (AGB), belowground biomass (BGB), total biomass, and the carbon percentage in both biomass and soil (SOC) at three age stages (young, medium, and mature) from selected date palm trees in Abu Dhabi Emirate. (Chapter 2),

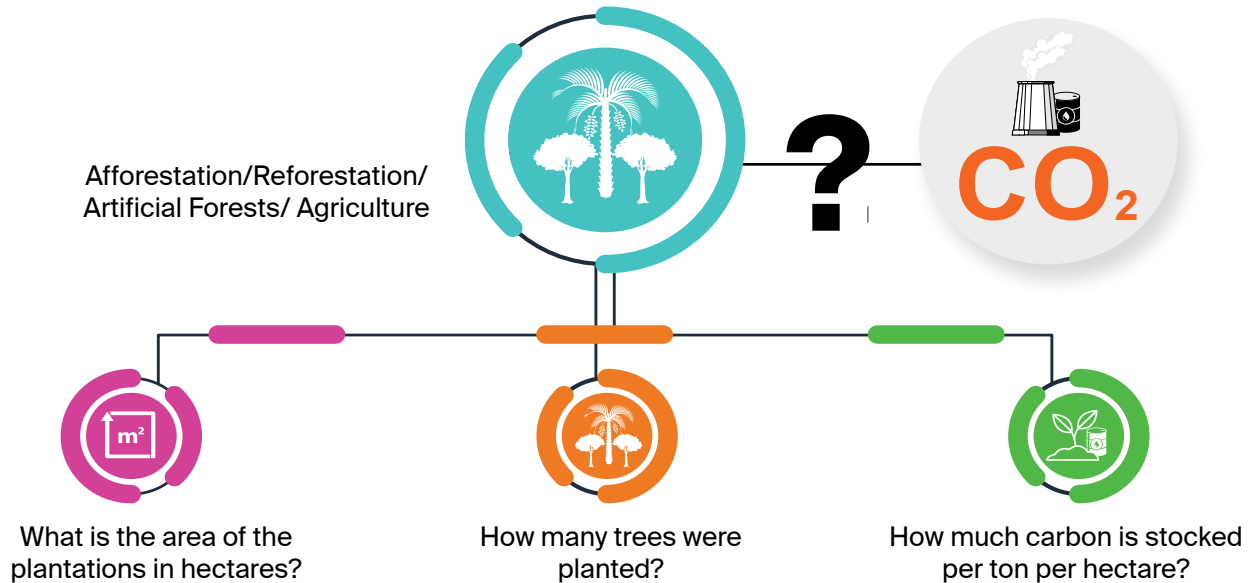
To develop date palm biomass allometric equations for estimating its biomass and CS assessment. (Chapter 2),

To map the main LULC classes in the study area and to extract and map the date palm trees in Abu Dhabi Emirate. (Chapter 3),

To build a RS-based spatial model for biomass and CS assessment of date palm. (Chapter 4), and

To quantify and visualize the amount of biomass and CS in Abu Dhabi Emirate, using the built RS-based spatial model. (Chapter 4).

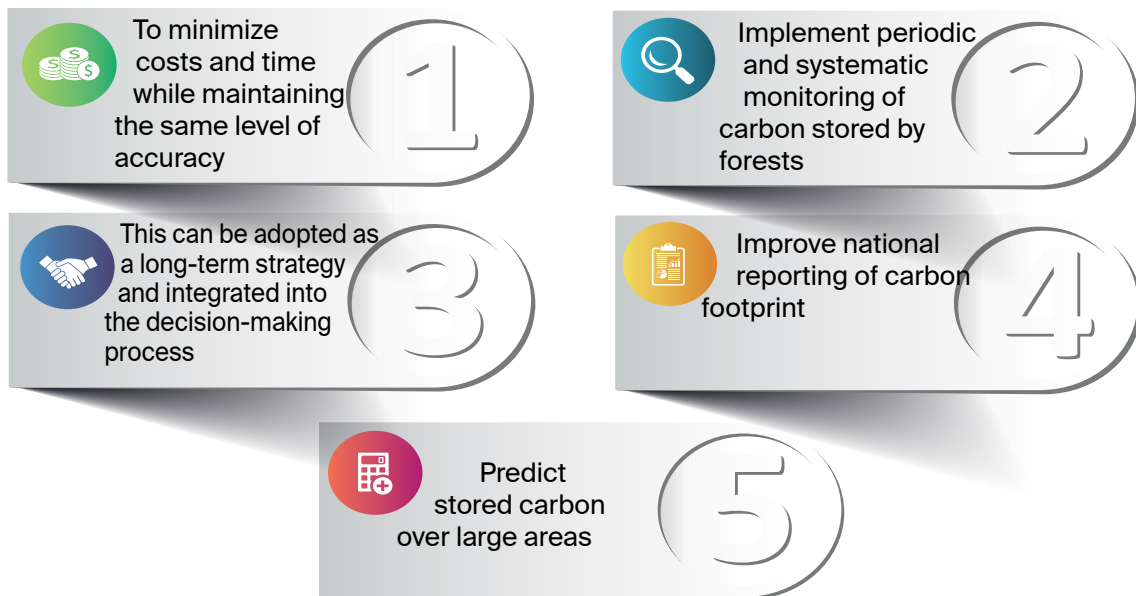
## Lack of implemented mechanism and tools



**Infographic 2:** Efforts to reduce its carbon footprint have not been accounted for due to a lack of tools to assess biomass and carbon sequestration in its territories.



## Impacts of the INNOVATIVE Method



**Infographic 3:** Geospatial techniques enhance natural resource management, particularly in biomass and carbon assessment, yielding positive results.



# 1.3.

## Literature Review

The substantive part of this Subsection has been published in peer reviewed journals. These published papers are:

- Dahy, B., Issa, S., Ksiksi, T., & Saleous, N. (2020). Geospatial Technology Methods for Carbon Stock Assessment: A Comprehensive Review. IOP Conference Series: Earth and Environmental Science, Volume 540.
- Issa, S., Dahy, B., Ksiksi, T., & Saleous, N. (2020). A Review of Terrestrial Carbon Assessment Methods Using Geo-Spatial Technologies with Emphasis on Arid Lands. Remote Sensing, 12(12), 2008.
- Dahy, B., Issa, S., Ksiksi, T., & Saleous, N. (2019). Non-Conventional Methods as a New Alternative for the Estimation of Terrestrial Biomass and Carbon Sequestered: Mini Review. World Journal of Agriculture and Soil Science.

### 1.3.1. Quantifying Terrestrial Carbon Sequestration

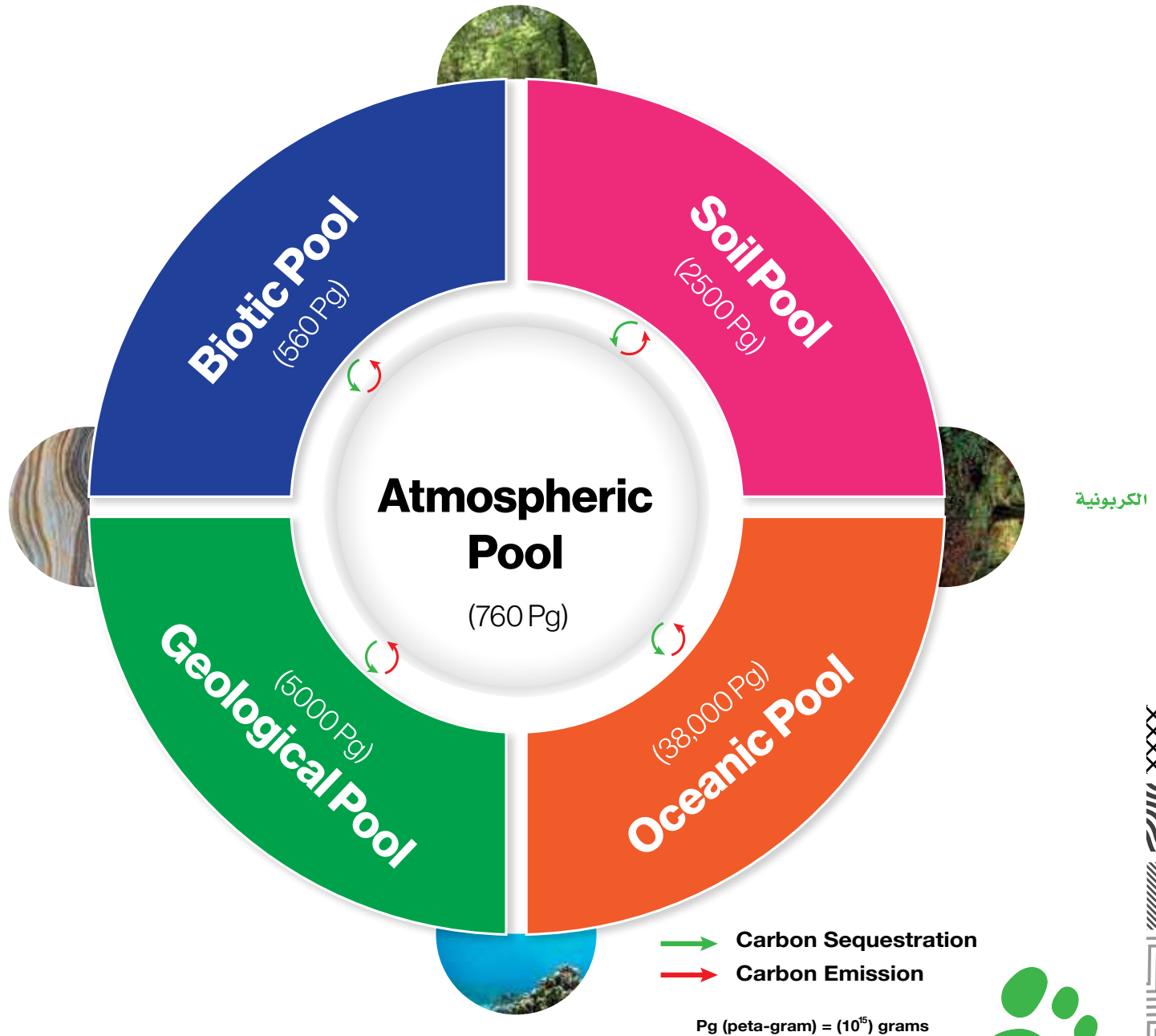
Carbon sequestration is the process of capturing of CO<sub>2</sub> gas in the atmosphere and its storing in liquid or solid state. This process is already occurring naturally through trees, the ocean, soil and live organic matter (Lackner, 2003). Any reservoirs or stores of carbon are called carbon pools. Specifically, CO<sub>2</sub> storing occurs in three levels: in plants and soil (Terrestrial Se-

questration), underground (Geological Sequestration) and deep in oceans (Ocean Sequestration) (Figure 1). Terrestrial or biologic sequestration is the process of storing atmospheric CO<sub>2</sub> as carbon in the stems, roots of plants and soil. The bulk of carbon sequestered terrestrially is stored in forest biomass.

Forests, as both carbon sources and sinks, can play a major role in combating global climate change (Dick OB, 2015; Ekoungoulou *et al.*, 2014). Estimation of CS and assessing the role of forest ecosystems in regional and global carbon cycles, is important for a better understanding of the impacts of land-cover changes on carbon fluxes, nutrient cycling and budgeting. Likewise, monitoring forest biomass, as a step in CS estimation, is not an environmental issue only; actually, more than 190 countries are committed to take action to implement and support sustainable management of forests and enhancement of forest CS according to Paris Agreement on Climate Change (United Nations, 2019).

Carbon sequestration is becoming an essential component in the fight against global warming. Afforestation projects and land use conversion to forest (reforestation) can be used to earn carbon credits and reduce the carbon footprint, hence providing a long-term reduction in greenhouse gases (GHGs) levels through carbon sequestration (Singh *et al.*, 2018). This attitude has a growing interest among policymakers and governments (Baral & Guha, 2004). Plantation cropping as a land use system has the potential to contribute to CS, maintain soil biodiversity and improve soil fertility (Prayogo *et al.*, 2018). It can add economic value by providing more job opportunities, better income and food security, especially the smallholder systems in developing countries, and the timber exploitation (Khalid & Hamid, 2017; Singh *et al.*, 2018).

The UN program for the reduction in emissions from deforestation and forest degradation (REDD+), is an international initiative to help nations earn financial incentives if they implement climate policies and if they demonstrate CO<sub>2</sub> emission reduction (Gibbs *et al.*, 2007).



الكربونية

**Figure 1:** Carbon pools. They include: (1) Terrestrial Sequestration pool (sequestering and storing of CO<sub>2</sub> in plants and soil); (2) Geological Sequestration (underground) pool; (3) Ocean Sequestration (deep in oceans) pool; and (4) Atmospheric pool. (Lal, 2004; Issa et al., 2020a).



Precise CS estimation is a necessary step to define carbon emission mitigation strategies and programs at the local and regional level (Clerici *et al.*, 2016a). This kind of studies is necessary for a better understanding of the long-term behaviour and drivers of carbon sequestration under different global climate change scenarios (Corona-Núñez *et al.*, 2018). The total CS in any terrestrial ecosystem is the sum of carbon in biomass and soil. A practical definition of forest biomass is the total amount of aboveground living organic matter in trees expressed as oven-dry tons per unit area (Brown, 1997). The estimation of biomass is a challenging task, especially in the areas with both complex stands and varying environmental conditions as well as in low vegetation cover density areas, such as arid

lands. Both types of ecosystems require the use of accurate and consistent measurement methods.

Eggleston *et al.* (2006) has listed five terrestrial ecosystem carbon pools involving biomass: above-ground biomass (AGB), below-ground biomass (BGB), litter, woody debris and soil organic matter. The total CS is estimated as the sum of two quantities representing the amounts of carbon in soil and in biomass. Therefore, two routes for achieving sequestered carbon estimation: First, estimating soil organic carbon (SOC) which is part of soil organic matter (SOM). Second, estimating vegetation biomass which can be achieved by estimating the AGB and then deriving the remaining components; BGB, Litter and Debris, from the AGB as shown in (Table 1).

**Table 1: Calculation methods of CS components in terrestrial ecosystems.**

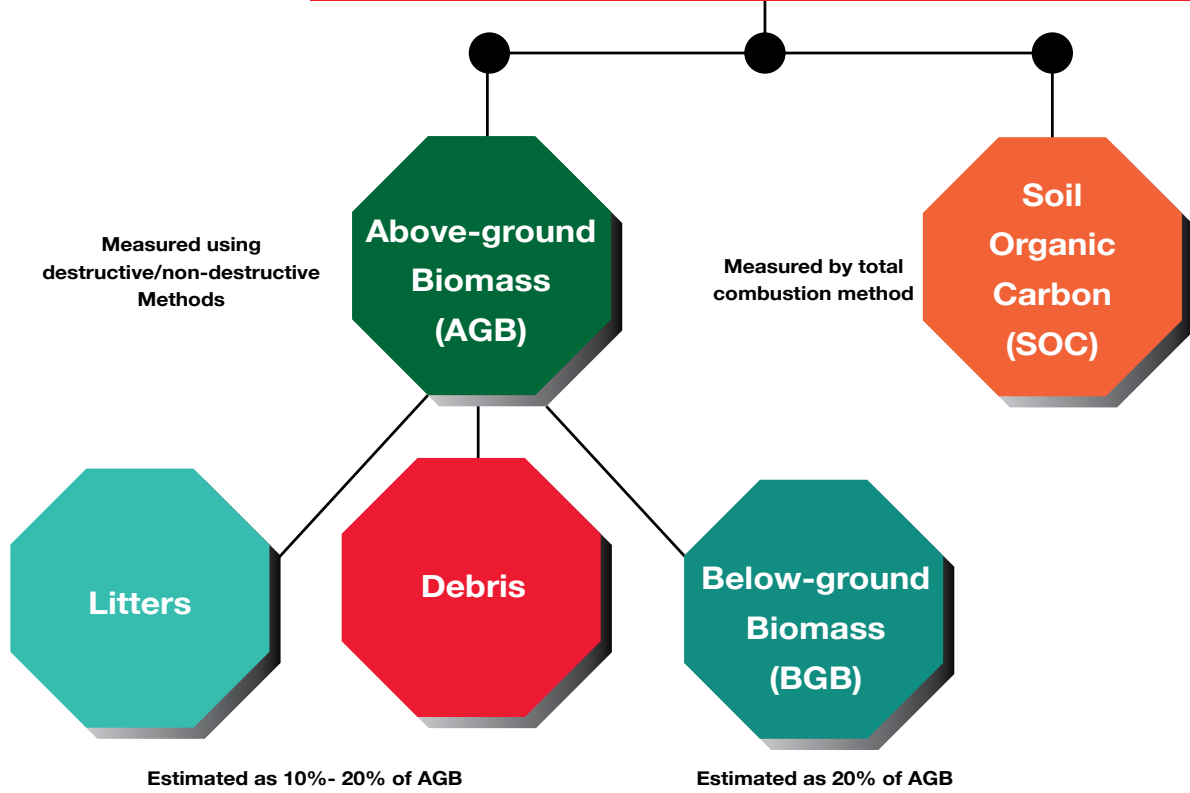
Component	Calculation Method	Source
<b>AGB</b>	Destructive OR Non-destructive Methods	(Gibbs <i>et al.</i> , 2007)
<b>BGB</b>	20% of Above-ground biomass	(Cairns <i>et al.</i> , 1997)
<b>Litters</b>	10-20% of Above-ground biomass	(Houghton <i>et al.</i> , 2009)
<b>Debris</b>		
<b>SOC</b>	Total combustion method	(Walkley & Black, 1934)

As for SOM, it is most commonly estimated through soil sampling at various layers; SOC is then estimated using the total combustion method, as explained in (Walkley & Black, 1934). The content of SOC included in SOM may change depending on many factors (ecosystems, type of organic residues and land management, etc.). Many studies estimate SOC from SOM using the conventional factor of 1.724 (~ 58% of SOM). This figure is widely used and has appeared in many studies and published papers in the last century; while Brady and Weil (1999) concluded that this value (58% of SOM) probably applies only to highly stabilized humus. After his statistical analysis of 481 studies, Pribyl (2010) found that conventional factor varies from 1.35 to 7.50 with a mean value of 2.20, concluding that

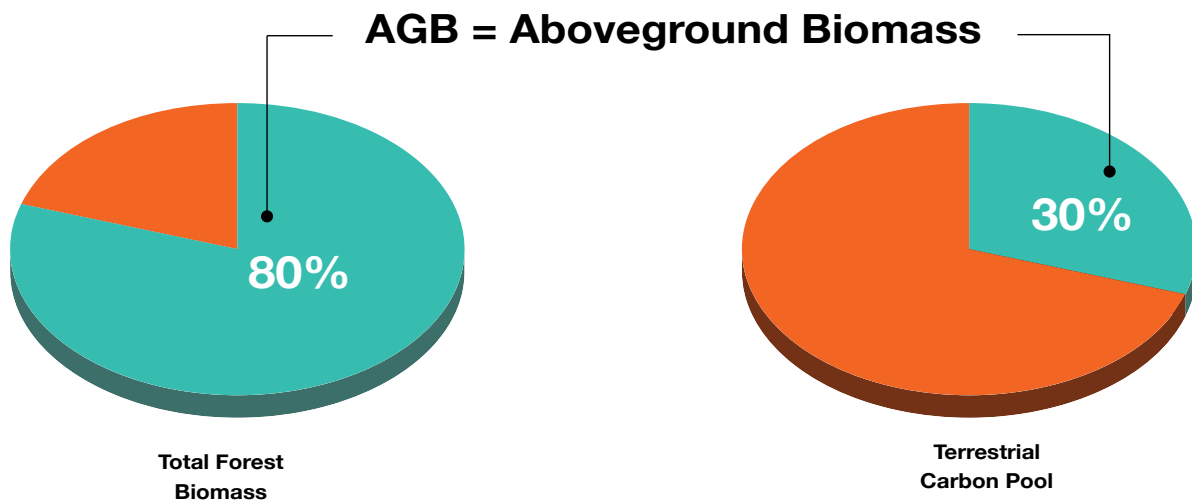
any single-number conversion factor, universally applied, has the potential for serious error when used to estimate the carbon content of soils. However, recent studies have accepted a generic quick, simple and inexpensive coefficient of 57% for measuring SOC as a percent of SOM (Ponce-Hernandez *et al.*, 2004).

Of the above five pools, AGB is the most visible, dominant, dynamic and important pool of the terrestrial ecosystem, constituting around 30% of the total terrestrial ecosystem carbon pool which, in turn, represents 70-90% of the total forest biomass (Cairns *et al.*, 1997). AGB estimation has received considerable attention over the last few decades because of increased awareness of climate warming and the role

Calculation Methods of the five components of Carbon Stock in terrestrial ecosystems



الكربونية



**Infographic 4:** The estimation of aboveground biomass (AGB) holds significance as it represents the most visible, dominant, dynamic, and critical component of the terrestrial ecosystem.



forest biomass plays in carbon sequestration and release of greenhouse gases due to deforestation (Kumar *et al.*, 2015). While SOM holds two to three times more carbon than the total biomass carbon pool on a global scale, much of the soil carbon is more protected and not easily oxidized (Davidson & Janssen, 2006).

On the other hand, AGB contributes to atmospheric carbon fluxes to a much greater extent due to fire, logging, land-use changes, etc., and so is of much greater interest. Therefore, it should be monitored and measured along the year, not only a one-time mapping; although the estimation of forest biomass is a scientific challenge as to identify efficient methods for its assessment at regional to national-levels (Gibbs *et al.*, 2007). Moreover, estimates of AGB can also be used to predict root biomass (BGB), which is generally estimated at 20% of the AGB based on the predictive relationship applied by many studies (Table 1) (Cairns *et al.*, 1997; Mokany *et al.*, 2006; Ramankutty *et al.*, 2007). In addition, CS of dead wood or litter (e.g., felled or dead trees, dead or broken branches, leaves, etc.) in mature forests are generally assumed to be equivalent to 10 to 20% of the calculated AGB (Gibbs *et al.*, 2007; Houghton *et al.*, 2009).

Producing accurate maps for biomass estimation distribution is a serious challenge which has to be addressed when calculating CS. As mentioned before, plant biomass can be measured or estimated by both direct (destructive) and indirect (non-destructive) methods. The direct method which is the most precise method for determining carbon biomass by destructively harvest all plants, partition each into various constituent components (e.g. stem, branches, leaves, flowers, fruits, roots) and subsequently determine the carbon content of the various components analytically or calculated as a fraction of measured biomass (indirect) (Yuen *et al.*, 2016). The destructive methods of biomass estimation are limited to a small area due to the destructive nature, time, expense and labor involved and sometime illegal especially for trees. In addition, these methods ultimately rely on ground measurement and can cause severe destruction to the forests

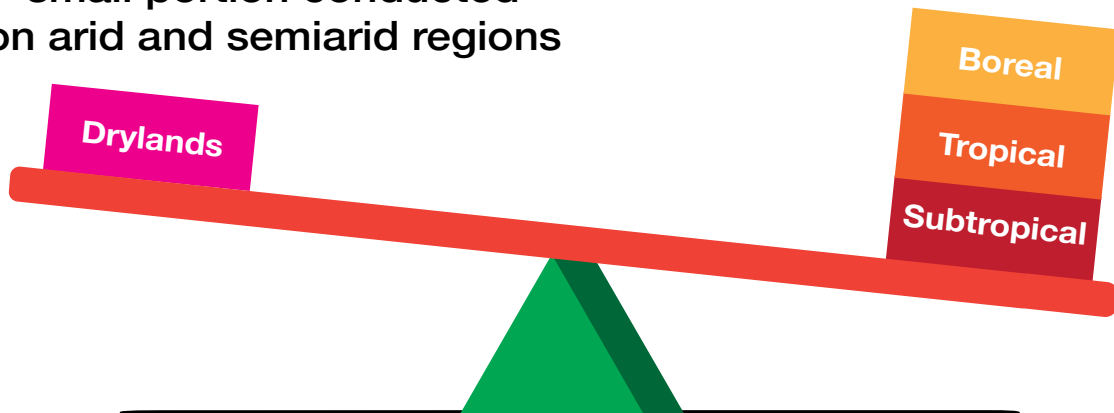
as well as a risk of environmental deterioration (Khalid & Hamid, 2017; Maulana *et al.*, 2016). The indirect methods include the estimation based on allometric equations (Subsection 1.2.2) or through non-conventional methods using RS and GIS (Subsection 1.2.3).

### 1.3.2. Biomass Allometric Equations

There are many reasons that make developing biomass equations a very essential step towards guarantying an alternative to destructive methods. The main objective in developing allometric equations is to avoid destructing forests when estimating their biomass, hence its CS, and provide a cost effective and environment-friendly option since it is done without harvesting (Brown *et al.*, 1989). In general, allometric equation is a statistical model to estimate the biomass of the trees using their biometrical characteristics (e.g., height, diameter at breast height (DBH) or crown size),

## Studies on forest biomass and carbon in different ecosystems

small portion conducted on arid and semiarid regions



**Infographic 5:** The majority of biomass and carbon estimation studies have predominantly focused on boreal and tropical forests, while comparatively fewer have been undertaken in arid and semiarid regions.

الكربونية

which are non-destructive and simpler to measure (Picard *et al.*, 2012). Therefore, non-destructive methods through allometric relationships are increasingly used. Such equations have also been proven to be fast, inexpensive, and more suitable for largescale estimation of forest CS (Koala *et al.*, 2017). Allometric models are commonly used in forest inventories and ecological studies (Brown *et al.*, 1989). The models relate biomass of an entire tree or individual tree components (e.g., stems, branches, leaves or roots) to one or more easily tree variables and dendrometric measures (e.g. height, diameter breast height or crown size), and to estimate CS (Ebuy *et al.*, 2011; Picard *et al.*, 2012). The proportions between height and diameter, between crown height and diameter, and between biomass and diameter follow rules that are common to all trees which are grown under the same conditions and become more useful in uniform forests or trees with similarly aged stands (Archibald & Bond, 2003; Bohlman & O'Brien, 2006; Dietze *et al.*, 2008; King, 1990; Kumar & Mutanga, 2017).

The selection of appropriate and robust models, therefore, have considerable influence on the accuracy of the obtained estimates (Mahmood *et al.*, 2019). As mentioned above the aim of using allometric equations is to estimate biomass without the need to cut trees. In order for those equations to be validated, cutting and weighting tree components is necessary (Vashum & Jayakumar, 2012). The number of trees destructively sampled to build allometric equations differs from one study to another. Currently, there is no consensus on that number, as this is often dependent on resource availability and permission to harvest trees (Yuen *et al.*, 2016). For example, Russell (1983) and Deans *et al.* (1996) used 15 and 14 trees, while Brown *et al.* (1995) and Khalid *et al.* (1999a) used only 8 and 10 trees, respectively to build their allometric equations. In their study of oil palm trees of Benin forests, Aholoukpè *et al.* (2018) used 25 palms from several ages and different genetic origins to build a species specific allometric equation. However, a recent study showed that smaller sample size ( $\leq 10$ ) results in biased allometric equations (Duncanson *et al.*, 2015).

للنخيل

Generally, there is no specific procedure to build allometric equations yet there is a recommended guideline for documenting allometric equations. (Jara *et al.*, 2015) recommended that researchers should only report all the details in methods section of how they build up their equations. Furthermore, sampled trees should be randomly selected, regardless of health condition or degree of damage, because sampling only trees with fully intact structural characteristics will likely result in an equation that overestimates biomass for the general case. In this respect, data outliers should not be removed simply to improve model fit metrics (Yuen *et al.*, 2016).

Many allometric equations have been developed for various plant species. For example, the Globe Allome Tree database contains over 706 equations from Europe, 2843 from North America and 1058 from Africa (Sileshi, 2014). Some of these are volume equations, while the others are biomass equations. The biomass can be calculated from volume of the biomass per hectare (VOB/ha) by using a generalized volume model, wood density and a biomass expansion factor (Brown *et al.*, 1995; Lugo & Brown, 1992). One of the limitations of volume equations is that it can only be applied to stem while allometric equations cover a wide range of vegetation components (Cheng *et al.*, 2014).

Allometric models can be developed for either individual or multiple plant species to represent a community or bioregion. They also can be developed to cover specific sites, regional or pan-tropical scales (Mahmood *et al.*, 2019; Yuen *et al.*, 2016). Most of biomass equations, species and multispecies, have been developed for tropical rainforests ecosystems because of their importance to the global carbon cycle (Basuki *et al.*, 2009; Brown, 1997; Chave *et al.*, 2005; Cole & Ewel, 2006; Makinde *et al.*, 2017). The multispecies equations are built because it is practically difficult to develop allometric equations for all species present in the ecosystem (Dick OB, 2015).

Chave *et al.* (2005) have shown that one hectare of a tropical forest may shelter as many as 300 different tree species. Hence, the multispecies allo-

metric models are more methodologically efficient for biomass estimation compared to those developed for individual species at specific locations. However, these models carry the potentiality to misrepresent local, species- or community-specific variations and anomalies. Therefore, they may fail to capture variations in both forest type and the full diversity of the natural vegetation communities hence leading to an increased level of uncertainty (Mahmood *et al.*, 2019).

Hence, a tailored equation for each specific species is needed for a better accuracy in estimating the biomass. Nevertheless, such an equation will still be conditioned by the ecological zone based on which it had been built. Hence, weakening the estimation's accuracy of the actual forest AGB when the equation is used in another area or region.

Due to the different characteristics of plant species from site to site, pre-existing equations developed at locations that are different from the one in consideration may have limited applicability, even if the equation is species-specific. In their review of allometric equations in Asia, Yuen *et al.* (2016) concluded that applying existing allometric equations out of convenience is potentially a key source of uncertainty in above- and below-ground CS estimates in many Asian landscapes. The selection of allometric equations can influence local, regional and global biomass estimates, therefore, there is an importance of site-specific equations for accurate estimation of biomass as generalized equations can overestimate AGB by 50% to 65% (Maulana *et al.*, 2016).

The locally developed models are expected to provide less uncertainty than generic equations (Jara *et al.*, 2015). Site and species specific allometric models should logically provide a greater level of accuracy at a given location to assist the assessment of biomass carbon sequestration and that make the locally built equation a better option to produce more accurate site-specific biomass estimation.

Finally, since the choice of the equations is the first critical step, there has been a rapid increase in efforts to develop locally appropriate equations (Sileshi,

2014). Only a few biomass assessment equations are available for plant species in desert land ecosystems. None of these measurements were used to fit one of the most important fruit crops in the arid regions, *Phoenix dactylifera* L., (date palm).

The mathematical model commonly used for modelling AGB is based on the power function (Yuen *et al.*, 2016). This was founded on the basis that the growth of a plant is characterized by the relation of proportionality between its total biomass and its size (Fonton *et al.*, 2017). Biometric variables measured in plant species were considered as independent variables (DBH, total height, crown variables, stem height, etc) and incorporated into a power function model (Da Silva *et al.*, 2015).

The allometry based on power model have good reliability as indicated by high coefficient of determination indices ( $R^2$ ) (Gevana & Im, 2016). Researchers involved in the development and application of biomass allometric equations are faced with many challenges. One of them is the choice between simple bivariate power-law (typical allometric) functions and models with multiple predictors (Sileshi, 2014). Different variables (structural and non-structural) were considered when building biomass allometric equations. Most equations for AGB, or biomass of any component (stem, branch, leaves, other) use equations with diameter and/or height as independent variables. Other variables such as girth, basal area and crown dimensions have been used even less frequently— usually in special cases (Yuen *et al.*, 2016).

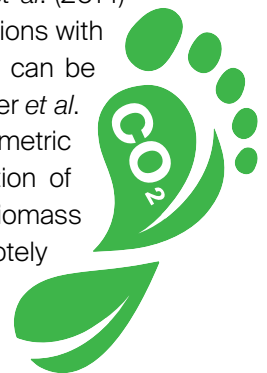
Using wood density, when it is available, as a predictor is considered as significantly improving the biomass prediction equation when dealing with multispecies dataset (Chave *et al.*, 2005). In their study to investigate the allometric equations in China, Cheng *et al.* (2014) found that the most frequently used predictive variable in single-variable models is DBH, and in two-variable models are DBH and tree height while wood density and crown diameter are presented in more complicated models. They found that diameter variables have a dominant proportion of 87.4% of the surveyed equations. However, DBH showed a weak cor-

relation with biomass quantity in specific species, like palm for example (Carlos *et al.*, 2015; Sajdak *et al.*, 2014).

Age can be used as a predictor for biomass estimation in many studies since there is a linear correlation between biomass accumulation and age (Henson & Chang, 2003; Singh *et al.*, 2018). Many studies have highlighted the importance of tree height as a predictor variable in the AGB equation (Fonton *et al.*, 2017; Khalid & Hamid, 2017; Picard *et al.*, 2012; Prayogo *et al.*, 2018). A single plant species can have more than one allometric equation, e.g., date palm varieties (Appendix 1). Furthermore, more than one allometric equation can be developed for each plant species. The reasons behind that can be:

1. difference in ecoregion sites that these equations developed for (Tropical or Amazonian forests etc.),
2. the decision of the developers of the allometric equations and choosing of the suitable variable/s (height, DBH, trunk height, etc.) to work as input (independent variable) to the model, and
3. the use of the allometric equations to cover either specific parts of the plant (AGB, crown biomass, trunk biomass, etc.) or specific age (young, mature, mixed, etc.), and
4. the selection of the mathematical equation form (power, linear, algorithmic, etc.).

The use of crown variables as indicators for biomass estimation became of more interest lately due to the developments in RS technologies. More recently, allometric equations have been used, coupled with RS and field-based structural variables measurements (Cihlar *et al.*, 2002; Dahy *et al.*, 2019; Salem Issa *et al.*, 2018, 2019). For example, Cheng *et al.* (2014) recommended to develop more equations with different field structural variables that can be linked to RS predictors. Likewise, Jucker *et al.* (2017) suggested in their review of allometric equations to develop a new generation of allometric equations that estimate biomass based on attributes which can be remotely sensed.



### 1.3.3. Geospatial Technologies for Estimation of Carbon Stock

While direct field data measurements of biomass are the most accurate, they are not adequate to map AGB distribution at large scales. On the other hand, geospatial technologies proved to be practical and cost-time effective, and allows for imaging and studying inaccessible places by traditional field measurements. Geospatial technologies procedures have been applied to natural resources management and biomass assessment, hence CS (Kankare *et al.*, 2013; Wannasiri *et al.*, 2013). RS can obtain biomass information over large areas with repetitive coverages, at a reasonable cost and with acceptable accuracy (Lu, 2006).

Various techniques and sensors have also been used and tested in numerous studies. RS, both active and passive, provide some of the most time-efficient and cost-effective approaches to derive AGB estimation at the national and regional scale. Moreover, the integration of RS data into GIS models provides advantages of both technologies, allowing for adding ancillary and field data to the analysis, besides increasing reliability in estimating AGB.

A textual search on Google Scholar was performed, in order to identify statistically relevant temporal patterns of the use of terms such as 'Carbon Sequestration', 'Carbon Sequestration + Remote Sensing' and 'Carbon Sequestration + GIS' in the literature. The search was customized to group results by ten-year intervals starting in 1951, to highlight the development of researches in the subject under review over time and the increase in the use of geospatial technologies in CS studies (Figure 2).

Statistical analysis of the data revealed an exponential increase with time in the number of scientific studies on carbon sequestration considering both RS and GIS in their methodology. This can be attributed to the increase in volume of available satellite imagery and the ease of access to their archives witnessed over the last two decades to be become available to

the end user either freely or commercially. Furthermore, the introduction of GIS in the late eighties contributed to this trend as well.

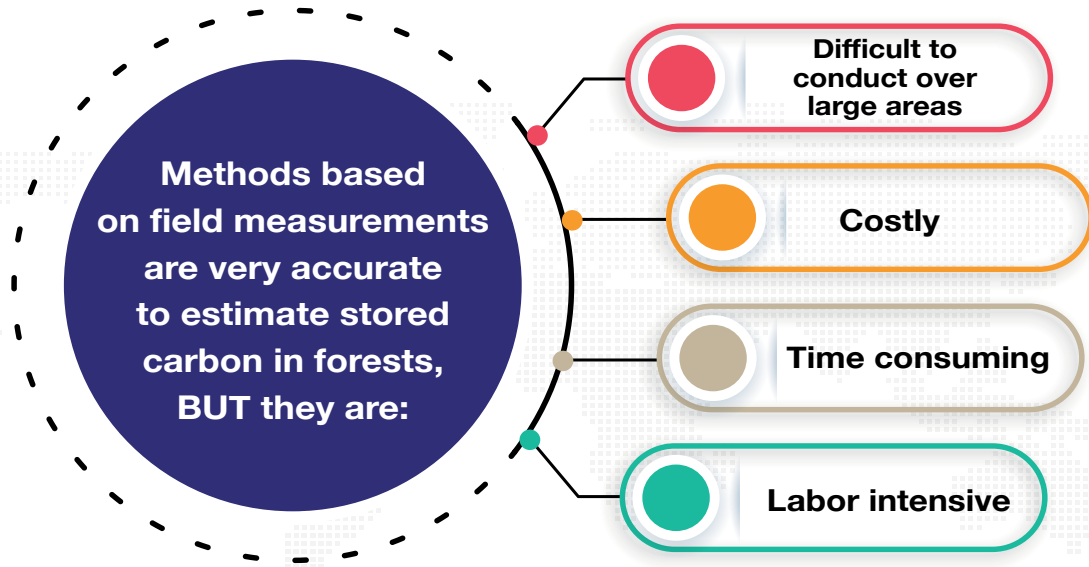
Furthermore, a systematic review was conducted in two databases other than Google Scholar, namely, Web of Science and Science Direct. The databases were accessed using the search terms: "carbon sequestration", "above-ground biomass", "remote sensing", and "GIS". The search was applied to articles that were published in peer-reviewed journals only. These searches collectively yielded 2,771 results. The results were pared down to 647 by applying three criteria:

1. the results were NOT "review papers" OR "conference proceeding" papers and only restricted to research articles;
2. the study belonged to terrestrial ecosystems excluding the marine and coastal ecosystems; and
3. the study is not a duplicate from a previous search.

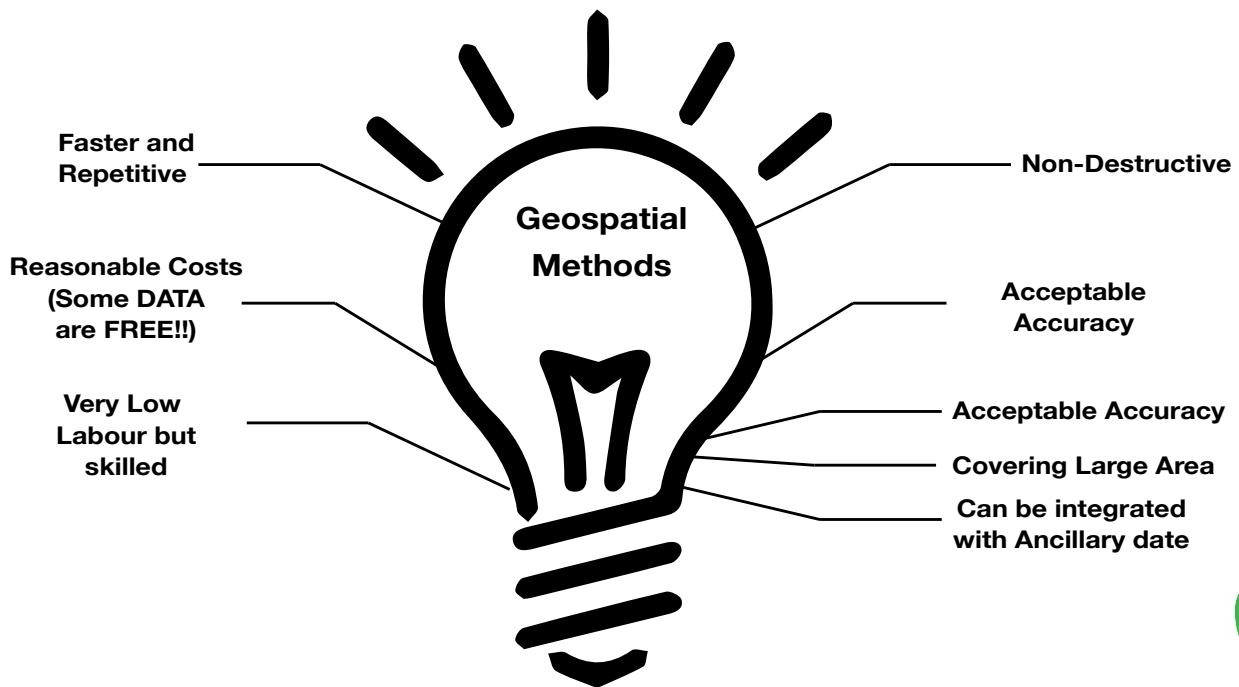
All these articles were downloaded and stored using the reference management software (ZOTERO). Based on reviewing the abstracts, the list was further reduced to 171 by retaining only articles that discuss correlation between AGB and RS-based parameters, and that use GIS in the analysis (not for mapping only!). Finally, the full-text assessment of the final articles was used to review geospatial technologies for estimation of CS.

The following subjects will be covered and evaluated: RS data types for estimating AGB and CS (Subsection 1.3.3.1); the RS-based methods used to attain a certain level of accuracy at the species/plant communities (multispecies) level (Subsection 1.3.3.2); surveys all biophysical predictors used in RS technology (Subsection 1.2.3.4); identifies significant RS variables (Subsection 1.3.3.5); highlights RS-GIS integrated models (Subsection 1.3.3.6); and presents arid lands case studies with challenges and opportunities (Subsection 1.3.4).

# PROBLEM & GAP



الكربونية



**Infographic 6:** Geospatial technologies for biomass and carbon assessment offer numerous advantages over traditional methods.



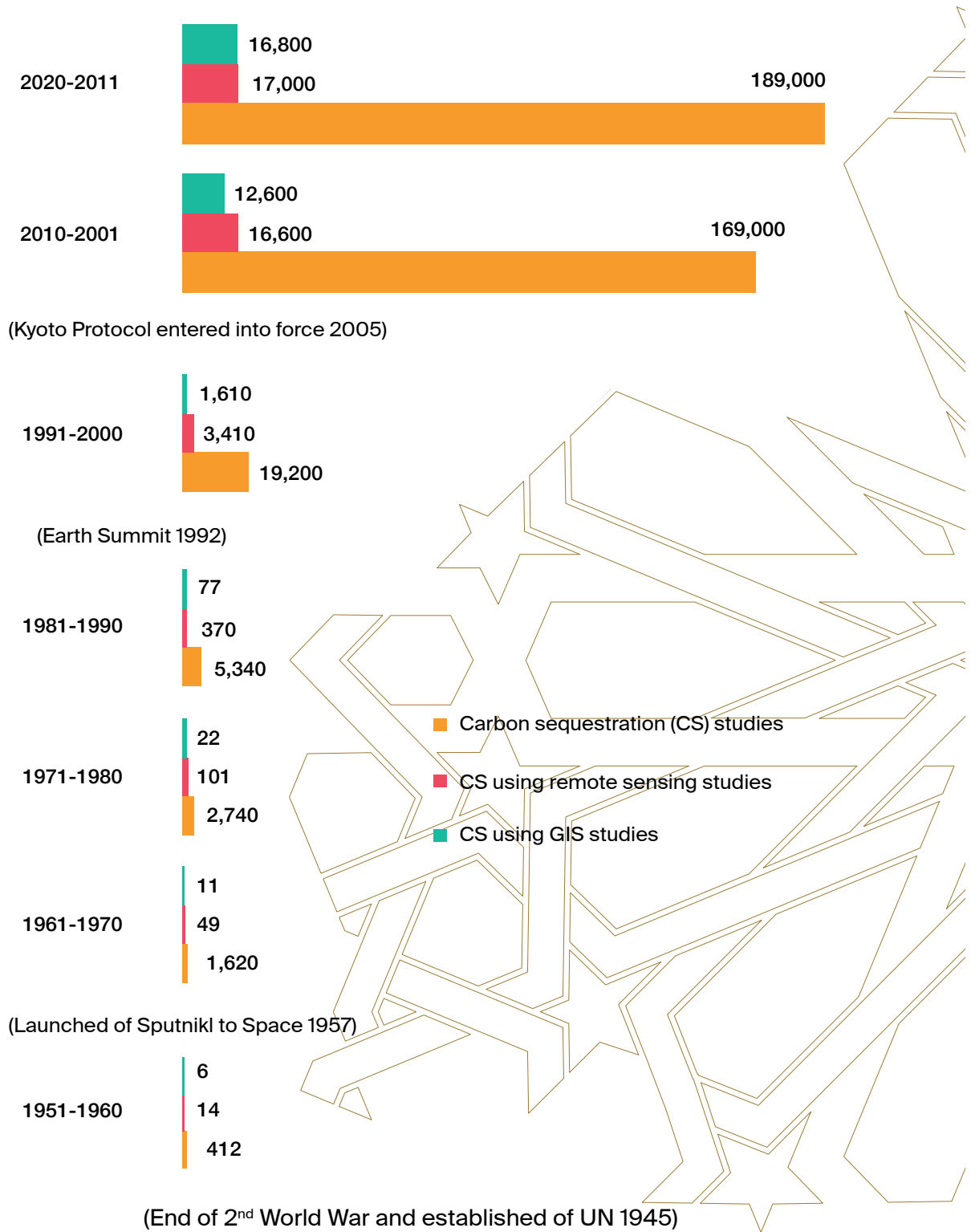


Figure 2: Textual analysis using Google Scholar. The terms used are: Carbon Sequestration, Remote Sensing and GIS. (Dahy et al., 2019, 2020; Salem Issa et al., 2020a).

### 1.3.3.1 Remote Sensing Data Types

Data from RS satellites are available at various scales, from local to global, and from several different platforms. There are also different types of sensors both passive, such as optical and thermal RS sensors, and active, such as Radar and Light Detection and Ranging (LiDAR) sensors, with each having its advantages and disadvantages. Benefits and limitations of these sensors are shown in Appendix 2. The optical sensors, sometimes called passive sensors, are RS systems relying on visible and reflected infrared light (Zhao *et al.*, 2016). Appendix 3 shows the specifications of the RS optical sensors most commonly used for AGB estimation. While active sensors are the sensors that emit and record backscatter values or interferometry technique in a portion of the electromagnetic spectrum (Ghasemi *et al.*, 2011).

Despite the successful application of any sensors in AGB estimation, there are challenges related to acquisition costs, area coverage (swath width), and limited availability. RS data are nowadays abundant and widely available for a fraction of the cost required only a decade ago. Furthermore, these data are captured with various, radiometric, spectral, spatial and temporal resolutions, hence meeting the needs for AGB detection, mapping and assessment. Selecting the “right” sensor is associated with the specific data availability of the area under study, project budget, technical skill requirements for data interpretation and software packages. The resolutions of the sensors used are pre-defined to meet the researcher’s needs and specifications, although it happens that a specific sensor’s data are the only available for a study area. Many software packages can perform digital images processing and spatial analysis like ERDAS imagine, ENVI, ArcGIS and other open-source software like QGIS and Google Earth Engine. These packages are relatively easy to use and can produce exceptional results.

Statistical analysis based on the 171 papers reviewed reveals that around two thirds of these studies used passive (optical) sensors (with different spatial resolutions), while the remaining third used active sensors (almost equally split between RADAR and LiDAR) (Figure 3).

Around 40% of the studies using optical sensors used coarse spatial resolution (>100 meters) sensors like MODIS and SPOT VEG. Almost the same percentage of studies (40%) used moderate spatial resolution (~10- 100 meter) sensors like Landsat, IRS, and SPOT. Additionally, around 20% of these studies used fine spatial resolution sensors (sub-meter to 5 meters) like IKONOS, Quickbird and World View.

To improve the accuracy of estimating AGB, integration of more than one sensor is becoming a trend (around 17% of the reviewed studies), as well as the integration with GIS-based approaches (around 14% of the reviewed studies). It was observed that more than 60 studies were conducted using these two approaches. Statistical results further showed that the number of studies that estimate AGB at plant species levels, instead of forests in general or mixed species, was increasing. Many plant species are not separable targets using RS because they are indistinguishable from other plants due to their spectral similarities (detecting, mapping, and classification of vegetation will be discussed in separate Subsection, 1.3.3.3).

Hence, resolution concerns such as high spatial resolution (e.g., IKONOS) and high spectral resolution (e.g., hyperspectral) should be taken into account as they help resolve such ambiguities and play essential roles in the quality of the resulting maps (Thenkabail *et al.*, 2004). Nowadays, RS data are widely available for a fraction of their cost only a decade ago. Figure 3 shows the proportion of utilizing different sensors with different number of bands for the estimation of the biomass and carbon sequestered.

Accurate image classification relies on the successful extraction of pure spectral signature for each species, which is often dictated by the spatial resolution of the observing sensor and the timing of observation (Xie *et al.*, 2008). For example, archived and recent Landsat imageries are available and are freely downloadable from the USGS website, providing a globally consistent record of archived imageries since 1972; other resources



are being continuously published and added to the internet. Bryceson (1991) used the habitat type, condition and soil type as the delineating parameters to locate *Chortoicetes terminifera* (Australian plague locust) by using Landsat-5 multispectral scanner data. Anderson *et al.* (1993) mapped *Ericameria austrotexana* infestation in a large homogenous area using Landsat Thematic Mapper (TM) imagery.

The spectral radiances in the red and near-infrared regions, in addition to others, were used for vegetation mapping by RS technology. The spectral signatures of photosynthetically and nonphotosynthetically active vegetation showed noticeable differences and could be utilized to estimate forage quantity and quality of grass prairies (Xie *et al.*, 2008). Moreover, discrimination of vegetation species from single imagery is only achievable where a combination of leaf chemistry, structure and moisture content culminates to form a unique spectral signature.

As the detection and estimation of biomass are sensed from space, the crown biomass component has gained prominence in the majority of the relevant studies (Cheng *et al.*, 2014; Clark *et al.*, 2005; Jucker *et al.*, 2017; N'aves & Økland, 2002; Ozdemir, 2008; Popescu *et al.*, 2003). The unique pattern of crown palm trees, for example, makes them easily distinguishable from other trees on satellite imagery (Shafri *et al.*, 2011).

It is worth mentioning that most of these studies were conducted on boreal and tropical forests with a small portion conducted on arid and semiarid regions (around 10%). This could be due to the early availability of geo-spatial technologies in the developed northern countries (boreal forests) and the relative importance of the tropical rainforests to the global carbon cycle (Figure 3).

### 1.3.3.2. Remote Sensing Based Methods

To explore the potential of RS-based methods for extracting biomass information in different environments, various techniques and sensors have been used and tested in numerous studies. Optical,

RADAR, and LiDAR data have been extensively used to estimate AGB with a variety of methods (Clerici *et al.*, 2016a). AGB studies using geospatial technologies can be aggregated according to the level of the methodological complexity to several tiers including different levels of detail and accuracy.

The Intergovernmental Panel on Climate Change (IPCC) proposed three tiers: Tier-1, Tier-2, and Tier-3 (Gibbs *et al.*, 2007; Henry *et al.*, 2011; TSITSI, 2016). Tier-1 is the basic method based on the 'biome average' approach. It is the simplest level using the globally available data, generalized equations, and provides a rough approximation of biomass, and hence CS, and could be used as a starting point for decision-makers; however, it can provide inaccurate results with a high level of uncertainty (Gibbs *et al.*, 2007). Tier-1 considered a generalized biomass equation for the ecological zones, and is typically used when no species-specific equations exist (Henry *et al.*, 2011).

Tier-2 is an intermediate level that is based on the volume equation and wood density. It is used when species-specific volume equations exist, and woody density for the specific plant species is available. The volume is then converted to biomass using wood density and a default biomass expansion factor (BEF) (Eggleston *et al.*, 2006; Henry *et al.*, 2011).

Finally, Tier-3, the most demanding in terms of complexity and data requirements, is based on using a species-specific biomass equation to calculate either total or partial biomass. Partial biomass is obtained by adding up the biomass estimates obtained from the species-specific equations for the different compartments.

Tier-2 and Tier-3 levels are more dependent on ground-based measurements of the tree (i.e., DBH and height) and building the predictive relationships (allometric equations) (Gibbs *et al.*, 2007). This makes these two levels more expensive to implement than Tier-1. It is worth noting here that the precision for a given species generally increases with the increase in the Tier number (Henry *et al.*, 2011).

A geospatial approach is widely used to collect information regarding forest AGB and vegetation structure as well as to monitor and map vegetation biomass and productivity at large scales (Iizuka & Tateishi, 2015; Main-Knorn *et al.*, 2011; Makinde *et al.*, 2017; Pflugmacher, 2011). Using RS, GIS and modeling to study the current state of carbon sequestration and its future dynamics, are promising and have a potential ability as an innovative approach to tackle the ecological assessment problems (Lal, 2002). RS-based methods have seen widespread use among the research community thanks to their unique characteristics either in data collection or in results presentation. RS data can sense and record spatial variability, spatial distributions, spatial patterns of forests and assess their changes over time (Zhao *et al.*, 2016).

For mapping vegetation using RS data, a multi-steps process is usually applied (detecting, mapping, and classification of vegetation will be discussed in separate Subsection, 1.2.3.3).

The first step involves image preprocessing and aims at enhancing the quality of original images. For example, panchromatic band with 15 m spatial resolution, in Landsat imagery, that can be used to pan-sharpen other bands and hence increase their interpretability, has been added to Landsat's multispectral sensors (Phiri & Morgenroth, 2017). Previous studies showed that such use of the panchromatic band helped achieve dramatic improvements (15%) in classification accuracies (Gilbertson *et al.*, 2017).

The second step involves determining the level of vegetation classification (at community or species level). The third step determines the correlation between the vegetation types and spectral characteristics of RS imagery. Vegetation data is identified by interpreting satellite images based on the elements such as image color, texture, tone, pattern and association information.

Lastly, the final step includes translating the spectral classes into vegetation types by assigning

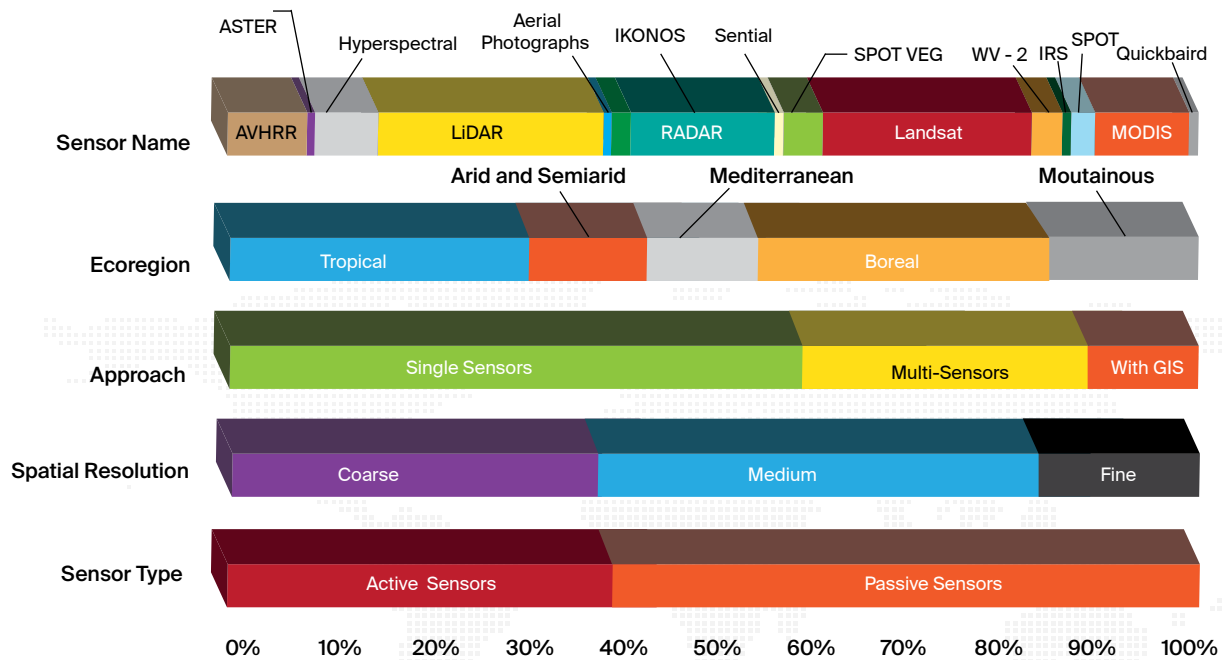
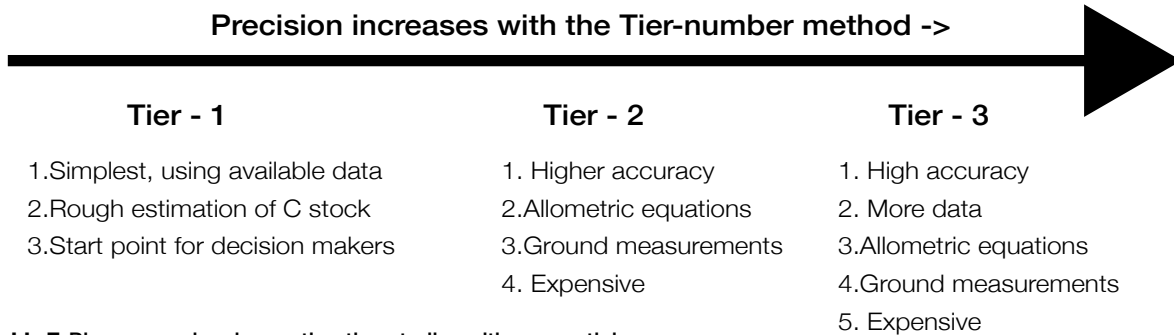


Figure 3: Geospatial input data used in reviewed papers at different forests. (Dahy *et al.*, 2019, 2020; Salem Issa *et al.*, 2020a).



- RS based methods for biomass estimation are still at an experimental stage and is challenging task because of their complex forest structure.
- Level of methodological complexity (IPCC)



**Infographic 7: Biomass and carbon estimation studies with geospatial technologies can be grouped by methodological complexity into tiers with varying detail and accuracy.**

each pixel of the scene to one of the vegetation groups defined in the vegetation classification system selected in the second step. Classification methods are broadly based on the pixel-based classification (PBC) approach or the object-oriented based classification (OOC) approach. Both methods have their advantages and disadvantages depending on their areas of applications, and most importantly, the RS datasets that are used for information extraction (Jawak *et al.*, 2015). OOC methods group several pixels with homogeneous properties into an object/objects instead of pixels, which are considered as the basic unit for analysis, while PBC approaches are based on combining reflectance pixel values into separated spectral clusters (Blaschke, 2010; Myint *et al.*, 2011a).

AGB and hence CS can be estimated from different RS data types using various approaches (Figure 4). Landsat series, for example TM, Enhanced Thematic Mapper (ETM+), and Operational Land Imager (OLI), have been historically used to map biomass and carbon in a variety of ecosystems, due to the relevance of their spectral bands, the continuity of the program, and the suitability of the 30 meter spatial resolution for regional mapping (Clerici *et al.*, 2016a).

Although biomass cannot be directly measured from space, the use of spectrally-derived parameters

from sensor reflectance (bands), including vegetation indices (VIs) that were created to improve prediction accuracy, enables increased biomass prediction accuracy when combined with field-based measurements (Pandit *et al.*, 2018).

RS data correlates with plot-based field measurements to estimate AGB and hence CS. In general, RS data are empirically linked to AGB measurements of field plots using different regression analyses and algorithms (Wani *et al.*, 2015).

There are many methods of image analysis that can be integrated to achieve a better accuracy. Algorithm development and implementation is an important subject in studies estimating biomass (Kumar & Mutanga, 2017). The advanced machine learning algorithms methods and/or other state-of-the-art processing techniques can reveal important information about the spatial and temporal biomass patterns by determining relationships between field measurements and RS data, especially over large areas (Kumar & Mutanga, 2017).

To determine the relationship between above-ground field biomass and RS data, researchers have used linear regression models with or without log transformations of field biomass data, and multiple

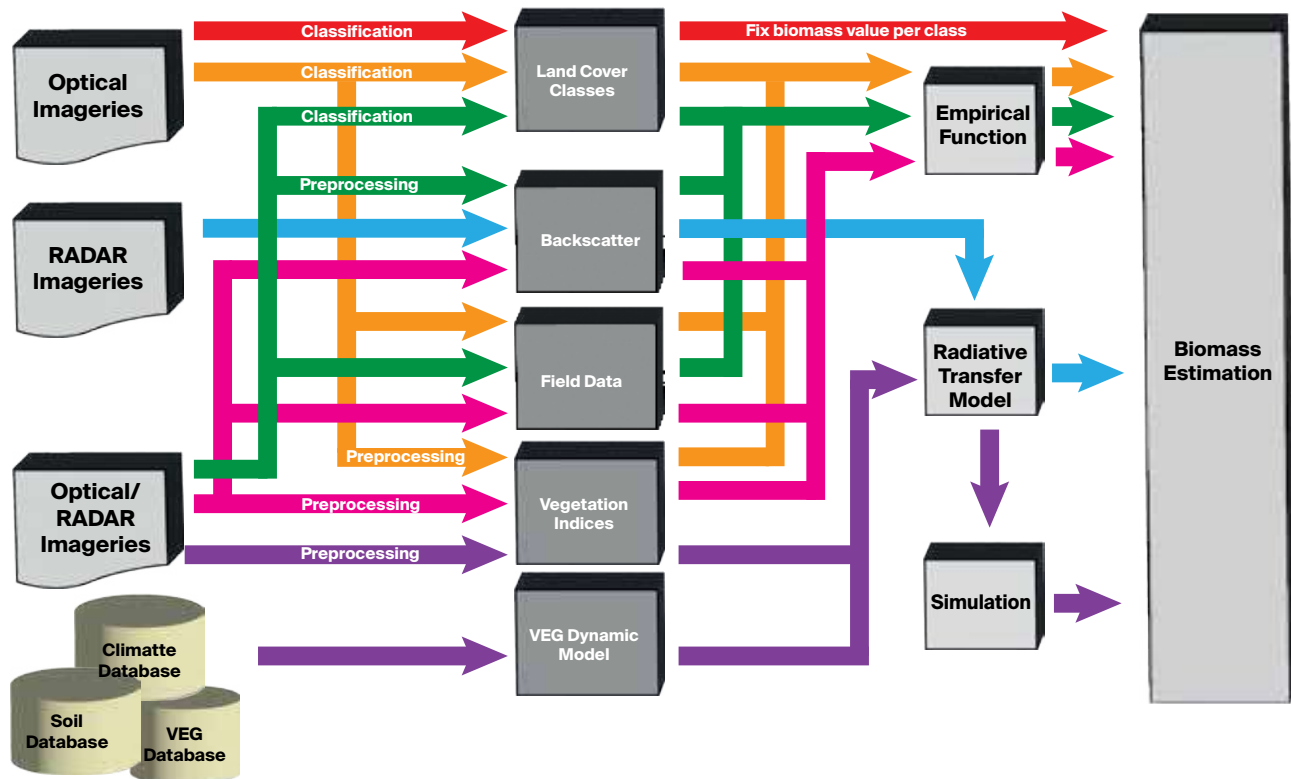


**Figure 4:** Different RS/GIS procedures available for estimating AGB and CS. (Eisfelder *et al.*, 2012; Salem Issa *et al.*, 2020a).

regressions with or without stepwise selection (Clewley *et al.*, 2012; Robinson *et al.*, 2013). Artificial neural networks, semi-empirical models, nonlinear regression, and nonparametric estimation techniques (e.g., k-nearest neighbor and k-means clustering) have also been used (Castel *et al.*, 2000; Lu, 2006; Wijaya & Gloaguen, 2009).

However, few studies have investigated approaches other than the empirical relationship with spectral bands or VIs (Eisfelder *et al.*, 2012). One of these approaches is Monteith's efficiency model for obtaining indirect estimates of absorbed photosynthetically active radiation (APAR) from the red and IR reflectance characteristics of the vegetation where APAR is used as an indication of how efficiently absorbed energy is converted to dry biomass (Monteith, 1972). Rosema (1993) used a simulation of vegetation development from daily total evapotranspiration with the in/out radiation of METESTAT in order to estimate

the herbaceous biomass in savannah grassland in Sahel countries.

Other studies used canopy functioning process-based models coupled with physical radiative transfer models to estimate biomass production from RS data (Williams, 2010). Fourier transform textural ordination (FOTO) was used by Morel *et al.* (2012) with SPOT5 data for estimation AGB in Thailand with the R value equal to 0.83. Regression, ordinary kriging, co-kriging, and stepwise linear regression have been used in various studies and it was found that the combination of RS and geo-statistics can improve the accuracy of biomass estimates more than the use stepwise linear regression only (Mutanga & Rugege, 2006).

Extensive field knowledge and expert knowledge may help improve classification accuracy. Studies have shown that



classification accuracy can be greatly improved after applying expert knowledge (empirical rules) and ancillary data to extract thematic features (e.g., vegetation groups) (Xie *et al.*, 2008). Fieldwork is the foundation for RS technology allowing to extend limited vegetation information to large scale predictions (Wu *et al.*, 2016). This direct mapping approach is more accurate at depicting variations in biomass across the landscape, making it easier to update the maps as needed (Kelsey & Neff, 2014).

### 1.3.3.3. Detecting and Mapping Plant Species Using Satellite Imagery

Accurate mapping of vegetation is a critical and important task for many environmental-related issues such as forest management, biomass estimation, or terrestrial CS quantification. Geospatial technologies (RS & GIS) are well established for their capabilities of measuring and estimating forest AGB and for monitoring and mapping vegetation biomass at large scales (Dahy *et al.*, 2019; Iizuka & Tateishi, 2015; Main-Knorr *et al.*, 2011; Makinde *et al.*, 2017; Maynard *et al.*, 2007; Pflugmacher, 2011; Salem Issa *et al.*, 2020a).

Methods for measuring and mapping vegetation cover using RS and GIS are well developed; however, they exhibit performance issues in certain ecosystems particularly, arid land ecosystems where a high background reflectance contribution to the pixel value remains a great challenge. Besides, several plant species are hardly distinguished from other objects because of their spectral resemblances. The advent of high spectral and spatial resolutions data helped in resolving such ambiguities and played an essential role in improving the quality of land cover maps (Thenkabail *et al.*, 2004).

Furthermore, satellite imagery variables are only capable of mapping and correlating environmental variables if the vegetation spectra are detectable within the pixel, a great challenge that can only be overcome in certain arid land environment (Aly *et al.*, 2016a; Oldeland *et al.*, 2010; Tian *et al.*, 2016). This last constraint presents a foremost challenge in the desert ecosys-

tem, usually with sparse vegetation cover, producing a weak spectral object requiring a higher resolutions' imagery to be captured (Bradley *et al.*, 2019).

Hyperspectral sensors showed plausible classification accuracies in mapping major forest species and predicting the susceptible areas of fruit malformation (Nagaraja, 2009). Hebbar *et al.* (2014) used LISS-IV data to classify fruit trees and found that old and mature trees were classified more accurately while young and recently planted ones (3 years or less) showed poor classification accuracy due to mixed spectral signature, wider spacing and poor stands of trees.

While high-resolution data offer more spatial detail, they present certain disadvantages including high cost especially when it applies to broad areas, the need for large data storage, complex technicalities and long processing times. Furthermore, moderate resolution satellites (e.g. Landsat, and SPOT) proved to be effective in land cover classification for different research purposes and in different regions (Aly *et al.*, 2016a; Elhag, 2016; Rembold *et al.*, 2000; Shaker *et al.*, 2012).

Such multispectral optical sensors have been widely utilized operationally in estimating and mapping AGB (Eisfelder *et al.*, 2012; Kumar *et al.*, 2015; Kumar & Mutanga, 2017; TSITSI, 2016; Vashum & Jayakumar, 2012). Indeed, moderate resolution satellite data offer plausible results after conducting specific approaches such as pan-sharpening or fusion techniques. Starting with Landsat-7 ETM+, a panchromatic band with 15 m spatial resolution, that can be used to pan-sharpen other bands and hence increase their interpretability, was added to the already existing Landsat's multispectral sensors (Phiri & Morgenroth, 2017; Shaharum *et al.*, 2018).

Previous studies showed that such use of the panchromatic band helped achieve dramatic improvements (more than 15%) in classification accuracies (Gilbertson *et al.*, 2017). The Landsat program, MSS, TM, ETM+ and the most recent Landsat-8 OLI, present unique advantages in land cover classification applications because:

1. it is the longest running uninterrupted Earth observation program since 1972;
2. its archives are the first to offer global images free of charge (free access approach since 2008) (Phiri & Morgenroth, 2017; Turner *et al.*, 2015);
3. the current effects of climate change make the research on land cover classification methods based on the archived Landsat images an important resource (Barbosa *et al.*, 2014; De Sy *et al.*, 2012);
4. it is a very good source for vegetation change detection over large areas due to its relatively high temporal resolution (16-days revisit) and large swath (185 km);
5. another benefit of Landsat is to offer atmospherically corrected reflectances. Atmospheric correction is a critical step to minimize aerosol and cloud contamination and;

the suitability of the spatial resolution of Landsat series for regional mapping of biomass and carbon in a variety of ecosystems (Clerici *et al.*, 2016b). Baumann *et al.* (2018) found that Landsat-8 OLI is reliable for mapping woody vegetation (tree cover and shrub cover) in their study in Gran Chaco, south America. In their study for mapping tree canopy cover and AGB in woodlands landscape of Burkina Faso using Landsat-8 OLI, Karlson *et al.* (2015) found that the image texture is more correlated to tree cover attributes, in particular AGB, in open canopy conditions compared to closed canopies due to its ability to capture shadow structures caused by large trees (Karlson *et al.*, 2015).

There is no universal classification system that can be used for all types of imagery, at different scales, and for different purposes. Classification methods are broadly divided in two categories: pixel-based classification (PBC) and object-based classification (OOC). They both have advantages and disadvantages depending on their areas of applications and, most importantly, the RS datasets they use for information extraction (Jawak *et al.*, 2015).

PBC methods are based on using reflectance values to group pixels into separate spectral clusters; while OOC methods group contiguous pixels with homogeneous properties into objects, referred to as segments, that serve as the basic units for analysis (Blaschke, 2010; Myint *et al.*, 2011b). OOC methods have gained increased interest with the advent of high and very high-resolution RS imagery (Jawak *et al.*, 2013). Furthermore, OOC paves the way for combining spectral and spatial information, and in doing so potentially offers a more comprehensive classification approach that increases the results' accuracy (Wang *et al.*, 2016).

However, under- and over-segmentation errors may occur in the segmentation phase and lead to a reduction of classification accuracy; especially when an image object covers multiple classes. This usually leads to classification errors as all pixels in each mixed image object are assigned to the same class (Jawak *et al.*, 2015; Liu & Xia, 2010).

PBC, on the other hand, has proven very successful with low to moderate spatial resolution data. It uses a combined spectral response from all pixels in a training set for a target class. The resulting signature comprises spectral responses from a group of different land covers in the training samples, while the classification system merely ignores the impact of mixed pixels (Lu & Weng, 2004). PBC is commonly divided into supervised and unsupervised classification methods. Both approaches, separately or together, were used widely to run LULC classification in many regions and both have advantages and disadvantages. The use of vegetation indices (such as NDVI, EVI, SAVI) is considered as part of the unsupervised classification method. These indices use vegetation spectral characteristics to assess the status of vegetation cover (see Subsection 1.2.3.5).

The conventional PBC is quite limited because images of medium to low resolutions present a high level of heterogeneity and internal class variation within the same



© Freepik





scene (Kux & Souza, 2012). OOC approach considers the organization of individual pixels into groups (segments) that correspond to real-world objects in the identification of classes. Object-oriented image analysis involves partitioning the image into meaningful segments that replace pixels as the basic processing units (Benz *et al.*, 2004).

In general, the OOC algorithm initially performs segmentation of the whole image, then, the user defines a set of knowledge-based classification rules (spectral, spatial, contextual and textual information) to describe each class. Thereafter, the classifier is chosen to assign each segment to the proper class according to the user-defined rules (Jawak *et al.*, 2015). The OOC procedure involves the selection of training samples that represent the features to be classified. These features (objects) are then defined within the software based on rules that are further used to model the individual or groups of objects based on color, size, shape, position, direction, distance, orientation, distribution throughout the image, texture, as well as other user-defined parameters.

Many algorithms were developed for tree crown detection and mapping, (Chepkochei, 2011; Hebbar *et al.*, 2014; Lack & Bleisch, 2010; Rizvi *et al.*, 2019; Sahay *et al.*, 2017). Nevertheless, different methods may give different results while working in the same environment. Consequently, the results of tree detection and mapping can be affected by algorithm features. It is imperative to select the proper algorithm to get appropriate results. Likewise, for any algorithm to work properly, crowns should be detectable and segmented as an object in the image before classification. Training sets of the different classes to be identified and mapped must be selected very carefully for not to contain any contribution from the background nor any other class reflectance. This can be done by visual analysis and based on the interpreter's expertise and knowledge of the study area.

Hybrid classification approaches that combine supervised and unsupervised algorithms have gained importance. Since the early 1990s, several hybrid methods have been tried and refined in many cases

to improve classification accuracy (Jawak *et al.*, 2015; Kamusoko & Aniya, 2009; Kuemmerle *et al.*, 2006; Lo & Choi, 2004; Pradhan *et al.*, 2010; Rozenstein & Karnieli, 2011; Shila, 2010). Hybrid methods have demonstrated significant improvement in results' interpretation where there is complex variability in the spectral data within information classes.

#### The algorithms of most hybrid methods involve:

1. initial arrangement of the imagery by spectral clustering,
2. assigning clusters to user-defined classes, and
3. classification of the entire image using supervised learning (Jawak *et al.*, 2015).

Lo and Choi (2004) suggested that a hybrid approach can be economically implemented in a standard image processing software package to produce LULC maps with higher accuracy (up to 96% in urban) from moderate spatial resolution data ETM+ (Lo & Choi, 2004). In their study in eastern Europe, Kuemmerle *et al.* (2006) combined the advantages from supervised and unsupervised methods to derive a land cover map from Landsat data (Kuemmerle *et al.*, 2006). They conducted unsupervised classification to minimize bias in the selection of training areas and seed signatures, then eighty class signatures were extracted to run the supervised classification using the maximum likelihood classifier. The accuracy of the approach was estimated at 84%, 87%, and 91% for agriculture area, forests, and dense forests, respectively.

Shila (2010), used a hybrid classification method in Isfahan, Iran from ETM+ to increase automation and improve the accuracy of image data classification by taking advantage of both supervised and unsupervised classification methods. They found that the accuracy of the produced map reached 93%. Rozenstein and Karnieli (2011) examined combining signatures from both supervised and unsupervised training data (hybrid classification) and showed that they provided significantly more accurate results in Negev desert using TM image.

The majority of the UAE's territory is formed of desert ecosystems representing the mainland cover class of the country's land area. Date palm (DP) trees are known for their resilience to hard conditions requiring minimum water supply, tolerating high temperatures and drought, and sustaining high levels of salinity.

Measurement and analysis of DP in the UAE, using RS and GIS techniques, are almost absent and have seen very limited application examples in the country and the Gulf Cooperation Council region at large (Issa & Al Shuwaihi, 2012). Such investigations are vital for DP planning, management, and related resource studies. Sohl (1999) used multi-temporal TM imageries to provide locational, quantitative, and qualitative information on land cover change within the Abu Dhabi Emirate. His main concern was mapping changes in vegetation cover in Abu Dhabi Emirate in general rather than DP.

Goudie *et al.* (2000) have applied a cartographic approach to study coastal changes in Ras Al Khaimah (UAE); they reconstructed the history of coastal change in the study area. Alhameli and Alshehhi (2004) used historical aerial photographs, images and old documents to describe the rapid development of the UAE on selected sites with no measurements or analysis of DP mapping or other related parameters. Abdi and Nandipati (2010) investigated land cover changes in Abu Dhabi capital city and surrounding regions from 1972 to 2000 using Landsat images. The study conducted a simple change detection analysis of four land cover classes; none of them focused on DP trees.

#### 1.3.3.4. Biophysical Predictors

The biophysical predictors of vegetation growth need to be considered in RS studies due to the different rates of growth of various parts of such vegetation (Chong *et al.*, 2017). These predictors can be detected by remote sensors and are manifested through shadow, roughness, and spectral response (McMorrow, 2001). RS variables measured and correlated with biomass quantification include the spectral reflectance of vegetation as the spectral properties of AGB obtained by the sensors have unique signature correlated with chlorophyll content in the plants (Lu, 2006).

The signals are sensitive to AGB structure and influenced by density, shadow, texture, soil moisture and roughness, and constitutes one of the RS variables used in estimating biomass (Baccini *et al.*, 2008; Eisfelder *et al.*, 2012). The biophysical predictors used for estimating biomass include leaf area index (LAI), chlorophyll content, leaf nutrient concentration, height, DBH, stand basal area, greenness of canopy, and crown measurements like crown area (CA) and crown diameter (CD). All of these predictors are traditionally used to estimate biomass, but only some are applicable for RS based estimation (Figure 5).

Xiaoming *et al.* (2005) observed a robust logarithmic correlation between LAI and AGB. LAI can be defined as the area of one-sided leaf tissue per unit ground and measures the density of the leaves surface in a canopy. Tan *et al.* (2013) estimated LAI of oil palm in Malaysia using UK-DMC2 and ALOS PALSAR. They concluded that an increase in the LAI shows a proportional increase in the spectral reflectivity or Normalized Difference Vegetation Index (NDVI) during the initial growth stage; however, it presents little to no increase once it attains the full canopy cover due to sensor saturation.

The ability of hyperspectral RS to collect reflectance in many narrow bands makes it particularly useful for extracting vegetation parameters, such as LAI, chlorophyll content, and leaf nutrient concentration (Im & Jensen, 2008). Large scale photographs have been used to measure various forest characteristics, such as tree height, CD, crown closure, and stand area (Clark *et al.*, 2005).

In their study on the indirect estimation of biomass, Popescu *et al.* (2003) used RS data to determine tree canopy parameters, such as CD, using multiple regression analysis and canopy reflectance models. The CA can be measured by satellite imageries and, thus, provide biomass estimation. Suganuma *et al.* (2006) found that medium-resolution or more detailed spatial resolution data could be used for the crown coverage.



Crown projection area (CPA), which is the canopy area that is covered by an individual tree, can be calculated by delineating trees using object-based image analysis (Chong *et al.*, 2017; McMorrow, 2001). Greenberg *et al.* (2005) have effectively used IKONOS data (spatial resolution 4 meter) for estimating crown projected area, DBH and stem density. Song *et al.* (2010) estimated tree crown size from IKONOS and Quickbird images and concluded that this approach could provide estimates of average tree crown size for hardwood stands.

Height information of a tree can be retrieved using various approaches of RS, e.g., LiDAR and Radar. Height has been shown to be a potentially successful indicator for age in oil palms, for example, and it is widely used in estimating forest biomass (Chong *et al.*, 2017). Radar backscatters (P and L bands) are positively correlated not only with tree height and age but also with other major biophysical forest parameters such as DBH, basal area, and total AGB (Kumar *et al.*, 2015).

LiDAR sensor can directly measure three-dimensional (3D) components of vegetation canopy structure and is widely used in the estimation of forest biophysical parameters (Appendix 2). LiDAR data are used for biomass estimation for different forest environments; tropical forest biomass, temperate mixed deciduous forest biomass, and in measurements of biophysical parameters such as tree height and stand volume, and CD and canopy structure in general.

The two-dimensional data (2D) have limitations in estimating vertical vegetation structures such as canopy height, which is one of the critical biophysical parameters for biomass estimation (Appendix 2).

Recently, optical data such as ALOS, panchromatic RS instrument for stereo mapping (PRISM), IKONOS stereo satellite images, and SPOT have been used to provide a stereo viewing capability that can be used to develop vegetation canopy height, thus improving biomass estimation performance. St-Onge *et al.* (2008) assessed the accuracy of the forest height and biomass estimates derived from an IKONOS stereo pair and a LiDAR digital terrain model.

Reinartz *et al.* (2005) used SPOT 5 HRS for forest height estimations in Bavaria and Spain, while Wallerman *et al.* (2010) investigated 3-D information derived from SPOT 5 stereo imagery to map forest variables such as tree height, stem diameter and volume.

### 1.3.3.5. Remote Sensing Variables

Vegetation indices are generally used to estimate biomass in many studies (Clewley *et al.*, 2012; Robinson *et al.*, 2013; Schlerf *et al.*, 2005; Salem Issa *et al.*, 2019; Terakunpisut *et al.*, 2007). VIs are calculated from mathematical transformations of the original spectral reflectance data and can be used to interpret land vegetation cover (Das & Singh, 2012). VIs are applied to remove the variations caused by spectral reflectance measurements while also measuring the biophysical properties that result from the soil background, sun view angles, and atmospheric conditions (Lu, 2006).

The notion of VI is well adapted for quantifying vegetation over large areas, for example, over areas covering many pixels of an image (Bannari *et al.*, 1995). VIs are quantitative measurements indicating the vigor of vegetation. They show better sensitivity for the detection of biomass than individual spectral bands (Bannari *et al.*, 1995).

Previous studies have shown a significant positive relationship between biomass and VIs (Patel *et al.*, 2007). In order to examine the relationship between AGB and RS variables including individual band reflectance values and VIs, Günlü *et al.* (2014) used Landsat TM in their study and found that VIs present better estimation of AGB in Anatolian pine forests with  $R^2$  equal to 0.606, compared to individual band reflectance with  $R^2$  of 0.465.

AGB models could be developed using many available predictors, grouped into two distinct categories: raw bands of the sensor as reflectance and VIs, including the simple ratio (SR), difference vegetation index (DVI), NDVI, ratio vegetation index (RVI), global environmental monitoring index (GEMI), soil adjusted vegetation index (SAVI), enhanced vegetation index (EVI), tasseled cap index of greenness (TCG), tasseled cap index of brightness (TCB), tasseled cap index of wetness (TCW), and many others.

All above indices can measure the presence and density of green vegetation, overall reflectance (e.g., differentiating light from dark soils), soil moisture content, and vegetation density and structure). Most VIs rely on red and infrared (IR) bands, which are the raw bands present in earth observation satellites and often contain more than 90% of the information related to vegetation (Baret *et al.*, 1989; Huete, 1988; Jiang *et al.*, 2008; Pinty & Verstraete, 1992; Turner *et al.*, 1999).

Early studies have shown that both the simple ratio (Near Infrared /Red) and the NDVI were closely related to dry matter accumulation (Baret *et al.*, 1989). The use of vegetation and other indices (e.g., NDVI, EVI, SAVI) are considered as part of the classification method.

The principle of applying NDVI, for example in vegetation mapping, is that vegetation is highly reflective in the near infrared (NIR) and highly absorptive in the visible red. The contrast between these channels can be used as an indicator of the vegetation greenness (Xie *et al.*, 2008, p. 200). Sonnenschein *et al.* (2011) used NDVI, SAVI and TCG from Landsat images for forests mapping in Greece.

In a study conducted in Saudi Arabia, Aly *et al.*, 2016b found that NDVI images of Landsat could be classified into three classes of vegetation cover in arid regions, namely dense vegetation cover (NDVI > 0.5), moderate vegetation cover (NDVI 0.25–0.5), and sparse vegetation cover (NDVI < 0.25).

The ability of VIs to separate the vegetation from its background varies from one ecoregion to another, and from one plant species to another. VIs commonly used to estimate biophysical variables such LAI, APAR and biomass include NDVI, EVI, and SAVI (Kumar *et al.*, 2015, p. 20). NDVI is a prominent and frequently used index with different spatial resolutions of the optical sensors (Figure 6).

Thenkabail *et al.* (2004) implemented a regression model using NDVI and optical bands reflectance number 3 and 4 of IKONOS for estimation of AGB for oil palm in Africa, with 64–72% accuracy. Morel *et al.*

(2012) found that the Normalized Difference Fraction Index (NDFI) of Landsat ETM+ data performs better when estimating AGB for oil palm in Malaysia with kappa coefficient equal to 0.87. Srestasathien and Rakwatin (2014) found that the best performing VI to separate oil palms from its background was the Normalized Difference Greenness Index (NDGI), which is a normalized ratio of green to the red band, and displays the highest discriminating power using a histogram dissimilarity metrics.

Nevertheless, these results could not be generalized as all VIs must be tested. Zhao *et al.* (2016) examined specific spectral bands of Landsat and their relationships with AGB in the Zhejiang province of Eastern China. They found that, when the forest stand structure is complex, VIs including shortwave infrared spectral bands (SWIR) had a higher correlation with AGB than others. However, the VIs including NIR wavelength improved correlations with AGB in relatively simple forest stand structures. VIs can maximize the sensitivity for recording the green vegetation situation (Günlü *et al.*, 2014).

The choice of adequately performing VIs depends on the type of ecosystem, the environmental conditions and the spectral information available. In their study on forests in Bogotá, Colombia, Clerici *et al.* (2016a) estimated AGB and found that the best performing AGB estimation model was based on the RVI, with  $R^2$  equal to 0.582. They also found that atmospheric and topographic correction was vital in improving model fit, especially in high aerosol and rugged terrain.

However, some studies had shown poor relationship between biomass and VIs compared with using raw bands (Onesimo, Mutanga & Skidmore, 2004). Singh *et al.* (2014) used two optical sensors (Landsat TM and SPOT 5) to assess their efficacy and evaluate disparities in forest composition and AGB in Sabah, Malaysia. They found that NDVI derived from SPOT 5 could distinguish between pristine forests and oil palm trees. In fact, the reflectance values of bands 3 (red sensitive) and 4 (NIR sen-



sitive) of Landsat TM were strongly correlated with the field-based AGB values while both VIs derived from Landsat TM and SPOT 5 (such as NDVI) were weakly correlated with the field-based AGB values. The data saturation problem in Landsat imagery is well recognized and is regarded as an important factor resulting in inaccurate forest AGB estimation, especially when AGB is high (>130 Mg.ha<sup>-1</sup>) and when the forest structure is heterogeneous (Zhao *et al.*, 2016). In a study to estimate total living biomass of Miombo woodlands of Tanzania, Gizachew *et al.* (2016) found no clear evidence of data spectral saturation at higher biomass value in open canopy woodlands. They suggested that Landsat-8 OLI derived NDVI could be used as suitable auxiliary information for carbon monitoring in the context of the reducing emissions from deforestation and forest degradation program (REDD+).

### 1.3.3.6. Remote Sensing/GIS Integrated Models

GIS is a platform hosting spatial databases capable of assembling and integrating geographically referenced data, running spatial analysis, and integrating various types and formats of spatial data (Ardö & Olsson, 2003; Deng *et al.*, 2011; Kamusoko & Aniya, 2009). A repository of various data sources (e.g., forest inventory, land use maps, elevation and RS data) can be used to measure vegetation parameters over large areas (Labrecque *et al.*, 2006). GIS is usually employed to process model inputs and to visualize results (Deng *et al.*, 2011). However, building GIS-based models to predict future scenarios for forest management and the implementation of afforestation plans is another, more valuable product. In RS-GIS integrated models, RS data are used as input to the GIS model; where GIS act as a platform for data layering and database build-

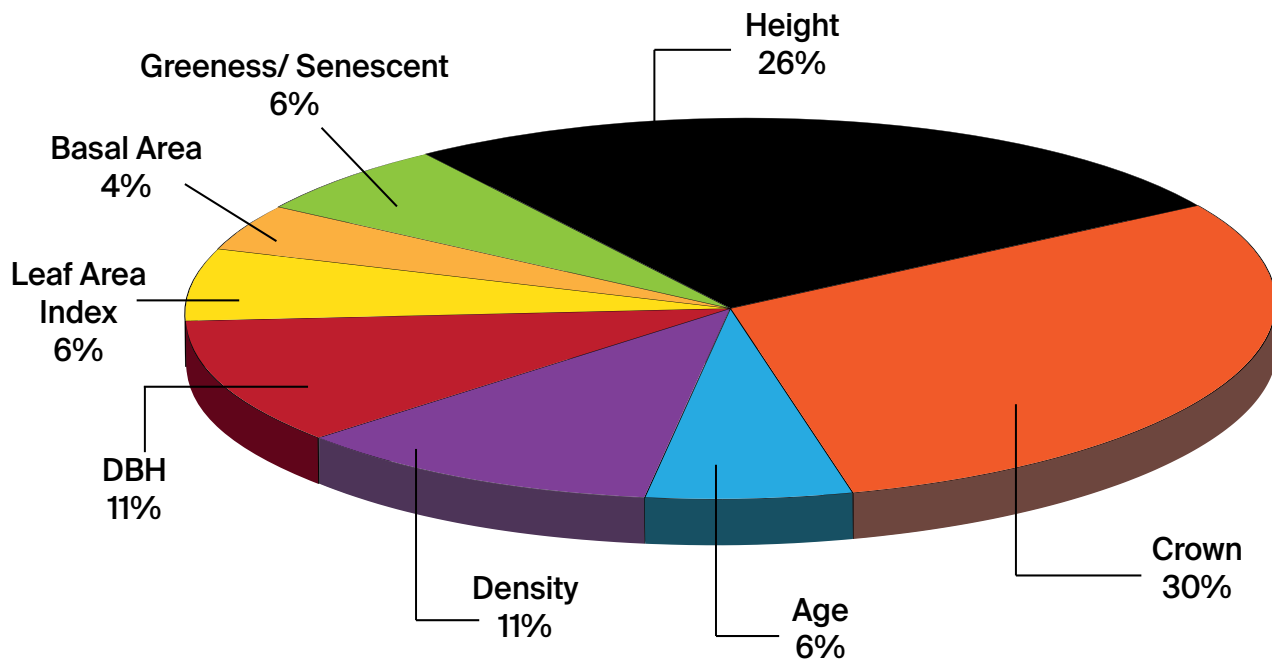


Figure 5: Different biophysical parameters used in RS based estimation of AGB. (Dahy *et al.*, 2020; Salem Issa *et al.*, 2020a).



© Freepik

الكريونية

للنخيل

A case study from the Emirate of Abu Dhabi, UAE.



ing in order to perform spatial data analysis and map creation. This not only saves time, but also allows for faster and better communication between research centers across the globe (Deng *et al.*, 2011). The use of geospatial modeling to study the current state of carbon sequestration and its future dynamics is a promising technique; it has the potential ability to tackle the ecological assessment problems (Rattan Lal, 2002). Furthermore, as mentioned above, the integration of RS data into GIS models enables adding ancillary and field data (soil, climate, topography, etc.), in the analysis and increasing reliability in estimating AGB. For example, there are different GIS-based AGB estimation models that integrate other data models such as: digital terrain model (DTM), rainfall models, canopy height models, atmospheric scattering models, biomass production models, grazing models, 3D forest structure models and regression models (Aranha *et al.*, 2008; G. Baumann, 2009; Cho *et al.*, 2012; Deng *et al.*, 2011; Gernhardt *et al.*, 2010; Greenberg *et al.*, 2005; Holm *et al.*, 2003; Le Maire *et al.*, 2008; Li *et al.*, 2008; Maynard *et al.*, 2007; Montaghi *et al.*, 2013; Ibrahim Ozdemir & Karnieli, 2011; Ramachandran *et al.*, 2007; Thakur & Swamy, 2012; Wang *et al.*, 2010). An integrated classification approach, coupled with GIS analysis, has been employed successfully to improve LULC, forest, and biomass mapping for Landsat data (Kamusoko & Aniya, 2009; Labrecque *et al.*, 2006; Ohmann & Gregory, 2002). Results show that an integration of RS and spatial analysis functions in GIS can increase the overall classification accuracy from 50.12% to 74.38% (Myint *et al.*, 2011a). Furthermore, the integration with GIS-based models are becoming more common, used in around 14% of the reviewed studies.

### 1.3.4. Arid Regions Case Studies

Mapping vegetation for accurate measuring of biomass and assessing CS is a significant challenge, specifically for arid lands, where RS has unique challenges that are not typically encountered in other sub-humid or humid regions. Major challenges include low vegetation signal-to-noise ratios, high soil background reflectance, presence of biological soil crusts, high spatial heterogeneity from plot to regional scales,

and irregular growing seasons due to unpredictable seasonal rainfall and frequent periods of drought (Bestelmeyer *et al.*, 2015; Cheng *et al.*, 2017; Haughton *et al.*, 2018; Wu & Archer, 2005). Additionally, there is a relative discontinuity in the long-term measurements in arid lands, which hampers reliable calibration and evaluation of RS data products. Consequently, RS techniques developed in other ecosystems often result in inaccurate estimates of arid lands ecosystem CS.

Arid lands, defined as regions where annual potential evapotranspiration substantially exceeds precipitation, are critically important to society, yet exceptionally vulnerable to climate change (Smith *et al.*, 2019). Arid lands make up to 40% of the Earth's land surface and provide ecosystem services to more than two billion people, including supporting significant crop production and forage for wildlife and domestic livestock (Bestelmeyer *et al.*, 2015). RS images can reduce the complexity of fieldwork by collecting quantitative and qualitative information at regular intervals and enabling the mapping of inaccessible places, as is the case in most arid regions (Abburu & Golla, 2015; Al-Ahmadi & Hames, 2009; Diouf & Lambin, 2001; Holm *et al.*, 2003; Mangiarotti *et al.*, 2008; McGwire *et al.*, 2000; Olsen *et al.*, 2015; Ibrahim Ozdemir & Karnieli, 2011; Qi, Huete, *et al.*, 1994; Ren *et al.*, 2011; Ritchie & Rango, 1996; Schucknecht *et al.*, 2015; T. Svoray *et al.*, 2001; Tal Svoray & Shoshany, 2003; Tucker *et al.*, 1985; Wylie *et al.*, 1995).

In their review, Eisfelder *et al.* (2012) stated that RS studies of vegetation in arid regions are scarce, and an additional methodological research is needed to address the specific challenges faced by RS techniques in these environments. In this study, out of the 171 reviewed research articles conducted from 1984 to 2020 to estimate AGB, only 15 studies were conducted in arid lands and another 24 studies in semi-arid ecosystems (more than a third of these studies were conducted in Niger and Senegal). Figure 7 shows the proportions of RS-based AGB estimation studies in arid and semi-arid regions taking into account the proportion of reviewed studies, sensors used and their spatial resolutions, the use of GIS tools and locations of the studies.

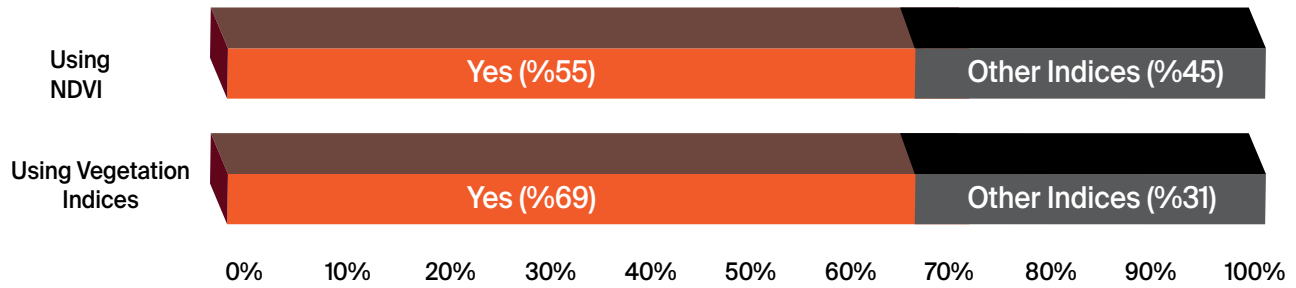


**Figure 6:** The use of vegetation indices and NDVI for estimating AGB. (Dahy *et al.*, 2020; Salem Issa *et al.*, 2020a).

As mentioned above, monitoring the spatiotemporal dynamics of arid lands ecosystem structure and function is therefore a high research priority. Although the methods detailing vegetation cover mapping and estimation integrating RS and GIS are well developed, research on RS-based biomass estimation for arid lands is relatively scarce compared to other ecosystems (tropical, subtropical, temperate and boreal forests) (Eisfelder *et al.*, 2012).

Very few biomass measurements are available for plant species in desert ecosystems. Although biomass per unit area is normally low in those regions, the vast extent of the Earth's arid lands gives it a significant role as a carbon pool and for the supply of essential ecosystem services (Zandler *et al.*, 2015). Studies showed a strong link between desertification and emission of CO<sub>2</sub> from soil and vegetation to the atmosphere (Lal, 2001).

Desertification, and degradation of soils and vegetation in arid lands resulting from climatic and anthropogenic factors, affects more than one billion hectares of soils and more than 2.5 billion hectares of rangelands globally. Furthermore, an alarming estimate of six billion hectares of land is affected by desertification per year (Lal, 2001).

Lal (2001) concluded that the total world historic loss of carbon due to desertification in the period between 1850 and 1998 was in the order of 19–29 petagram (Pg), an amount that could have been sequestered (1 Pg = 10<sup>15</sup> gram). Information on biomass helps to quantify the resilience of arid land systems and is

thus essential for sustainable land-use management (G. Baumann, 2009). Hence, suitable methods to map biomass in arid land regions still need to be developed (Mangiarotti *et al.*, 2008).

If plant species are very scattered, which is the case for most arid land's ecosystems, where vegetation is characterized by its patchiness pattern, the background reflection is mostly related to the soil. Hence, the selection of sites must be characterized by their relatively high density of plant species under study in order to reduce the background effects as much as possible. In addition, the selected sites must be relatively large in area and be homogenous, to enable the extraction of real spectral signature that represent the species to be mapped or to use a minimum number of field plots within each pixel as well as to increase the spatial/spectral resolution of the sensors used (Eisfelder *et al.*, 2012).

Moreover, using satellite images to map and correlate biomass is only possible if the target vegetation spectra are strong enough to be identified within the pixel (Aly *et al.*, 2016b; Oldeland *et al.*, 2010; Tian *et al.*, 2016). This presents a major challenge in the desert where vegetation is usually sparse, offering a small spectral target that requires higher resolutions to be detected (Bradley *et al.*, 2019). In the desert environment in China, Ren *et al.* (2011) estimated crop biomass of individual components (e.g., leaves, stems) for the whole season using red edge reflectance of hyperspectral data.

الكربونية



Optical RS probably provides the best alternative to biomass estimation using RS due to its historic global coverage, repetitiveness and cost-effectiveness and thus is useful and operational in dry lands. Such regions can be found in most of the low-income developing or least developed countries. Zandler *et al.* (2015) used Landsat 8 OLI in the arid regions of Tajikistan to model total biomass in extremely low vegetation cover. The coverage of the SWIR spectral region showed the importance in detecting shrubs or nonphotosynthetic vegetation. To deal with soil brightness, the study used additional soil adjusted VIs variations such as SAVI, transformed soil-adjusted vegetation index (TSAVI), and modified soil-adjusted vegetation index (MSAVI) as VIs suffer from various soil effects, especially when vegetation cover is low.

The above study indicated that biomass quantification in this arid setting is feasible but is subject to large uncertainties. One of the main challenges is the extreme aridity and the associated strong influence of soil background. Another challenge is the fact that large parts of arid or desert plants consist of nonphotosynthetic, woody matter and hence the photosynthetic signal, captured by most spectral bands and indices, may be low in relation to the biomass amount.

### 1.3.5. Learning Lessons from the Literature Review

**Geospatial technologies** are practical, feasible and can provide an adequate mean for AGB assessment monitoring, modeling and management of carbon sequestration. This conclusion is the main outcome of this literature review and is consistent with the consensus of numerous scientific papers on the subject published in the last five decades. The use of these technologies is an efficient tool, especially for developing countries, for measuring, mapping, monitoring, modeling and management of their CS in biomass and soil; leading to improve soil and plant productivity, to increase food security, and to control land degradation. In their turn, these countries can

play a significant role in reducing the negative impact of climate change, by mitigating carbon emissions. Of course, there are many methods that can be used for estimating CS, and all of them have their advantages and disadvantages. Traditional methods, relying on heavy fieldwork measurements, are the most accurate, however, they require significant time, expense and labor, and can be damaging for the ecosystems.

**Building allometric equations** can help avoid the destructive nature and other disadvantages of the fieldwork method. However, most of the allometric equations are mixed species-equations and not tailored for single one specie; most of them are also built for specific sites and ecosystems (less applicable for arid regions). Also, it is now more and more recommended to build allometric biomass equations that are correlated with and rely more on geospatial techniques to estimate biomass and CS (crown and height attributes). Building a database including the rates of carbon sequestered and stored for each plant species, especially those with high economic values, will fill the gap and increase the understanding of the atmospheric carbon sequestration potential of plant species and ecosystems.

**The use of geospatial technologies** should always be accompanied by ground measurements for verification and model validation of results which are required at some stages in the estimation of biomass. The best fit methodology relies on both fieldwork and the analysis of RS data and GIS techniques. The suggested process involves three steps, including: pre-field preparations to identify sample areas of interest, fieldwork that includes sample collection and measurement of plant characteristics, and post-field activity that focuses on processing RS data, classification, GIS model development and validation. Assessing CS remotely and consistently over large areas varies greatly depending on the type of instruments used, and the platforms. Nevertheless, these difficulties can be solved and tackled using different sensor options and other innovative methods, and hence avoiding the limitations that relate to these aspects such as scale, cost, and associated errors and uncertainties.



Figure 7: Studies on estimating AGB using RS in arid/semi-arid ecosystems. (Salem Issa et al., 2020a).

**High resolution RS data** are the most accurate. However, moderate resolution satellite data, such as Landsat, have shown to be effective in estimating AGB and, consequently, CS, with good accuracy. Furthermore, these sensors provide invaluable historical data to monitor the change of CS over time. Developing algorithms that combine more than one remote sensor is highly important for tackling the challenges associated with estimating AGB and subsequently assessing carbon sequestration. Merging and fusion of more than one set of data have the potential to reduce uncertainty errors in biomass estimation. In such studies, it is important to consider the effects of bioclimatic factors depending on parameters such as plant age, species, forest type, rainfall, topography, vegetation structural variations, heterogeneity of landscapes, and seasonality. One of the common challenges in achieving this, is mapping the spatial patterns of vegetation and soil carbon and producing geo-referenced estimates of carbon. Such maps provide a better understanding of carbon dynamics and help quantify the regional and global carbon budgets. In addition, this will provide decision-makers with a strong knowledge base to be able to identify and focus on the most essential issues.

**The arid lands RS-GIS research** should be given a high research priority, especially given that more than 2 billion people depend on services provided by arid lands ecosystems. A combination of the field-based measurements and geo-spatial approaches reviewed have the potential to help improve carbon estimation to reduce emissions resulting from deforestation and forest degradation, and to design incentive programs in arid land regions. Therefore, it can be applied to enhance the decision-making process on sustainable monitoring and management of carbon sequestration like afforestation, reforestation, and forest conservation projects.

الكربونية



## 1.4

# Structure of the Book

- **Chapter 2** illustrates the results of developing date palm biomass allometric equations and calculating the carbon stock both, in date palms and their soils.

Subsections 2.3., 2.4., and 2.5. focus on calculating the biomass of date palm at different biomass components,

while Subsection 2.6. focuses on estimating the carbon stock in date palm at different age-stages.

- **Chapter 3** presents mapping & counting of date palm trees in Abu Dhabi Emirate using satellite imageries.

Subsections 3.2. and 3.3. focus on the mapping of LULC and vegetated areas of Abu Dhabi using the moderate resolution of Landsat-8 OLI images

Subsections 3.4. focus on mapping of the young, medium, and mature date palms in Abu Dhabi using sub-meter world view-2 images.

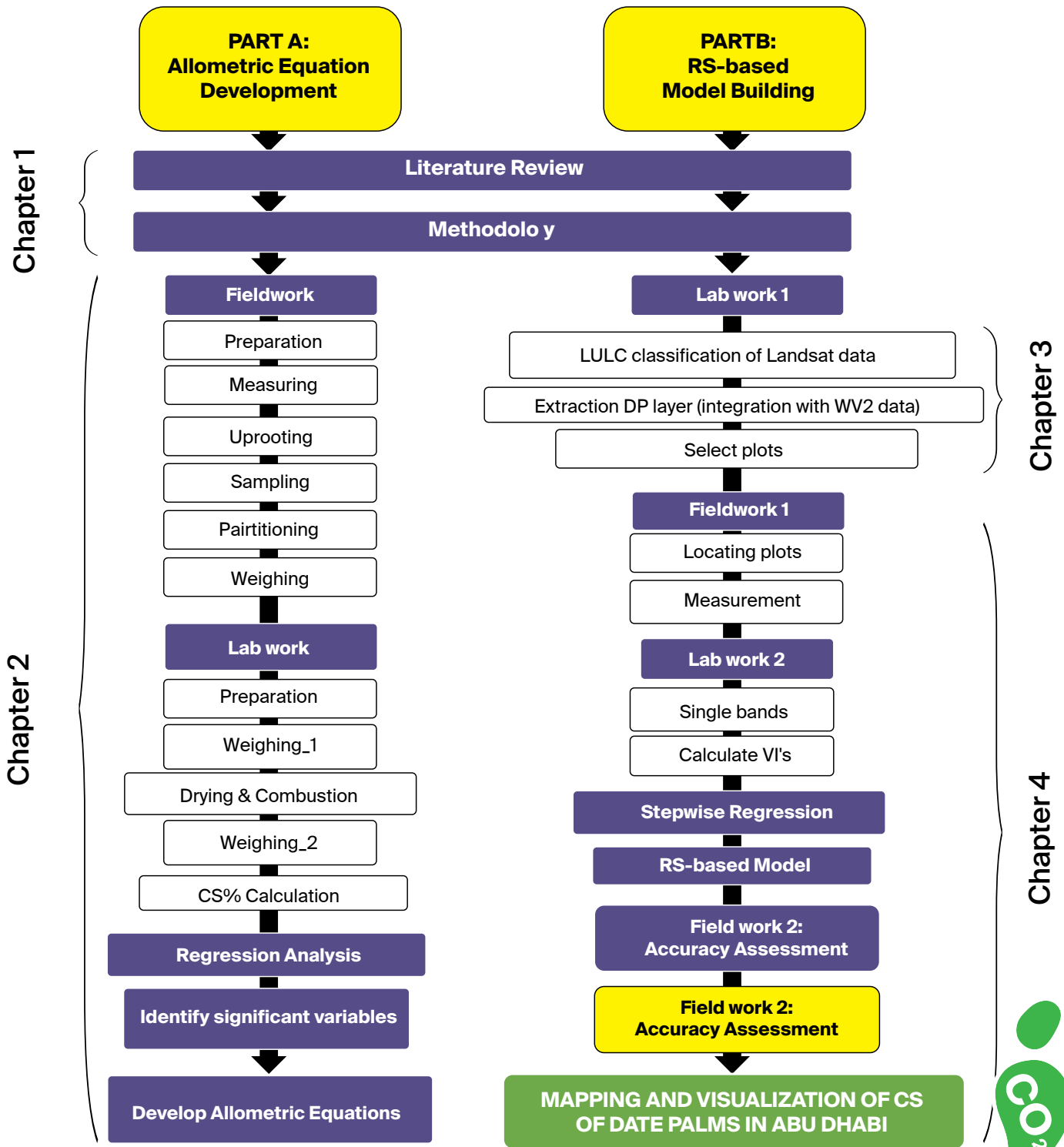
Subsections 3.5. focus on assessing the accuracy of the produced maps and counting the date palms of Abu Dhabi at different age stages using a remote sensing approach.

- **Chapter 4** displays the results of conducting a regression analysis between remote sensing variables (single bands and vegetation indices) with 54 field plots covering different age stages of date palms in the emirate of Abu Dhabi.

Subsection 4.4.1. and 4.4.2. presents the final RS-based models and their validation to estimate biomass and carbons stock in mature ( $> 10$  years) and non-mature date palms ( $\leq 10$  years). The chapter ends up with an assessment map of the carbon stock by date palms of Abu Dhabi.

- **Chapter 5** discusses some critical issues which have emerged during the course of this study, while
- **Chapter 6** concludes the whole learned lessons and recommendations for this book.

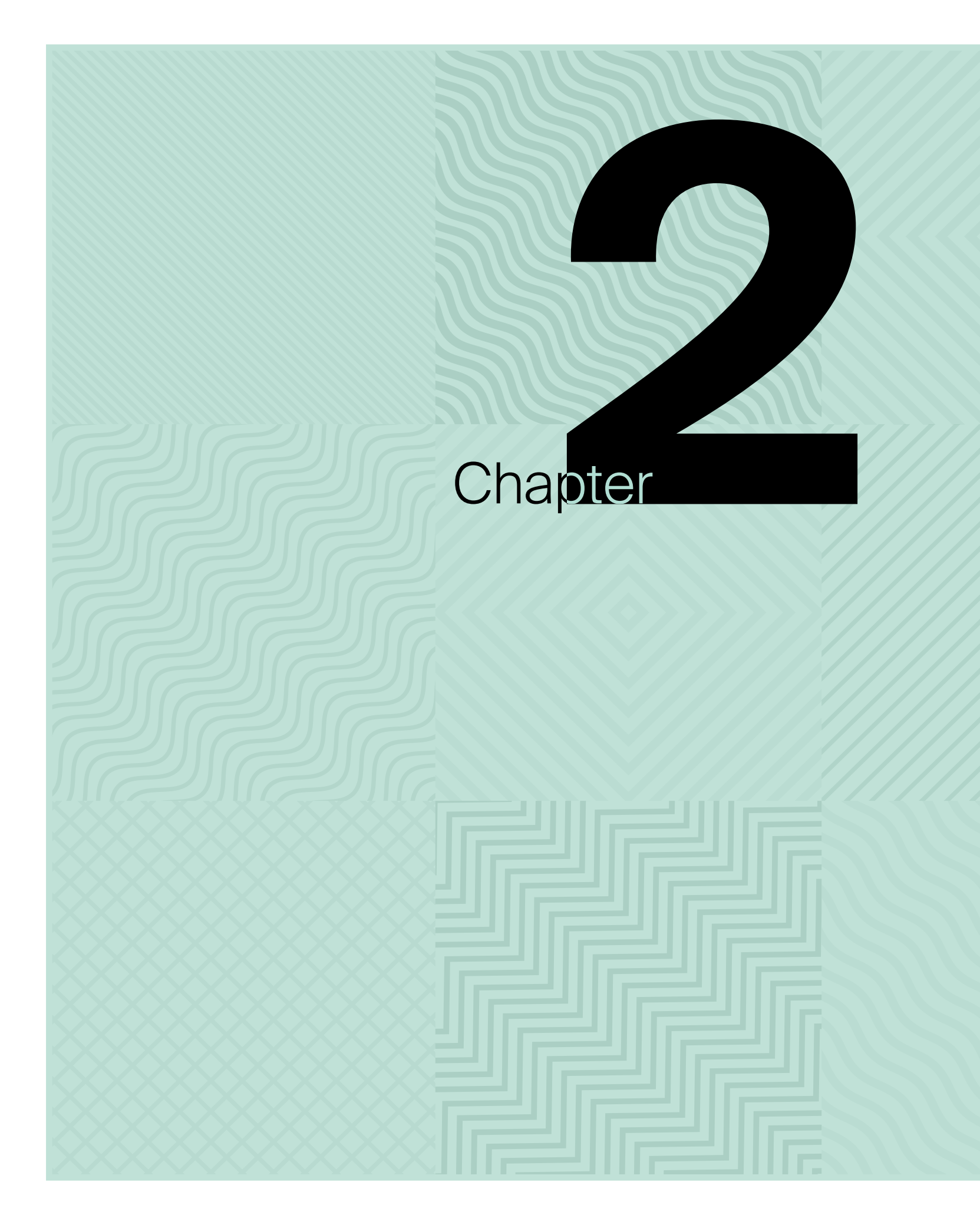
الكربونية



الكربونية

**Infographic 8:** The comprehensive methodology flowchart and their corresponding chapters within this book.



The background is a light green color with a grid of squares. Each square contains a different geometric pattern: some have wavy lines, some have concentric diamonds, and some have zig-zag lines. A large, bold black number '2' is centered on the page, overlapping the patterns.

# 2

Chapter



# **Calculation of Carbon Stock in Date Palm Trees for Biomass and Soil**

© Freepik





## 2.1.

## Overview

**A**fforestation projects can be used to earn carbon credits and reduce the carbon footprint. This type of supportive efforts has a growing interest among policymakers and governments (Baral & Guha, 2004). Therefore, estimation of CS in forests and trees is an important measure towards assessing mitigation effects on global change (Ebuy et al., 2011). Many destructive techniques (felling or harvesting) exist to directly estimate CS (Gibbs et al., 2007). Although these techniques provide the most accurate measure of biomass, they ultimately rely on ground measurements and can cause severe destruction to the forests as well as a risk of environmental deterioration (Khalid & Hamid, 2017; Maulana et al., 2016). In addition, such methods are tedious and time consuming (Ebuy et al., 2011), hence they cannot be used routinely.

Therefore, developing biomass equations (allometry) that rely on non-destructive measurements, is very essential in estimating biomass. Subsequently, allometric equations have been developed and used to estimate tree biomass and CS from dendrometric measures, such as tree diameters and height (Ebuy et al., 2011; Picard et al., 2012). Notwithstanding, the number of trees destructively sampled to build allometric equations is not constant and differs from one study to another. Currently, there is no consensus on that num-

ber, as this is often dependent on resource availability and permission to harvest trees (Yuen et al., 2016). For example, Russell (1983), and Moran and Grace (1996) used 15 and 14 trees, while Brown et al. (1995) and Khalid et al. (1999a) used only 8 and 10 trees, respectively to build their allometric equations.

Different quantitative variables were considered when building oil palm biomass allometric equations (Korom & Mastuura, 2016) (Appendix 1). Henson and Chang (2003) used age as a predictor to estimate the standing biomass of oil palm in tons per hectare. Others used structural variables such as total height and trunk height (Dewi et al., 2009; Khalid et al., 1999a; Thenkabail et al., 2004), while Corley et al. (1971) used DBH, number of fronds, leaf area, rachis and petiole length, rachis and petiole cross-sectional area at intervals, and volume of petiole sections in their pioneer study to estimate the average yield of oil palms.

More recently, allometric equations have been used, coupled with RS and field-based structural variables measurements (Fonton et al., 2017; Salem Issa et al., 2019). Furthermore, Cheng et al. (2014) recommended to develop more equations with different field structural variables that can be linked to RS predictors. Likewise, Jucker et al. (2017) suggested in their review of allometric equations to develop a new generation of allometric equations that estimate biomass based on attributes which can be remotely sensed.

Most biomass equations, whether species-specific or multispecies, have been developed for tropical rainforest ecosystems because of their relevance to the global carbon cycle (Basuki et al., 2009; Brown, 1997; Chave et al., 2005; Cole & Ewel, 2006; Makinde et al., 2017). A few plant species biomass assessment equations are available for desert ecosystems. Nonetheless, none of these were used to fit one of the most important fruit crops in arid regions, *Phoenix dactylifera* L., date palm (DP). More than 90% of the UAE territory is covered by desert ecosystems representing more than two-thirds of the country's land area. DP species are a good alternative for CS in such arid ecosystems. To estimate DP biomass and its carbon content, it is



© Freebik

necessary to quantify the biomass in all palm components. Moreover, it would be more accurate to include both the AGB and BGB in estimating the CS, as both are available for recycling in the ecosystem at replanting (Khalid *et al.*, 1999b).

**Specifically, Chapter 2 aims at:**

1. Identifying the most relevant structural field variables for the estimation of DP biomass;
2. Developing specific allometric biomass equations that can be correlated with RS variables;
3. Estimating CS in date palms; and
4. Assessing the potential of DP species to improve soil CS in such desert ecosystems.

## 2.2.

# *Phoenix dactylifera* L. Date Palm

**D**ate palms (*Phoenix dactylifera* L.) are resilient, productive over long terms, and possess multipurpose economic and environmental advantages (Figure 8). Moreover, date palms have been considered an important crop and part of the farming systems in arid and semi-arid regions, especially in the oases and in the forms of small farm units or as large-scale trees (FAO, 1982). Date palms are considered precious, and have strong religious, traditional and nutritional significance (Shahin & Salem 2014).

الكربونية

In the Arabian gulf states, date palms are heavily planted and maintained, particularly in the UAE, using abundant desalinated water and can thus be considered as a good alternative for carbon sequestration in such arid ecosystems. The UAE's economy has prospered since the discovery of oil, and the country witnessed an unprecedented pace of growth supported by revenues from oil. The government invested heavily in planting and maintaining green areas, including farms many of which are date palm trees. During the past decades, the UAE date production increased, as an outcome of increased demand as the population swelled (AOAD, 2008).



للنخيل

The date palm in Arab countries, in general, has been an integral part of the people's culture and tradition. However, the number of the date palm, production, and consumption vary from one country to another due to varying ecological conditions (El-Juhany, 2010). The world's highest production and consumption of dates is found in the Arabian Peninsula countries, such as UAE (Zohary & Hopf, 1993). According to Food and Agriculture Statistics Database (FAOSTAT, 2013), the total world number of date palms is about 120 million trees, distributed in 30 countries and producing nearly 7.5 million tons of fruit per year. Over two-thirds of this amount is found in the Arab countries; three of the top 10 dates producers worldwide are in the Arabian Peninsula, namely: Saudi Arabia, UAE, and Oman (Kader & Hussein, 2009; AOAD, 2008). It is estimated that

the UAE has the largest number of date palms for any single country in the world with a minimum of 200 cultivars, 68 of which are commercially considered to be the most important (El-Juhany, 2010).

Arid lands in particular, have received less attention in recent decades despite their importance to society and their exceptional vulnerability to climate change. They provide ecosystem services to more than two billion people, including significant crop production and forage for wildlife and domestic livestock (Bestelmeyer *et al.*, 2015). While arid lands are sparsely vegetated with low annual productivity, they have been identified as an important player in the global trends and variability in atmospheric CO<sub>2</sub> concentrations (Ahlström *et al.*, 2015; Biederman *et al.*, 2017; Humphrey

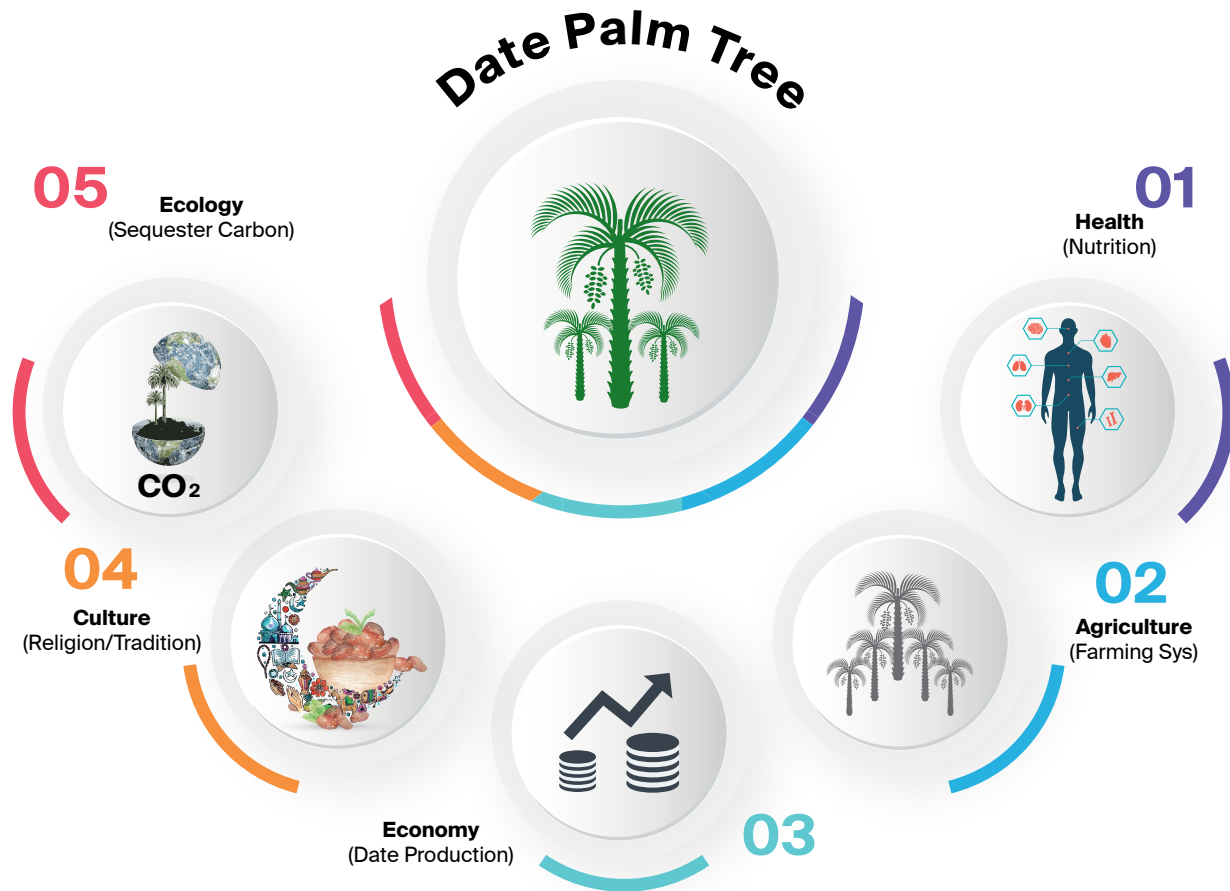


**Figure 8:** Multipurpose advantages of date palms. The present book is focused on the ecological advantages of date palm by assessing and quantifying the carbon stock by date palm trees.

*et al.*, 2018; Poulter *et al.*, 2014). Although biomass per unit area in arid and semiarid regions is normally low, their large extent gives them a significant role as a carbon pool for the supply of essential ecosystem services (Zandler *et al.*, 2015).

Monitoring the spatiotemporal dynamics of arid lands ecosystem structure and function is, therefore, a high research priority. Satellite RS particularly, has been instrumental in exposing the role of arid lands within the context of global carbon cycling and the broader Earth system (Humphrey *et al.*, 2018; Poulter *et al.*, 2014). Yet, none of the plant biomass assessment measurements and its capacity of storing and sequestering carbon, were conducted for the most important fruit crops in arid regions, Phoenix dactylifera, date palm.

In UAE, where more than two-thirds of its land area is covered by desert ecosystems, date palm species is a good alternative for CS in such ecosystems. Date palm requires minimum water supply and tolerate harsh growth conditions such as high temperatures, drought, and high levels of salinity. In fact, it is the most salt tolerant plant of all fruit crops (Alhammedi & Kurup, 2012; El-Juhany, 2010; Zohary and Hopf, 2000). Some palm species are considered keystone and provide multiple ecosystem services, such as CS (van der Hoek *et al.*, 2019).

The amount of carbon that can be sequestered in palms is relatively high compared to some other plant species. In their study of the relationship between land use and CS in northeastern Brazil, Carlos *et al.* (2015) found that land planted with palms provided 40 t. C ha<sup>-1</sup> while lands used for pasture and agriculture provided only 8 t. C ha<sup>-1</sup> and 5 t. C ha<sup>-1</sup>, respectively. In another study in Northeast India, Singh *et al.* (2018) recorded considerably higher amounts of carbon in oil palm trees than in shifting cultivation fallows. They concluded that a 10 years old oil palm plantation could sequester up to 3.7 t. C ha<sup>-1</sup> year<sup>-1</sup>. Hence, palms generate economic benefit and contribute to carbon storage in a more sustainable way especially when planted in areas of low productivity or on degraded lands.



© Shutterstock

الكربونية

## 2.3. Structural Field Variables of Date Palm

**A** number of DP were selected to measure AGB and BGB in order to build specific allometric equations and calculate the CS in both biomass and soil for DP trees in the study area. Age is one of the most important factors that influence the biomass of the palm and its structural measurements (Sunaryathy et al., 2015).

A substantial amount of research has been undertaken and published on the estimation of oil palm biomass at various ages (Husin *et al.*, 1987; Kamarudzaman *et al.*, 1995; Khalid *et al.*, 1999a; Rees & Tinker, 1963). In the current study, a similar approach has been adopted to estimate DP' biomass at three different age stages:

- Age stage One (young) for trees younger than 5 years;
- Age stage Two (medium) for trees between 5 and 10 years; and
- Age stage Three (mature) for trees exceeding 10 years of age.

Accordingly, five DP were selected, prepared and uprooted to represent each age stage. Another influencer factor in DP biomass storing is variety. Indeed, DP in the study area differ in their cultivars (varieties) with different palm growth rates as well. Therefore, field samples were selected to represent the different varieties as well as the three different age stages in the study area including Fardh, Bumaan, Khunaizi, Khlalas, Baghel, Jabri, Shahem, Jash Ramli, and Neghal (see Appendix 4).

A fieldwork campaign was conducted during the fourth week of April 2018 where five DP were uprooted for each age stage (total of 15 palms). Each sampled palm was partitioned into three parts: crown, trunk and roots (Khalid *et al.*, 1999a). The term biomass, in this research, refers to the value of dry weight unless indicated otherwise. Although some researchers prefer to use the fresh weight instead of dry weight for building their equations (Dewi *et al.*, 2009; Khalid *et al.*, 1999a) (Appendix 1). Hence, AGB is calculated as the sum of the crown and trunk weight while BGB is calculated as the weight of the root system. A large commercial scale balance was used to get the fresh weight of crown, trunk and roots in (Kg). From each part of the uprooted palms, three samples were collected (3 crown samples, 3 trunk samples and 3 root samples), (Figure 9).

Structural variables of uprooted DP including total palm height, trunk height, diameter breast height (DBH), crown diameter (CD), crown area (CA) and number of fronds (#FronD), were measured and later used in the regression analysis to build specific biomass allometric equations of date palm (Figure 10). Before uprooting the palm, the following variables were measured:

- i. DBH in cm by measuring the circumferences of the trunk at 1.3 m height and dividing by the number  $\pi$ . For small palms, with no developed trunk, the diameter was measured at the base of the palm,
- ii. Number of palm fronds (#FronD),
- iii. CD in meter, and (iv) CA in square meter was cal-



Figure 9: Uprooting, partitioning, and weighing date palms. (Salem Issa et al., 2018, 2020b).

culated using the sphere equation ( $CA = \pi CD^2/4$ ), assuming a rounded palm crown. After uprooting the palm, the following variables were measured:

- a. Palm height (H) in meter,
- b. Palm trunk height (Ht) in meter, and
- c. Crown depth ( $\Delta$ height), defined as the difference between total and trunk heights in meter.

A total of 120 biomass samples were collected during the fieldwork: (15 Crown + 10 Trunk + 15 Root) x 3 replicates. Only 10 x 3 trunk samples were collected due to the absence of developed trunk in young palms. Four soil samples were collected from underneath each palm canopy, referred to as “In”. A total of 60 soil samples: 15 palms x 4 replicates were collected during the campaign. More soil samples were collected away from the palms’ canopy, referred to as “Out”, from two DP farms: [2 farms x 4 replicates], for

comparison and quantification of the effect of DP contribution to soil carbon sequestration.

Immediately after reaching the UAEU/ Biology department’s Labs, the fresh weights of all samples were measured. Then, samples were air dried and transferred to paper bags to be ready for oven drying at 80°C for 72-96 hours to measure the dry weight (Allen *et al.*, 1974; Corley *et al.*, 1971; Khalid *et al.*, 1999a). Samples were prepared and grinded to calculate the biomass components’ parameters using the formula listed in Table 2.

Samples were weighted to get the percentage of dry weight to original fresh weight in each sample (dry to fresh factor=DF) (Figure 11). Finally, samples were combusted for 4 hours at 550°C (Allen *et al.*, 1974) to calculate organic matter (OM) and organic carbon (OC) as per the formula in Table 3.

**Table 2:** Calculation of different date palms biomass components.

Parameter	Formula
Dry Weight of each palm part	Crown Dry Weight (kg) = Crown Fresh Weight × Crown DF* Trunk Dry Weight (kg) = Trunk Fresh Weight × Trunk DF Root Dry Weight (kg)= Root Fresh Weight × Root DF
Percentage of BGB (Root system) from the AGB**	BGB:AGB ratio = BGB/AGB × 100
AGB weight in each palm	AGB (kg) = Crown Dry Weight + Trunk Dry Weight
Total Biomass of each palm	Total Biomass (kg) = AGB Weight + Root biomass Weight (BGB)

**\*DF is dry to fresh factor**

**\*\* The ratio of each biomass component (crown, trunk, and roots) to the total biomass were calculated as well.**

**\*\* The ratio of each biomass component (crown, trunk, and roots) to the total biomass were calculated as well.**

Soil samples were first air dried and prepared for further processing (Allen *et al.*, 1974). They were then placed in crucibles and oven-dried at 105°C for 72 hours.

The different soil samples’ parameters were calculated using formulae listed in Table 4 following the approach described in (Ksiksi, 2012; Lemenih & Itanna, 2004).

**Table 3:** Calculation of OM and OC of the collected samples.

Item	Formula
The percentage of OM to dry weight in each sample	%OMD* = (1- Combustion Weight 550 /Dry Weight 80) × 100
The OM Weight for palm parts in each palm	Crown OM Weight (kg) = Crown Dry Weight × % Crown OMD Trunk OM Weight (kg)= Trunk Dry Weight × % Trunk OMD Root OM Weight (kg) = Root Dry Weight × % Root OMD
The OC weight palm parts in each palm**	Crown OC Weight (kg) = Crown OM Weight × 0.58 Trunk OC Weight (kg) = Trunk OM Weight × 0.58 Root OC Weight (kg) = Root OM Weight × 0.58
The OC in AGB for each palm	OC in AGB (kg) = Crown OC Weight + Trunk OC Weight
Total OC in each palm	Total OC (kg) = OC in AGB + OC in Root biomass

\* OMD is OM to dry factor

\*\* OC is equal OM multiply by 0.58

**Table 4:** Formulae used to calculate the different soil parameters.

Item	Formula
% Moisture content	= (Initial Weight–Dry Weight 105)/Initial Weight × 100
Bulk density (g/cm <sup>3</sup> )	= dried-oven Weight (g)/ Total volume of the sample
% SOM*	= (Dry Weight 105 – Loss of Combustion)/ Dry Weight 105 × 100
% OC**	= OM × 0.58
Soil carbon (g/cm <sup>2</sup> )***	= Z × BD × C × 10
Soil carbon in Kg/palm	= (Soil C. (g/m <sup>2</sup> ) × CA) / 1000

\* Combustion was performed for 4 hours at 550 to estimate % SOM

\*\*% OC is estimated as 0.58 of the calculated OM

\*\*\* Where Z = thickness of each sample depth (10 cm), BD = bulk density (1.7 g/m<sup>3</sup>) of each sample depth and C is the carbon concentration (g.C/Kg soil) of each sample depth. Results are reported in tons per hectare.

The total CS in and contributed by the DP is calculated as the sum of CS in the DP biomass itself plus the CS in the soil underneath the palm as explained and formulated as per equation 1 below:

$$\text{Total CS} = \text{Biomass C} + \text{Soil C} \quad \text{Equation (1)}$$

The correlation coefficients between fresh and dry weight for the palm's crown trunk and root

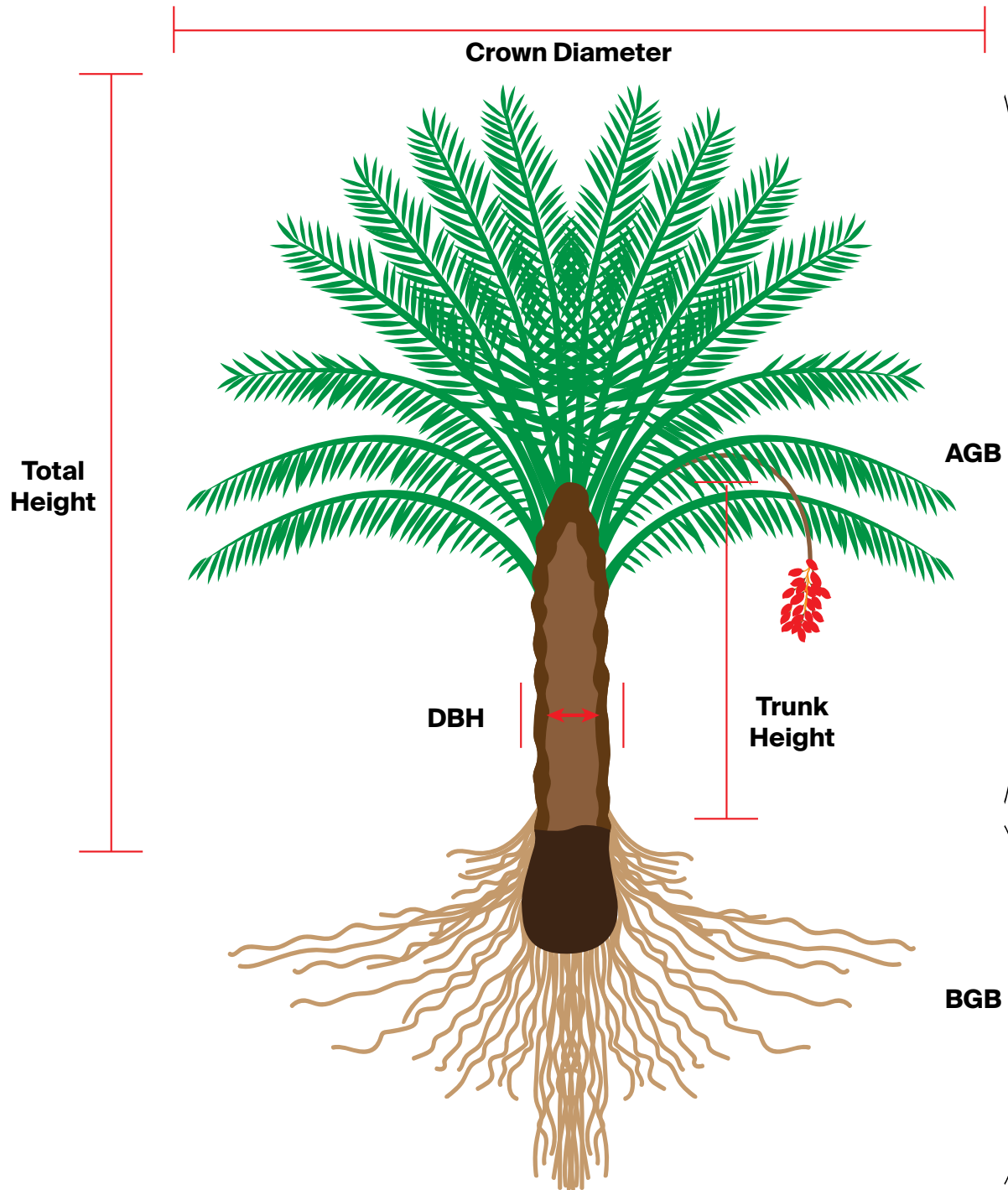
components were estimated at 0.99, 0.97 and 0.97, respectively; while the correlation between the total fresh weight and the total dry weight gave a value of 0.99. Furthermore, the dry to fresh ratio or factor (DF), for the BGB was estimated at 0.45, while that of the AGB was calculated at 0.40 (Table 5).





© Freepik





الكريونية

**Figure 10:** Structural field variables of date palm. ( AGB: Aboveground Biomass, BGB: Belowground Biomass, and DBH: Diameter at Breast Height )



**Table 5:** Average of dry to fresh weight factor for each DP component.

All Ages	Crown DF	Trunk DF	Root DF	Total DF	AGB DF
(Mean ± SE)	(0.41 ± 0.01)	(0.37 ± 0.02)	(0.45 ± 0.02)	(0.42 ± 0.01)	(0.4 ± 0.02)

\*DF is dry to fresh factor calculated as a ratio between dry to fresh weights.

\*\*AGB includes crown plus trunk only.

\*\*\* SE is the standard error.

As for the non-structural variables, age proved to be an important factor influencing the storing of DP biomass (P < 0.05). The significant correlation

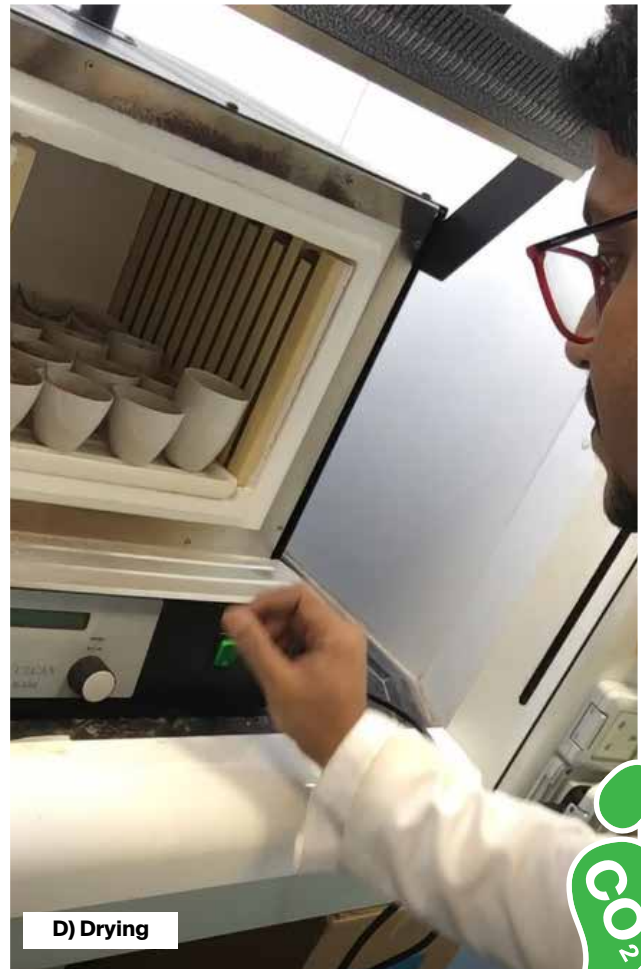
between age of DP and its total biomass/ AGB remains positively strong for either fresh or dry weights (Table 6).

**Table 6:** Field variables of DP used to assess allometric equations.

Field Variables	Young (< 5 year) (Mean ± SE)	Medium (5-10 year) (Mean ± SE)	Mature (> 10 year) (Mean ± SE)
DBH (cm)	33.87 ± 2.28	43.29 ± 7.45	51.57 ± 5.1
H (m)	4 ± 0.167	4.85 ± 0.206	8.38 ± 0.48
Ht (m)	-	0.764 ± 0.196	3.21 ± 0.52
Δ height (m)	4 ± 0.17	4.086 ± 0.22	5.17 ± 0.36
CD (m)	3.09 ± 0.46	5.66 ± 0.25	7.2 ± 0.08
CA (°)	8.15 ± 2.57	25.36 ± 2.28	40.73 ± 0.86
# Fronds	29.8 ± 2.27	35 ± 5.17	61.6 ± 2.32
<b>Weight of fresh component (Kg.palm<sup>-1</sup>)</b>			
Crown	50.65 ± 5.43	171.08 ± 34.47	367.24 ± 78.56
Trunk	-	74.18 ± 13.61	365.28 ± 30.65
Root	21.43 ± 6.39	187.36 ± 27.91	282.06 ± 25.25
Total weight	72.08 ± 11.19	432.62 ± 66.41	1014.58 ± 95.92
AG weight*	50.65 ± 5.43	245.26 ± 42.99	732.52 ± 91.38
<b>Weight of dry component (Kg.palm<sup>-1</sup>)</b>			
Crown	22.51 ± 3.06	65.17 ± 11.87	148.5 ± 35.85
Trunk	-	29.53 ± 8.62	135.91 ± 19.62
Root	7.46 ± 1.88	87.61 ± 14.87	141.23 ± 13.59
Total	29.97 ± 4.17	182.3 ± 32.07	425.63 ± 45.6
AG weight*	22.51 ± 3.06	94.69 ± 18.45	284.41 ± 43.15

\*Aboveground weight equals crown weight plus trunk weight of the palm.

\*\*SE is the standard error.



الكربونية

Figure 11: Lab works, preparing samples, grinding, weighing, and drying.



## 2.4. Ratios of Date Palm Biomass Components (Crown, Trunk, and Root)



الكربونية

**G**iven that the correlation between fresh and dry weights of DP (0.99 for both aboveground and total weights) was found to be very strong; dry weight was used in all subsequent calculations as well as for building the biomass allometric equations of DP. For young DP, with non-developed trunk, CB ranged between 17.2 Kg and 34.1Kg with a mean value of 22.5 Kg, contributing 75.1% of the total palm biomass. While the BGB contributed about 24.9% of that total biomass (Table 6).

It is worth noting that in the case of young DP, the AGB consists of only the CB. The contribution of the crown and root to the total biomass increased with age hence, with trunk growth of the palm. The ratio of CB to total biomass decreased to 35.75% and 34.89% of the total biomass for medium and mature DP, respectively. While the root system's contribution to the total biomass increased to 35.38% as the palms grew older (Table 7).

The trunk contained 16.20% of the total biomass in medium DP palms and 31.93% of the total biomass in mature DP. The mean % of TB in all palm age stages (with no trunk in young palm) approaches 15.98% of the total biomass (Table 7).

**Table 7:** DP component's biomass calculated as a ratio of total or AGB.

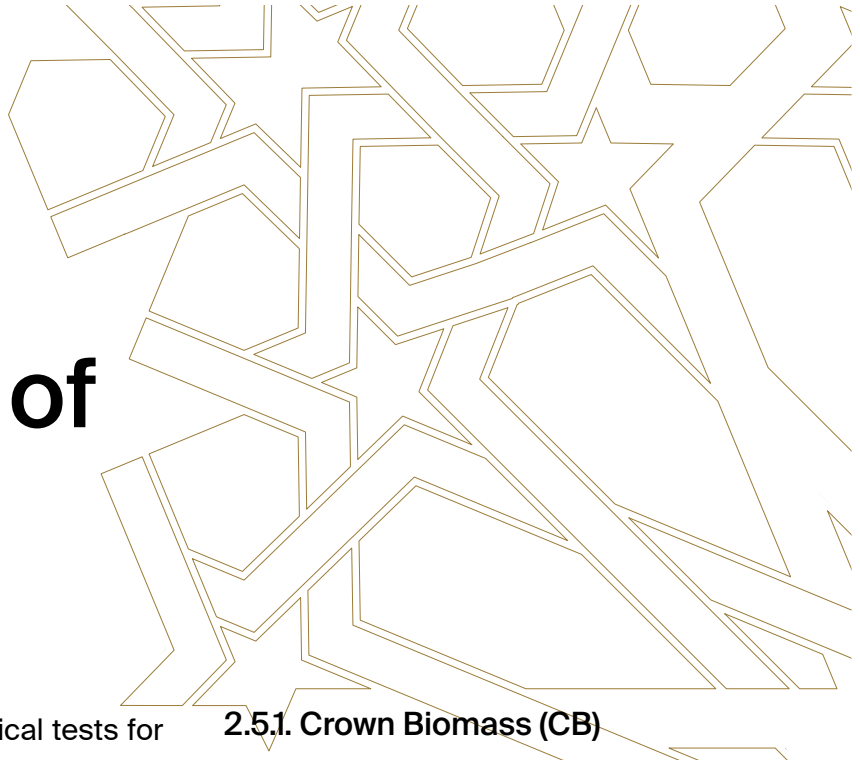
Component	To	Young DP%	Medium DP%	Mature DP%	Mean%
CB	Total	75.11	35.75	34.89	48.59
TB		-	16.2	31.93	15.98
BGB		24.89	48.06	33.18	35.38
AGB		75.11	51.94	66.82	64.31
CB	AGB	100	68.82	52.21	73.68
TB		-	31.18	47.79	26.32
BGB		33.15	92.52	49.66	58.44

Where CB is crown biomass, TB is trunk biomass, BGB is below ground biomass, AGB is above ground biomass, and Total is total biomass.

The AGB alone contained most of the DP biomass with an average of 75.11%, 51.94% and 66.82% for young, medium and mature DP, respectively. The crown was found to retain most of the AGB at all ages. It was noted that each component of the DP followed a different rate of biomass storing at each age stage. The BGB to AGB ratios changed considerably during growth stages of the DP with values of 33.15%, 92.52% and 49.66% for young, medium and mature DP, respectively. The average mean percentage of BGB to AGB was 58.44% when averaged over all age stages. It increased to 71.1% when including DP with developed trunks from the medium and mature stages only (Table 7).



## 2.5. Biomass Allometric Equations of Date Palm



الكربونية

All statistical and graphical tests for the models were performed using SPSS and Excel software packages. First, correlation coefficients between biomass in each DP part (crown, trunk and root) and all collected field variables were calculated. Linear, logarithmic, exponential, power and polynomial expressions, were fitted in the regression analyses to identify the highest coefficient of determination ( $R^2$ ). Single-variable models are most frequently used in estimating the biomass as they are easy to apply compared to those with multiple variables (Cheng et al., 2014). In the current case, the linear and non-linear regression analyses were run to develop single-variable models to predict the biomass. Individual single field measurements were considered as the independent variables (i.e., H, Ht, CD, CA, etc.), while the predicted biomass (AGB) was the dependent variable. Then, the associated  $R^2$  values for each model were calculated at  $P < 0.05$ .

### 2.5.1. Crown Biomass (CB)

All field variables showed significant correlation with CB except DBH and  $\Delta$ Height (Table 8). The four field variables that gave the highest correlation with CB were: Age, CA, CD and H. After applying different types of relationships (linear, polynomial, power, logarithmic, and exponential equations), it was found that the power equation (2) with 'Age' as independent variable had the highest  $R^2$  (equal to 0.857) (see Table 8).

$$CB = 6.4575 \times Age^{1.019} \quad \text{Equation (2)}$$

However, age is a non-structural variable and cannot be measured directly in the field. It has to be obtained from farmers or from the farm's records. Furthermore, it was intended to identify potential field structural variables to develop specific DP allometric equations that would be used in a RS based CS assessment model of DP in the region. Therefore, the use of other well-correlated structural variables such as CA to estimate CB was very appropriate. Equation (3) applying an exponential expression with CA as independent variable and depicted graphically in Figure 12, was found to have the best  $R^2$  (equal to 0.8354) (see Table 8).

$$CB = 14.034 \times e^{0.0554 \times CA} \quad (CA \neq 0) \quad \text{Equation (3)}$$

**Table 8:** Best prediction equations for crown biomass estimation of DP.

Regression Equations	Variable	R <sup>2</sup>	P value
CB= 6.4575 × Age <sup>1.1019</sup>	Age	0.857***	0.00002
CB= 0.2506 × DBH <sup>1.4548</sup>	DBH	0.3054*	0.229
CB= 1.0874 × H <sup>2.3225</sup>	Height	0.8114***	0.00002
CB= 2.4525 Ht <sup>2</sup> + 29.201 Ht + 30.12	Ht	0.7602**	0.00003
CB= 0.3013 × Δ Height <sup>3.5402</sup>	Δ Height	0.4466*	0.02
CB= 5.8364 × e <sup>0.4231 × CD</sup>	CD	0.8143***	0.002
CB= 14.034 × e <sup>0.0554 × CA</sup>	CA	0.8354***	0.001
CB= 0.1113×#Frond <sup>2</sup> -6.4461×#Frond +125.63	#Fronds	0.7181**	0.0003

\*weakly significant

\*\*moderately significant

\*\*\*strongly significant

الكربونية

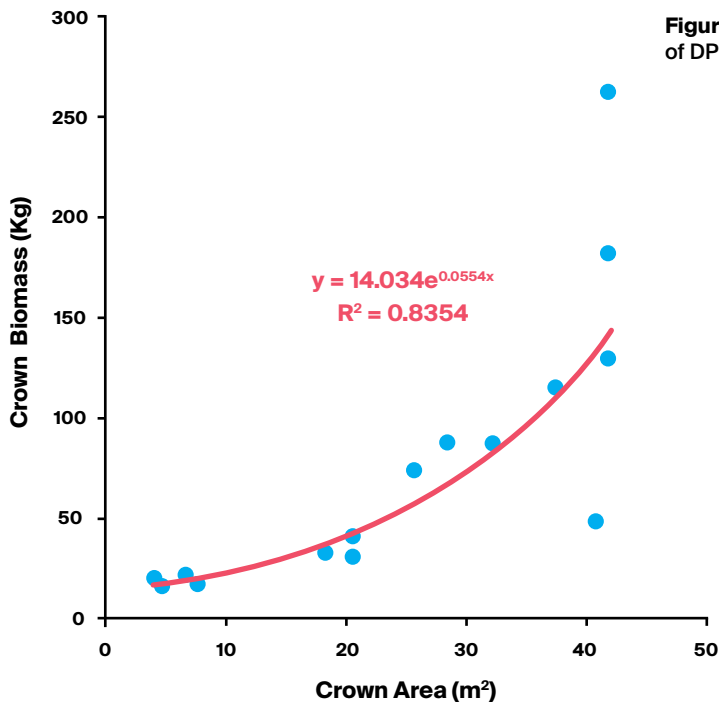


**Figure 12:** Allometric equation for estimating CB of DP as function of CA (Salem Issa et al., 2020b).



### 2.5.2. Trunk Biomass (TB)

All field variables were significantly correlated with TB except DBH and  $\Delta$ Height (Table 9). The three field variables that gave the highest correlation with TB were: Ht, H, and CA (Table 9). It was found that the

power equation (4) using Ht as the independent variable, had the best  $R^2$  (equal to 0.828) (see Table 9 and Figure 13).

$$TB = 40.725 \times Ht^{0.9719} \quad \text{Equation (4)}$$

**Table 9:** Best prediction equations for trunk biomass estimation of DP.

Regression Equations	Variable	$R^2$	P value
$TB = 0.5808 \times Age^{1.9271}$	Age	0.753	0.002
$TB = 0.0816 \times DBH^{1.7212}$	DBH	0.3967	0.197
$TB = 0.2879 \times H^{2.8666}$	Height	0.8017	0.001
$TB = 40.725 \times Ht^{0.9719}$	Ht	0.8276	0.0004
$TB = 0.4644 \times \Delta Height^{3.1733}$	$\Delta$ Height	0.3252	0.176
$TB = 0.1286 \times e^{0.9487 \times CD}$	CD	0.7556	0.008
$TB = 2.356 \times e^{0.0966 \times CA}$	CA	0.7566	0.008
$TB = 0.008 \times \#FronD^{2.3274}$	#FronDs	0.7403	0.008

### 2.5.3. Aboveground Biomass

AGB is the resulting sum of crown biomass (CB) and trunk biomass (TB). It can be estimated from CA (Equation 3) and Ht (Equation 4) that were found to be the most significant field structural variables for predicting crown and trunk biomass, respectively. Finally, the resulting allometric equation to estimate AGB of DPs is given in equation (5) below.

$$AGB = CB + TB \quad \text{Equation (5)}$$

**Where:**  $CB = 14.034e^{0.0554 \times CA}$  (with  $CA \neq 0$ ), and  $TB = 40.725 \times Ht^{0.9719}$ .

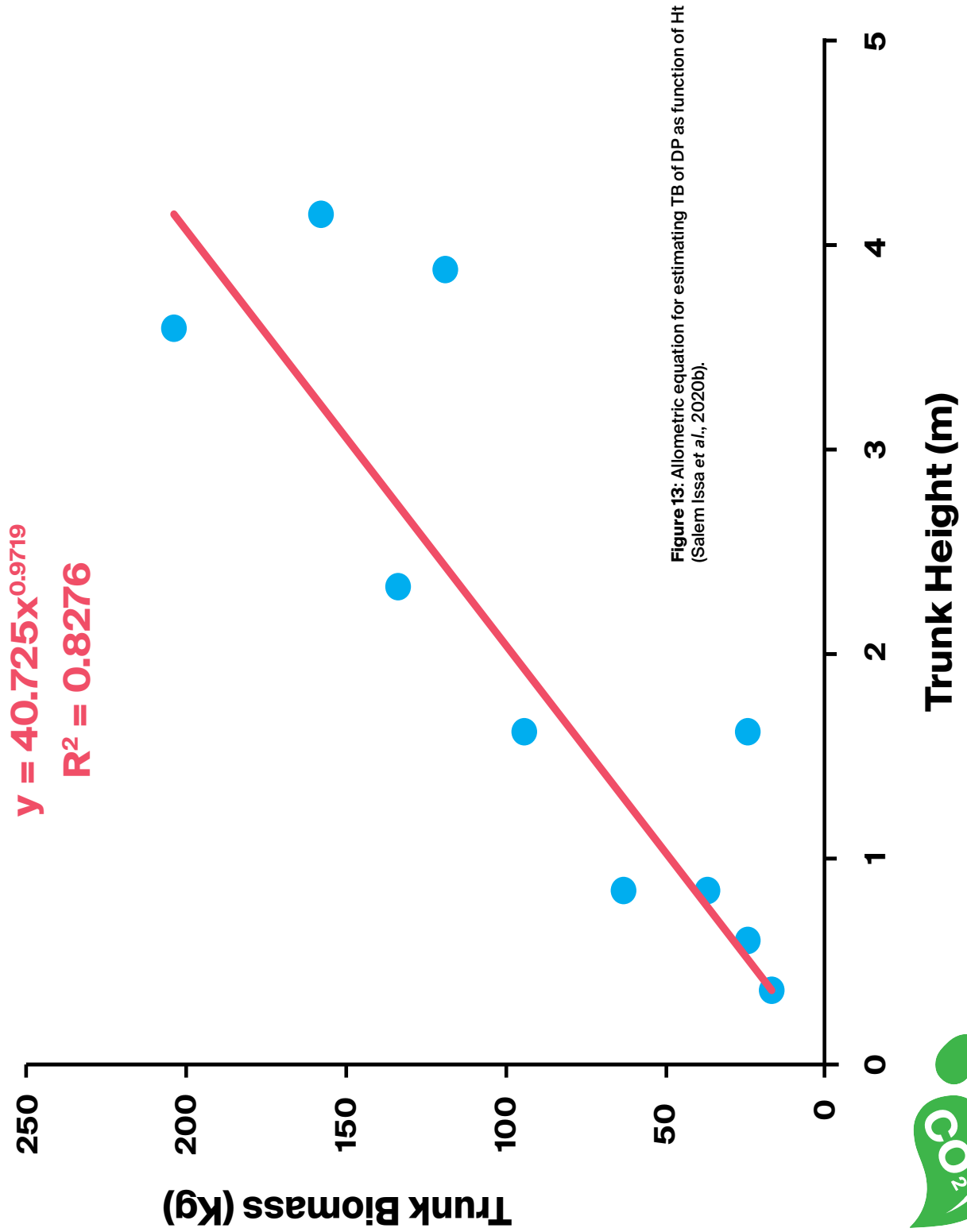


Figure 13: Allometric equation for estimating TB of DP as function of Ht (Salem Issa et al., 2020b).



# 2.6. Carbon Stock in Date Palm Trees at Different Age-Stages

Overall trunk of DP had a higher organic matter (OM) content of its dry weight than crowns and roots with averages of 93.3%, 92.43% and 88.39%, respectively (Table 10). The average percent OM was 91.38% for the whole DP (i.e. sum of the 3 components) and 92.87% for AGB. The same was noted about the organic carbon (OC) content to dry weight of DP. The trunk had higher OC content than crown and roots (54.12%, 53.61% and 51.27%, respectively). The percentage of carbon content in the root system of DP (BGB) was found to be 51.27%, which is slightly lower than the carbon content in the AGB.

The average percentage of OC for whole DP was 53% of the AGB. The total OM and OC stocks in the various DP components expressed per palm are shown in Table 10. The whole DP contains about 15.88 Kg of OC for young DP with increasing values of a maximum of 96.62 Kg and 225.58 Kg for medium and mature DP, respectively. While the AGB contained averages of 11.93 Kg, 50.19 Kg and 150.74 Kg of OC for young, medium and mature DP, respectively.

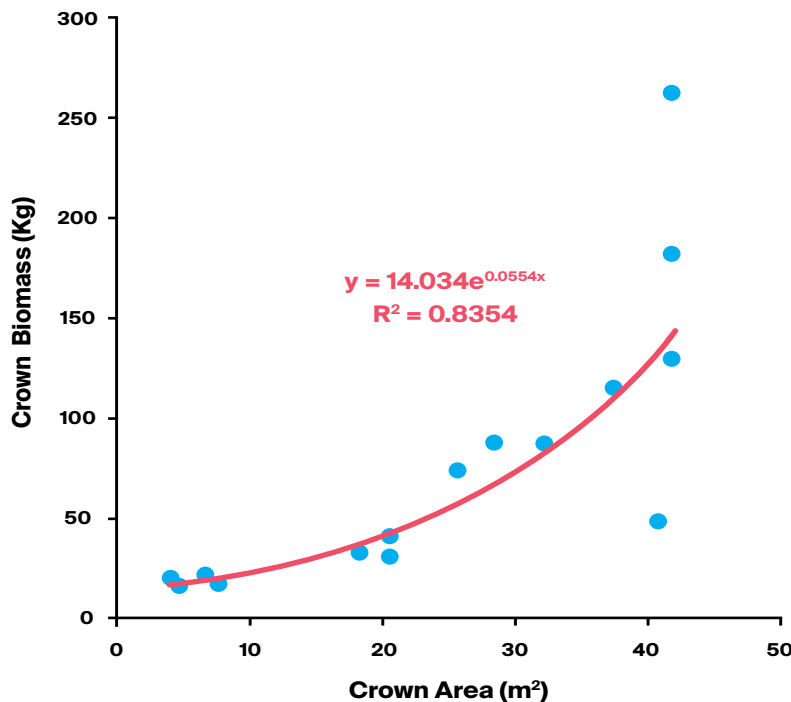


**Figure 14:** Prediction equation of soil organic carbon as function of CA (Salem Issa et al., 2020b) the authors demonstrated that combinations of visible and short wave single bands (Red, SWIR1, SWIR2).

**Table 10: OM and OC (Kg. palm<sup>-1</sup>) in DP components at different age stages.**

DP Component	Age Stage	Dry Weight	OM		OC	
Crown	Young	22.51	92.43%	20.81	53.61%	12.07
	Medium	65.17		60.24		34.94
	Mature	148.50		137.26		79.61
Trunk	Young	-	93.31%	-	54.12%	-
	Medium	29.53		27.55		15.98
	Mature	135.91		126.82		73.55
Root	Young	7.46	88.39%	6.59	51.27%	3.82
	Medium	87.61		77.44		44.92
	Mature	141.23		124.83		72.41
Total Biomass	Young	29.97	91.38%	27.39	53.00%	15.88
	Medium	182.30		166.59		96.62
	Mature	425.63		388.94		225.58
AGB	Young	22.51	92.87%	20.91	53.87%	12.13
	Medium	94.69		87.94		51.01
	Mature	284.41		264.13		153.21

The average SOM content of samples taken from underneath the DP canopy (labeled “In”) increased with age, registering 4.28%, 5.02% and 5.06% for young, medium and mature DP, respectively, with an overall mean of 4.79% (Table 11). On the other

hand, the average SOM content of samples taken away from the DP canopy (labeled “Out”) registered 3.0%. This percent represents only about two-third of that recorded from samples taken beneath (“In”) the date palms (Table 11).

الكربونية

**Table 11: Percent SOM and SOC for different canopy positions.**

Underneath/ Far Away DP	Soil Organic Matter (%)		Soil Organic Carbon (%)	
	In	Out	In	Out
<b>Qattara Farm</b>	5.06	4.1	2.6	2.38
<b>Masakin Farm</b>	4.28	1.9	2.48	1.1
<b>Average</b>	4.67	3.0	2.54	1.74

Percent SOC was transformed into bulk tons of SOC per hectare (Table 12), The average bulk density ranged from 0.74 to 1.24 g/cm<sup>3</sup> with a mean of 0.88 g/cm<sup>3</sup>. An estimated total of about 22.26 tons of SOC was added per hectare in the areas dominated by DP. Variations between different age stages were also detected. The average SOC at young, medium and mature DP were 20.29, 23.66 and 22.83 tons per hectare, respectively. At the individual palm level, the average SOC was 18.09 Kg.palm<sup>-1</sup>, 62.59 Kg.palm<sup>-1</sup>, and 92.91

Kg.palm<sup>-1</sup> for young, medium and mature DP, respectively, with an overall average of 57.87 Kg.palm<sup>-1</sup> (Table 12). There was a strong correlation between SOC (Kg.palm<sup>-1</sup>) and palm CA (m<sup>2</sup>) with R<sup>2</sup> equal 0.9523 (Figure 14). Thus, CA can be used as a suitable predictor to estimate SOC using the power regression given in Equation (6).

$$\text{SOC (Kg.palm}^{-1}\text{)} = 1.5474 \times \text{CA}^{1.144} \quad \text{Equation (6)}$$



Table 12: SOM and SOC at 10 cm depth under DP at three different age stages.

DP Age Stage	Age (year)	CA (m <sup>2</sup> )	SOM (%)	SOC (%)	SOC (g/m <sup>2</sup> )	SOC (Kg.palm <sup>-1</sup> )	SOC (ton.ha <sup>-1</sup> )
Young	2.5	3.98	3.08	1.79	1731.58	6.88	17.32
	2.5	4.52	4.48	2.6	1932.42	8.74	19.32
	3	7.55	3.75	2.18	2126.36	16.05	21.26
	3	6.61	3.48	2.02	1740.43	11.5	17.4
	4	18.1	6.59	3.82	2613.07	47.29	26.13
	Mean	8.152	4.276	2.482	2028.772	18.092	20.286
Medium	5	20.43	3.99	2.31	2003.73	40.93	20.04
	7	28.27	4.58	2.65	2359.16	66.7	23.59
	8	25.52	4.95	2.87	2430.97	62.03	24.31
	9	32.17	8.36	4.85	3446.96	110.89	34.47
	10	20.43	3.22	1.87	1587.22	32.42	15.87
	Mean	25.364	5.02	2.91	2365.608	62.594	23.656
Mature	11	40.72	4.06	2.35	2277.49	92.73	22.77
	14	41.85	7.27	4.22	3151.01	131.88	31.51
	16	37.39	5.74	3.33	2392.35	89.46	23.92
	18	41.85	3.79	2.2	1571.99	65.79	15.72
	20	41.85	4.46	2.59	2023.26	84.68	20.23
	Mean	40.732	5.064	2.938	2283.22	92.908	22.83
<b>Averages</b>			4.79	2.78	2225.87	57.87	22.26

## 2.7. Summary

In Chapter 2, specific allometric biomass equations were developed that can be integrated into a RS-based model for assessing carbon sequestered in DP. Assessing the potential of DP to improve soil carbon sequestration was another objective. The average amounts of DP biomass, organic matter, organic carbon, and soil organic carbon at different age stages were presented on Appendix 5. Here and based on field and lab work, relevant structural variables were identified and used in the development of allometric equations.

Results showed that the crown area (CA) best estimated both crown biomass (CB) and soil organic carbon (SOC). Likewise, the trunk height (Ht) was the best estimator of trunk biomass (TB). Using these variables, allometric equations were developed for date palms at different age stages and were used to estimate CB, TB and SOC with coefficients of determination ( $R^2$ ) of: 0.884, 0.835 and 0.952, respectively. Furthermore, the average ratios of below ground biomass (BGB) to above ground biomass (AGB) varied with palm maturity stages averaging 0.332, 0.925 and 0.496 for young, medium and mature palms, respectively.

Moreover, the results demonstrated that the amounts of organic carbon (OC) stored in date palms were considerable with values of: 15.88 Kg. palm<sup>-1</sup> for young DP, 96.62 Kg. palm<sup>-1</sup> for medium DP, and 225.58 Kg. palm<sup>-1</sup> for mature DP. Substantially higher amounts of SOC were measured compared to other local plants with values of: 18.092 Kg. palm<sup>-1</sup>, 62.594 Kg. palm<sup>-1</sup>, and 92.908 Kg. palm<sup>-1</sup> under young, medium and mature DP palms, respectively.

The main achievement was the development of new and unprecedented allometric equations for DP species in arid land. Such equations allow the development and calibration of a RS-based model for estimating biomass and CS of date palms in the region with high accuracy.

الكربونية



## Summary of statistics on palm biomass and sequestered carbon

Item	Average amount (Kg palm <sup>-1</sup> )		
	Young (< 5 year)	Medium (5 - 10 years)	Mature (>10 years)
Crown Biomass (CB)	22.51	65.17	148.5
Trunk Biomass (TB)	0	29.53	135.91
AGB	22.51	94.69	284.41
BGB	7.46	87.61	141.23
Total Biomass	29.97	182.3	425.63
Organic Matter (OM)	27.39	166.56	388.94
Organic Carbon (OC)	15.88	96.62	225.58
SOC	18.09	62.59	92.91
Total Carbon Stock (CS)	33.97	159.21	318.49

الكربونية

**CA**  
is Crown Area

### Above ground biomass (BGB)

$$\text{CROWN BIOMASS} = 14.034 \times 1.057^{\text{CA}}$$

$$\text{TRUNK BIOMASS} = 40.725 \times \text{Ht}^{0.9719}$$

$$R^2 = 0.8354, p\text{-value} = 6 \times 10^{-4}$$

$$\text{AGB} = \text{CROWN BIOMASS} + \text{TRUNK BIOMASS}$$

### Below ground biomass (BGB)

is calculated a ratio with AGB:

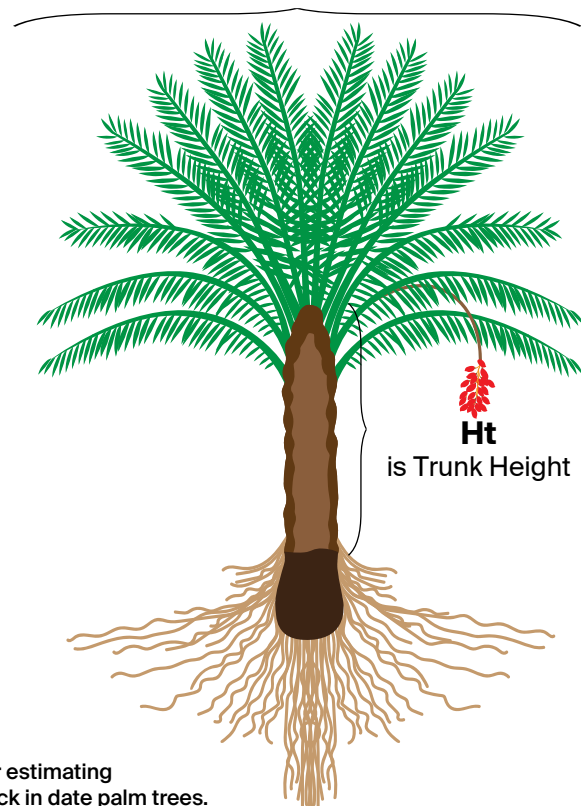
$$\text{BGB for Young date palm} = 0.332$$

$$\text{BGB for Medium date palm} = 0.925$$

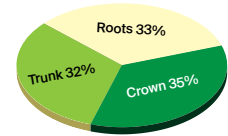
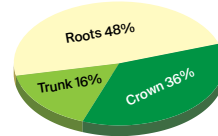
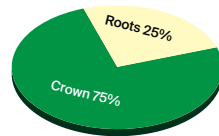
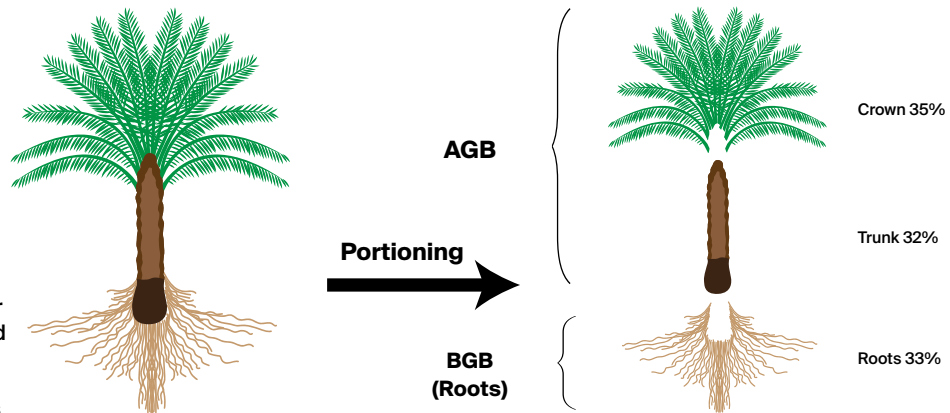
$$\text{BGB for Mature date palm} = 0.496$$

- Carbon is 53.87% of AGB
- Soil Carbon (SOC) is 22.26 t/ha

**Infographic 9:** Summary of statistics, equations, and ratios for estimating aboveground biomass, belowground biomass, and carbon stock in date palm trees.

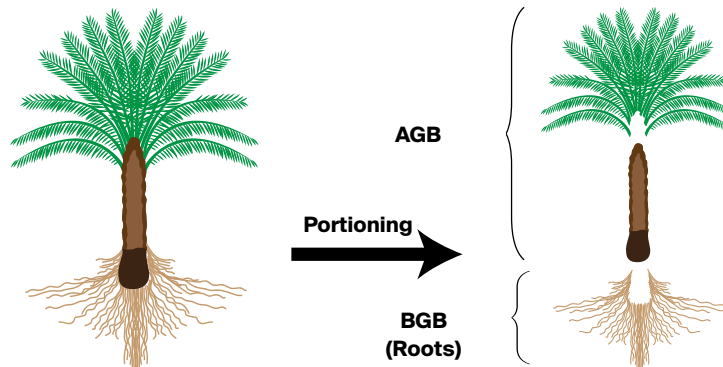


**Infographic 10:** Summary of statistics, equations, and ratios for estimating aboveground biomass, belowground biomass, and carbon stock in date palm trees.



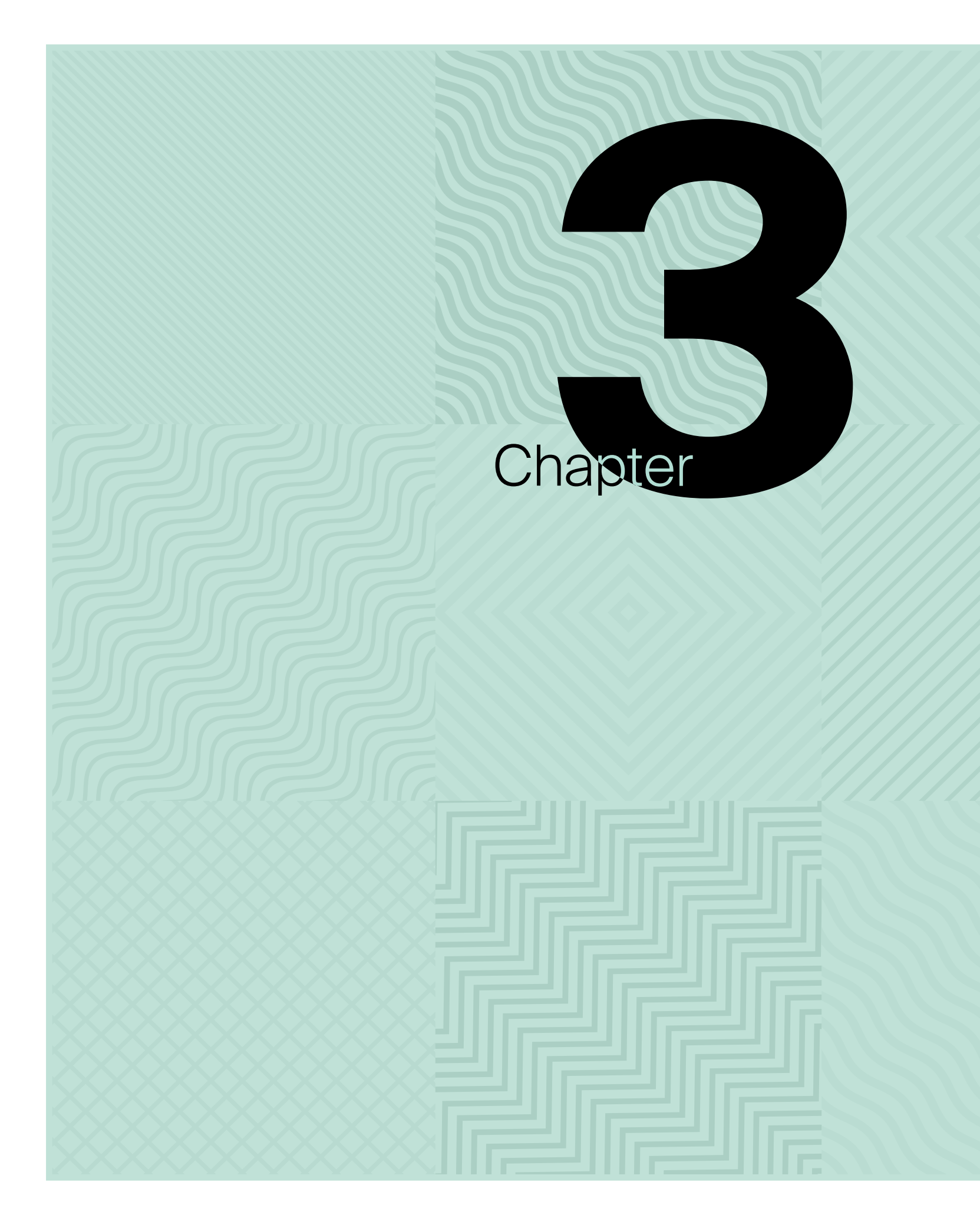
Item	% from total BIOMASS		
	Young (< 5 year)	Medium (5 - 10 years)	Mature (>10 years)
Crown	75.11	35.75	34.89
Trunk	0	16.2	31.93
<b>AGB</b>	<b>75.11</b>	<b>51.95</b>	<b>66.82</b>
BGB (Roots)	24.89	48.06	33.18

الكربونية



Item	% from AGB		
	Young (< 5 year)	Medium (5 - 10 years)	Mature (>10 years)
Crown	100	68.82	52.21
Trunk	0	31.18	47.79
<b>BGB: AGB Ratio</b>			
BGB (Roots)	0.33	0.93	0.5



The background is a light green color with a grid of six rectangular panels, each containing a different geometric pattern. The top-left panel has a fine, dense grid of small squares. The top-right panel features a pattern of concentric, slightly irregular diamond shapes. The middle-left panel shows a series of wavy, horizontal lines that resemble a topographic map. The middle-right panel contains a pattern of wavy, vertical lines. The bottom-left panel has a pattern of interlocking, zig-zagging lines. The bottom-right panel features a pattern of wavy, horizontal lines, similar to the middle-left panel but with a different scale and orientation. A large, bold, black number '3' is centered in the upper right portion of the image, overlapping the top-right and middle-right panels. The word 'Chapter' is written in a white, sans-serif font, positioned below the number '3' and overlapping the middle-right and bottom-right panels.

# 3

Chapter



# **Mapping & Counting of Date Palm Trees in Abu Dhabi Emir- ate Using Satellite Imageries**



©KIADPAI - Khaled Juma Al Blooshi



# 3.1. Overview

In this Chapter, a hybrid classification method (HCM) was developed to produce a classified map of the study area comprising seven land use/land cover (LULC) classes. A GIS-based semi-automatic approach, benefiting from the researcher's prior knowledge of the study area, was then implemented to group the classes and to produce a bitmap (binary mask) of only two types: vegetation and non-vegetation (the vegetation bitmap). Finally, a set of high-resolution WorldView-2 (WV-2) imagery was used to classify and map date palm trees at different age stages, within the vegetation bitmap, to create an accurate and reliable DP map. The output product will be used as an input to the built RS-based biomass model to assess CS in DP trees in the study area (see Chapter 4).

Figure 15 demonstrates the pre-processing and processing of RS data in details. First, each pan-sharpened scene of Landsat-8 OLI was classified using a the HCM (supervised and unsupervised classification) to create LULC maps (for RS data used, see appendix 6A).

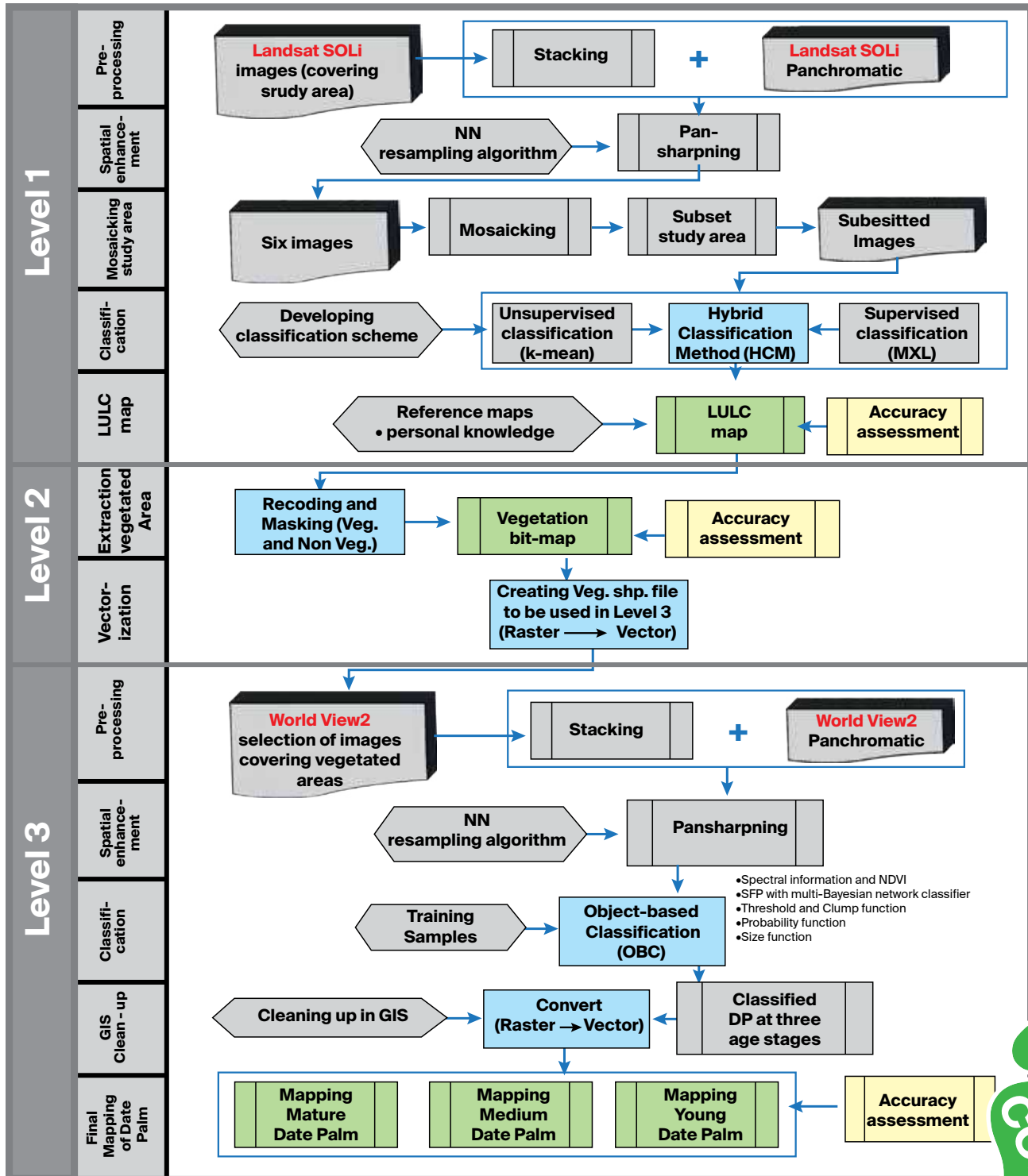
Next, the maps were recoded (reclassified) to create a bitmap comprising only two classes: vegetation and non-vegetation. The HCM was applied to the areas covered by the vegetation class in order to delineate the date palms and create a bitmap containing date palms and non-date palms classes (DP and non-DP). However, at this stage of the classification, only

mature DP trees were depicted due to the limitations of Landsat-8 OLI to differentiate soil background from the non-mature DP trees (less than 10 years) with average crown diameter less than 5 meters.

In order to map the other two age stages (medium, and young), object-oriented classification (OOC) method was applied on the already produced vegetation bitmap. At this level, about 829 sub-meter world view -2 (WV-2) images were used covering only the vegetated areas (see Appendix 6B). The HIA classification method was able to depict the three age stages of date palms: young, medium, and mature.

To validate the interim and final maps, an accuracy assessment procedure was implemented at different levels for the evaluation of the LULC maps, the vegetation bit-map, and the detailed DP maps. An error matrix was produced and helped determine the overall, user's, and producer's accuracies, in addition to the kappa coefficient. All processes were implemented using ERDAS Imagine 2020 and ArcGIS 10.7.1 software packages.

For the purpose of tree crown detection and delineation, many algorithms were developed (Chepkochei, 2011; Hebbar *et al.*, 2014; Lack & Bleisch, 2010; Rizvi *et al.*, 2019; Sahay *et al.*, 2017). However, results of tree detection and delineation can be affected by algorithm characteristics. Indeed, different approaches may give different results despite working in the same environment. Thus, it is important to select the appropriate algorithm to get the suitable results. Moreover, for any algorithm to work properly, crowns should be, at least, detectable and segmented as an object in the image before classification.



الكريونية

Figure 15: The flowchart of methods for land use/land cover (LULC) classification and mapping of date palm trees.



Training areas of the classes that are to be extracted must be chosen very carefully for not to include any background pixels and non-targeted classes based on visual analysis and on previous knowledge of the area by the interpreter. By using the pan-sharpened WV-2 images (spatial resolution 0.5 meter) (see Chapter 2, Subsection 2.3), DP crowns can be differentiated from the background (soils, grasses, and weeds) and other shrubs and trees using colour, tone, texture, size and planting arrangement (Figure 16). In general, the steps followed could be divided to multi-levels:

1. raster data analysis which includes identifying DP from other vegetation and classifying their age stages (mature, medium, and young) according to their crowns, and
2. vectorising, cleaning up the vector layers and creating the maps.

Furthermore, a pixel-based classifier relying on spectral, textural and site information, is used in the raster analysis part (Figure 17b, and 17c). The second level of analysis was done on the vector data model by first vectorising the three raster outputs (mature, medium, and young), smoothing the polygons, calculating the areas, and cleaning up the maps manually (Figures 17d, 17e, and 17f).

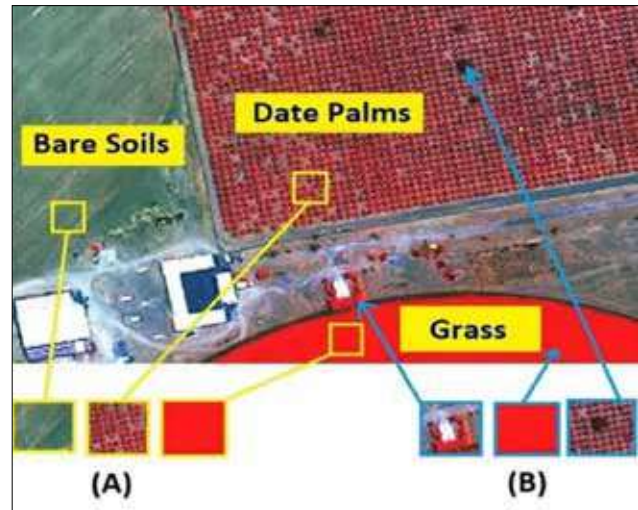


**Figure 16:** A subset of pan-sharpened WV-2 image. Green, red, and NIR1 bands were used with a spatial resolution of 0.5 meters. The image is displayed in false color. (A) The DP can be differentiated from bare soils and grass visually by using color, tone, and texture; and (B) The DP can be differentiated from other vegetation (grasses, trees, and shrubs) visually using the mentioned tools plus the planting arrangements and spacing.

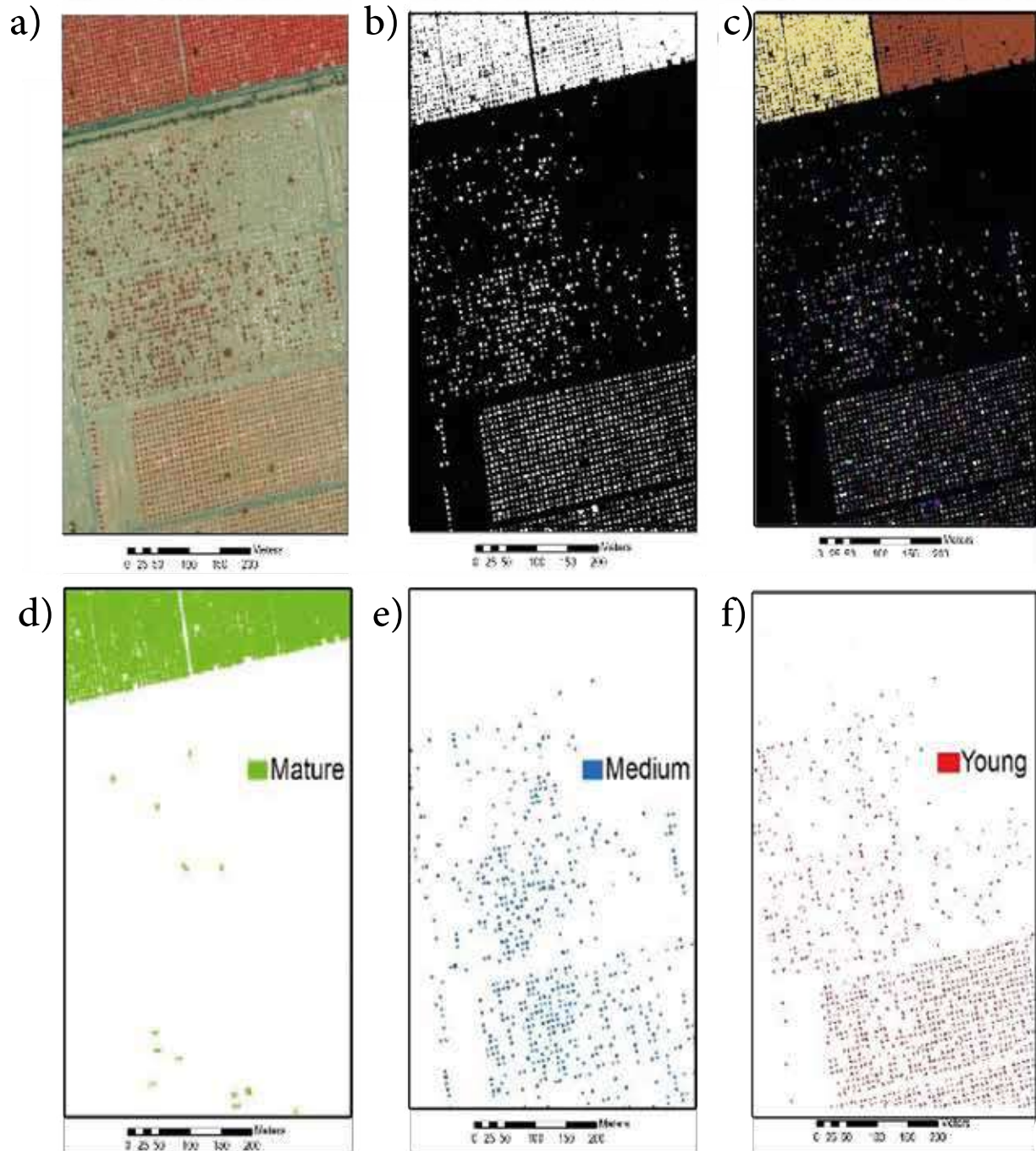


**Figure 17:** Separating age classes of date palm trees. The example is from Al Foah DP farm: (a) Original WV-2 image (RGB:7,5,4); (b) SFP using Bayesian network; (c) Threshold and clump applied; (d) Mature palms layer; (e) Medium palms layer; and (f) Young palms layer (Salem Issa *et al.*, 2020).



# 3.2. Land Use/ Land Cover Classification of the Emirate of Abu Dhabi

الكربونية

Anderson classification scheme (Level 1) was adopted, to classify the Landsat data (Al-Ahmadi & Hames, 2009; Anderson, 1976; Rozenstein & Karnieli, 2011). Seven LULC classes were used to represent: vegetation, urban, sand sheets, sand dunes, deep water and shadows, shallow water, and sabkhas.

The HCM approach was implemented: starting by performing unsupervised classification to minimize bias in the selection of training areas and seed signatures; then, a set of spectral class signatures was created to be used as training data for the supervised classification phase (Bakr *et al.*, 2010; Kuemmerle *et al.*, 2006; Rozenstein & Karnieli, 2011). Each image was initially clustered into 80 classes with a maximum

of 80 iterations (the optimum number of iteration for Landsat data), permitting the clustering process to stop naturally as it reaches the convergence threshold of 0.990 (Al-Shuwaihi, 2009; Kuemmerle *et al.*, 2006; Mundia & Aniya, 2005; Yang & Lo, 2002).

Next, all images were classified using the previously created signatures corresponding to the seven classes present in the study area. The signatures were collected by delineating polygons on the images to collect the training samples (total of 720 training sets). The signatures were assessed and evaluated by plotting the mean signature values of each class against the Landsat-8 OLI bands. The maximum likelihood classifier (MXL) was used and the resulting classes were then merged and recoded to form the final seven LULC classes. The resulting LULC map was smoothed and cleaned up using a Majority Filter with a window size of (3x3). Then, certain class boundaries were manually adjusted using the Fill Tool module in ERDAS Imagine. This is achieved by filling the misclassified pixels with the right values. Finally, the thematic LULC map was created and the area of each of the seven classes was computed in hectare.

The evaluation of spectral signatures separability (total of 740 training sets) is displayed in Figure 18 where the Y-axis represents the mean signature value of each class (pixel or DN value) and the X-axis represents the Landsat-8 OLI bands. Shortwave infrared bands (SWIR1& SWIR2) had the best separability power of all Landsat 8 OLI bands.

Figure 19 displays the class distribution and Table 13 shows their respective areas and percentages in the study area. Sand dunes formed about 70% of the study area with nearly 5 million hectares. Sabkhas occupied 15.51%, while sand sheets, including gravel, made up 8.6% of the study area. Finally, Urban and Vegetation classes constituted only 0.49% with 32,333 hectares and 0.6% with 40,102.6 hectares of the study area, respectively.

**Table 13:** The area and percentage of each class LULC of Abu Dhabi.

LULC Class	Deep Water	Shallow Water	Urban	Vegetation	Sand Dunes	Sand Sheets	Sabkha
Area (ha)	9,677.7	11,847.2	40,102.6	32,333.3	4,957,180	572,665	1,032,170
(%)	0.15	0.18	0.6	0.49	74.48%	8.6	15.15

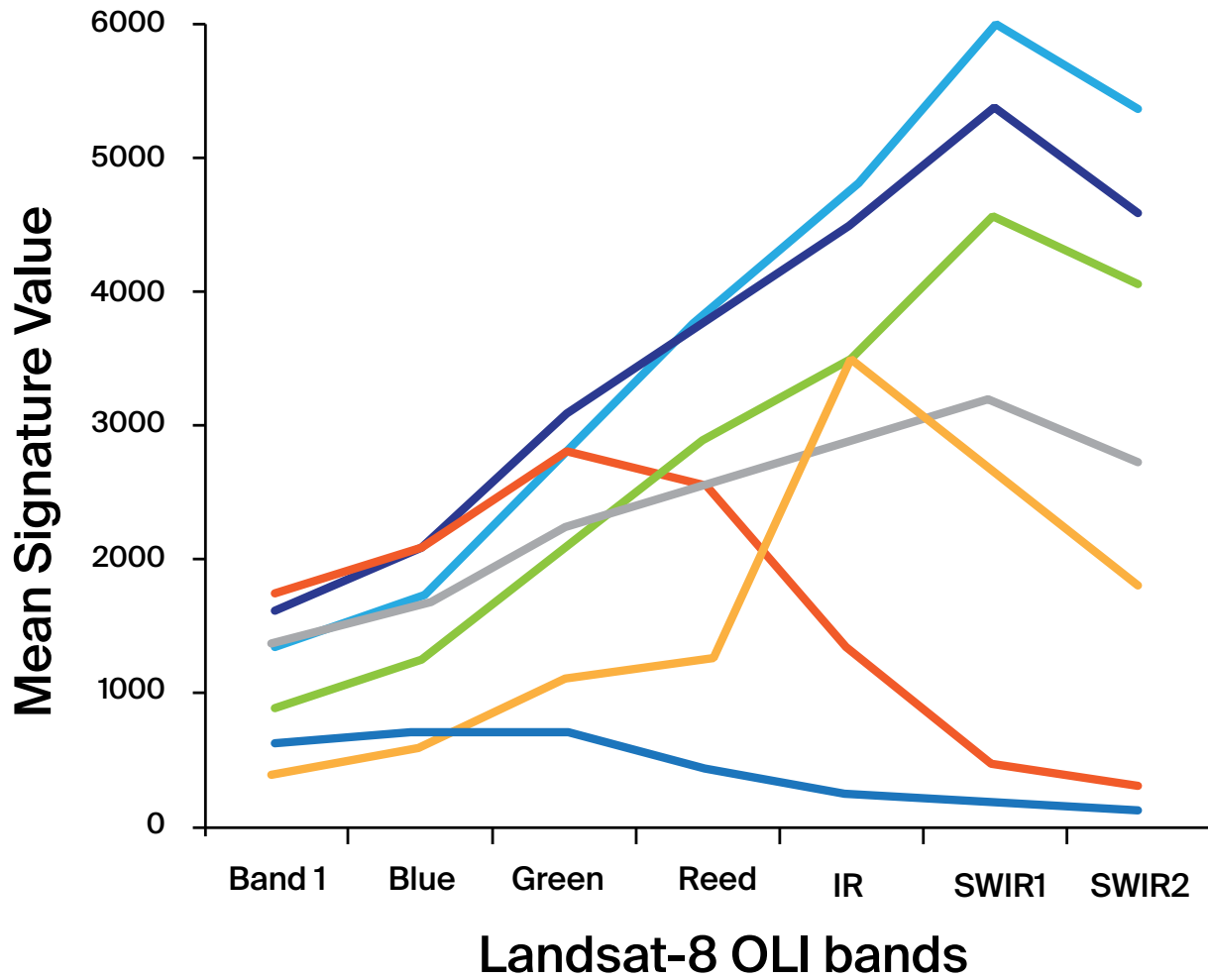


Figure 18: Mean signature value of LULC classes vs. Landsat-8 bands.



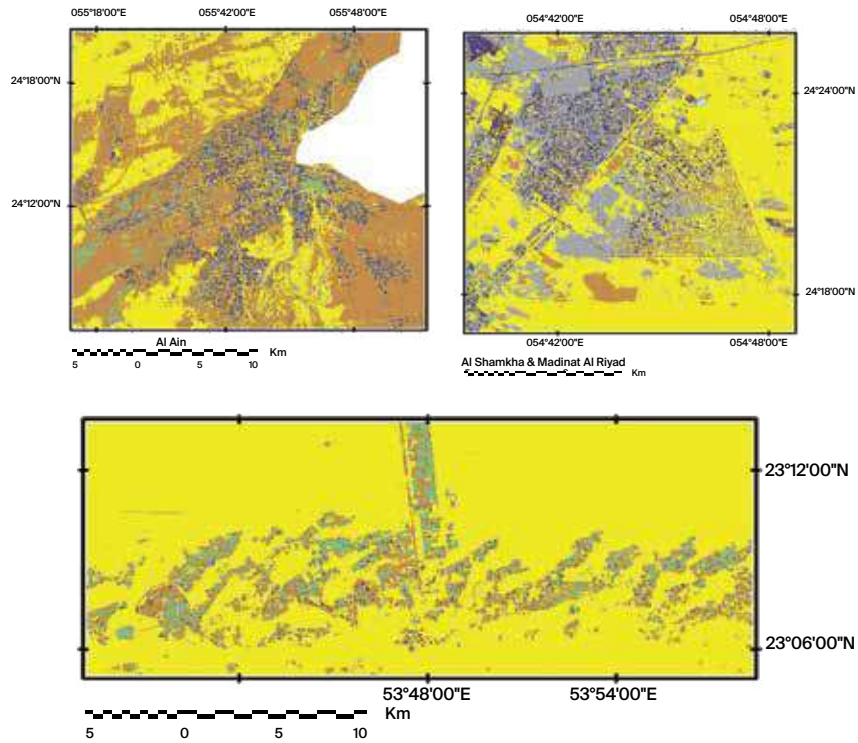
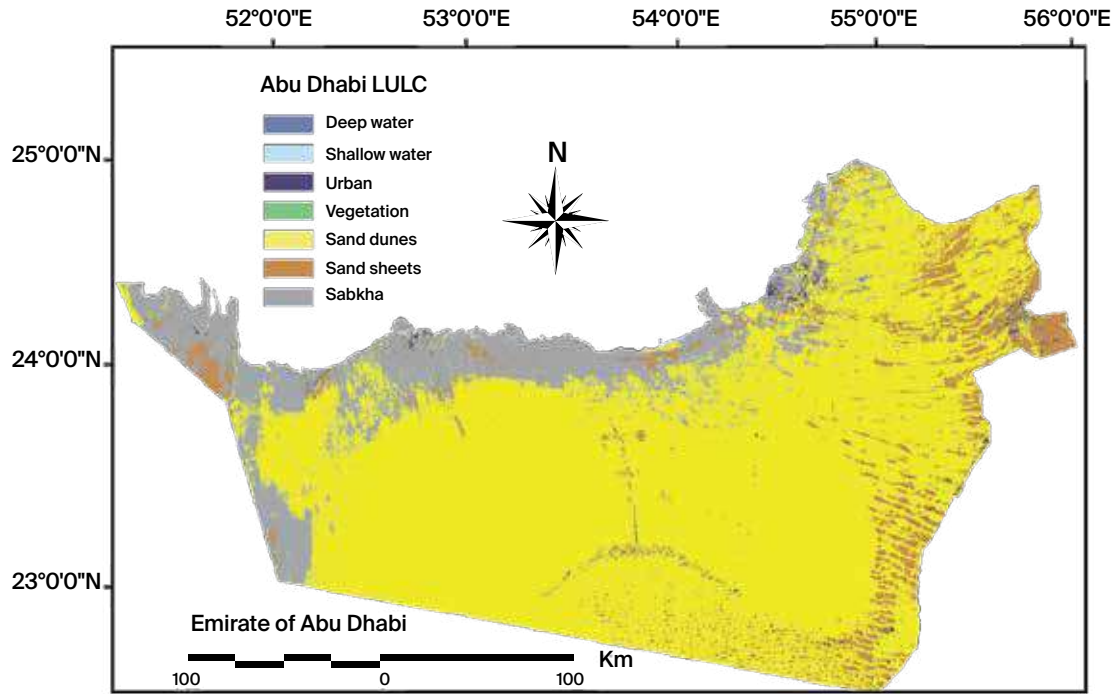


Figure 19: LULC map of the study area.

### 3.3.

# Mapping Vegetation and Date Palm Using Landsat-8 OLI Sensor

The Landsat-8 OLI images were first processed to produce a bitmap with two land cover classes: vegetated / non-vegetated (Al-Shuwaihi, 2009; Southworth et al., 2002). To that end, the LULC map of Abu Dhabi was converted to a binary map by merging all non-vegetation classes: urban, sand sheets, sand dunes, deep water, shallow water, and sabkhas, into one class named non-vegetation.

A "Recode" function was used in the process to create a vegetation bitmap having two values: 1 for vegetated area class and 0 for non-vegetated class. Vegetated areas (pixels) were extracted from the original images by masking the non-vegetated pixels using Subset/Mask functions in ERDAS Imagine. To separate the DP trees from other vegetation types, the HCM was run within the vegetated areas following the

same procedure described above. The DP trees were mapped and their areas in hectare were computed; however, only the mature DP trees were depicted due to the limitations of Landsat-8 OLI to differentiate soil background from the non-mature DP trees.

Consequently, the vegetation bitmap was transformed and converted to vector format and exported to a vector shapefile using ArcGIS 10.7.1. The shapefile will then be used for the selection of the corresponding WV-2 scenes that cover the vegetated areas present in the study area. The OOC classification method is applied to classify the high-resolution WV-2 images for the separation and mapping of DP age classes and calculating their statistics.

All non-vegetated classes of the LULC map were merged to produce one non-vegetated class; where the vegetated class was given the value of One, while the non-Vegetated class was set to Zero (Figure 20).

Pure spectral signatures of DP were selected from pixels representing DP planted in Abu Dhabi Emirate. They all were collected during intensive field visits to different locations of DP farms in the study area. These DP farms are different in their phenological cycle (mature, medium, and young). Besides, they have different farming systems, management practices (irrigation and fertilizing) and healthy conditions (stressed/ not stressed). In order to separate and map DP from other vegetation types, the spectral signature values (minimum, maximum, and mean) of DP trees were analyzed. It was revealed that only mature DP had good separability and hence could be detected at this stage, using Landsat-8 OLI. This is due to the limitations of Landsat-8 OLI to differentiate soil background from the non-mature DP trees.

The results are displayed in Figure 21; where the Y-axis represents the signature values (pixel or DN value) of DP (mature DP) while the X-axis represents the Landsat-8 OLI bands. It was noticed that the best discriminatory bands of the Landsat-8 OLI for mature DP spectral separation are found in the Red-Red edge-IR boundaries.

الكربونية



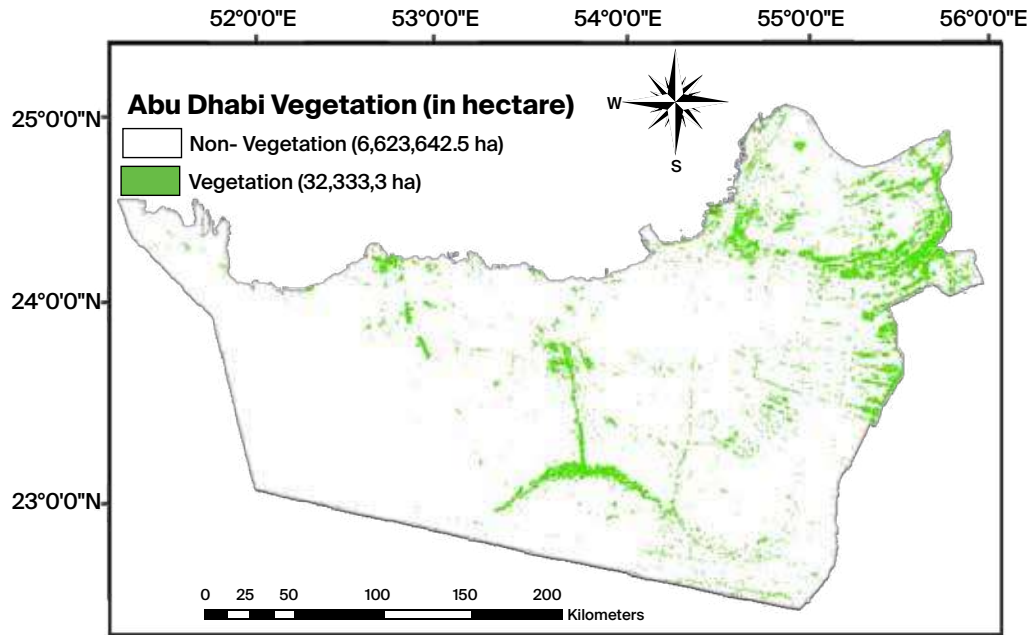


Figure 20: Vegetation bitmap of Abu Dhabi.

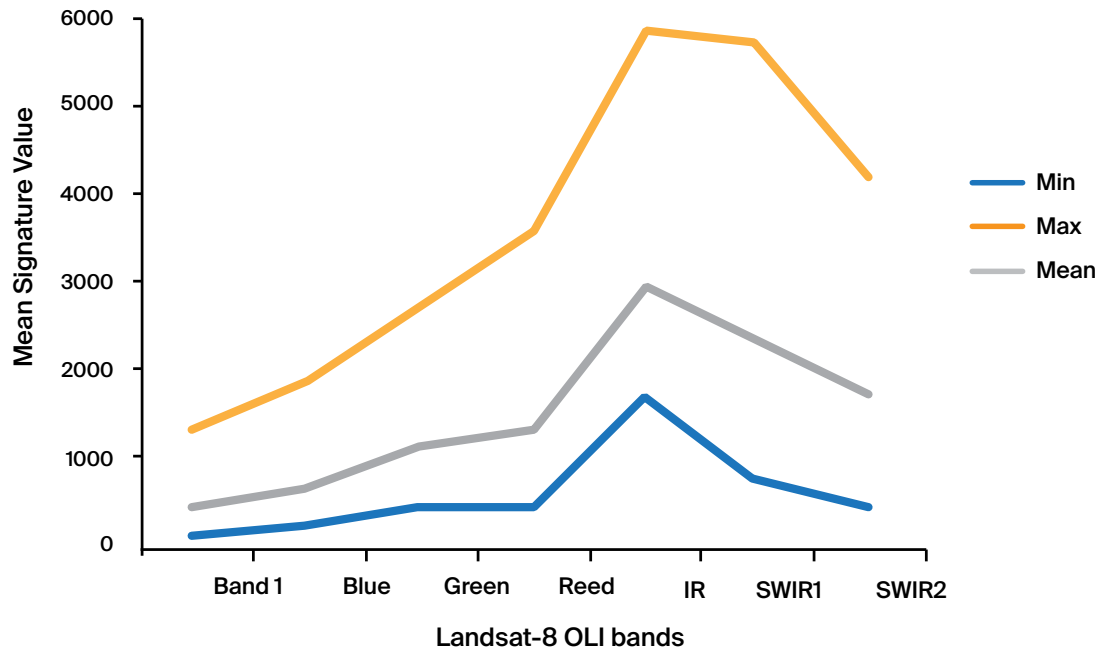
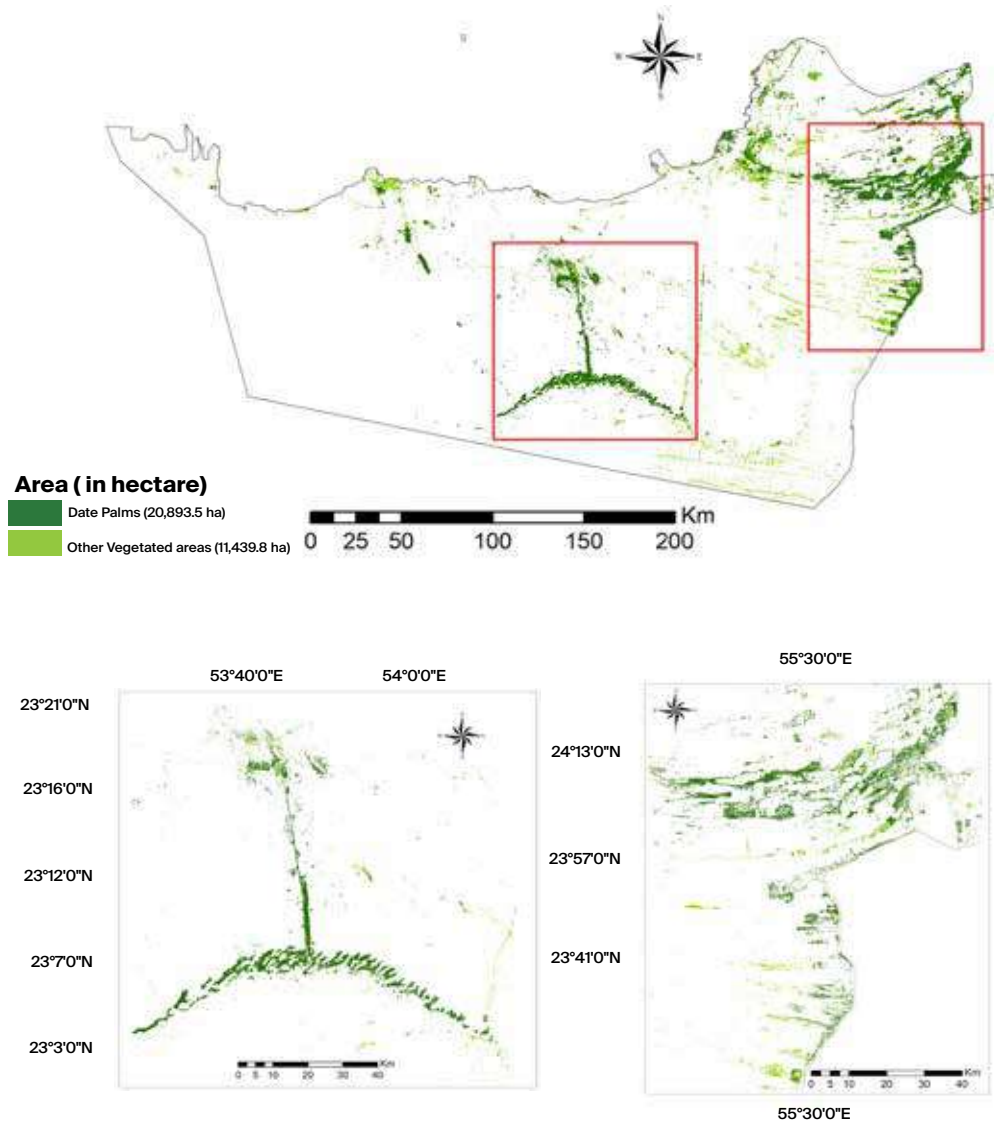


Figure 21: Min., max., and mean signature value of date palm trees versus Landsat bands.

Therefore, non-mature DP (medium and young) were not mapped, and only mapping of mature DP was performed using the Landsat-8 OLI imagery at this stage. The HCM was applied to the vegetation bitmap produced previously and, the same procedure described above was implemented. Maps were created and their areas in hectare were computed (Figure 22).

The area (in hectare) of the DP trees was estimated at 20,893.5 ha, hence contributing to more than 64% of the vegetated areas in the emirate. Most of DP trees were found in AI Ain (east of the emirate) and Liwa (south of the emirate). Note that these figures represent only the mature DP trees (> 10 years) of Abu Dhabi as Landsat-8 OLI couldn't depict the non-mature DP (medium and young) of an average crown diameter less than 5 meters due to mixed spectral signature with soil background and wider spacing.



**Figure 22:** Abu Dhabi Emirate DP trees map (mature DP) using Landsat-8 OLI. It is shown that most of the DP trees are found in AI Ain City (right box) and Liwa (left box).



## 3.4. Accurate Mapping of Date Palm at Different Age-Stages Using WorldView-2 Sensor



than 60,000 palms of different ages and cultivars and was subject to many visits during the study period (Issa *et al.*, 2018; Issa *et al.*, 2019, Issa *et al.*, 2020c). The FMT was then run on the entire WV-2 sharpened images (Lack & Bleisch, 2010). This model became the basis for the extraction of DP at different age stages which consisted of several sequenced “process nodes” (Figure 23). Best parameters were selected and trained following a trial-and-error approach.

At this level of the classification, the 829 WV-2 scenes acquired in 2014 were used (for RS data used, see appendix 6B). The vegetated areas, in each of the 829 scenes, were visually interpreted and subset to run the OOC. A semi-automatic object-oriented feature model has been implemented for the detection and mapping of DP using ERDAS Objective Imagine (Chepkochei, 2011; Lack and Bleisch, 2010; Rizvi *et al.*, 2019; Issa *et al.*, 2020b).

The same Al Foah farms area, north of Al Ain city (Figure 23) was used as a pilot area to create and calibrate the Feature Model Tree (FMT). It contains more

Maps of DP at three age stages: young, medium, and mature were created using the sub-meter WV-2 imagery. GIS tools for cleaning up the vector shapefile resulting from the OOC method were used successfully to enhance and improve highly the accuracy of the final maps. Figure 24 shows the final DP map at three different age stages in AD emirate (mature, medium, and young); while Table 22 displays areas (in hectare) of each category with a total area equal to 7,588.04 ha. It can be noted that more than half of the Abu Dhabi DP trees areas were mature DP (> 10 years).

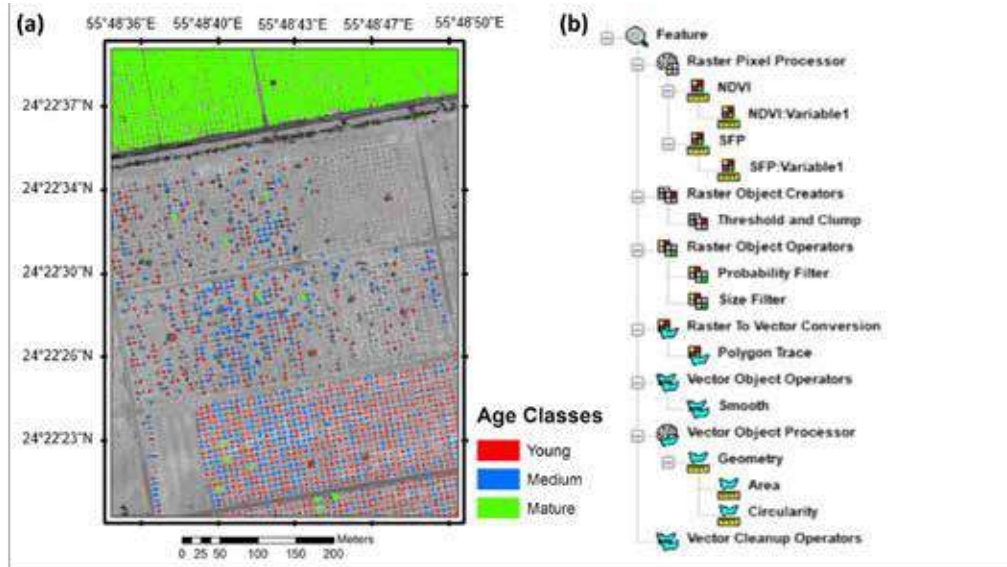


**Figure 23:** Object-oriented classification of DP in Abu Dhabi. (a) The three age stages of date palms produced, after applying the object-oriented approach on WV-2 images on a testing area in Al Foah DP farms area, to optimize the selected parameters. (b) FMT for the extraction of DP trees with three age stage.

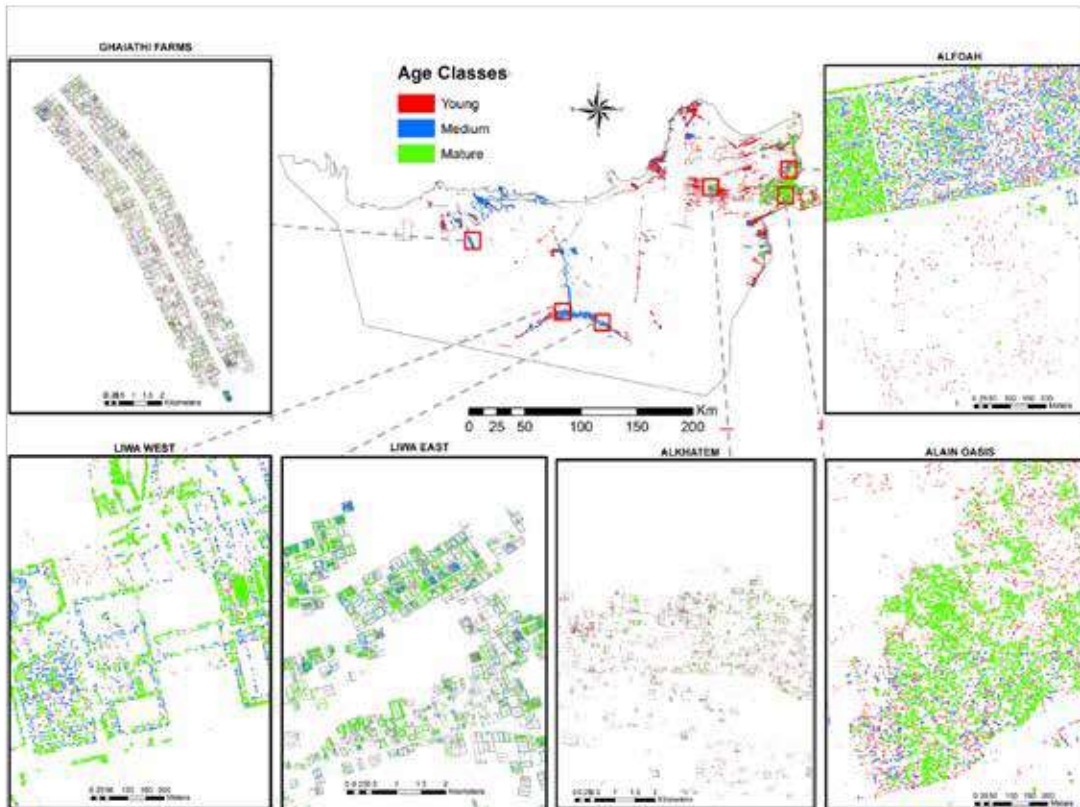


**Figure 24:** Map of DP trees showing three age stages using WV-2. The boxes represent the DP maps at different scales and different locations (Alfoah, Alain Oasis, Alkhatem, Liwa west, Liwa east, and Ghiathi).



# 3.5. Maps Validation

The accuracy of the classified maps was assessed using standard statistical tools. The results are summarized and shown in (Table 14), they show a good overall per-

formance of the classification process with an overall accuracy of about 81.7% for LULC map and 87% for the vegetation bit-map using Landsat-8 OLI. Furthermore, the overall accuracies of the DP maps, produced using the sub-meter WV-2, at different age stages, were determined to be 86.8%, 88% to 90.7%, for young, medium, and mature DP trees, respectively.

Also, the accuracy of the DP map derived from WV-2 was assessed for all three age stages combined (considered as one DP class only). The resulting map had an overall accuracy of 94.5% and a kappa coefficient of 88% (Table 14). These figures are considered a great achievement considering the efforts exerted by the government to inventory DP in the emirate.

**Table 14:** Accuracy assessment of the classified maps.

Data Source	Classified map	Producer's Accuracy %	User's Accuracy %	Overall Accuracy %	Overall Kappa
Landsat-8	LULC (7 classes)			81.71	0.8094
	Deep Water	92.68	76.00		
	Shallow Water	95.65	88.00		
	Urban	85.71	72.00		
	Vegetation	74.07	80.00		
	Sand Dunes	81.81	90.00		
	Sand Sheets	74.07	80.00		
	Sabkha	74.14	86.00		
Landsat-8	Vegetation bitmap			87.00	0.7400
	Vegetation	97.44	76.00		
	Non-vegetation	80.33	98.00		
Landsat-8	DP bitmap			77.5	0.5500
	DP	92.24	61.67		
	Non-DP	70.89	93.33		
WV-2	Mature	100.0	81.48	90.74	0.8148
	Medium	95.34	80.00	88.00	0.7600
	Young	93.75	78.95	86.82	0.7368
	All Ages			94.5	0.888
	DP	94.59	95.45		
	Non-DP	94.38	93.33		



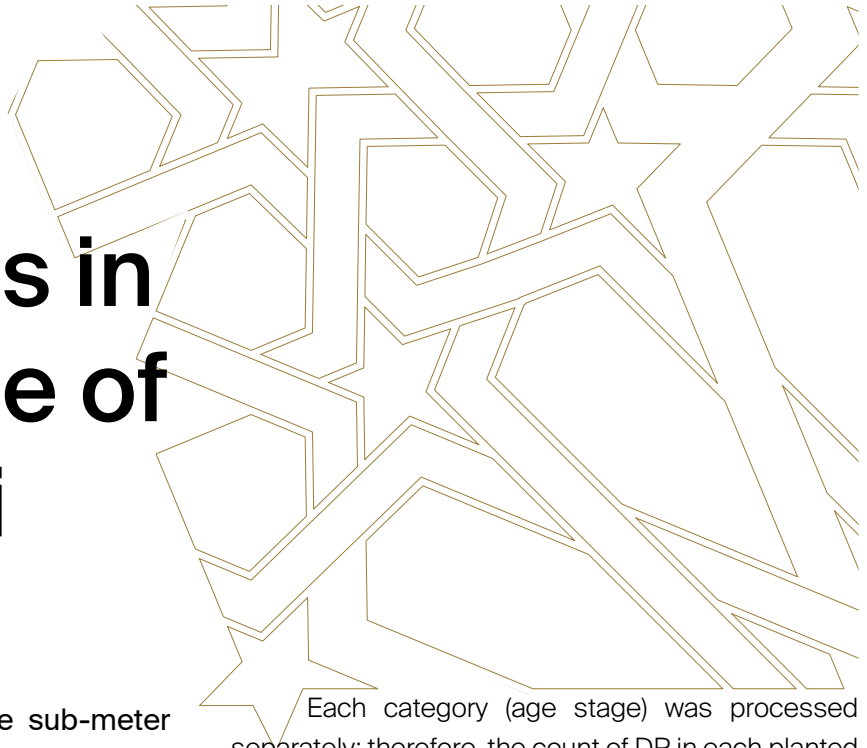
© Shutterstock

الكرونية

للنخيل



## 3.6. Counting Date Palms in the Emirate of Abu Dhabi



الكربونية

**M**apping DP using the sub-meter WV-2 instrument allowed not only to delineate the edges of DP crowns but also provide with the ability to count their numbers in Abu Dhabi. The counting of DP was simpler for non-mature DP (medium and young), where there is no overlapping between DP crowns, hence each palm was delineated by only one polygon “one entity”. However, the counting became more complicated for mature DP (i.e., full canopy producing non-district objects representing each mature DP) or, in dense planting farming systems (small spacing among palms is the common practice), where the straight forward method of counting polygons become difficult.

Each category (age stage) was processed separately; therefore, the count of DP in each planted area (young, medium, and mature) was determined by dividing the area (in meter) by the mean crown area (CA) of each DP age stage which were: 2.41 m<sup>2</sup>, 17.72 m<sup>2</sup>, and 47.78 m<sup>2</sup>, for young, medium, and mature, respectively. The total number of DP planted in the study area counted an estimated number of: 8,966,826 palms (Table 15).

**Table 15:** The preliminary results of the total numbers of the DP in AD.

Age stage (year)	Number (palm)
Young (< 5)	7,145,436
Medium (5 - 10)	943,646
Mature (> 10)	877,744
<b>Total</b>	<b>8,966,826</b>

## 3.7. Summary

**A** framework for mapping DP in the study area with varying age stages and based on integrating multi-source/multi-sensor data in a hierarchical integrated approach (HIA) was proposed. Landsat-8 OLI scenes succeeded in delineating and mapping mature DP trees with acceptable accuracy. However, it failed to depict young and medium DP, because of inadequate sensor resolutions at such level of detail.

Consequently, an object-oriented classification (OOC) approach was applied using sub-meter World-View-2 (WV-2) imagery, at the DP plantation level, to depict and map medium and young aged DP. GIS helped in converting from raster to vector formats, allowing for manual editing of certain polygons hence, increasing the accuracy of the produced maps, more specifically for young DP.

### Date Palm Area in Abu Dhabi

Class	Mature DP	Medium DP	Young DP	Total
Area (ha)	4,193.86	1,672.14	1,722.05	7,588.05
Percentage (%)	55.27	22.04	22.69	100%

The outcomes of the implemented approach were the creation of detailed and accurate maps of DP at three age stages. This step is essential in the building process of the RS-based biomass estimation model, for the assessment of the CS of DP (see Chapter 4). The produced maps were validated using existing ancillary data and field checks. The overall accuracies for young, medium, and mature DP trees were 86.8%, 88% to 90.7%, respectively; while for mixed-ages DP the value reached up to 94.5%, with an overall Kappa statistics estimated at 0.888.

الكربونية



Chapter

# 4



# **Remote Sensing Based Models for Assessing Date Palm Biomass and Carbon Stock**

©KIADPAI - Ahmed Alsaby





# 4.1. Overview

The flowchart below used to develop and validate the RS-based biomass model is presented in (Figure 25). It shows the main components of the model:

- identification of RS predictors that can be used to estimate AGB;
- selection of sample plots representing different age classes of DP (mature, medium, and young);
- collection of field data necessary to estimate AGB using the DP-specific biomass allometric equations;
- building the RS-based biomass estimation model using various regression methods and validating it by using different statistical metrics, and
- producing a map showing CS distribution throughout the emirate, by creating the AGB distribution map first, then converting it into CS distribution map. Our model was developed and implemented using ERDAS Imagine 2020, and ArcGIS 10.7 software packages.

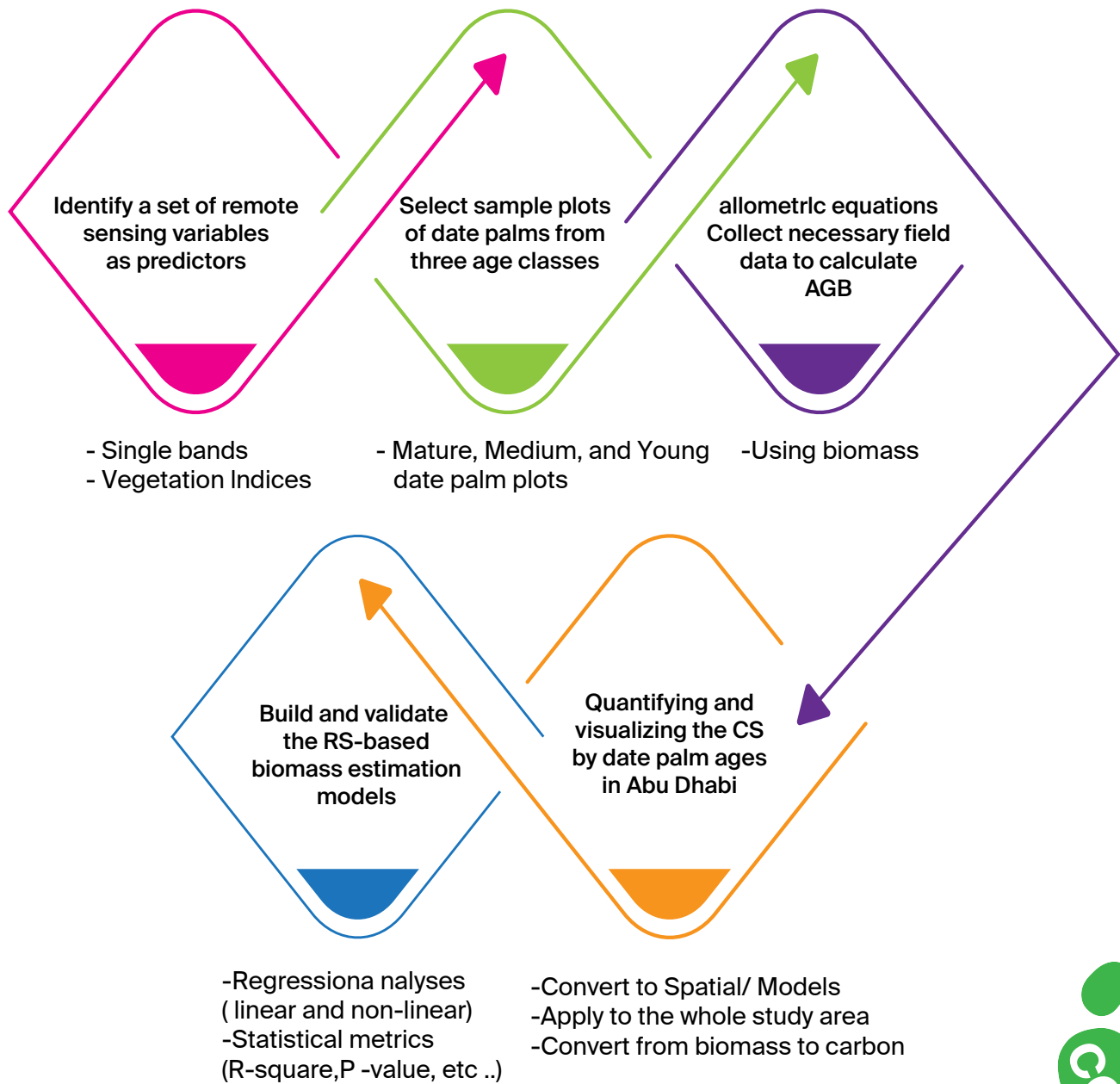
DP trees in the study area were classified according to their age into three classes: mature date palm (MDP) (more than 10 years), medium date palm (MeDP) (5-10 years), and young date palm (YDP) (less than 5 years). Two extensive field visits were conducted in Emirate of Abu Dhabi at the end of summer and during winter of 2018 targeting farms with different age stages trees, to collect data from sample units representing the three DP age stages (for geographical and environmental settings of the study area, see Appendix (7).

The first visit took place from 10<sup>th</sup> to 18<sup>th</sup> September and the second from 14<sup>th</sup> to 6<sup>th</sup> December. In all, 54 plots of DP trees were selected using a randomized probability sampling design (stratified random design) according to their age stage (MDP, MeDP, and YDP).

The plot survey included 17 representing MDP, 19 representing MeDP, and 18 representing YDP. The dimension of the plots were 40 m × 40 m, to ensure that one Landsat 30x30 meter pixel fell within each plot (Figure 26) (Issa *et al.*, 2019). The coordinates of the plot's center and the number of DP in each of the 54 plots were recorded. The mean values of these variables (single bands and VIs) for all plots were calculated using a 3 × 3 window centered over each plot and consequently used in the model development. 3x3 window was used to reduce the uncertainties in RS data resulting from plot positioning errors that could be created because of the mismatching of sample plots with the image pixels introduced when the x and y coordinates of sample plots were located using GPS (Figure 26).

Trunk height (Ht) and crown diameter (CD) for each palm were measured and subsequently used to calculate its crown area (CA), assuming a spherical palm crown ( $CA = \pi CD^2/4$ ). It is worth mentioning that we initially selected 83 field plots for surveying but had to exclude 29 of them leaving 54 only. The reasons for exclusion were: (1) sparse distribution of DP per plot (< 20 palm per plot), (2) suffering of DP from abiotic stresses (e.g., drought: direct observation in the field or/and through discussion with the farmers as some DP were deliberately not irrigated to get rid of them), and (3) the large level of heterogeneity not representing, accurately, the age stage class (mature, medium, and young).

The AGB at the plot level was estimated by using DP biomass allometric equations previously developed, specifically for DP of Abu Dhabi under arid land ecosystem conditions (Issa *et al.* 2020b). AGB for each DP was first estimated by adding crown biomass (CB) and trunk biomass (TB) using the equations presented in Table 16. AGB at the plot level was then predicted by summing



الكربونية

**Figure 25:** The flowchart for developing and validating the RS-based biomass model (Dahy et al., 2023).



the AGB for all palms in the plot and converting the results to biomass density in tons per hectare (t. ha<sup>-1</sup>).

**Table 16:** The Crown and Trunk biomass equations used for AGB (kg. palm<sup>-1</sup>) estimation of DP in study area.

Biomass Component	Allometric Equation	R <sup>2</sup>	P-value	Reference
CB	= 14.034 × 1.057 <sup>CA</sup>	0.8354	0.001	(Issa <i>et al.</i> 2020b)the authors demonstrated that combinations of visible and short wave single bands (Red, SWIR1, SWIR2
TB	= 40.725 × Ht <sup>0.9719</sup>	0.8276	0.0004	
AGB	= CB + TB			

where CB is crown biomass, TB is trunk biomass, AGB (= CB+TB) is the above-ground biomass, CA is crown area (m<sup>2</sup>), Ht is trunk height, R<sup>2</sup> is coefficient of determination.

Atmospherically corrected (Level-2) Landsat 8 OLI scenes, were used to build the RS-based model. The data which comprised different types of DP trees were

geo-registered to the UTM coordinate system (Zone 40, WGS 84). Seven bands were selected, stacked, and stored using ERDAS software package (Table 17).

**Table 17:** Details of dataset used in the current research.

Scene (Path/Row)	Date (2017)	Landsat 8 OLI Level 2 Bands (µm)	Resolution/ Swath
160/43	24 <sup>th</sup> April	Coastal (B1): 0.433–0.453, Blue (B): 0.450–0.515, Green (G): 0.525–0.600 Red (R): 0.630–0.680, NIR: 0.845–0.885, SWIR1: 1.560–1.660, and SWIR2: 2.100–2.300	30 meters. Swath area is 185 km.
160/44	26 <sup>th</sup> May		
161/43	15 <sup>th</sup> April		
161/44	15 <sup>th</sup> April		
162/43	22 <sup>nd</sup> April		
162/44	22 <sup>nd</sup> April		

الكربونية

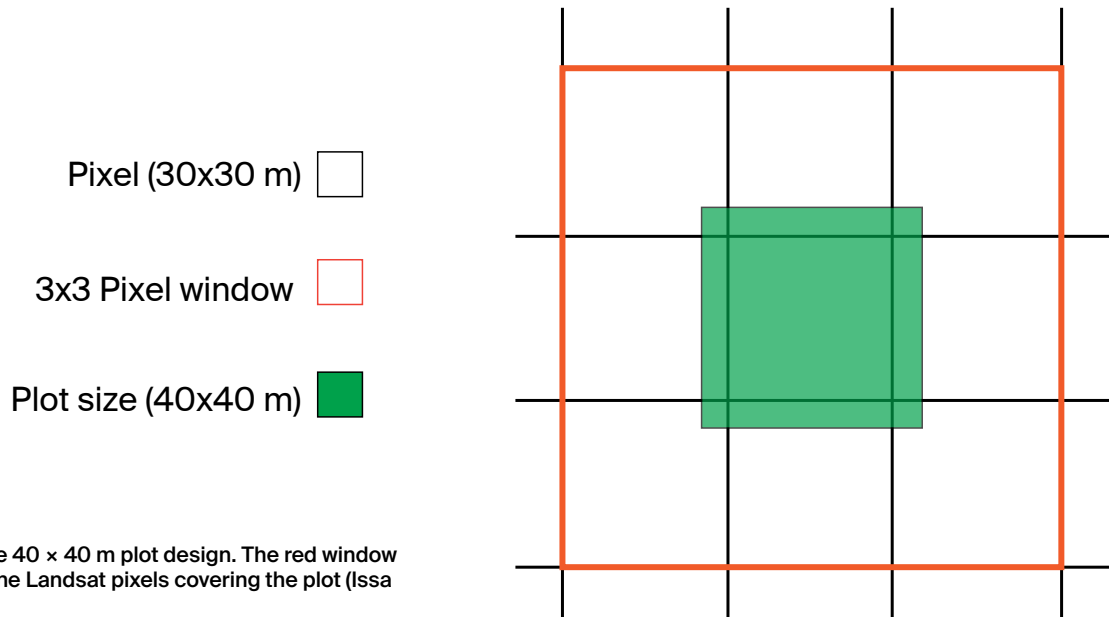


**Figure 26:** The 40 × 40 m plot design. The red window delimits the nine Landsat pixels covering the plot (Issa *et al.* 2019).

A combination of individual reflective bands and VIs were used as remote sensing predictors

to estimate AGB. Both reflective bands listed in Table 18.

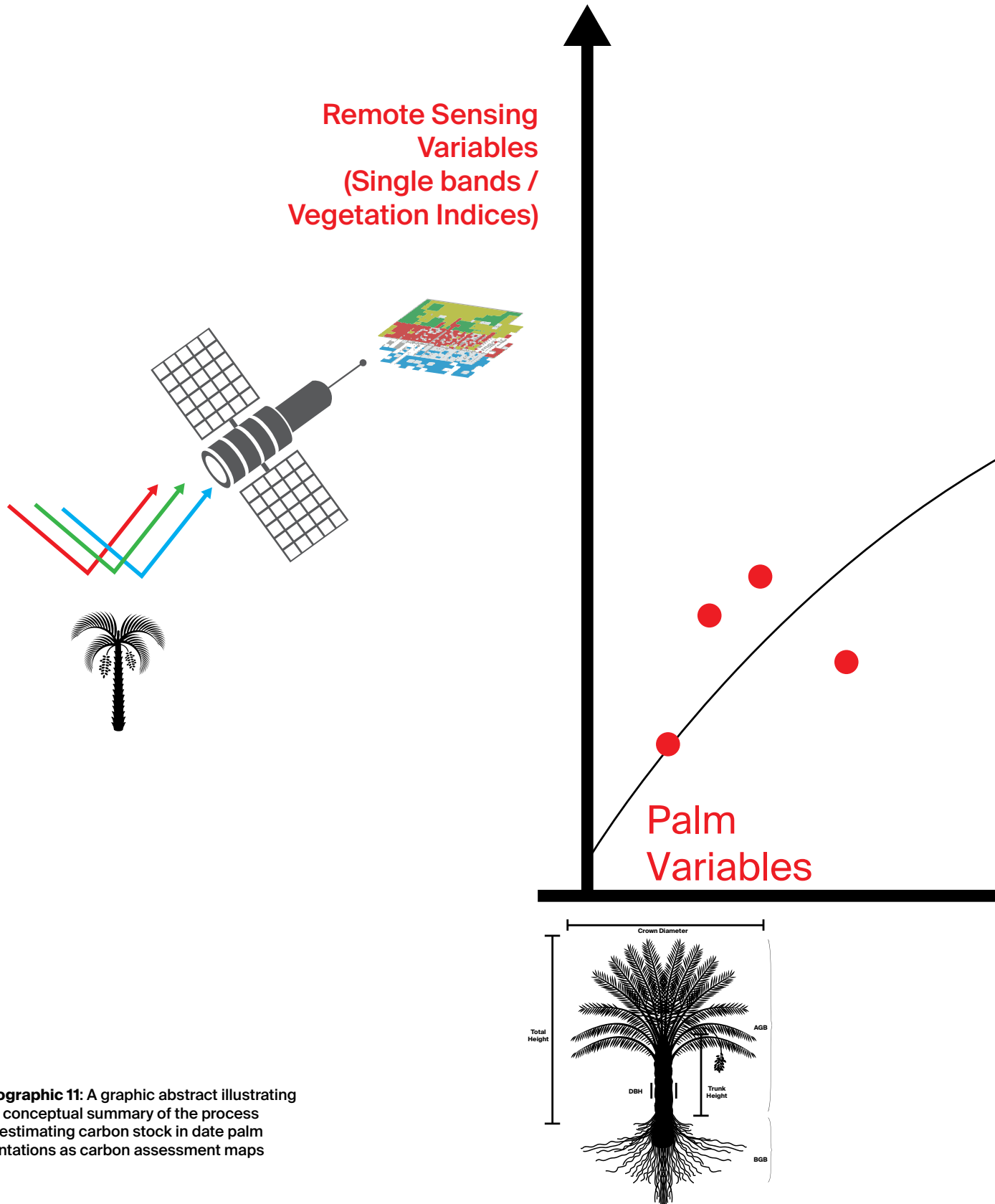
**Table 18:** Selected Landsat 8 OLI-derived vegetation indices (VIs).

VIs	Equation	Source
SR	$NIR/R$	(Birth and McVey, 1968)
RVI	$R/NIR$	(Pearson and Miller, 1972)
DVI	$NIR-R$	(Tucker, 1979)
NDGI	$(G-R)/(G+R)$	(Courel <i>et al.</i> , 1991)
NDVI	$(NIR-R)/(NIR+R)$	(Rouse, 1974)
TVI	$\sqrt{(NDVI + 1)}$	(Srestasathiern and Rakwatin, 2014)
GNDVI	$(NIR-G)/(NIR+G)$	(Gitelson <i>et al.</i> , 1996)
RDVI	$(NIR - R)/\sqrt{(NIR + R)}$	(Roujean and Breon, 1995)
SAVI	$(1.5 \times (NIR - R))/(NIR + R + 0.5)$	(Huete, 1988)
MSAVI	$0.5 \times [2 R_{NIR} + 1 - \sqrt{(2 R_{NIR} + 1)^2 - 8 (R_{NIR} - R_{red})}]$	(Qi <i>et al.</i> , 1994) however, the L factor should vary inversely with the amount of vegetation present. A modified SAVI (MSAVI
TCG	$-0.2941 \times B - 0.2430 \times G - 0.5424 \times R + 0.7276 \times NIR + 0.0713 \times SWIR1 - 0.1608 \times SWIR2$	(Baig <i>et al.</i> , 2014)
TCB	$0.3029 \times B + 0.2786 \times G + 0.4733 \times R + 0.5599 \times NIR + 0.5080 \times SWIR1 + 0.1872 \times SWIR2$	(Baig <i>et al.</i> , 2014)
TCW	$0.1511 \times B + 0.1973 \times G + 0.3283 \times R + 0.3407 \times NIR - 0.7117 \times SWIR1 - 0.4559 \times SWIR2$	(Baig <i>et al.</i> , 2014)

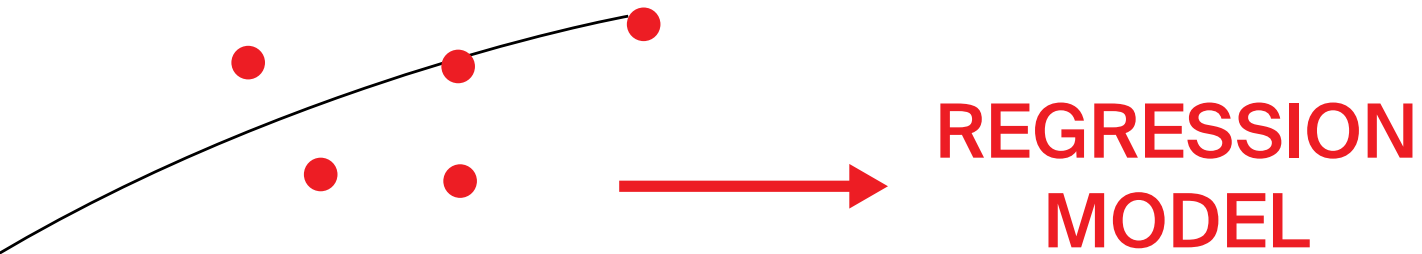
where SR is the simple ratio, RVI is the ratio vegetation index, DVI is the difference vegetation index, NDGI is the normalized difference greenness index, NDVI is the normalized difference vegetation index, TVI is the transformed vegetation index, GNDVI is the green normalized difference vegetation index, RDVI is the renormalized difference vegetation index, SAVI is the soil-adjusted vegetation index, MSAVI is the modified soil adjusted vegetation index, TCG is the tasseled cap transformation index for greenness, TCB for brightness and TCW for wetness.

Different regression types (linear and non-linear) were considered to evaluate the relationships between RS predictors and AGB values for each plot predicted from ground measurements and allometric equations. Linear regression model was first tested, and their performance assessed based on their coefficients of determination ( $R^2$ ) and significance ( $P$ -value < 0.05). A stepwise multiple linear regression analysis, involving several single bands and VIs, was subsequently applied to achieve improved correlation.





**Infographic 11:** A graphic abstract illustrating the conceptual summary of the process for estimating carbon stock in date palm plantations as carbon assessment maps



**REGRESSION  
MODEL**

الكربونية

**Field  
Variables**

**(Biomass / Carbon)**



**Mapping  
the Carbon Stock**



للنخيل

The AGB estimation model was assessed using cross-validation for each plot; Root Mean Square Error (RMSE), RMSE%, and the systematic prediction error (SPER)s, were estimated in percentage after randomly splitting the plot measurements dataset into a calibration dataset (80%), and a validation dataset (20%). The RMSE, RMSE%, and SPER were estimated using the equations 7, 8, and 9.

$$\text{RMSE} = \sqrt{\frac{\sum(\hat{y}_i - y_i)^2}{n}} \quad \text{Equation (7)}$$

$$\text{RMSE \%} = 100 \times \frac{\text{RMSE}}{\bar{y}} \quad \text{Equation (8)}$$

$$\text{SPER} = \hat{y}_i - \bar{y}_i \quad \text{Equation (9)}$$

where ( $\hat{y}_i$ ) is the predicted  $\hat{\text{AGB}}$  of the  $i$ th plot, ( $\bar{y}_i$ ) is the observed AGB of the  $i$ th plot, ( $y$ ) is the mean of predicted  $\hat{\text{AGB}}$ , and ( $\bar{y}$ ) is the mean observed AGB.

Maps of DP trees, created in a previously published study (Dahy *et al.*, 2021), were used in the model to delineate the location of DP at different age stages. The reported accuracy of these maps was significantly high with overall classification accuracy of 94.5%, and a kappa coefficient of 0.888. They showed that DP trees covered an area of about 7,588.04 hectares (22.69% for YDP, 22.04% for MeDP, and 55.27% for MDP). Subsets of Landsat 8 OLI images corresponding to DP trees as defined in the DP maps were extracted using ERDAS imagine and used as input to the RS-based biomass model.

The spatial model that estimates the amount of AGB ( $\text{t. ha}^{-1}$ ) for each Landsat pixel was implemented and run in the Spatial Model Editor within ERDAS Imagine to estimate and create an AGB map of the study area. The produced map was subsequently used as input to estimate the density of above-ground carbon ( $\hat{\text{AGC}}$ ) for each pixel according to equation 10, based on a previously published carbon content to AGB ratio of 53.87% (Issa *et al.*, 2020b).

$$\text{AGC (t. ha}^{-1}\text{)} = 0.5387 \times \text{AGB (t. ha}^{-1}\text{)} \quad \text{Equation (10)}$$

To estimate AGB and AGC content (in ton),  $\hat{\text{AGB}}$  and  $\hat{\text{AGC}}$  density values ( $\text{t. ha}^{-1}$ ) produced by the model for each pixel were multiplied by the pixel size using the Attribute Table Function in ERDAS Imagine.  $\hat{\text{AGB}}$  (in ton) was subsequently used to estimate the other carbon components involving biomass as described below.

The total amount of CS was estimated as the sum of the carbon content of each of the following five biomass components: AGB, below-ground biomass (BGB), litter, woody debris, and soil organic matter (SOM) (Eggleston *et al.*, 2006). BGB, litter, and debris were predicted from the estimated AGB value. The soil organic carbon (SOC) was deduced from the SOM amount which was estimated as 91.38%.

### Below-ground biomass (BGB)

BGB is generally estimated at 20% of the AGB in several published studies (Cairns *et al.*, 1997; Koala *et al.*, 2017; Mokany *et al.*, 2006; Niether *et al.*, 2019). However, we found different ratios among different DP age stages with averages of 0.332, 0.925, and 0.496 for YDP, MeDP, and MDP, respectively (Issa *et al.* 2020b). Therefore, the following equations (11, 12, and 13) were developed to estimate BGB of DP:

$$\text{BGB}_{\text{MDP}} (\text{t}) = \text{AGB} (\text{t}) \times 0.496 \quad \text{Equation (11)}$$

$$\text{BGB}_{\text{MeDP}} (\text{t}) = \text{AGB} (\text{t}) \times 0.925 \quad \text{Equation (12)}$$

$$\text{BGB}_{\text{YDP}} (\text{t}) = \text{AGB} (\text{t}) \times 0.332 \quad \text{Equation (13)}$$

On the other hand, the percentage of carbon content in the root system of DP (BGB) was found to be 51.27% (Issa *et al.*, 2020b), which is slightly lower than the carbon content in the AGB. Therefore, below-ground carbon ( $\hat{\text{BGC}}$ ) was estimated in tons by multiplying the resulting values from equations 11, 12, or 13 by a factor of 0.5127 (equation 14).

$$\text{BGC} (\text{t}) = 0.5127 \times \text{BGB} (\text{t}) \quad \text{Equation (14)}$$

### Litters, and Woody Debris

Carbon content of dead wood or litter and woody debris were assumed to be between 10 and 20% of the AGB (Gibbs *et al.*, 2007; Houghton *et al.*, 2009; Issa *et al.*, 2020a). The borders between dead biomass and litter, and between dead biomass and SOM, are rather subjective (Houghton *et al.*, 2009). Based on extensive field visits to DP farms at different age stages, it was observed that litter and debris ratio to AGB of DP varied depending on the palm age stage. The more the palm matures, the more it produces litter and debris. The researchers adopted the following percentages to be applied to predict litter and debris (in ton) from AGB (in ton), for DP trees; 10% for YDP, 15% for MeDP, and 20% for MDP.

### Soil Organic Carbon (SOC)

The DPs contribute about 22.26 tons of SOC per hectare in trees (Issa *et al.*, 2020b). This number was calculated by performing the combustion method for 4 hours at 550°C on soil samples taken at top soil (10 cm) from underneath the DP canopy, and then deriving of the SOM, and the SOC. Furthermore, the SOC (in ton) of DP for the three age stages were calculated as per equation 15.

$$\text{SOC} = \text{Area} \times 22.26 \text{ t. ha}^{-1} \quad \text{Equation (15)}$$

where the total areas of MDP, MeDP, and YDP in the study area were estimated to be 4,193.86 ha, 1,672.14 ha, and 1,722.05 ha, respectively (Dahy *et al.*, 2021).

Finally, ERDAS spatial modelling tools were used to produce the AGB map for the whole study area utilizing the selected model built from the RS variables as estimated by the results of our analyses. AGC map was then created by multiplying the estimated AGB by 0.5387 as per the equation 10.



## 4.2.

# Descriptive Statistics of the Structural Field Variables Assessed



الكربونية

Structural variables of 2063 palms included in the 54 plots were measured in the field. Statistics about these measurements including the number of DP for each age stage class, average CA, Ht, and densities of DP per hectare, are summarized in Table 19. The average palm CA in me-

ter and its standard error ( $\pm$ SE) of the MDP, MeDP, and YDP plots were 36 ( $\pm$ 1.64), 22.51 ( $\pm$ 1.22), and 6.65 ( $\pm$ 0.67) m<sup>2</sup>, respectively.

The average palm Ht's of the MDP, MeDP, and YDP plots were 2.89 ( $\pm$ 0.22), 1.07 ( $\pm$ 0.08), and 0.15 ( $\pm$ 0.03) m, respectively. It is obvious that the increase in DP age results in an increase in CA and Ht. The averages of DP number per plot of MDP, MeDP, and YDP were 41, 38, and 35, respectively, which, based on a plot area of 1600 m<sup>2</sup>, amounts to around 258, 238, and 221 palm. ha<sup>-1</sup>, respectively.

**Table 19:** Crown area (CA), trunk height (Ht), and density values of DP for each age stage.

DP Age Stage	No. Palms	Average CA (m <sup>2</sup> )	Average Ht (m)	Avg. Density (palm. ha <sup>-1</sup> )
MDP	701	36 (19.54 - 44.15)	2.89 (1.90 - 5.07)	258 (131 - 600)
MeDP	725	22.51 (11.85 - 32.45)	1.07 (0.39 - 1.64)	238 (131 - 450)
YDP	637	6.65 (2.52 - 13.94)	0.15 (0 - 0.37)	221 (144 - 306)

where MDP is mature date palm, MeDP is medium date palm, and YDP is young date palm. The numbers in the parenthesis represent the minimum and maximum values.

## 4.3. The Field Based Biomass Estimation Model of Date Palm and Estimating its Carbon

**A**  $\hat{C}B$  was estimated from the field measurement in all 54 plots. Table 6 shows the average and range of

AGB in ( $t. ha^{-1}$ ) for DP at the three age stages. The largest  $\hat{C}B$  was found in MDP plots while the lowest  $\hat{C}B$  was found in YDP plots.

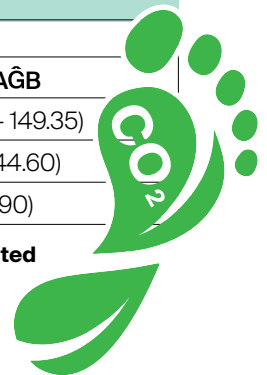
الكربونية

These outcomes were affected by the average CA of the plots (Table 20). Similarly,  $\hat{T}B$  was affected by the Ht average (Table 20). The averages of  $\hat{A}GB$  in tons per hectare ( $\pm SE$ ) of MDP, MeDP, and YDP were estimated at 59.39 ( $\pm 7.8$ ), 23.33 ( $\pm 2.5$ ), and 6.15 ( $\pm 0.5$ )  $t. ha^{-1}$ , respectively. The  $\hat{A}GC$  in ( $t. ha^{-1}$ ) was estimated by multiplying the average  $\hat{A}GB$  in tons per hectare by 0.5387 (see equation 10). Therefore, the averages  $\hat{A}GC$  ( $\pm SE$ ) for MDP, MeDP, and YDP plots were estimated at 31.99 ( $\pm 4.2$ ), 12.57 ( $\pm 1.4$ ), and 3.31 ( $\pm 0.3$ )  $t. ha^{-1}$ .

**Table 20:** The averages and ranges of  $\hat{A}GB$  ( $\hat{C}B$  and  $\hat{T}B$ ) at each DP age stage.

DP Age Stages	No. Plots	Biomass ( $t. ha^{-1}$ )		
		$\hat{C}rown$ Biomass	$\hat{T}runk$ Biomass	$\hat{A}GB$
MDP	17	29.02 (12.45 - 49.49)	30.37 (11.95 - 106.76)	59.39 (24.41 - 149.35)
MeDP	19	13.34 (5.62 - 27.21)	9.98 (4.18 - 20.63)	23.33 (11.11 - 44.60)
YDP	18	4.85 (2.72 - 8.16)	1.30 (0 - 4.08)	6.15 (2.72 - 9.90)

where MDP is mature date palm, MeDP is medium date palm, YDP is young date palm, and  $\hat{A}GB$  is the estimated above-ground biomass. The numbers in the parenthesis represent the minimum and maximum values.



## 4.4. The Remote Sensing Based Biomass Estimation Models

الكربونية

As the DP age has an important role in their biomass (Table 20), the regression analysis linking the field variables with the RS predictors was conducted according to the DP age stages defined earlier.

### 4.4.1. Mature Date Palm Model

In MDP plots (17 plots), the linear correlation between AGB and single bands was only significant for SWIR bands; at the same time, it was significant for all tested VIs except TCB and TCG (appendix 8). The highest correlation was for SWIR1 and SWIR2 bands with R2 values of 0.302 and 0.290, respectively. While for VIs, NDGI and SR showed the highest correlation, with R2 values of 0.609 and 0.545, respectively.

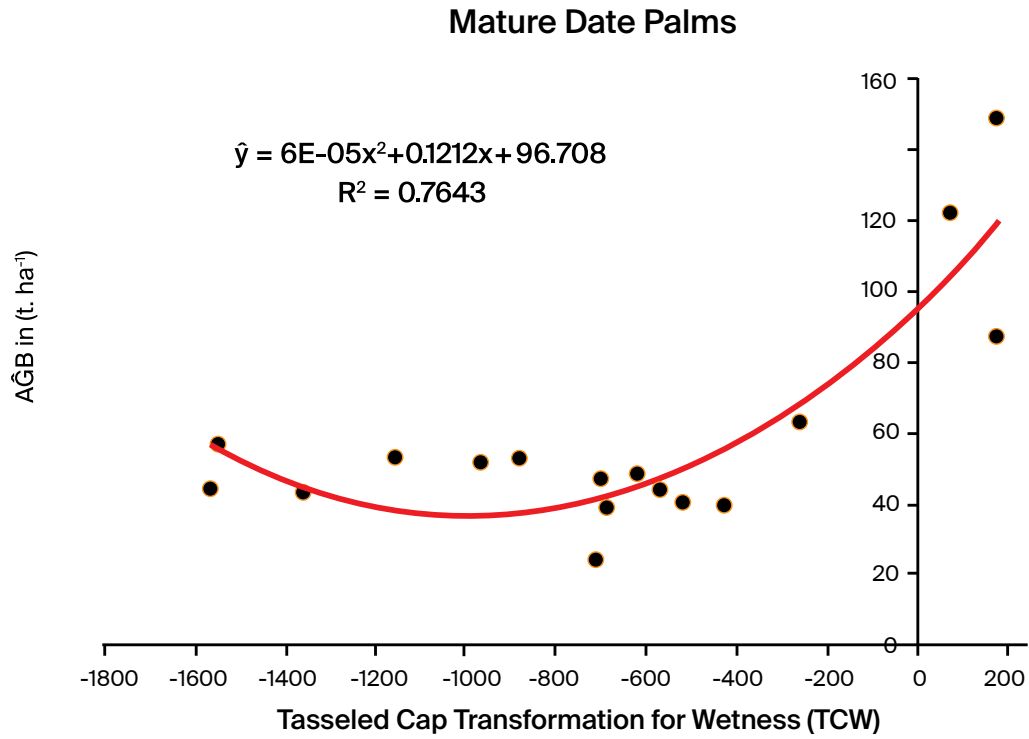
On the other hand, TCW showed the strongest correlation to AGB using a second-order polynomial model. Additionally, stepwise multiple regression analysis on AGB of the MDP revealed that a grouping of single bands or of VIs did not improve the R2. Therefore, the second-order polynomial model that uses only TCW as RS predictor was found to be the strongest model to estimate the biomass of MDP with R<sup>2</sup> equal 0.7643 and P-value equal of 0.007 (equation 16 and Figure 27).

$$\text{AGBMDP (t. ha}^{-1}\text{)} = 0.00006 \times \text{TCW}^2 + 0.1212 \times \text{TCW} + 96.708 \quad \text{Equation (16)}$$

### 4.4.2. Non-Mature Date Palm Model

It was found that R2 could be improved by considering medium and young DP as one age class, the non-mature class (Non-MDP) (appendix 8). Running the regression analysis for Non-MDP (37 plots: the combination of MeDP and YDP) resulted in a stronger correlation between AGB and RS predictors. All of Landsat 8 OLI single bands with the exception of B, G, and NIR, and all the VIs except NGVI, exhibited significant correlation with AGB. The stepwise regression analysis on AGB of the Non-MDP revealed that a grouping of single bands or VIs did not improve the R2. The exponential regression model using RDVI yielded the strongest correlation with an R2 value of 0.4987 and P-value equals 0.00002 (equation 17 and Figure 27).

$$\text{AGB}_{\text{Non-MDP}} \text{ (t. ha}^{-1}\text{)} = 0.8257 \times e^{0.1469 \times \text{RDVI}} \quad \text{Equation (17)}$$



الكربونية

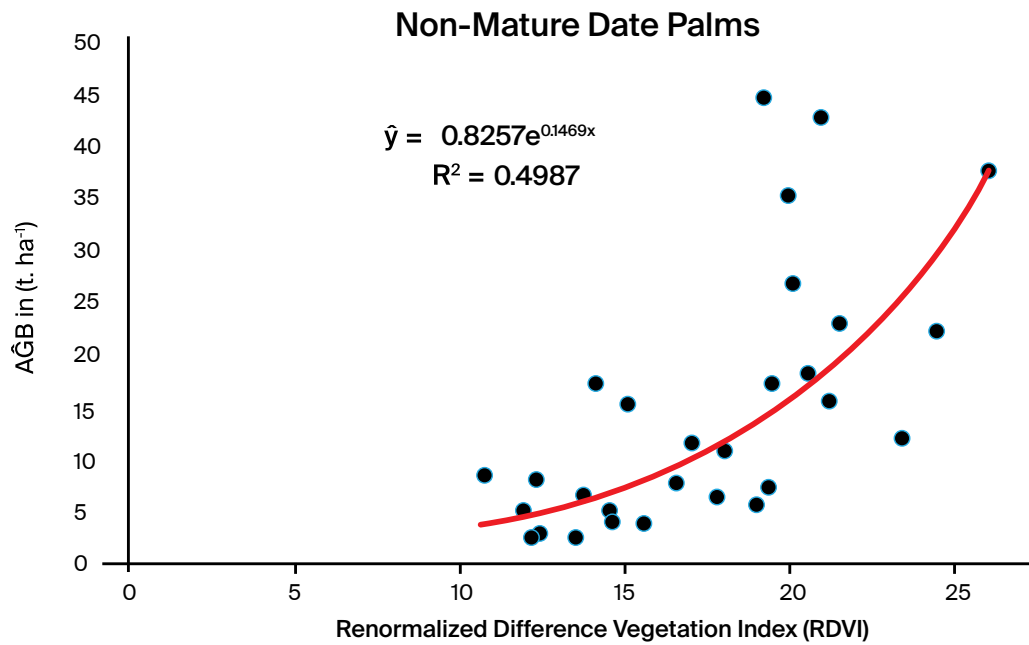


**Figure 27:** AGB for DP as function of TCW and RDVI. (a) for mature DP, and (b) for non-mature DP.



## 4.5. Models Validation

Field measurements and the statistical accuracy assessment were used to validate the developed AGB model. The accuracy statistics included RMSE, RMSE%, and SPEr. Table 21 summarizes the selected regression models for the estimation of the AGB from Landsat 8 OLI single bands and VIs.

**Table 21:** Model(s) used for AĜB estimation (t. ha<sup>-1</sup>) for mature and non-mature date palms

Regression Model	DP Class	R2	P-value	RMSE	RMSE%	SPEr
$A\hat{G}B = 0.00006(TCW)^2 + 0.1212(TCW) + 96.708$	Mature	0.764	0.007	6.322	14.912	1.43
$A\hat{G}B = 0.8257 \times 1.1582^{(RDVI)}$	Non-mature	0.4987	0.00002	8.040	51.376	-5.04

الكربونية

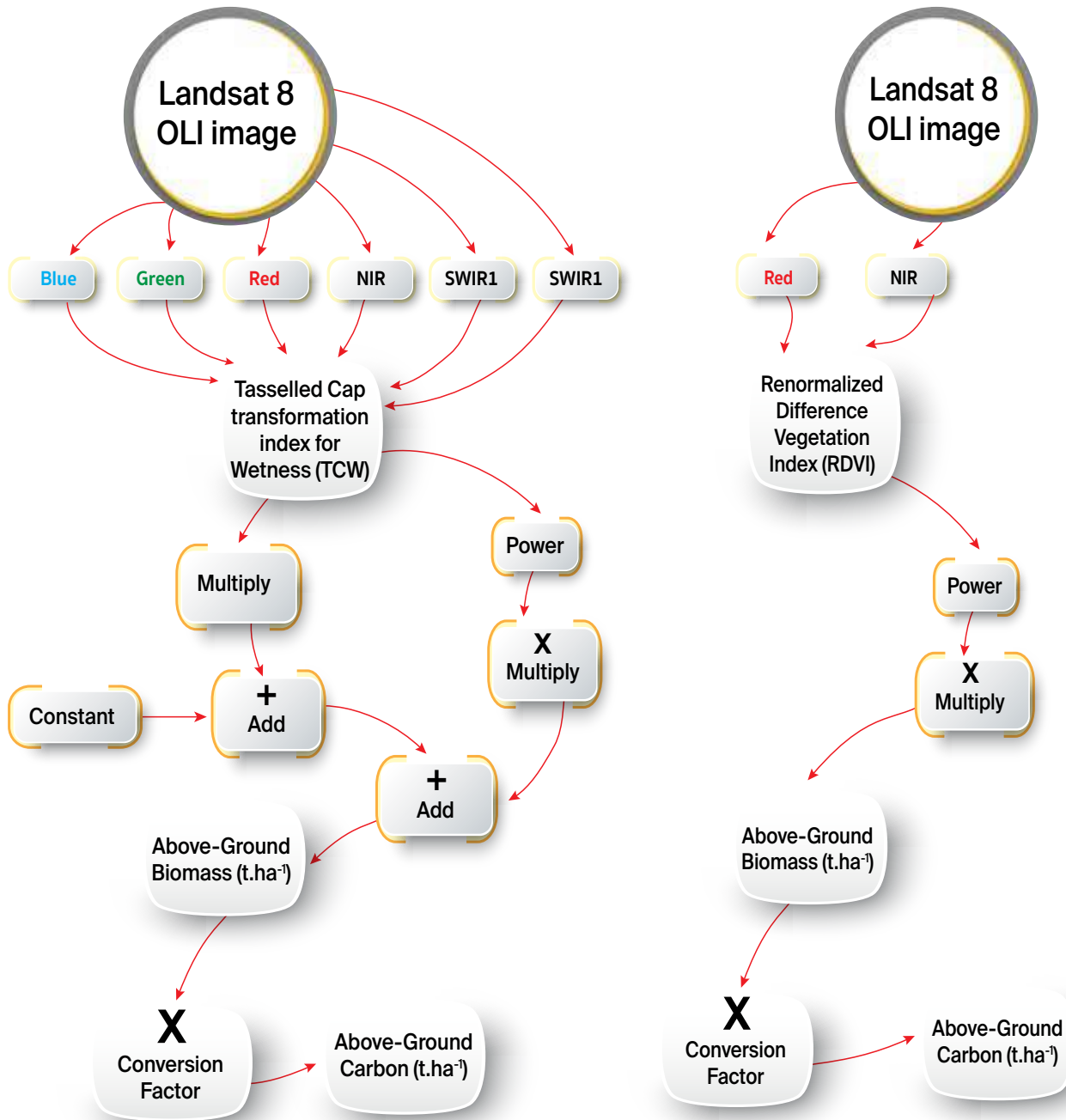


**Figure 28:** Pipeline of the spatial modeler used to build the two sub-models for calculating CS in DP: (a) MDP model and (b) Non-MDP Model.



## 4.6. Creation of the Aboveground Carbon Map of Date Palm Trees

الكربونية

The final AGB map was created using the regression models shown in Table 21. The two sub-models that use TWC for MDP and RDVI for Non-MDP are depicted in Figure 28.

The map of AGC, shown in Figure 29, is predicted from AGB map using equation 10.

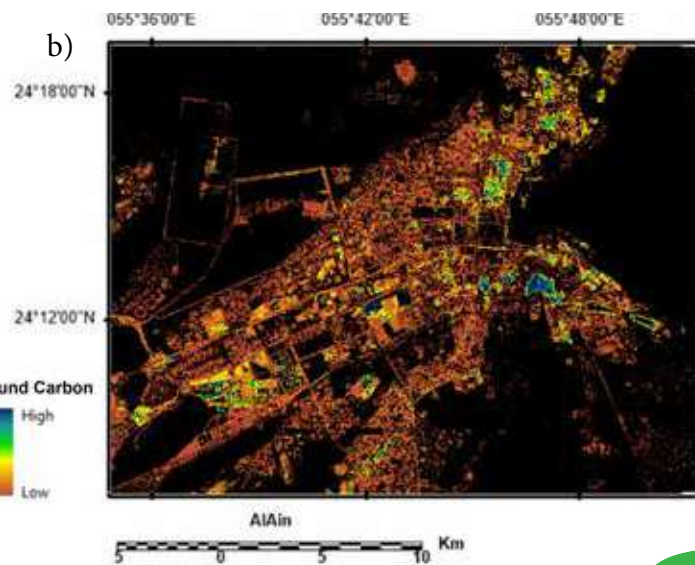
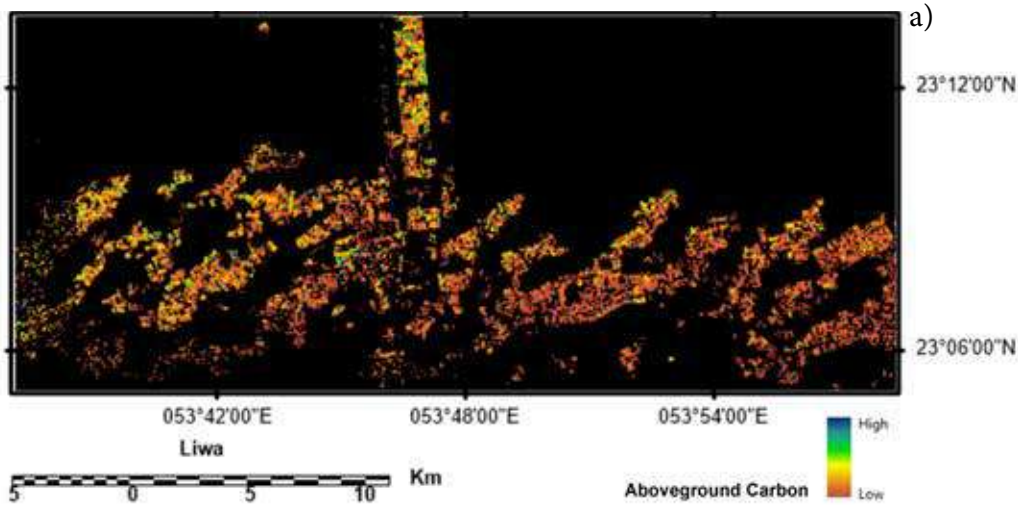
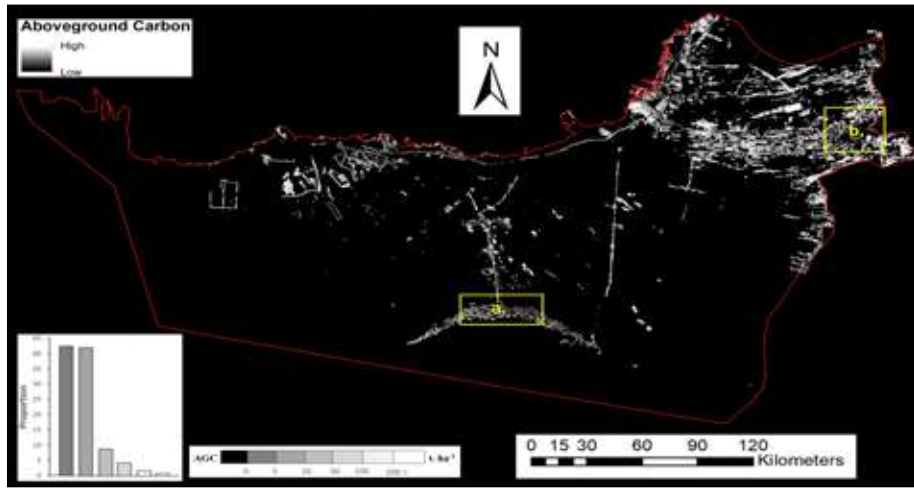


**Figure 29:** The aboveground carbon (AGC) map of DP in the study area (Abu Dhabi). Two areas were zoomed where the different shades of greyscale are obvious: (a) Liwa and (b) Al Ain. The lighter pixels (digital number), the more amount of AGC (t. ha<sup>-1</sup>). The black color represents areas without DP.

الكربونية



# 4.7. Estimating the Total Carbon Stock of Date Palm Trees



الكربونية

Table 22 summarizes the results of the CS analysis. We found that the overall CS by DP trees in Abu Dhabi was **2,447,856.87** tons.

**Table 22: The total CS (in Mt) by DP trees in Abu Dhabi, UAE.**

DP Class	Above-Ground		Below-Ground		Litter & Debris		SOC	Total
	A <sup>g</sup> B	A <sup>g</sup> C	B <sup>g</sup> B	B <sup>g</sup> C	Biomass	C		
MDP	1.210	0.652	0.600	0.308	0.242	0.130	0.093	<b>1,183</b>
MeDP	0.384	0.207	0.356	0.182	0.058	0.031	0.037	<b>0.458</b>
YDP	1.008	0.543	0.335	0.172	0.101	0.054	0.038	<b>0.807</b>
Total	2.602	1.402	1.290	0.662	0.400	0.216	0.169	<b>2.448</b>

Mt = 1 million tons.

# 4.8. Summary

Data from Landsat 8 OLI were used to assess the correlation between spectral reflectance and different VIs on one side, and AGB derived from ground measurements on the other. RS data of moderate resolution such as the freely available long record of Landsat satellite imagery were used successfully to build a RS-based biomass estimation models at different age stages of DP (mature DP and non-mature DP).

The allometric equations developed previously (see Chapter 2) provided an important element in the design, libration, and implementation of a novel approach to assess AGB (ton. ha<sup>-1</sup>) and to estimate CS stored (ton. ha<sup>-1</sup>) in DP trees. The relationships between the estimated AGB and parameters derived from RS data were tested using single and multiple linear regression analysis.

The obtained results helped identify the RS predictors that exhibited the highest and most significant

correlation with AGB calculated from field measurements and the allometric equations developed in this study. Models using these predictors were adopted to estimate AGB from RS data for the different age classes of DP consequently map and estimate CS for the whole study area (see Table 23).

For mature DP class alone (>10 years), the strongest correlation between AGB and RS predictors was found for the VI TCW using a second-order polynomial equation with R<sup>2</sup> equal to 0.7643 and P value equal to 0.007. For medium DP, the second-order polynomial equation that uses only DVI as RS predictor is the strongest model to estimate the biomass of medium DP with R<sup>2</sup> equal to 0.2286 and P value equal to 0.049. While for young DP, the linear regression equation that uses only NIR as RS predictor is the strongest model to estimate the biomass of young DP with R<sup>2</sup> equal to 0.2828 and P value equal to 0.023.

However, combining these two classes into one non-mature class yielded a stronger and more significant correlation. An exponential regression equation that uses RDVI as RS predictor was the best single VI and had the strongest correlation among all RS variables of Landsat 8 OLI for AGB of non-mature DP, with an R2 value of 0.4987 and P value equal 0.00002. Finally, the models applied on the DP maps of Abu Dhabi that were produced previously (see Chapter 4) to map and quantify the CS of DP of Abu Dhabi. The overall CS by DP trees in Abu Dhabi (including the five components: AGB, BGB, litter, debris, and SOC) is 2,447,856.87 tons with an average of 322.6 ton.ha-1 (see Table 22).

الكربونية

**Table 23: RS predictive variables used in the RS based biomass models**

RS Model	Vegetation Indices	Significant Variables
<p><b>Model 1 (Mature):</b></p> $AGB = 0.00006(TCW)^2 + 0.1212(TCW) + 96.708$	<p>TCW:  <math>(= 0.1511 \times B + 0.1973 \times G + 0.3283 \times R + 0.3407 \times NIR - 0.7117 \times SWIR1 - 0.4559 \times SWIR2)</math></p>	<p>B (0.450–0.515 μm)                      G (0.525–0.600 μm)                      R (0.630–0.680 μm)                      NIR (0.845–0.885 μm)                      SWIR1(1.560–1.660 μm)                      SWIR2 (2.100–2.300 μm)</p>
<p><b>Model 2 (Non-Mature):</b></p> $AGB = 0.8257 \times 1.1582^{(RDVI)}$	<p>RDVI:  <math>(NIR - R) / (NIR + R)</math></p>	<p>R (0.630–0.680 μm)                      NIR (0.845–0.885 μm)</p>

Where B is blue band, G is green band, R is red band, NIR is near infrared band, and SWIRs are shortwave infrared bands.



Chapter

# 5



# Discussion

© KIADPAI - Abdullah Al Rwais





# 5.1. Biomass Allometric Equations & Carbon Stock of Date Palm

الكربونية

One of the first steps in the development of models for estimation CS was the development of allometric equations that relate AGB to palm structural variables. In previous studies, some authors used fresh weight to build allometric equations, as it was the case in some southern Asia oil palms studies (Dewi et al., 2009; Khalid et al., 1999a). Others used dry weight as in some tropical and west African regions (Corley et al., 1971; Thenkabail et al., 2004) (see Appendix 1). For DP, it was found that the correlation coefficient between the total fresh and dry weights of DP to be 0.99, in agreement with values usually recorded in palm experiments (Corley et al., 1971).

Consequently, dry weight was adopted as a surrogate to develop specific allometric equations for the calculation of AGB of DP in the UAE. Results showed

that the dry weight of DP averaged 42% of their fresh weight (Chapter 2, Table 5). When considering the trunk alone, that ratio averaged around 37%. This is higher than trunk dry/wet ratios of 20% reported in other studies (Khalid *et al.*, 1999a) and can be attributed to the conditions of desert ecosystems where plants adapt to water stress due to the limited availability of water intake (Aronson *et al.*, 1992; Felker, 2009; Figueiredo *et al.*, 1999; Kappen *et al.*, 1972; Mwanamwenge *et al.*, 1999; Ramos *et al.*, 2003).

The total palm biomass was calculated as the sum of AGB and BGB, where BGB was derived from AGB using different ratios according to age stage. The ratio of BGB to AGB in DP was estimated at 0.33 for young DP. Such ratio increased to 0.92 for medium DP and decreased to about 0.5 for mature DP. The increase observed in medium age may be attributed to the substantial growth of the palm's root system at this age stage to support the emergence of the trunk and help the palm keep balance.

Resource allocation within plants generally is affected by biotic and abiotic stresses (Ketterings *et al.* 2001; Koala *et al.* 2017; Litton and Boone Kauffman 2008; Adam and Jusoh 2018; Diédhiou *et al.* 2017). Still, in the current case the BGB to AGB ratios in DP, at all age stages, were found to be consistently higher than the ratio of 0.2, commonly used by many researchers for other forest species biomass estimation (Achard *et al.*, 2002; Cairns *et al.*, 1997; Gibbs *et al.*, 2007; Houghton *et al.*, 2009; Mokany *et al.*, 2006; Ramanikutty *et al.*, 2007).

It is important to note that these published ratios were derived from regular tree species, other than palms, in tropical, boreal and temperate ecosystems which are completely different from those growing in desert ecosystems (Mokany *et al.*, 2006). DP species in particular, show unique plant architecture and anatomical characteristic (Da Silva *et al.*, 2015).

Age stages have substantially affected biomass accumulating in DP. In young DP, with no developed trunk, the AGB averaged 22.5 Kg.palm<sup>-1</sup>. Progressively,

AGB increased with age where medium palms AGB increased to an average of 94.7 Kg.palm<sup>-1</sup> due to the trunk development and the increase in number and diameter of crown fronds (Figure 30). The increase in AGB continued in mature palms to exceed 284 Kg.palm<sup>-1</sup>. The percentage of AGB to total biomass also varied during growth with averages of 75.1%, 51.9% and 66.8% for young, medium and mature palms, respectively. The average AGB to total biomass ratio was found to be 64.3%.

The high correlation between age and biomass indicated that age was the best parameter to estimate AGB of DP with three distinguished stages of storing biomass.

Firstly, young DP stage, where most of the biomass was stored in its crown representing about 75.11% of the total biomass.

Secondly, medium aged DP where trunk started developing and taking a portion from the total biomass (around 16.2%). This portion was offset by dou-

bling that of the root biomass from 24.89% to 48.06% of the total biomass.

Thirdly, mature DP where the dry biomass was distributed equally among the three palm components (crown, trunk and root).

Similarly, Henson and Chang (2003) used age to calculate the standing biomass of oil palm while Corley and Tinker (2008) found that the density of dry trunk increased with palm age. The regression analysis of age with AGB of the DP showed that CB increased at about 14% per year and that TB increased 18% yearly.

Nonetheless, age is a non-structural variable that cannot account for biomass variations within the same stage in a plantation and measured directly in the field (Korom *et al.*, 2016). In addition, it does not satisfy the aim of identifying variables that can be directly measured by RS and hence provide an alternative approach to estimating the biomass and CS in DP trees (Salem Issa *et al.*, 2019).

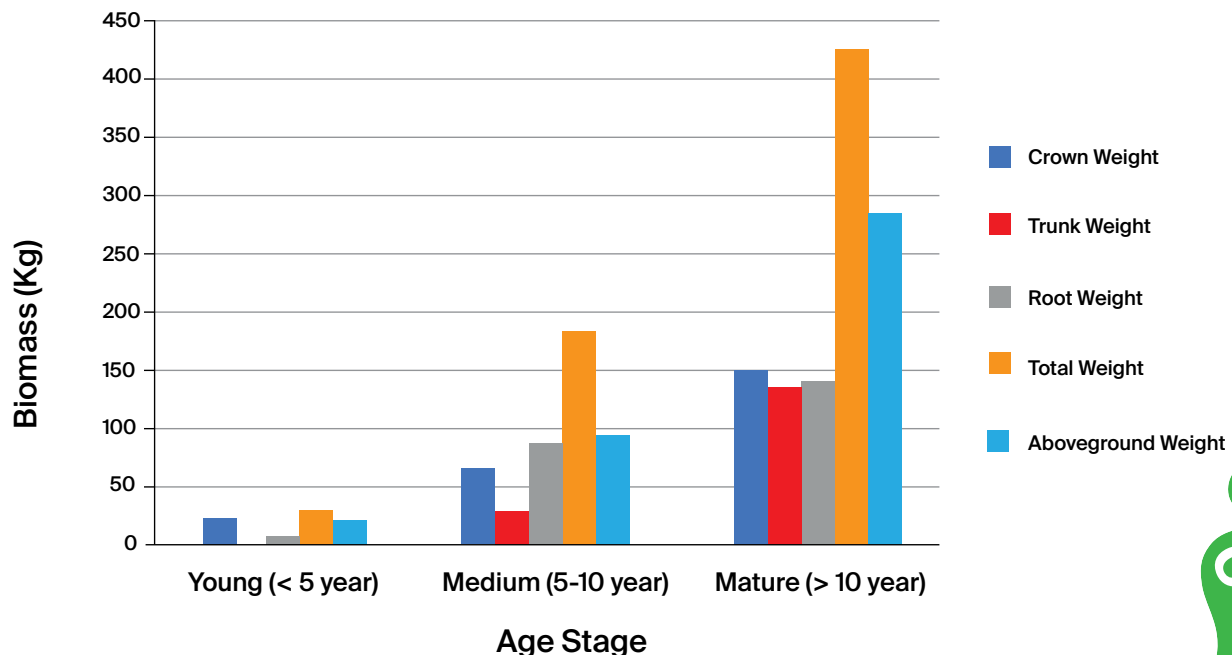


Figure 30: The biomass (dry weight) of DP versus age stages.



Therefore, using structural variables such as H, Ht and DBH, to build AGB regression equations are preferred (Corley & Tinker, 2008; Dewi *et al.*, 2009; Khalid *et al.*, 1999a; Thenkabail *et al.*, 2004). Generally, DBH is widely used in biomass equations in tropical regions because of the high correlation between DBH and AGB (Brown, 1997). However, in the current study, a weak to intermediate correlation between DBH and biomass was found. The correlation was insignificant with both CB (P value = 0.229) and TB (P value = 0.197) (see Chapter 2, Tables 8 and 9).

This may be due to the growing effects of the palm trunk where the DBH becomes more stable and there is no significant increase in DBH from medium to mature DP. In addition, palms being monocots, have a different anatomy and form than other trees. The DBH does not increase with age, which may explain the weak relationship observed with biomass (Sajdak *et al.*, 2014).

As the AGB is the resulting sum of crown and trunk biomasses, it could be estimated from CA and Ht, which were found to be the most significant field predictors (see Chapter 2, Tables 8 and 9). CB was highly correlated with CA with the highest  $R^2$  of 0.8354 obtained using an exponential regression equation. While the TB was highly correlated with the Ht with the highest  $R^2$  of 0.828 reached using a power regression equation. Correlations between CB and CA in one hand, and TB and Ht in the other, were also observed by others.

Carlos *et al.* (2015), for instance, found that foliage (crown) biomass was strongly correlated with palm crown variables in Brazil. Similarly, Korom and Matsuur (2016) studied the AGB of oil palms in Malaysia and analyzed different allometric equations. They reported that AGB could be estimated using CD of oil palms consistently at all ages with  $R^2$  ranging between 0.95 and 0.97. The same can be said about CA as it could be calculated from CD using sphere equation ( $CA = \pi CD^2/4$ ), assuming a rounded palm crown.

Palm trees height was reported to be more useful as an independent variable than DBH in AGB estimations (Yuen *et al.*, 2016). Likewise, in a study conducted in Malaysia, Asari *et al.* (2013) concluded that palm height was more strongly associated with age. Carlos *et al.* (2015) found that the biomass was strongly correlated with age and very strongly with Ht.

Recently, Singh *et al.* (2018) found that AGB was highly correlated with the Ht in their study on oil palm trees in India. This could be explained by the fact that palm species growth pattern were nonlinear and each biomass component had its unique characteristics which would be reflected in the allometric model for estimating biomass (Korom *et al.*, 2016; Da Silva *et al.*, 2015). Crown dimensions have been used less frequently in equations for AGB or biomass of any component (Yuen *et al.*, 2016). However, as the detection of biomass and its estimation by RS techniques greatly increase the efficiency in forest monitoring and measurement (Holmgren *et al.*, 1994), CB component has gained prominence in most research (Kumar & Mutanga, 2017).

The novelty introduced in the current study highlighted the value of integrating allometric equations with RS. The predictive power of such variables derived from moderate resolution satellite data, such as Landsat TM and ETM+ imagery, were valid to estimate palm biomass. The results of the regression analysis for the estimation of AGB and CS from the allometric equations on one hand, and the RS indicators on the other (Issa *et al.*, 2019), showed high correlation (see Chapter 4, Table 23).

The significant correlations reported here supported the aim of the study to ultimately use RS data for estimating CS. The approach provided a significant advantage by enabling the calculation of AGB and CS for large areas based on field measurements at a limited number of representative sites used to derive the allometric equations.

The regression analysis yielded positive correlation between CA and SOC with a coefficient of 0.903 ( $P < 0.0001$ ), concluding that for DP's CA could be used as a good predictor of SOC in DP. The average SOC added to the area dominated by DP ranged from 15.7 ton. ha<sup>-1</sup> to 34.5 ton. ha<sup>-1</sup> with a mean of 22.26 ton. ha<sup>-1</sup> (see Chapter 2, Table 12).

These figures were determined from the fifteen DP destructively sampled measurements belonging to age stages ranging from 2.5 to 20 years. Comparatively, in Southern Ethiopia, Lemenih & Itanna (2004) found that semiarid acacia woodland added 14.7 ton. ha<sup>-1</sup> of SOC in the top 10 cm of the soil, while Nyssen *et al.* (2008) found that grazing lands of Ethiopia could add 26 ton. ha<sup>-1</sup> of SOC. In the UAE, *Acacia tortilis* added around 14.7 tons of SOC per hectare while *Colotropis procera* added only 6.6 tons of SOC per hectare (Ksiksi, 2012).

It is worth noting that different land management practices can lead to differences in the accumulation of SOC in different date palms trees (El Tahir *et al.*, 2009). Likewise, plant species differ markedly in their impact on soil carbon concentration and distribution, mainly because of differences in their root systems (Ksiksi, 2012; Lal, 2002). LULC change leads to change in SOC stock (Guo & Gifford, 2002). Afforestation, for instance, results in sequestration of new C and stabilization of old C in physically protected SOM fractions, associated with micro-aggregates and silt and clay (Nyssen *et al.*, 2008).



## 5.2. Mapping of Date Palm Trees at Three Age- Stages

## الكربونية

The accuracy of capturing all DPs is crucial to the current research, as these layers are used as an input to a RS-based biomass and CS estimation model (see Chapter 4, Subsection 4.1). Because of the reasons explained in Chapter 1 (Subsections 1.2.3.3), the moderate resolution Landsat-8 OLI imagery was chosen. However, this choice raised many challenges, particularly when mapping the non-mature DP (< 10 years), with an average CD of fewer than 5 meters.

The low canopy cover combined with the high contribution of desert background reflectance limited the efficiency of capturing the less developed and sparse DP trees at moderate resolution. Therefore, an integrated approach was proposed in this research, the HIA, applied to the multi-source / multi-resolution data from moderate Landsat-8 OLI and high-resolution WV-2 integrated with GIS. The HIA was able to depict the three age stages of DPs: mature, medium, and young with high accuracy.

First, a LULC map of the major seven classes in the study area was created, namely: urban, vegetation (including DP), sand sheets, sand dunes, deep water and shadows, shallow water, and sabkhas. The PBC method was applied to the Landsat-8 OLI scenes to perform this task, which was achieved successfully. The seven LULC classes were mapped and their spectral reflectance separability was achieved effectively. Although the overall accuracy of the LULC map was below the 85% level set as satisfactory for planning and management purposes (Anderson, 1976). However, there is a debate about the usefulness to take this level as standard; many publications reported accuracies mostly below the usually advised 85% target (Foody, 2002; Rozenstein & Karnieli, 2011).

Further light was shed by examining the user's and the producer's accuracies, which measure the commission and omission errors, respectively. The analysis of misclassified pixels in the LULC map indicates that most of the errors are mainly of omission (see the accuracies of vegetation, sand dunes, sand sheets, and sabkhas layers at the LULC map in Chapter 3, Table 14). The HCM, which combines both supervised and unsupervised classification, seems to provide an acceptable accuracy especially in the case of arid lands. This fact has also been reported by other researchers (Rozenstein & Karnieli, 2011) as well as in other ecoregions (Kamusoko & Aniya, 2009; Lo & Choi, 2004).

The created LULC map showed that vegetated and urban areas constituted only 0.6% with 40,102.6 hectares, and 0.49% with 32,333 hectares of the total area of the emirate, respectively. It is worth noting that sand dunes, sabkhas, and sand sheets areas were the dominant LULC classes in the whole emirate, making up more than 98% of the total area (see Chapter 3, Figure 24). Finally, the overall classification accuracy of the LULC maps was 81.71% with an overall Kappa Statistics equal to 0.81.

Second, a vegetation bitmap of Abu Dhabi was created by merging all non-vegetation classes into one class. The "recode" function in ERDAS Imagine was used to produce the binary mask with only two



© Shutterstock

الكريونية

للتخيل

A case study from the Emirate of Abu Dhabi, UAE.



values: the value of “1” for the vegetation class, and the value of “0” for the non-vegetation class. Vegetation in the study area were sparse and small in size (=32,333.3 ha, representing only 0.49% of the total study area). The overall classification accuracy of the created vegetation bitmap was 87%, with a Kappa coefficient equal to 0.74 (see Chapter 3, Table 14).

The second phase of the classification approach of DP was run on the vegetation bitmap using the same HCM to isolate the DP plantation pixels. However, at this stage of the classification, only the mature DP trees were depicted due to the limitations of Landsat-8 OLI to differentiate soil background from the non-mature DP trees ( $\leq 10$  years and have an average CD of fewer than 5 meters). Therefore, a different approach using different sensor characteristics was needed to map the other DP categories (medium and young) with accuracy.

Third, mapping of DP at all age stages was achieved using the OOC method applied to the sub-meter WV-2 imagery. Using high-resolution sensors such as WV-2, to detect low-density DP and map of the spatial distribution of DP in AD at different age stages: young ( $< 5$  years), medium (5-10 years), and mature ( $> 10$  years), proved very successful and added innovation to the actual research. Indeed, many studies upraised the use of high spatial-resolution for depicting and revealing information about the distribution and type of vegetation, especially in arid lands, and hence increase their distinguishability (Bradley *et al.*, 2019; Immitzer *et al.*, 2012; Li *et al.*, 2015; Mugiraneza *et al.*, 2019; Xie *et al.*, 2008).

Several software packages supporting OOC and feature extraction are available. ERDAS Imagine 2020 Objective tool was used, it employs “feature model tree” which applies to objects created by image segmentation and other pixel-based algorithms which, after being vectorized, can be processed using geometric and textural parameters (Lack & Bleisch, 2010).

The “cue metrics” are the result of many trials and errors. There were two-level steps of analysis: (1) raster data analysis and, (2) vectorizing (the three raster outputs: mature, medium, and young) and cleaning up the vector layers by visual interpretation to remove erroneous vector if any.

The OOC comprised many steps summarized as follows: i) starting with 0.5 m pan-sharpened WV-2 images covering a test site (AlFoah farm, east of study area), optimum RS parameters were initially selected, analyzed and defined, for discriminating DP trees at three different age stages; ii) applying the produced parameters to the whole WV-2 dataset; iii) differentiating DP crowns visually from the background; iv) training areas were carefully selected to exclude any background pixel and; v) pixels of individual palms were submitted to compute pixel cue metrics to train the classifier. However, it should be noted here that, one should familiarize himself with the study area to be able to train the representative signatures.

Evaluation of the three classified maps was carried out using classification accuracy assessment in terms of mapping accuracy where results are summarized in Table 14 (see Chapter 3). The overall accuracies of DP maps were 86.8%, 88%, and 90.7% for young, medium, and mature DP, respectively. The area of each category was calculated and found to be 4,193.86 ha, 1,672.14 ha, and 1,722.05 ha for mature, medium, and young DP trees, respectively. It was revealed that the total DP trees areas represented around 64.62% of the total vegetated areas in Abu Dhabi (mostly located in the east and south parts). This was expected due to the importance given to DP in the farming system of the emirate and the adopted government policies in granting farms to the local population.

Furthermore, comparing the results of DP maps produced using Landsat-8 OLI and WV-2 imagery, showed a big difference between the two methods. Landsat-8 OLI gave an area equal to 20,893.5 ha while; classifying WV-2 images gave an area of only 7,588.05 ha. It is well known that, in general, classifying the Landsat-8 OLI images would overestimate the areas of DP trees compared to the classified WV-2 ones. A similar remark was noticed also by (Stych *et al.*, 2019) who ran a comparison study between Landsat-8 OLI and WV-2 for the classification of forests in Czech and they found that the area of wetland class was almost doubled on the classified Landsat-8 OLI images compared to the classified WV-2 images. This is explained by the fact that DP class areas estimated by the classified Landsat-8 images include the spacing areas (empty areas) among DP while the classified WV-2 images completely excluded these empty areas considering them as part of the pure soil class. Hence, only DP crowns were delineated and mapped (especially for non-mature DP where there is no overlapping of DP crowns). This is illustrated in a practical example in Figure 31.

Furthermore, it was observed that mature DP showed better overall classification accuracy followed by medium and young DP, respectively. This could be attributed to the less background contribution in the overall reflectance of the pixel because of large crown areas covering mature DP; while medium and younger (smaller canopy cover) result in wider spacing and higher exposure of the soil background resulting in a mixed spectral signature. Finally, a marginal improvement in classification was achieved through manual intervention editing in a GIS. The implemented approach proved very promising, with little cost compared to more complex algorithms and expensive data, especially for researches with limited budget, which is the case in most developing countries.

Figure 31: Differences in estimating DP trees areas at the same farm. The classifying of Landsat-8 OLI image as present in (a) gave 14.02 hectares of DP (yellow color), while (b) classifying of WV-2 image gave 3.77 hectares only (yellow color). This difference is caused by spacing areas among palms that were added to the DP total cover with Landsat-8 images (because of low resolution); while the classified WV-2 images captured and classified these areas as background (non-DP).

الكربونية



للنخيل

## 5.3. Estimating the Total Carbon Stock in Date Palm Trees

## الكربونية

The main purpose of the current study is to build a geospatial model for the estimation of carbon stock (CS) of date palms (DP) and mapping its geographical distribution in the emirate of Abu Dhabi (UAE), at three age stages: mature, medium and young. It is worth noting that parts of our findings have already been published.

However, the novelty in the current study is reflected in many aspects including, the scope and objectives, the sample sizes, the datasets used, the model built, and the results and visualization. Indeed, the current study has been extended to cover the whole emirate involving larger sample sizes and comprising most cultivars of UAE's date palms. The integration between the finer resolution WV-2 scenes, which served at depicting and mapping all DP trees at different age stages (Dahy *et al.*, 2021), with Landsat Level 2 dataset to identify and measure more accurate RS predictors, allowed to build our final improved model.

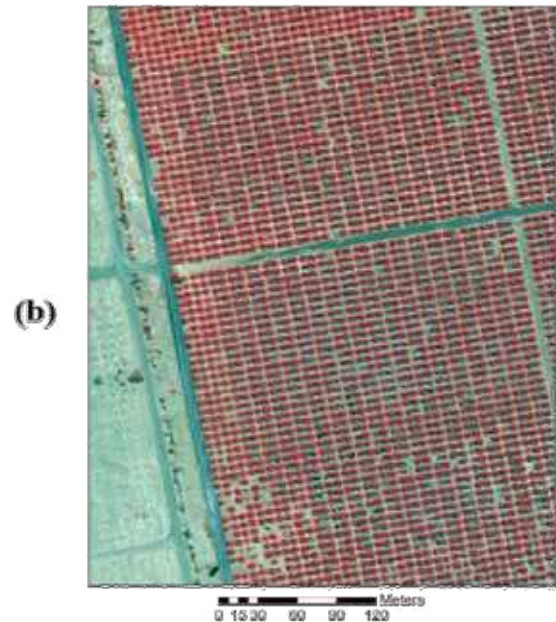
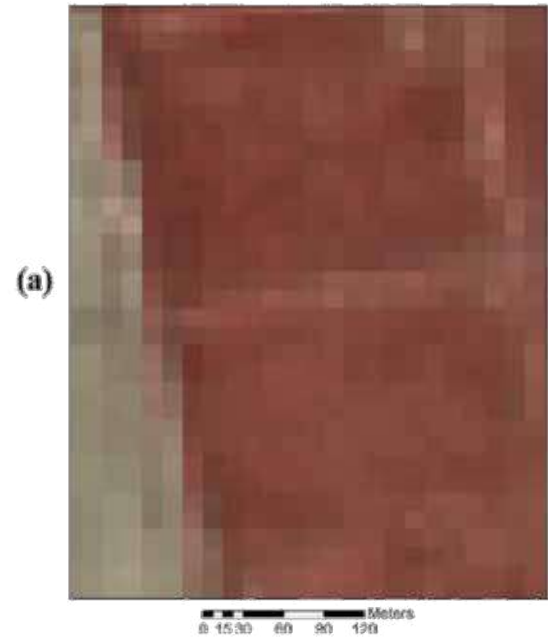
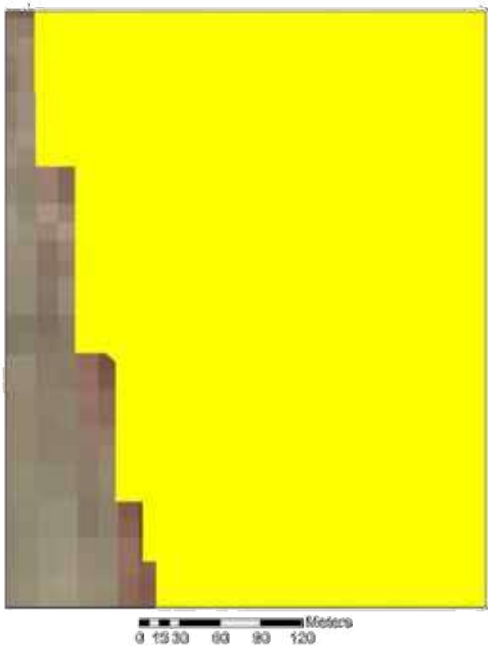


**Figure 31:** Differences in estimating DP trees areas at the same farm. The classifying of Landsat-8 OLI image as present in (a) gave 14.02 hectares of DP (yellow color), while (b) classifying of WV-2 image gave 3.77 hectares only (yellow color). This difference is caused by spacing areas among palms that were added to the DP total cover with Landsat-8 images (because of low resolution); while the classified WV-2 images captured and classified these areas as background (non-DP).



Another novelty of the current research is that the generally adopted ratio of BGB estimated at 20% of the AGB in several published studies (Cairns *et al.*, 1997; Koala *et al.*, 2017; Mokany *et al.*, 2006; Niether *et al.*, 2019), was not valid for our model. Instead, our results showed different ratios among different DP age stages with averages of 0.332, 0.925, and 0.496 for YDP, MeDP, and MDP, respectively (Issa *et al.*, 2020b). Therefore, equations (11, 12, and 13) were developed and implemented to estimate BGB of DP instead.

On the other hand, the percentage of carbon content in the root system of DP (BGB) was found to be 51.27% (Issa *et al.*, 2020b), which is slightly lower than the carbon content in the AGB. Therefore, below-ground carbon (BGC) was estimated in tons by multiplying the resulting values from equations 11, 12, or 13 by a factor of 0.5127 (equation 14). Furthermore, carbon content of dead wood or litter and woody debris are usually assumed to be between 10 and 20% of the AGB (Gibbs *et al.*, 2007; Houghton *et al.*, 2009; Issa *et al.*, 2020a).

However, based on extensive field visits to DP farms at different age stages, it was observed that litter and debris ratio to AGB of DP varied depending on the palm age stage. The more the palm matures, the more it produces litter and debris. The researchers adopted the following percentages to be applied to predict litter and debris (in ton) from AGB (in ton), for DP trees; 10% for YDP, 15% for MeDP, and 20% for MDP.

Three models were initially built to estimate AGB for the three age stages: mature, medium, and young. However, the large contribution of background reflectance in the study area reduced the accuracy of separating the young and medium DP. This, in turn, weakened the statistical relationship between AGB of medium and young DP with RS variables derived from Landsat-8 OLI. Subsequently, young, and medium DP classes were merged to form one non-mature DP (Non-MDP) class, substantially improving the statistical relationship between AGB and RS variables. Therefore, we opted for the creation of two sub-models only: one for Non-MDP and another for MDP.

الكربونية



Our study showed that when using single band to predict AGB, the SWIR bands of Landsat OLI produced the highest and most significant correlation for both MDP and Non-MDP trees. These results were in line with findings from a previous study in Tajikistan where the authors found that SWIR1, 2 of Landsat 8 were convenient in detecting arid land's vegetation (Zandler *et al.*, 2015). While our work on AGB of the MDP showed that a grouping of single bands or VIs does not improve the R<sup>2</sup>, it was noticed that VIs provided better predictors of AGB than single bands. Our results were also consistent with other studies that used Landsat imagery to estimate biomass in different regions such as the study reported in (Günlü *et al.*, 2014).

The decision of selecting the effectively performing VIs is function of the type of ecosystem, environmental conditions, and spectral characteristics of the sensor. Spectral band saturation, for instance, is a well-recognized problem and can affect VI performance and lead to inaccurate estimation of AGB (Zhao *et al.*, 2016). However, this was not a major factor in our study region.

Observed structural differences in DP trees influenced the calculation of AGB. Indeed, varied palms spacing were found in some plots; while sparse distribution of DP with no regular spacing, caused by human interferences, were found in others. It was also noted that regardless of the DP age, other factors affected date palm's CA and Ht and consequently the palm's capacity to accumulate biomass and sequester carbon. Cultivar and land management practices are examples of such factors.

The largest average of DP density was found on MDP plots. In two cases of MDP plots, the number of DP reached 88 and 96 palms per plot which corresponds to around 550 and 600 palm.ha<sup>-1</sup>, respectively. This could be attributed to the old farming systems, where MDP were planted irregularly in the farm with short spacing among palms to benefit from the traditional irrigation systems (e.g. Aflaj irrigation systems). Nowadays, the palms are distributed in a more organized manner with wider spacing among them (7m×7m, 8m×8m, and 9m×9m) leading to lower densities, allowing agricultural tractors and machinery to navigate

more easily. It is noticeable that an overlap between the crown area ranges of MDP and MeDP is found in some cases. This is due to regular pruning of DP fronds practiced in new trees.

The pruning process aims to keep a specific number of fronds in the palm allowing more carbohydrates to go to the fruits (dates) than the fronds. It is rare to find Ht of DP taller than 5 meters in modern DP farms as the farmers tend to remove tall palms reaching certain height, as they are more difficult to maintain and manage. However, during field measurement, the researchers observed some DP that exceeded 5 meters, and some were extremely tall with very high Ht reached up to 15.2 m especially in the oases. In contrast, it was found that most YDP had Ht equal to zero and some of them had CA equal 0.07 m<sup>2</sup> since their fronds were attached by cord with no trunk. These structural variations impacted the performance of spectral bands and VIs as predictors, affected the estimation of AGB and influenced the choice of estimation model.

The approach implemented aimed at selecting the most appropriate regression model among the tested models to estimate AGB of DP at multiple age stages. It considered the use of linear and non-linear regression models with multiple single band, single VIs, and stepwise multivariate regression to estimate the most appropriate model from the tested models based on correlation, significance and RMSE. The model that provided the best estimate of AGB in the case of MDP, consisted in the use of a second-order polynomial where TCW served as the only RS predictor.

This model yielded the strongest correlation and significance with R<sup>2</sup> equal to 0.7643 and a P-value equal to 0.007 with RMSE of 6.322 t.ha<sup>-1</sup>. For Non-MDP, an exponential model that uses RDVI as RS predictor provided the strongest estimate of biomass with R<sup>2</sup> equal to 0.4987 and P-value equal to 0.00002, while the model validation showed RMSE of 8.040 t.ha<sup>-1</sup>. These results were consistent with published literature for other species and study areas where Landsat 8 was used for mapping and predicting AGB in woodlands (Karlson *et al.*, 2015).

The DP age stage class derived from the WV-2 data was processed to select the proper model from the tested models to use when estimating AGB. The resulting map was an emirate wide map of AGB that was subsequently used to predict CS. This step highlights the strength and uniqueness of our approach where RS-based model, once calibrated, enabled the creation of CS maps from remote sensing data without the need for additional field measurements.

The accurate total carbon stock estimation of DP trees in Abu Dhabi depends on the accurate estimation of its biomass, specifically AGB that is predicted by using biomass allometric equations. Therefore, one source of uncertainty could come from the equations themselves. To overcome this issue, the authors used published allometric equations developed from represented field samples of DP considering the different varieties as well as the three different age stages in the study area.

The other source of uncertainty for the estimation of the biomass of DP, hence their carbon stock, could come from RS models that were built during the current study. The authors identified and selected a number of plot samples representing homogeneous DP trees with strict criteria excluding the plots that have a sparse distribution of DP/plot, stressed DP, large level of heterogeneity, and not representing the age stage class. The plot design with 40m × 40m dimension ensured that the area on the ground occupied at least one full pixel of Landsat 8 OLI image with a 30-m pixel resolution (Issa *et al.*, 2019). Landsat 8 OLI spectral variables (mean values) for all the plots were extracted for a 3 × 3 window centered over each plot to reduce the uncertainties in RS data resulting from plot positioning errors that could be created because of the mismatching of sample plots with the image pixels introduced when the x and y coordinates of sample plots were located using GPS (D. Lu *et al.*, 2002).

The RS models for estimating DP biomass were estimated from Level 2 product of Landsat to identify and measure more accurate RS predictors, however, Landsat with moderate spatial resolution, was not able to differentiate and map DP at all age stages. Therefore, we used accurate maps of DP at all age stages derived from fine-resolution WV-2 scenes as input to our final biomass models (Dahy *et al.*, 2021). Hence, we succeeded in predicting and visualizing the amounts of CS in all DP trees in the whole study area.



Chapter

# 6



# Conclusions & Recommendations

One of the key objectives of this study was to develop specific allometric biomass equations for assessing carbon sequestration in DP of the UAE and to estimate the potential of DP species to improve soil carbon sequestration in such desert ecosystems (see Chapter 1). Allometric equations using structural variables that could be linked to RS observations were developed for DP at different age stages. Based on field and lab works, CA was found to best estimate CB and SOC, while Ht was the best estimator of TB. The allometric equations developed using these variables allowed the estimation of CB, TB and SOC with coefficients of determination (R<sup>2</sup>) of 0.884, 0.835 and 0.952, respectively (see Chapter 2). The allometric equations developed in the early stages of the dissertation were crucial for the development of the RS-based model to predict AGB as they provided the needed input to calibrate the model without further recourse to destructive procedures for measuring AGB in the field.

Furthermore, the dissertation showed that the average ratios of the BGB to AGB in DP varied with their maturity stages at values of 0.332 for young, 0.925 for medium (due to the substantial growth of the palm's root system at this stage to support the emergence of the trunk) and 0.496 for mature DP. Additionally, the study showed that the amounts of CS in or contributed by DP were substantial, with significantly higher amounts of SOC compared to other local plants.

The development of AGB and OC estimation equations using RS data enabled the calculation of CS over large areas without further need for extensive field work, a key tool to accomplish the other objectives of this book (see Chapter 3 and 4). RS data sets (Landsat-8 OLI and WV-2 imageries) were used for the ac-

curate delineation of DP trees at different age stages for the whole study area. The dissertation proposes a novel framework based on using multi-source/ multi-sensor data in a hierarchical integrated approach (HIA) to map DP trees in the Emirate of Abu Dhabi at different age stages (see Chapter 3).

First, each pan-sharpened scene of Landsat-8 OLI was classified using an HCM (supervised and unsupervised classification) to create LULC maps. The evaluation of the spectral signatures separations was performed to select the best discriminatory Landsat-8 OLI bands. Interpretation of the seven signatures demonstrated that the shortwave infrared (SWIR1& SWIR2) had the best separability power of all Landsat 8 OLI bands. However, some other combinations were found to be efficient in identifying and mapping the vegetation class such as (RED, SWIR1, SWIR2), (RED, GREEN, SWIR1), (RED, GREEN, SWIR2) or (GREEN, SWIR1, SWIR2). Next, the maps were reclassified (recoded) to create a vegetation bitmap encompassing only two classes: vegetation and non-vegetation. The HCM was applied to the vegetation bitmap to delineate and map DP in the study area. However, at this stage of the classification, mature DP trees only were depicted due to the limitations of Landsat-8 OLI to separate soil background from the non-mature DP trees ( $\leq 10$  years, with average crown diameter less than 5 meters).

Therefore, the sub-meter WV-2 imagery, covering vegetated areas, were classified using the object-oriented classification (OOC) method, to separate and map the other two DP age stages (medium, and young). At this level, about 829 sub-meter WV-2 images were classified and interpreted to extract and map all categories of DP in the study area. The suitability of the WV-2 satellite data for the identification of tree species was demonstrated. Furthermore, the OOC proved to outperform the pixel-based approach with the near-infrared, red-edge, and green bands being always more important than the other bands to classification.

The areas of DP trees at the various age stages was calculated and were found to be 4,193.86 ha, 1,672.14 ha, and 1,722.05 ha for mature, medium, and young DP, respectively. The total DP trees areas represented around 65% of the total vegetated areas in Abu Dhabi (mostly located in the eastern and southern parts of the emirate). This was expected due to the importance given to DP in the farming system of the emirate and the adopted government policies in granting farms to the local population.

Furthermore, comparing the results of DP maps produced using Landsat-8 OLI and WV-2 imagery, showed a big difference between the two methods. This is because DP class areas estimated by the classified Landsat-8 images include the spacing areas (empty areas) among DP while the classified WV-2 images completely excluded these empty areas considering them as part of the pure soil class. Note that the difference between Landsat and WV-2 results can be reduced if the OOC is tuned to segment the whole farm rather than patches of DP.

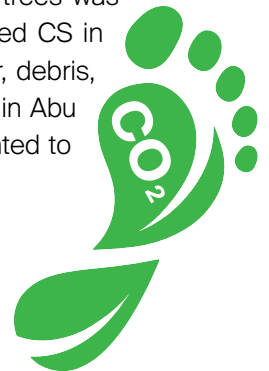
The results of the classified maps accuracy assessment indicated a good overall performance of the classification process with an overall accuracy value of about 81.7% for the LULC map and 87% for the vegetation bit-map using Landsat-8 OLI as source data. For DP age stages maps using WV-2 data, the overall accuracies were 86.8%, 88% to 90.7% for young, medium, and mature DP, respectively. Besides, the accuracy of the DP map considering all DP ages had an overall accuracy of 94.5% and a kappa coefficient of 88%.

Furthermore, it was observed that mature DP showed better overall classification accuracy followed by medium DP and young DP, respectively. This could be attributed to the less background contribution in the overall reflectance of the pixel because of large crown area coverage of mature DP; while medium and younger (smaller canopy cover) result in wider spacing and higher exposure of the soil background resulting in a mixed spectral signature.

Finally, a marginal improvement in classification was achieved through manual editing in a GIS. A final and accurate DP map at three age stages in the emirate of Abu Dhabi (mature, medium, and young) was created. Most of the DP trees in Abu Dhabi were found to be in Al Ain (east of the emirate) and Liwa (south of the emirate) with more than half of those at the mature stage (> 10 years). The produced DP map was converted to a GIS layer and used as an input to a RS-based biomass model to assess CS in DP trees in the study area (see Chapter 4).

A geospatial model of carbon stock assessment of date palm at different age stages was developed. Allometric equations, previously developed and published by the authors, were utilized to design, calibrate, and implement the model to predict the amounts of AGB and AGC in DP. Different types of regression analysis (single and multiple) were tested to create relationships linking the AGB to RS predictors. Using an expanded number of 54 field plots showed that TCW has the most significant correlation estimated using a second-order polynomial model to estimate the biomass of MDP with  $R^2$  equal to 0.7643 and P-value equal to 0.007.

On the other hand, the exponential regression model that used RDVI as RS predictor provided the strongest correlation with AGB of Non-MDP, with an  $R^2$  value of 0.4987 and a P-value of 0.00002. The development of a remote sensing-based biomass and carbon estimation model enabled the prediction and visualization of CS over extended areas with minimum fieldwork. Using previously produced DP age classification maps, the RS-based model was applied to Landsat-8 imagery to map and predict the CS of DP in Abu Dhabi. The total CS in DP trees was estimated as the sum of the estimated CS in the five components: AGB, BGB, litter, debris, and SOC. The overall CS by DP trees in Abu Dhabi predicted from this map amounted to 2,447,856.87 tons.



The main limitation is related to the use of moderate spatial resolution RS product to estimate the biomass and CS amounts. Landsat with moderate spatial resolution was not able to accurately differentiate and map DP at all age stages. Therefore, we used accurate maps of DP at all age stages derived from fine-resolution WV-2 scenes as input to our final biomass models.

Consequently, a weak statistical relationship between AGB of medium and young DP with RS variables derived from Landsat-8 OLI was observed. Subsequently, young, and medium DP classes were merged to form one non-mature DP (Non-MDP) class. To overcome this challenge one suggested solution is to use finer spatial resolution of satellite imagery for the building the DP biomass model.

The implemented approach proved very promising, with minimal cost compared to more complex algorithms and data, especially for limited-budget researches, which is the case in most developing countries. The approach was successful in identifying and mapping mature, medium, and young DP in the study area with high accuracies. The accurate mapping of three age stages permitted for a better estimation of their CS. The created maps opened the road toward applying a non-destructive approach and to build a RS-based biomass estimation model for assessing AGB and CS in DP in the arid environment of UAE (see Chapter 4). Moreover, the approach can easily be extended to larger areas in the region.

RS-based biomass assessment models for DP were built for quick and reliable estimation of the amounts of AGB and CS which allow for the establishment of a benchmark DP CS map for the Emirate of Abu Dhabi. The methodology proposed in this book relied on both fieldwork and analysis of RS data. The work procedures included pre-field preparations to identify sample areas of interest, fieldwork that included sample collection and measurement of plant characteristics, and post-field activity that focused on processing RS data and model development and validation.

Our applied methods used in this project can be generalized to other areas in the Gulf region with minimal cost. It can also be modified to use other publicly available moderate resolution imagery such as Sentinel-2. RS-based biomass estimating model for DP were built for a quick and reliable method for the creation and visualization of a standard DP CS map for the Emirate of Abu Dhabi. Thus, it can be further employed to boost the decision-taking process on durable and sustainable management of CS in other similar ecosystems.

In conclusion, the field-based measurements and geospatial approach introduced in this study has the potential to help improve carbon estimation in DP trees to reduce emissions resulting from deforestation and forest degradation (REDD+) and to design incentive programs in the UAE.



© Freepik

الكريونية



للنخيل

A case study from the Emirate of Abu Dhabi, UAE.



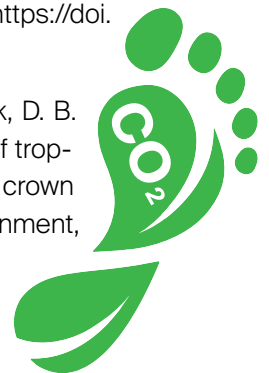
# REFERENCES

1. Abburu, S., & Golla, S. B. (2015). Satellite image classification methods and techniques: A review. *International Journal of Computer Applications*, 119(8), 20–25.
2. Abd Rabou, A. F. N. (2017). The current status of the date palm (*Phoenix dactylifera*) and its uses in the Gaza Strip, Palestine. *Biodiversitas, Journal of Biological Diversity*, 18(3). <https://doi.org/10.13057/biodiv/d180324>
3. Abdi, A. M., & Nandipati, A. (2010). Abu Dhabi Island: Analysis of Development and Vegetation Change Using Remote Sensing (1972–2000). In *Advances in Earth Observation of Global Change* (pp. 43–53). Springer.
4. Abu Dhabi State of Environment Report: From: <https://www.soe.ae/>. (2017). Retrieved on 20 April, 2021.
5. Achard, F., Eva, H. D., Stibig, H.-J., Mayaux, P., Gallego, J., Richards, T., & Malingreau, J.-P. (2002). Determination of deforestation rates of the world's humid tropical forests. *Science*, 297(5583), 999–1002.
6. Adam, N. S., & Jusoh, I. (2018). Allometric Model for Predicting Aboveground Biomass and Carbon Stock of Acacia Trees in Sarawak, Malaysia. *BioResources*, 13(4), 7381–7394.
7. Ahlström, A., Raupach, M. R., Schurgers, G., Smith, B., Arneeth, A., Jung, M., Reichstein, M., Canadell, J. G., Friedlingstein, P., & Jain, A. K. (2015). The dominant role of semi-arid ecosystems in the trend and variability of the land CO<sub>2</sub> sink. *Science*, 348(6237), 895–899.
8. Al-Ahmadi, F. S., & Hames, A. S. (2009). Comparison of four classification methods to extract land use and land cover from raw satellite images for some remote arid areas, kingdom of Saudi Arabia. *Earth*, 20(1), 167–191.
9. Alhameli, S., & Alshehhi, M. (2004). Images are an outstanding evidence of rapid development “A perfect example from United Arab Emirates (UAE)”. *Proceedings of the ISPRS XXth Congress, Commission PS IC, Working Group II/4, XXXV, Part B, 4, 505, Istanbul, Turkey*.
10. Alhammadi, M. S., & Kurup, S. S. (2012). Impact of salinity stress on date palm (*Phoenix dactylifera* L)-A review. In *Crop Production Technologies*. InTech.
11. Allen, S. E., Grimshaw, H. M., Parkinson, J. A., & Quarmby, C. (1974). *Chemical analysis of ecological materials*. Blackwell Scientific Publications.
12. Al-Shuwaihi, A. (2009). Monitoring Al Ain City urban growth dynamics between 1972 and 2000 by integrating remote sensing and GIS techniques. Master thesis, UAE University, UAE.
13. Aly, A. A., Al-Omran, A. M., Sallam, A. S., Al-Wabel, M. I., & Al-Shayaa, M. S. (2016a). Vegetation cover change detection and assessment in arid environment using multi-temporal remote sensing images and ecosystem management approach. *Solid Earth*, 7(2), 713–725.
14. Anderson, G. L., Hanson, J. D., & Haas, R. H. (1993). Evaluating Landsat Thematic Mapper derived vegetation indices for estimating above-ground biomass on semiarid rangelands. *Remote Sensing of Environment*, 45(2), 165–175.
15. Anderson, J. R. (1976). A land use and land cover classification system for use with remote sensor data (Vol. 964). US Government Printing Office.
16. AOAD, Arab Organization for Agricultural Development. (2008). *Arab Agricultural Statistics Yearbook, PART III: Plant Production*. Statistics Division 28.
17. Aranha, J. T., Viana, H. F., & Rodrigues, R. (2008). Vegetation classification and quantification by satellite image processing. A case study in North Portugal. *International Conference and Exhibition on Bioenergy*, 7. April 6th – 9th 2008, Portugal.
18. Archibald, S., & Bond, W. J. (2003). Growing tall vs growing wide: Tree architecture and allometry of *Acacia karroo* in forest, savanna, and arid environments. *Oikos*, 102(1), 3–14.
19. Ardö, J., & Olsson, L. (2003). Assessment of soil organic carbon in semi-arid Sudan using GIS and the CENTURY model. *Journal of Arid Environments*, 54(4), 633–651.



20. Aronson, J., Kigel, J., Shmida, A., & Klein, J. (1992). Adaptive phenology of desert and Mediterranean populations of annual plants grown with and without water stress. *Oecologia*, 89(1), 17-26.
21. Asari, N., Suratman, M. N., Jaafar, J., & Khalid, M. M. (2013). Estimation of above ground biomass for oil palm trees using allometric equations. 4th International Conference on Biology, Environment and Chemistry. Selangor, Malaysia.
22. Attarchi, S., & Gloaguen, R. (2014). Improving the estimation of above ground biomass using dual polarimetric PALSAR and ETM+ data in the Hyrcanian mountain forest (Iran). *Remote Sensing*, 6(5), 3693-3715.
23. Avery, T. E., & Burkhart, H. E. (2015). *Forest measurements*. Waveland Press.
24. Baccini, A., Laporte, N., Goetz, S. J., Sun, M., & Dong, H. (2008). A first map of tropical Africa's above-ground biomass derived from satellite imagery. *Environmental Research Letters*, 3(4), 045011. <https://doi.org/10.1088/1748-9326/3/4/045011>
25. Bakr, N., Weindorf, D. C., Bahnassy, M. H., Marei, S. M., & El-Badawi, M. M. (2010). Monitoring land cover changes in a newly reclaimed area of Egypt using multi-temporal Landsat data. *Applied Geography*, 30(4), 592-605.
26. Bannari, A., Morin, D., Bonn, F., & Huete, A. R. (1995). A review of vegetation indices. *Remote Sensing Reviews*, 13(1-2), 95-120.
27. Baral, A., & Guha, G. S. (2004). Trees for carbon sequestration or fossil fuel substitution: The issue of cost vs. carbon benefit. *Biomass and Bioenergy*, 27(1), 41-55.
28. Barbosa, J. M., Broadbent, E. N., & Bitencourt, M. D. (2014). Remote sensing of aboveground biomass in tropical secondary forests: A review. *International Journal of Forestry Research*, 2014, 10-14.
29. Baret, F., Guyot, G., & Major, D. J. (1989). TSAVI: A vegetation index which minimizes soil brightness effects on LAI and APAR estimation. *Geoscience and Remote Sensing*
30. Basuki, T. M., Van Laake, P. E., Skidmore, A. K., & Hussin, Y. A. (2009). Allometric equations for estimating the above-ground biomass in tropical lowland Dipterocarp forests. *Forest Ecology and Management*, 257(8), 1684-1694.
31. Baumann, G. (2009). How to assess rangeland condition in semiarid ecosystems? The indicative value of vegetation in the High Atlas Mountains, Morocco. Universität zu Köln.
32. Baumann, M., Levers, C., Macchi, L., Bluhm, H., Waske, B., Gasparri, N. I., & Kuemmerle, T. (2018). Mapping continuous fields of tree and shrub cover across the Gran Chaco using Landsat 8 and Sentinel-1 data. *Remote Sensing of Environment*, 216, 201-211.
33. Benz, U. C., Hofmann, P., Willhauck, G., Lingenfelder, I., & Heynen, M. (2004). Multi-resolution, object-oriented fuzzy analysis of remote sensing data for GIS-ready information. *ISPRS Journal of Photogrammetry and Remote Sensing*, 58(3-4), 239-258.
34. Bestelmeyer, B. T., Okin, G. S., Duniway, M. C., Archer, S. R., Sayre, N. F., Williamson, J. C., & Herrick, J. E. (2015). Desertification, land use, and the transformation of global drylands. *Frontiers in Ecology and the Environment*, 13(1), 28-36.
35. Biederman, J. A., Scott, R. L., Bell, T. W., Bowling, D. R., Dore, S., Garatuza-Payan, J., Kolb, T. E., Krishnan, P., Krofcheck, D. J., & Litvak, M. E. (2017). CO<sub>2</sub> exchange and evapotranspiration across dryland ecosystems of southwestern North America. *Global Change Biology*, 23(10), 4204-4221.
36. Blaschke, T. (2010). Object based image analysis for remote sensing. *ISPRS Journal of Photogrammetry and Remote Sensing*, 65(1), 2-16.

37. Bohlman, S., & O'Brien, S. (2006). Allometry, adult stature and regeneration requirement of 65 tree species on Barro Colorado Island, Panama. *Journal of Tropical Ecology*, 22(2), 123-136.
38. Bradley, A. V., Haughan, A. E., Al-Dughairi, A., & McLaren, S. J. (2019). Spatial variability in shrub vegetation across dune forms in central Saudi Arabia. *Journal of Arid Environments*, 161, 72-84.
39. Brady, N. C., & Weil, R. R. (1999). *The nature and properties of soil* 12th ed. Prentice-Hall Inc. Upper Saddle River, New Jersey.
40. Brown, I. F., Martinelli, L. A., Thomas, W. W., Moreira, M. Z., Ferreira, C. C., & Victoria, R. A. (1995). Uncertainty in the biomass of Amazonian forests: An example from Rondonia, Brazil. *Forest Ecology and Management*, 75(1), 175-189.
41. Brown, S. (1997). Estimating biomass and biomass change of tropical forests: A primer (Vol. 134). Food & Agriculture Org.
42. Brown, S., Gillespie, A. J., & Lugo, A. E. (1989). Biomass estimation methods for tropical forests with applications to forest inventory data. *Forest Science*, 35(4), 881-902.
43. Bryceson, K. P. (1991). Likely locust infestation areas in western New South Wales, Australia, located by satellite. *Geocarto International*, 6(4), 21-37.
44. Cairns, M. A., Brown, S., Helmer, E. H., & Baumgardner, G. A. (1997). Root biomass allocation in the world's upland forests. *Oecologia*, 111(1), 1-11.
45. Campbell, J. B., & Wynne, R. H. (2011). *Introduction to remote sensing*. Guilford Press.
46. Carlos, R. S., Sylvio, P., eacute llicoNetto, Ana, P. D. C., Aur eacute lio, L. ccedil o R., Alexandre, B., & Mateus, N. I. S. (2015). Quantifying biomass and carbon stocks in oil palm (*Elaeis guineensis* Jacq.) in Northeastern Brazil. *African Journal of Agricultural Research*, 10(43), 4067-4075. <https://doi.org/10.5897/AJAR2015.9582>
47. Castel, T., Guerra, F., Ruiz, A., Albarran, V., Caraglio, Y., & Houllier, F. (2000). Retrieval biomass of a large Venezuelan pine plantation using JERS-1 SAR data. *Geoscience and Remote Sensing Symposium*, 2000. Proceedings. IGARSS 2000. IEEE 2000 International, 1, 396-398.
48. Chave, J., Andalo, C., Brown, S., Cairns, M. A., Chambers, J. Q., Eamus, D., Fölster, H., Fromard, F., Higuchi, N., & Kira, T. (2005). Tree allometry and improved estimation of carbon stocks and balance in tropical forests. *Oecologia*, 145(1), 87-99.
49. Cheng, T., Song, R., Li, D., Zhou, K., Zheng, H., Yao, X., Tian, Y., Cao, W., & Zhu, Y. (2017). Spectroscopic Estimation of Biomass in Canopy Components of Paddy Rice Using Dry Matter and Chlorophyll Indices. *Remote Sensing*, 9(4), 319. <https://doi.org/10.3390/rs9040319>
50. Cheng, Z., Gamarra, J. G. P., & Birigazzi, L. (2014). Inventory of allometric equations for estimation tree biomass-a database for China. Rome, Italy: UNREDD Programme.
51. Chepkochei, L. C. (2011). Object-oriented image classification of individual trees using Erdas Imagine objective: Case study of Wanjohi area, Lake Naivasha Basin, Kenya. *Proceedings of the Kenya Geothermal Conference*, Nairobi, Kenya, 2123.
52. Chong, K. L., Kanniah, K. D., Pohl, C., & Tan, K. P. (2017). A review of remote sensing applications for oil palm studies. *Geo-Spatial Information Science*, 20(2), 184-200.
53. Cihlar, J., Denning, S., Ahem, F., Arino, O., Belward, A., Bretherton, F., Cramer, W., Dedieu, G., Field, C., & Francey, R. (2002). Initiative to quantify terrestrial carbon sources and sinks. *Eos, Transactions American Geophysical Union*, 83(1), 1-7. <https://doi.org/10.1029/2002EO000002>
54. Clark, M. L., Roberts, D. A., & Clark, D. B. (2005). Hyperspectral discrimination of tropical rain forest tree species at leaf to crown scales. *Remote Sensing of Environment*, 96(3), 375-398.



55. Clerici, N., Rubiano, K., Abd-Elrahman, A., Posada Hoestettler, J. M., & Escobedo, F. J. (2016b). Estimating aboveground biomass and carbon stocks in periurban Andean secondary forests using very high resolution imagery. *Forests*, 7(7), 138. <https://doi.org/10.3390/f7070138>
56. Clewley, D., Lucas, R., Accad, A., Armston, J., Bowen, M., Dwyer, J., Pollock, S., Bunting, P., McAlpine, C., & Eyre, T. (2012). An approach to mapping forest growth stages in Queensland, Australia through integration of ALOS PALSAR and Landsat sensor data. *Remote Sensing*, 4(8), 2236–2255.
57. Cole, T. G., & Ewel, J. J. (2006). Allometric equations for four valuable tropical tree species. *Forest Ecology and Management*, 229(1), 351–360.
58. Corley, R. H. V., Hardon, J. J., & Tan, G. Y. (1971). Analysis of growth of the oil palm (*Elaeis guineensis* Jacq.) I. Estimation of growth parameters and application in breeding. *Euphytica*, 20(2), 307–315.
59. Corley, R. Hereward V., & Tinker, P. B. (2008). *The oil palm*. John Wiley & Sons.
60. Corona-Núñez, R. O., Campo, J., & Williams, M. (2018). Aboveground carbon storage in tropical dry forest plots in Oaxaca, Mexico. *Forest Ecology and Management*, 409, 202–214.
61. Da Silva, F., Suwa, R., Kajimoto, T., Ishizuka, M., Higuchi, N., & Kunert, N. (2015). Allometric equations for estimating biomass of *Euterpe precatoria*, the most abundant palm species in the Amazon. *Forests*, 6(2), 450–463.
62. Dahy, B., Issa, S., & Saleous, N. (2023). Geo-spatial modelling of carbon stock assessment of date palm at different age stages: An integrated approach of fieldwork, remote sensing and GIS. *Ecological Modelling*, 481, 110377. <https://doi.org/10.1016/j.ecolmodel.2023.110377>
63. Dahy, B., Issa, S., Ksiksi, T., & Saleous, N. (2019). Non-Conventional Methods as a New Alternative for the Estimation of Terrestrial Biomass and Carbon Sequestered: Mini Review. *World Journal of Agriculture and Soil Science*. <https://doi.org/10.33552/WJASS.2019.04.000579>
64. Dahy, B., Issa, S., Ksiksi, T., & Saleous, N. (2020). Geospatial Technology Methods for Carbon Stock Assessment: A Comprehensive Review. *IOP Conference Series: Earth and Environmental Science*, 540, 012036. <https://doi.org/10.1088/1755-1315/540/1/012036>
65. Das, S., & Singh, T. P. (2012). Correlation analysis between biomass and spectral vegetation indices of forest ecosystem. *International Journal of Engineering Research and Technology*, 1(5), 1-13.
66. De Sy, V., Herold, M., Achard, F., Asner, G. P., Held, A., Kellndorfer, J., & Verbesselt, J. (2012). Synergies of multiple remote sensing data sources for REDD+ monitoring. *Current Opinion in Environmental Sustainability*, 4(6), 696–706.
67. Deans, J. D., Moran, J., & Grace, J. (1996). Biomass relationships for tree species in regenerating semi-deciduous tropical moist forest in Cameroon. *Forest Ecology and Management*, 88(3), 215–225.
68. Deng, S., Shi, Y., Jin, Y., & Wang, L. (2011). A GIS-based approach for quantifying and mapping carbon sink and stock values of forest ecosystem: A case study. *Energy Procedia*, 5, 1535–1545.
69. Dewi, S., Khasanah, N., Rahayu, S., Ekadinata, A., & Van Noordwijk, M. (2009). Carbon footprint of Indonesian palm oil production: A pilot study. Bogor, Indonesia. World Agroforestry Centre-ICRAF, SEA Regional Office, 8.
70. Dick OB, W. N. (2015). Estimating above Ground Biomass and Carbon Stock in the Lake Hawassa Watershed, Ethiopia by Integrating Remote Sensing and Allometric Equations. *Forest Research: Open Access*, 04(03). <https://doi.org/10.4172/2168-9776.1000151>
71. Diédhiou, I., Diallo, D., Mbengue, A. A., Hernandez, R. R., Bayala, R., Diémé, R., Diédhiou, P. M., & Sène, A. (2017). Allometric equations and carbon stocks in tree biomass of *Jatropha curcas* L. in Senegal's Peanut Basin. *Global Ecology and Conservation*, 9, 61–69.

72. Dietze, M. C., Wolosin, M. S., & Clark, J. S. (2008). Capturing diversity and interspecific variability in allometries: A hierarchical approach. *Forest Ecology and Management*, 256(11), 1939–1948.
73. Diouf, A., & Lambin, E. F. (2001). Monitoring land-cover changes in semi-arid regions: Remote sensing data and field observations in the Ferlo, Senegal. *Journal of Arid Environments*, 48(2), 129–148.
74. Duncanson, L., Rourke, O., & Dubayah, R. (2015). Small sample sizes yield biased allometric equations in temperate forests. *Scientific Reports*, 5, 1–13.
75. Ebuy, J., Lokombe, J. P., Ponette, Q., Sonwa, D., & Picard, N. (2011). Allometric Equation for Predicting Aboveground Biomass of Three Tree Species. *Journal of Tropical Forest Science*, 23(2), 125–132.
76. Eggleston, H. S., Buendia, L., Miwa, K., Ngara, T., & Tanabe, K. (2006). IPCC guidelines for national greenhouse gas inventories. Institute for Global Environmental Strategies, Hayama, Japan, 2, 48–56.
77. Eisfelder, C., Kuenzer, C., & Dech, S. (2012). Derivation of biomass information for semi-arid areas using remote-sensing data. *International Journal of Remote Sensing*, 33(9), 2937–2984.
78. Ekoungoulou, R., Liu, X., Loumeto, J. J., Ifo, S. A., Bocko, Y. E., Fleury, E. K., & Niu, S. (2014). Tree Allometry in Tropical Forest of Congo for Carbon Stocks Estimation in Above-Ground Biomass. *Open Journal of Forestry*, 4(5), 481. <http://www.scirp.org/journal/PaperInformation.aspx?PaperID=50690&#abstract>
79. El Tahir, B. A., Ahmed, D. M., Ardö, J., Gaafar, A. M., & Salih, A. A. (2009). Changes in soil properties following conversion of Acacia senegal plantation to other land management systems in North Kordofan State, Sudan. *Journal of Arid Environments*, 73(4–5), 499–505.
80. Elhag, M. (2016). Evaluation of different soil salinity mapping using remote sensing techniques in arid ecosystems, Saudi Arabia. *Journal of Sensors*, 2016. <https://doi.org/10.1155/2016/7596175>
81. El-Juhany, L. I. (2010). Degradation of date palm trees and date production in Arab countries: Causes and potential rehabilitation. *Australian Journal of Basic and Applied Sciences*, 4(8), 3998–4010.
82. Elzinga, C. L., Salzer, D. W., & Willoughby, J. W. (1998). *Measuring & Monitoring Plant Populations*. US Bureau of Land Management Papers.
83. EU EDGAR. (2021). Emissions Database for Global Atmospheric Research. [https://edgar.jrc.ec.europa.eu/report\\_2022?vis=pop#emissions\\_table](https://edgar.jrc.ec.europa.eu/report_2022?vis=pop#emissions_table) (Date accessed on 1st June 2023 at 7:45 PM Abu Dhabi)
84. FAO. (1982). *Plant Production and Protection*. Date Production and Protection Paper No. 35. p. 294. <http://www.fao.org/3/w5897e/w5897e6c.htm>
85. FAOSTAT. (2013). *Crop Production, Statistics Division*. Food and Agriculture Organization of the United Nations.
86. Felker, P. (2009). Unusual physiological properties of the arid adapted tree legume *Prosopis* and their applications in developing countries. *Perspectives in Biophysical Plant Ecophysiology: A Tribute to Park S Nobel*. Mexico City: Universidad Nacional Autónoma de México, 221–55.
87. Figueiredo, M. V. B., Vilar, J. J., & Burity, H. A. (1999). Alleviation of water stress effects in cowpea by *Bradyrhizobium* spp. Inoculation. *Plant and Soil*, 207(1), 67–75.
88. Fonton, N. H., Medjibé, V., Djomo, A., Kondaoulé, J., Rossi, V., Ngomanda, A., & Maïdou, H. (2017). Analyzing accuracy of the power functions for modeling aboveground biomass rediction in Congo basin tropical forests. *Open Journal of Forestry*, 7(4), 388–402.
89. Foody, G. M. (2002). Status of land cover classification accuracy assessment. *Remote Sensing of Environment*, 80(1), 185–201.
90. Gernhardt, S., Adam, N., Eineder, M., & Bamler, R. (2010). Potential of very high resolution SAR for persistent scatterer interferometry in urban areas. *Annals of GIS*, 16(2), 103–111.



91. Gevana, D., & Im, S. (2016). Allometric models for *Rhizophora stylosa* Griff. In dense monoculture plantation in the Philippines. *Malaysian Forester*, 79, 39–53.
92. Ghasemi, N., Sahebi, M. R., & Mohammadzadeh, A. (2011). A review on biomass estimation methods using synthetic aperture radar data. *International Journal of Geomatics and Geosciences*, 1(4), 776–788.
93. Gibbs, H. K., Brown, S., Niles, J. O., & Foley, J. A. (2007). Monitoring and estimating tropical forest carbon stocks: Making REDD a reality. *Environmental Research Letters*, 2(4), 045023. <https://iopscience.iop.org/article/10.1088/1748-9326/2/4/045023>.
94. Gilbertson, J. K., Kemp, J., & Van Niekerk, A. (2017). Effect of pan-sharpening multi-temporal Landsat 8 imagery for crop type differentiation using different classification techniques. *Computers and Electronics in Agriculture*, 134, 151–159.
95. Gizachew, B., Solberg, S., Næsset, E., Gobakken, T., Bollandsås, O. M., Breidenbach, J., Zahabu, E., & Mauya, E. W. (2016). Mapping and estimating the total living biomass and carbon in low-biomass woodlands using Landsat 8 CDR data. *Carbon Balance and Management*, 11(1), 1–14.
96. Goudie, A. S., Parker, A. G., & Al-Farraj, A. (2000). Coastal change in Ras al Khaimah (United Arab Emirates): A cartographic analysis. *Geographical Journal*, 166(1), 14–25.
97. Greenberg, J. A., Dobrowski, S. Z., & Ustin, S. L. (2005). Shadow allometry: Estimating tree structural parameters using hyperspatial image analysis. *Remote Sensing of Environment*, 97(1), 15–25.
98. Günlü, A., Ercanli, I., Başkent, E. Z., & Çakır, G. (2014). Estimating aboveground biomass using Landsat TM imagery: A case study of Anatolian Crimean pine forests in Turkey. *Annals of Forest Research*, 57(2), 289–298.
99. Guo, L. B., & Gifford, R. M. (2002). Soil carbon stocks and land use change: A meta analysis. *Global Change Biology*, 8(4), 345–360.
100. Houghton, N., Abramowitz, G., De Kauwe, M. G., & Pitman, A. J. (2018). Does predictability of fluxes vary between FLUXNET sites? *Biogeosciences*, 15(14). <https://doi.org/10.5194/bg-15-4495-2018>.
101. Hebbar, R., Ravishankar, H. M., Subramoniam, S. R., Uday, R., & Dadhwal, V. K. (2014). Object oriented classification of high resolution data for inventory of horticultural crops. *The International Archives of Photogrammetry, Remote Sensing and Spatial Information Sciences*, 40(8), 745. doi:10.5194/isprsarchives-XL-8-745-2014
102. Henson, I. E., & Chang, K. C. (2003). Oil palm trees and forest loss an objective appraisal. *Proceedings of the PIPOC 2003 International Palm Oil Congress*, Malaysian Palm Oil Board, 960–974.
103. Holm, A. M., Cridland, S. W., & Roderick, M. L. (2003). The use of time-integrated NOAA NDVI data and rainfall to assess landscape degradation in the arid shrubland of Western Australia. *Remote Sensing of Environment*, 85(2), 145–158.
104. Holmgren, P., Masakha, E. J., & Sjöholm, H. akan. (1994). Not all African land is being degraded: A recent survey of trees on farms in Kenya reveals rapidly increasing forest resources. *Ambio*, 23(7), 390–395.
105. Houghton, R. A., Hall, F., & Goetz, S. J. (2009). Importance of biomass in the global carbon cycle. *Journal of Geophysical Research: Biogeosciences*, 114(G2). <https://doi.org/10.1029/2009JG000935>
106. Huete, A. R. (1988). A soil-adjusted vegetation index (SAVI). *Remote Sensing of Environment*, 25(3), 295–309.
107. Humphrey, V., Zscheischler, J., Ciais, P., Gudmundsson, L., Sitch, S., & Seneviratne, S. I. (2018). Sensitivity of atmospheric CO<sub>2</sub> growth rate to observed changes in terrestrial water storage. *Nature*, 560(7720), 628–631.
108. Husch, B., Miller, C. I., & Beers, T. W. (1982). *Forest measurements*. John Wiley & Sons, Inc., New York.

109. Husin, M., Zakaria, Z. Z., & Hassan, A. H. (1987). Potentials of oil palm by-products as raw materials for agro-based industries. *IPMKSM*.
110. Im, J., & Jensen, J. R. (2008). Hyperspectral remote sensing of vegetation. *Geography Compass*, 2(6), 1943–1961.
111. Imagine Objective tools. (ERDAS Imagine User Guide, 2020). Imagine Objective tools.
112. Immitzer, M., Atzberger, C., & Koukal, T. (2012). Tree species classification with random forest using very high spatial resolution 8-band WorldView-2 satellite data. *Remote Sensing*, 4(9), 2661–2693.
113. Jara, M. C., Henry, M., Réjou-Méchain, M., Wayson, C., Zapata-Cuartas, M., Piotto, D., Guier, F. A., Lombis, H. C., López, E. C., & Lara, R. C. (2015). Guidelines for documenting and reporting tree allometric equations. *Annals of Forest Science*, 72(6), 763–768.
114. Jawak, S. D., Devliyal, P., & Luis, A. J. (2015). A comprehensive review on pixel oriented and object oriented methods for information extraction from remotely sensed satellite images with a special emphasis on cryospheric applications. *Advances in Remote Sensing*, 4(03), 177. doi: 10.4236/ars.2015.43015
115. Jawak, S. D., Luis, A. J., Panditrao, S. N., Khopkar, P. S., & Jadhav, P. S. (2013). Advancement in landcover classification using very high resolution remotely sensed 8-band WorldView-2 satellite data. *International Journal of Earth Sciences and Engineering*, 6(02), 1742–1749.
116. Jiang, Z., Huete, A. R., Didan, K., & Miura, T. (2008). Development of a two-band enhanced vegetation index without a blue band. *Remote Sensing of Environment*, 112(10), 3833–3845.
117. Joshi, H. G., & Ghose, M. (2014). Community structure, species diversity, and aboveground biomass of the Sundarbans mangrove swamps. *Tropical Ecology*, 55(3), 283–303.
118. Jucker, T., Caspersen, J., Chave, J., Antin, C., Barbier, N., Bongers, F., Dalponte, M., van Ewijk, K. Y., Forrester, D. I., & Haeni, M. (2017). Allometric equations for integrating remote sensing imagery into forest monitoring programmes. *Global Change Biology*, 23(1), 177–190.
119. Kader, A. A., & Hussein, A. M. (2009). Harvesting and postharvest handling of dates. *ICARDA, Aleppo, Syria*, 4, 15. <https://doi.org/10.1002/9781118292419.ch5>
120. Kamarudzaman, A., Mohd Hashim, T., Mohd, A., & Teah, C. H. (1995). Zero burning-An environmentally friendly replanting technique. *PORIM International Palm Oil Congress: Update and Vision (Agriculture) September 22–25 Kuala Lumpur, Malaysia*.
121. Kamusoko, C., & Aniya, M. (2009). Hybrid classification of Landsat data and GIS for land use/cover change analysis of the Bindura district, Zimbabwe. *International Journal of Remote Sensing*, 30(1), 97–115.
122. Kankare, V., Vastaranta, M., Holopainen, M., Rätty, M., Yu, X., Hyyppä, J., Hyyppä, H., Alho, P., & Viitala, R. (2013). Retrieval of forest aboveground biomass and stem volume with airborne scanning LiDAR. *Remote Sensing*, 5(5), 2257–2274.
123. Kappen, L., Lange, O. L., Schulze, E.-D., Evenari, M., & Buschbom, U. (1972). Extreme water stress and photosynthetic activity of the desert plant *Artemisia herba-alba* Asso. *Oecologia*, 10(2), 177–182.
124. Karlson, M., Ostwald, M., Reese, H., Sanou, J., Tankoano, B., & Mattsson, E. (2015). Mapping tree canopy cover and aboveground biomass in Sudano-Saharan woodlands using Landsat 8 and random forest. *Remote Sensing*, 7(8), 10017–10041.
125. Kelsey, K. C., & Neff, J. C. (2014). Estimates of aboveground biomass from texture analysis of Landsat imagery. *Remote Sensing*, 6(7), 6407–6422.
126. Ketterings, Q. M., Coe, R., van Noordwijk, M., & Palm, C. A. (2001). Reducing uncertainty in the use of allometric biomass equations for predicting above-ground tree biomass in mixed secondary forests. *Forest Ecology and Management*, 146(1–3), 199–209.



127. Khalid, H., Zin, Z. Z., & Anderson, J. M. (1999a). Quantification of oil palm biomass and nutrient value in a mature plantation. I. Above-ground biomass. *Journal of Oil Palm Research*, 11(1), 23–32.
128. Khalid, H., Zin, Z. Z., & Anderson, J. M. (1999b). Quantification of oil palm biomass and nutrient value in a mature plantation. II. Below-ground biomass. *Journal of Oil Palm Research*, 11(2), 63–71.
129. Khalid, N., & Hamid, J. R. A. (2017). Development of Allometric Equation for Estimating Aboveground Biomass in Ampang Forest Reserve, Malaysia. *J Biodivers Manage Forestry* 6: 1. Of, 4, 2. doi:10.4172/2327-4417.1000173
130. King, D. A. (1990). Allometry of saplings and understorey trees of a Panamanian forest. *Functional Ecology*, 27–32.
131. Koala, J., Sawadogo, L., Savadogo, P., Aynekulu, E., Heiskanen, J., & Saïd, M. (2017). Allometric equations for below-ground biomass of four key woody species in West African savanna-woodlands. *Silva Fennica*.
132. Korom, A., & Matsuura, T. (2016). Relationships between crown size and aboveground biomass of oil palms: An evaluation of allometric models. *Sains Malaysiana*, 45(4), 523–533.
133. Ksiksi, T. S. (2012). *Acacia trolilis* and *Calotropis procera*: Do They Substantially Promote Soil Carbon Sequestration? *Open Journal of Soil Science*, 2(02), 116. doi.org/10.4236/ojss.2012.22017
134. Kuemmerle, T., Radeloff, V. C., Perzanowski, K., & Hostert, P. (2006). Cross-border comparison of land cover and landscape pattern in Eastern Europe using a hybrid classification technique. *Remote Sensing of Environment*, 103(4), 449–464.
135. Kumar, L., & Mutanga, O. (2017). Remote Sensing of Above-Ground Biomass. *Remote Sensing*, 9(9), 935. https://doi.org/10.3390/rs9090935
136. Kumar, L., Sinha, P., Taylor, S., & Alqurashi, A. F. (2015). Review of the use of remote sensing for biomass estimation to support renewable energy generation. *Journal of Applied Remote Sensing*, 9(1), 097696–097696.
137. Kux, H. J., & Souza, U. D. (2012). Object-based image analysis of WORLDVIEW-2 satellite data for the classification of mangrove areas in the city of São Luís, Maranhão State, Brazil. *ISPRS Ann. Photogramm. Remote Sens. Spat. Inf. Sci*, 4, 95–100.
138. Labrecque, S., Fournier, R. A., Luther, J. E., & Piercey, D. (2006). A comparison of four methods to map biomass from Landsat-TM and inventory data in western Newfoundland. *Forest Ecology and Management*, 226(1), 129–144.
139. Lack, N., & Bleisch, S. (2010). Object-based change detection for a cultural-historical survey of the landscape—from cow trails to walking paths. *The International Archives of the Photogrammetry, Remote Sensing and Spatial Information Sciences*, 38. 38 Proceedings of the Geographic object-based image analysis (GEOBIA) Ghent, Belgium.
140. Lackner, K. S. (2003). A guide to CO<sub>2</sub> sequestration. *Science*, 300(5626), 1677–1678.
141. Lal, Rattan. (2001). Potential of desertification control to sequester carbon and mitigate the greenhouse effect. *Climatic Change*, 51(1), 35–72.
142. Lal, Rattan. (2002). Soil carbon dynamics in cropland and rangeland. *Environmental Pollution*, 116(3), 353–362.
143. Le Maire, G., François, C., Soudani, K., Berveiller, D., Pontailier, J.-Y., Bréda, N., Genet, H., Davi, H., & Dufrêne, E. (2008). Calibration and validation of hyperspectral indices for the estimation of broadleaved forest leaf chlorophyll content, leaf mass per area, leaf area index and leaf canopy biomass. *Remote Sensing of Environment*, 112(10), 3846–3864.
144. Lemenih, M., & Itanna, F. (2004). Soil carbon stocks and turnovers in various vegetation types and arable lands along an elevation gradient in southern Ethiopia. *Geoderma*, 123(1–2), 177–188.

145. Li, D., Ke, Y., Gong, H., & Li, X. (2015). Object-based urban tree species classification using bi-temporal WorldView-2 and WorldView-3 images. *Remote Sensing*, 7(12), 16917-16937.
146. Li, M., Tan, Y., Pan, J., & Peng, S. (2008). Modeling forest aboveground biomass by combining spectrum, textures and topographic features. *Frontiers of Forestry in China*, 3(1), 10-15.
147. Litton, C. M., & Boone Kauffman, J. (2008). Allometric models for predicting aboveground biomass in two widespread woody plants in Hawaii. *Biotropica*, 40(3), 313-320.
148. Liu, D., & Xia, F. (2010). Assessing object-based classification: Advantages and limitations. *Remote Sensing Letters*, 1(4), 187-194.
149. Lo, C. P., & Choi, J. (2004). A hybrid approach to urban land use/cover mapping using Landsat 7 Enhanced Thematic Mapper Plus (ETM+) images. *International Journal of Remote Sensing*, 25(14), 2687-2700.
150. Lu, Dengsheng. (2006). The potential and challenge of remote sensing-based biomass estimation. *International Journal of Remote Sensing*, 27(7), 1297-1328.
151. Lu, Dengsheng, & Weng, Q. (2004). Spectral mixture analysis of the urban landscape in Indianapolis with Landsat ETM+ imagery. *Photogrammetric Engineering & Remote Sensing*, 70(9), 1053-1062.
152. Lugo, A. E., & Brown, S. (1992). Tropical forests as sinks of atmospheric carbon. *Forest Ecology and Management*, 54(1), 239-255. [https://doi.org/10.1016/0378-1127\(92\)90016-3](https://doi.org/10.1016/0378-1127(92)90016-3)
153. Mahmood, H., Siddique, M. R., Costello, L., Birigazzi, L., Abdullah, S. R., Henry, M., Siddiqui, B. N., Aziz, T., Ali, S., & Al Mamun, A. (2019). Allometric models for estimating biomass, carbon and nutrient stock in the Sal zone of Bangladesh. *IForest-Biogeosciences and Forestry*, 12(1), 69. doi: <https://doi.org/10.3832/ifer2758-011>
154. Main-Knorn, M., Moisen, G. G., Healey, S. P., Keeton, W. S., Freeman, E. A., & Hostert, P. (2011). Evaluating the remote sensing and inventory-based estimation of biomass in the western Carpathians. *Remote Sensing*, 3(7), 1427-1446.
155. Makinde, E. O., Womiloju, A. A., & Ogundeko, M. O. (2017). The geospatial modelling of carbon sequestration in Oluwa Forest, Ondo State, Nigeria. *European Journal of Remote Sensing*, 50(1), 397-413.
156. Mangiarotti, S., Mazzega, P., Jarlan, L., Mougin, E., Baup, F., & Demarty, J. (2008). Evolutionary bi-objective optimization of a semi-arid vegetation dynamics model with NDVI and  $\delta^{13}C$  satellite data. *Remote Sensing of Environment*, 112(4), 1365-1380.
157. Maulana, S. I., Wibisono, Y., & Utomo, S. (2016). Development of local allometric equation to estimate total aboveground biomass in Papua tropical forest. *Indonesian Journal of Forestry Research*, 3(2), 107-118.
158. Maynard, C. L., Lawrence, R. L., Nielsen, G. A., & Decker, G. (2007). Modeling vegetation amount using bandwise regression and ecological site descriptions as an alternative to vegetation indices. *GIScience & Remote Sensing*, 44(1), 68-81.
159. McGwire, K., Minor, T., & Fenstermaker, L. (2000). Hyperspectral mixture modeling for quantifying sparse vegetation cover in arid environments. *Remote Sensing of Environment*, 72(3), 360-374.
160. McMorrow, J. (2001). Linear regression modelling for the estimation of oil palm age from Landsat TM. *International Journal of Remote Sensing*, 22(12), 2243-2264.
161. Mokany, K., Raison, R., & Prokushkin, A. S. (2006). Critical analysis of root: Shoot ratios in terrestrial biomes. *Global Change Biology*, 12(1), 84-96.
162. Montagni, A., Corona, P., Dalponte, M., Gianelle, D., Chirici, G., & Olsson, H. (2013). Airborne laser scanning of forest resources: An overview of research in Italy as a commentary case study. *International Journal of Applied Earth Observation and Geoinformation*, 23, 288-300.



163. Monteith, J. L. (1972). Solar radiation and productivity in tropical ecosystems. *Journal of Applied Ecology*, 9(3), 747-766.
164. Morel, A. C., Fisher, J. B., & Malhi, Y. (2012). Evaluating the potential to monitor aboveground biomass in forest and oil palm in Sabah, Malaysia, for 2000-2008 with Landsat ETM+ and ALOS-PALSAR. *International Journal of Remote Sensing*, 33(11), 3614-3639. <https://doi.org/10.1080/01431161.2011.631949>
165. Mugiraneza, T., Nascetti, A., & Ban, Y. (2019). WorldView-2 Data for Hierarchical Object-Based Urban Land Cover Classification in Kigali: Integrating Rule-Based Approach with Urban Density and Greenness Indices. *Remote Sensing*, 11(18), 2128. <https://doi.org/10.3390/rs11182128>
166. Mundia, C. N., & Aniya, M. (2005). Analysis of land use/cover changes and urban expansion of Nairobi city using remote sensing and GIS. *International Journal of Remote Sensing*, 26(13), 2831-2849.
167. Mutanga, O., & Rugege, D. (2006). Integrating remote sensing and spatial statistics to model herbaceous biomass distribution in a tropical savanna. *International Journal of Remote Sensing*, 27(16), 3499-3514.
168. Mutanga, Onesimo, & Skidmore, A. K. (2004). Narrow band vegetation indices overcome the saturation problem in biomass estimation. *International Journal of Remote Sensing*, 25(19), 3999-4014.
169. Mwanamwenge, J., Loss, S. P., Siddique, K. H. M., & Cocks, P. S. (1999). Effect of water stress during floral initiation, flowering and podding on the growth and yield of faba bean (*Vicia faba* L.). *European Journal of Agronomy*, 11(1), 1-11.
170. Myint, S. W., Gober, P., Brazel, A., Grossman-Clarke, S., & Weng, Q. (2011b). Per-pixel vs. Object-based classification of urban land cover extraction using high spatial resolution imagery. *Remote Sensing of Environment*, 115(5), 1145-1161.
171. Naesset, E., & Økland, T. (2002). Estimating tree height and tree crown properties using airborne scanning laser in a boreal nature reserve. *Remote Sensing of Environment*, 79(1), 105-115.
172. Nagaraja, A. (2009). Predicting susceptible areas of mango malformation through remote sensing and GIS [PhD Dissertation]. Indian Agricultural Research Institute, New Delhi, India.
173. Nyssen, J., Temesgen, H., Lemenih, M., Zenebe, A., Haregeweyn, N., & Haile, M. (2008). Spatial and temporal variation of soil organic carbon stocks in a lake retreat area of the Ethiopian Rift Valley. *Geoderma*, 146(1-2), 261-268.
174. Ohmann, J. L., & Gregory, M. J. (2002). Predictive mapping of forest composition and structure with direct gradient analysis and nearest-neighbor imputation in coastal Oregon, USA. *Canadian Journal of Forest Research*, 32(4), 725-741.
175. Oldeland, J., Dorigo, W., Wesul, D., & Jürgens, N. (2010). Mapping bush encroaching species by seasonal differences in hyperspectral imagery. *Remote Sensing*, 2(6), 1416-1438.
176. Ozdemir, I. (2008). Estimating stem volume by tree crown area and tree shadow area extracted from pan-sharpened Quickbird imagery in open Crimean juniper forests. *International Journal of Remote Sensing*, 29(19), 5643-5655.
177. Ozdemir, Ibrahim, & Karnieli, A. (2011). Predicting forest structural parameters using the image texture derived from WorldView-2 multispectral imagery in a dryland forest, Israel. *International Journal of Applied Earth Observation and Geoinformation*, 13(5), 701-710.
178. Pandit, S., Tsuyuki, S., & Dube, T. (2018). Estimating above-ground biomass in sub-tropical buffer zone community Forests, Nepal, using Sentinel 2 data. *Remote Sensing*, 10(4), 601. <https://doi.org/10.3390/rs10040601>
179. Patel, N. K., Saxena, R. K., & Shiwalkar, A. (2007). Study of fractional vegetation cover using high spectral resolution data. *Journal of the Indian Society of Remote Sensing*, 35(1), 73-79.

180. Pflugmacher, D. (2011). Remote sensing of forest biomass dynamics using Landsat-derived disturbance and recovery history and lidar data. Oregon State University.
181. Phiri, D., & Morgenroth, J. (2017). Developments in Landsat land cover classification methods: A review. *Remote Sensing*, 9(9), 967. <https://doi.org/10.3390/rs9090967>
182. Picard, N., Saint-André, L., & Henry, M. (2012). Manual for building tree volume and biomass allometric equations: From field measurement to prediction, FAO; Food and Agricultural Organization of the United Nations.
183. Pinty, B., & Verstraete, M. M. (1992). GEMI: A non-linear index to monitor global vegetation from satellites. *Vegetatio*, 101(1), 15–20.
184. Ponce-Hernandez, R., Koochafkan, P., & Antoine, J. (2004). Assessing carbon stocks and modelling win-win scenarios of carbon sequestration through land-use changes (Vol. 1). Food & Agriculture Org.
185. Popescu, S. C., Wynne, R. H., & Nelson, R. F. (2003). Measuring individual tree crown diameter with lidar and assessing its influence on estimating forest volume and biomass. *Canadian Journal of Remote Sensing*, 29(5), 564–577.
186. Poulter, B., Frank, D., Ciais, P., Myneni, R. B., Andela, N., Bi, J., Broquet, G., Canadell, J. G., Chevallier, F., & Liu, Y. Y. (2014). Contribution of semi-arid ecosystems to interannual variability of the global carbon cycle. *Nature*, 509(7502), 600–603.
187. Pradhan, R., Ghose, M. K., & Jeyaram, A. (2010). Land cover classification of remotely sensed satellite data using bayesian and hybrid classifier. *International Journal of Computer Applications*, 7(11), 1–4.
188. Prayogo, C., Sari, R. R., Asmara, D. H., Rahayu, S., & Hairiah, K. (2018). Allometric Equation for Pinang (Areca catechu) Biomass and C Stocks. *AGRIVITA, Journal of Agricultural Science*, 40(3), 382–389.
189. Ramachandran, A., Jayakumar, S., Haroon, R. M., Bhaskaran, A., & Arockiasamy, D. I. (2007). Carbon sequestration: Estimation of carbon stock in natural forests using geospatial technology in the Eastern Ghats of Tamil Nadu, India. *Current Science*, 323–331.
190. Ramankutty, N., Gibbs, H. K., Achard, F., Defries, R., Foley, J. A., & Houghton, R. A. (2007). Challenges to estimating carbon emissions from tropical deforestation. *Global Change Biology*, 13(1), 51–66.
191. Ramos, M. L. G., Parsons, R., Sprent, J. I., & James, E. K. (2003). Effect of water stress on nitrogen fixation and nodule structure of common bean. *Pesquisa Agropecuária Brasileira*, 38(3), 339–347.
192. Rees, A. R., & Tinker, P. B. H. (1963). Dry-matter production and nutrient content of plantation oil palms in Nigeria. *Plant and Soil*, 19(1), 19–32.
193. Reinartz, P., Müller, R., Hoja, D., Lehner, M., & Schroeder, M. (2005). Comparison and fusion of DEM derived from SPOT-5 HRS and SRTM data and estimation of forest heights. *Proc. EARSeL Workshop on 3D-Remote Sensing, Porto, Vol. 1, Portugal*.
194. Rembold, F., Carnicelli, S., Nori, M., & Ferrari, G. A. (2000). Use of aerial photographs, Landsat TM imagery and multidisciplinary field survey for land-cover change analysis in the lakes region (Ethiopia). *International Journal of Applied Earth Observation and Geoinformation*, 2(3–4), 181–189.
195. Ren, H., Zhou, G., & Zhang, X. (2011). Estimation of green aboveground biomass of desert steppe in Inner Mongolia based on red-edge reflectance curve area method. *Biosystems Engineering*, 109(4), 385–395.
196. Ritchie, J. C., & Rango, A. (1996). Remote sensing applications to hydrology: Introduction. *Hydrological Sciences Journal*, 41(4), 429–431.



197. Rizvi, R. H., Newaj, R., Srivastava, S., & Yadav, M. (2019). MAPPING trees on farmlands using OBIA method and high resolution satellite data: a case study of Koraput district, ODISHA. ISPRS - International Archives of the Photogrammetry, Remote Sensing and Spatial Information Sciences, XLII-3/W6, 617-621. <https://doi.org/10.5194/isprs-archives-XLII-3-W6-617-2019>
198. Robinson, C., Saatchi, S., Neumann, M., & Gillespie, T. (2013). Impacts of spatial variability on aboveground biomass estimation from L-band radar in a temperate forest. *Remote Sensing*, 5(3), 1001-1023.
199. Rosema, A. (1993). Using METEOSAT for operational evapotranspiration and biomass monitoring in the Sahel region. *Remote Sensing of Environment*, 46(1), 27-44.
200. Rozenstein, O., & Karnieli, A. (2011). Comparison of methods for land-use classification incorporating remote sensing and GIS inputs. *Applied Geography*, 31(2), 533-544.
201. Russell, C. E. (1983). Nutrient cycling and productivity of native and plantation forests at Jari Florestal, Para, Brazil. University of Georgia.
202. Sahay, B., Chakraborty, A., Chaudhary, K. K., Laxman, B., Murthy, C., & Rao, P. (2017). Mapping Multiple Horticulture Crops using Object Oriented Classification Techniques. 9. In: 38th Asian Conference on Remote Sensing.
203. Sajdak, M., Velázquez-Martí, B., & López-Cortés, I. (2014). Quantitative and qualitative characteristics of biomass derived from pruning Phoenix canariensis hort. Ex Chabaud. And Phoenix dactilifera L. *Renewable Energy*, 71, 545-552.
204. Salem Issa, & Al Shuwaihi, A. (2012). Characterization of Al Ain city urban growth using multi-temporal remote sensing data and GIS. *Int Geoinformatics Res Dev J*, 3, 1-17.
205. Salem Issa, Dahy, B., Ksiksi, T., & Saleous, N. (2018). Development of a new allometric equation correlated with RS variables for the assessment of date palm biomass. *Proceedings of the 39th Asian Conference on Remote Sensing (ACRS 2018)*, Kuala Lumpur, Malaysia, 15-19 October 2018. Link: <https://a-a-r-s.org/proceeding/ACRS2018/ACRS%202018%20PROCEEDING.pdf>
206. Salem Issa, Dahy, B. S., & Saleous, N. (2020). Accurate mapping of date palms at different age-stages for the purpose of estimating their biomass. *ISPRS Annals of Photogrammetry, Remote Sensing and Spatial Information Sciences*, V-3-2020, 461-467. <https://doi.org/10.5194/isprs-annals-V-3-2020-461-2020>
207. Salem Issa, Dahy, B., Ksiksi, T., & Saleous, N. (2020a). A Review of Terrestrial Carbon Assessment Methods Using Geo-Spatial Technologies with Emphasis on Arid Lands. *Remote Sensing*, 12(12), 2008. <https://doi.org/10.3390/rs12122008>
208. Salem Issa, Dahy, B., Ksiksi, T., & Saleous, N. (2020b). Allometric equations coupled with remotely sensed variables to estimate carbon stocks in date palms. *Journal of Arid Environments*, 182, 104264. <https://doi.org/10.1016/j.jaridenv.2020.104264>
209. Salem Issa, Dahy, B., Saleous, N., & Ksiksi, T. (2019). Carbon stock assessment of date palm using remote sensing coupled with field-based measurements in Abu Dhabi (United Arab Emirates). *International Journal of Remote Sensing*, 0(0), 1-20. <https://doi.org/10.1080/01431161.2019.1602795>
210. Schlerf, M., Atzberger, C., & Hill, J. (2005). Remote sensing of forest biophysical variables using HyMap imaging spectrometer data. *Remote Sensing of Environment*, 95(2), 177-194.
211. Schreuder, H. T., Gregoire, T. G., & Wood, G. B. (1993). Sampling methods for multiresource forest inventory. John Wiley & Sons.
212. Schucknecht, A., Meroni, M., Kayitakire, F., Rembold, F., & Boureima, A. (2015). Biomass estimation to support pasture management in Niger. *The International Archives of Photogrammetry, Remote Sensing and Spatial Information Sciences*, 40(7), 109. doi: 10.5194/isprsarchives-XL-7-W3-109-2015.

213. Shafri, H. Z., Hamdan, N., & Saripan, M. I. (2011). Semi-automatic detection and counting of oil palm trees from high spatial resolution airborne imagery. *International Journal of Remote Sensing*, 32(8), 2095–2115.
214. Shaharum, N. S. N., Shafri, H. Z. M., Gambo, J., & Abidin, F. A. Z. (2018). Mapping of Krau Wildlife Reserve (KWR) protected area using Landsat 8 and supervised classification algorithms. *Remote Sensing Applications: Society and Environment*, 10, 24–35.
215. Shahin, S. M., and M. Salem. (2014). "Review Future Concerns on Irrigation Requirements of Date Palm Tree in the United Arab Emirates (UAE): Call for Quick Actions". The 5th International Date Palm Conference, Date Palm Improvement Section, Abu Dhabi, March 16–18, 255–262.
216. Shaker, A., Yan, W. Y., & El-Ashmawy, N. (2012). Panchromatic satellite image classification for flood hazard assessment. *Journal of Applied Research and Technology*, 10(6), 902–911.
217. Shila, H. (2010). Comparison of Land Covers Classification Methods in Etm+ Satellite Images (Case Study: Ghamishloo Wildlife Refuge). *Journal of Environmental Research and Development*, 5(2), 279–293.
218. Shiver, B. D., & Borders, B. E. (1996). Sampling techniques for forest resource inventory. John Wiley and Sons.
219. Sileshi, G. W. (2014). A critical review of forest biomass estimation models, common mistakes and corrective measures. *Forest Ecology and Management*, 329, 237–254.
220. Singh, M., Malhi, Y., & Bhagwat, S. (2014). Evaluating land use and aboveground biomass dynamics in an oil palm-dominated landscape in Borneo using optical remote sensing. *Journal of Applied Remote Sensing*, 8(1), 083695. <https://doi.org/10.1117/1.JRS.8.083695>
221. Singh, S. L., Sahoo, U. K., Kenye, A., & Gogoi, A. (2018). Assessment of Growth, Carbon Stock and Sequestration Potential of Oil Palm Trees in Mizoram, Northeast India. *Journal of Environmental Protection*, 9(09), 912. doi 10.4236/jep.2018.99057
222. Smith, W. K., Dannenberg, M. P., Yan, D., Herrmann, S., Barnes, M. L., Barron-Gafford, G. A., Biederman, J. A., Ferrenberg, S., Fox, A. M., Hudson, A., Knowles, J. F., MacBean, N., Moore, D. J. P., Nagler, P. L., Reed, S. C., Rutherford, W. A., Scott, R. L., Wang, X., & Yang, J. (2019). Remote sensing of dryland ecosystem structure and function: Progress, challenges, and opportunities. *Remote Sensing of Environment*, 233, 111401. <https://doi.org/10.1016/j.rse.2019.111401>
223. Song, C., Dickinson, M. B., Su, L., Zhang, S., & Yaussey, D. (2010). Estimating average tree crown size using spatial information from Ikonos and QuickBird images: Across-sensor and across-site comparisons. *Remote Sensing of Environment*, 114(5), 1099–1107.
224. Sonnenschein, R., Kuemmerle, T., Udelhoven, T., Stellmes, M., & Hostert, P. (2011). Differences in Landsat-based trend analyses in drylands due to the choice of vegetation estimate. *Remote Sensing of Environment*, 115(6), 1408–1420.
225. Southworth, J., Nagendra, H., & Tucker, C. (2002). Fragmentation of a landscape: Incorporating landscape metrics into satellite analyses of land-cover change. *Landscape Research*, 27(3), 253–269.
226. Srestasathiern, P., & Rakwatin, P. (2014). Oil palm tree detection with high resolution multi-spectral satellite imagery. *Remote Sensing*, 6(10), 9749–9774.
227. St-Onge, B., Hu, Y., & Vega, C. (2008). Mapping the height and above-ground biomass of a mixed forest using lidar and stereo Ikonos images. *International Journal of Remote Sensing*, 29(5), 1277–1294.
228. Stych, P., Jerabkova, B., Lastovicka, J., Riedl, M., & Paluba, D. (2019). A comparison of worldview-2 and landsat 8 images for the classification of forests affected by bark beetle outbreaks using a support vector machine and a neural network: A case study in the sumava mountains. *Geosciences*, 9(9), 396. <https://doi.org/10.3390/geosciences9090396>



229. Suganuma, H., Abe, Y., Taniguchi, M., Tanouchi, H., Utsugi, H., Kojima, T., & Yamada, K. (2006). Stand biomass estimation method by canopy coverage for application to remote sensing in an arid area of Western Australia. *Forest Ecology and Management*, 222(1), 75–87. <https://doi.org/10.1016/j.foreco.2005.10.014>
230. Sunaryathy, P. I., Kanniah, K. D., & Tan, K. P. (2015). Estimating Aboveground Biomass of Oil Palm Trees by Using the Destructive Method. *World Journal of Agricultural Research*, 3(1), 17–19.
231. Svoray, T., Shoshany, M., Curran, P. J., Foody, G. M., & Perevolotsky, A. (2001). Relationship between green leaf biomass volumetric density and ERS-2 SAR backscatter of four vegetation formations in the semi-arid zone of Israel. *International Journal of Remote Sensing*, 22(8), 1601–1607.
232. Svoray, Tal, & Shoshany, M. (2003). Herbaceous biomass retrieval in habitats of complex composition: A model merging SAR images with unmixed Landsat TM data. *IEEE Transactions on Geoscience and Remote Sensing*, 41(7), 1592–1601.
233. Terakunpisut, J., Gajasen, N., & Ruankawe, N. (2007). Carbon sequestration potential in aboveground biomass of Thong Pha Phum national forest, Thailand. *Applied Ecology and Environmental Research*, 5(2), 93–102.
234. Thakur, T., & Swamy, S. L. (2012). Analysis of land use, diversity, biomass, C and nutrient storage of a dry tropical forest ecosystem of India using satellite remote sensing and GIS techniques. *Proceedings of International Forestry and Environment Symposium*, 15. pp. 273–278.
235. Thenkabail, P. S., Stucky, N., Griscom, B. W., Ashton, M. S., Diels, J., van der Meer, B., & Enclona, E. (2004). Biomass estimations and carbon stock calculations in the oil palm trees of African derived savannas using IKONOS data. *International Journal of Remote Sensing*, 25(23), 5447–5472. <https://doi.org/10.1080/01431160412331291279>
236. Tian, F., Brandt, M., Liu, Y. Y., Verger, A., Tageson, T., Diouf, A. A., Rasmussen, K., Mbow, C., Wang, Y., & Fensholt, R. (2016). Remote sensing of vegetation dynamics in drylands: Evaluating vegetation optical depth (VOD) using AVHRR NDVI and in situ green biomass data over West African Sahel. *Remote Sensing of Environment*, 177(Supplement C), 265–276. <https://doi.org/10.1016/j.rse.2016.02.056>
237. Tsitsi, B. (2016). Remote sensing of aboveground forest biomass: A review. *Tropical Ecology*, 57(2), 125–132.
238. Tucker, C. J., Vanpraet, C. L., Sharman, M. J., & Van Ittersum, G. (1985). Satellite remote sensing of total herbaceous biomass production in the Senegalese Sahel: 1980–1984. *Remote Sensing of Environment*, 17(3), 233–249.
239. Turner, D. P., Cohen, W. B., Kennedy, R. E., Fassnacht, K. S., & Briggs, J. M. (1999). Relationships between leaf area index and Landsat TM spectral vegetation indices across three temperate zone sites. *Remote Sensing of Environment*, 70(1), 52–68.
240. Turner, W., Rondinini, C., Pettorelli, N., Mora, B., Leidner, A. K., Szantoi, Z., Buchanan, G., Dech, S., Dwyer, J., & Herold, M. (2015). Free and open-access satellite data are key to biodiversity conservation. *Biological Conservation*, 182, 173–176.
241. United Nation. (2019). The Kyoto Protocol—Status of Ratification | UNFCCC [<https://unfccc.int/process/the-kyoto-protocol/status-of-ratification>]. Retrieved on 20 April 2021.
242. Van der Hoek, Y., Solas, S. Á., & Peñuela, M. C. (2019). The palm *Mauritia flexuosa*, a keystone plant resource on multiple fronts. *Biodiversity and Conservation*, 1–13.
243. Vashum, K. T., & Jayakumar, S. (2012). Methods to estimate above-ground biomass and carbon stock in natural forests—A review. *J. Ecosyst. Ecogr*, 2(4), 1–7.
244. Walkley, A., & Black, I. A. (1934). An examination of the Degtjareff method for determining soil organic matter, and a proposed modification of the chromic acid titration method. *Soil Science*, 37(1), 29–38.

245. Wallerman, J., Fransson, J. E., Bohlin, J., Reese, H., & Olsson, H. (2010). Forest mapping using 3D data from SPOT-5 HRS and Z/I DMC. 2010 IEEE International Geoscience and Remote Sensing Symposium, 64–67.
246. Wang, J., Chen, J., Ju, W., & Li, M. (2010). IA-SDSS: A GIS-based land use decision support system with consideration of carbon sequestration. *Environmental Modelling & Software*, 25(4), 539–553. <https://doi.org/10.1016/j.envsoft.2009.09.010>
247. Wang, L., Shi, C., Diao, C., Ji, W., & Yin, D. (2016). A survey of methods incorporating spatial information in image classification and spectral unmixing. *International Journal of Remote Sensing*, 37(16), 3870–3910.
248. Wani, A. A., Joshi, P. K., & Singh, O. (2015). Estimating biomass and carbon mitigation of temperate coniferous forests using spectral modeling and field inventory data. *Ecological Informatics*, 25, 63–70.
249. Wannasiri, W., Nagai, M., Honda, K., Santitam-nont, P., & Miphokasap, P. (2013). Extraction of mangrove biophysical parameters using airborne LiDAR. *Remote Sensing*, 5(4), 1787–1808.
250. Wijaya, A., & Gloaguen, R. (2009). Fusion of ALOS Palsar and Landsat ETM data for land cover classification and biomass modeling using non-linear methods. *Geoscience and Remote Sensing Symposium, 2009 IEEE International, IGARSS 2009*, 3, pp. III-581.
251. Williams, C. A. (2010). Integration of remote sensing and modeling to understand carbon fluxes and climate interactions in Africa. *Ecosystem Function in Savannas: Measurement and Modeling at Landscape to Global Scales*, Edited by: Hill, MJ and Hanan, N., CRC Press, Boca Raton, FL, 327–346.
252. Wu, C., Shen, H., Wang, K., Shen, A., Deng, J., & Gan, M. (2016). Landsat imagery-based above ground biomass estimation and change investigation related to human activities. *Sustainability*, 8(2), 159. <https://doi.org/10.3390/su8020159>
253. Wu, X. B., & Archer, S. R. (2005). Scale-dependent influence of topography-based hydrologic features on patterns of woody plant encroachment in savanna landscapes. *Landscape Ecology*, 20(6), 733–742.
254. Wylie, B., Denda, I., Pieper, R., Harrington, J., Reed, B., & Southward, G. (1995). Satellite-Based Herbaceous Biomass Estimates in the Pastoral Zone of Niger. *Journal of Range Management*, 48(2), 159–164. <https://doi.org/10.2307/4002804>
255. Xiaoming, F., Yingshi, Z., & Yan, L. (2005). Remote sensing linked modeling of the aboveground biomass of semiarid grassland in Inner Mongolia. *Geoscience and Remote Sensing Symposium, 2005. IGARSS'05. Proceedings. 2005 IEEE International*, 5, 3047–3050.
256. Xie, Y., Sha, Z., & Yu, M. (2008). Remote sensing imagery in vegetation mapping: A review. *Journal of Plant Ecology*, 1(1), 9–23.
257. Yang, X., & Lo, C. P. (2002). Using A time series of satellite imagery to detect land use and cover changes in Atlanta, Georgia. *International Journal of Remote Sensing*, 23(9), 1775–1798.
258. Yuen, J. Q., Fung, T., & Ziegler, A. D. (2016). Review of allometric equations for major land covers in SE Asia: Uncertainty and implications for above-and below-ground carbon estimates. *Forest Ecology and Management*, 360, 323–340.
259. Zahabu, E., Mugasha, W. A., Malimbwi, R. E., & Katani, J. Z. (2018). Allometric biomass and volume models for coconut trees. E&D Vision Publishing Ltd.
260. Zandler, H., Brenning, A., & Samimi, C. (2015). Quantifying dwarf shrub biomass in an arid environment: Comparing empirical methods in a high dimensional setting. *Remote Sensing of Environment*, 158, 140–155.
261. Zhao, P., Lu, D., Wang, G., Wu, C., Huang, Y., & Yu, S. (2016). Examining spectral reflectance saturation in Landsat imagery and corresponding solutions to improve forest aboveground biomass estimation. *Remote Sensing*, 8(6), 469. <https://doi.org/10.3390/rs8060469>
262. Zohary, D., & Hopf, M. (2000). *Domestication of plants in the Old World: The origin and spread of cultivated plants in West Asia. Europe, and the Nile Valley* Oxford University Press, New York.



The background features a light teal color with several abstract geometric elements. In the upper right, there is a large triangular shape filled with a grid of black dots. Below this, there are several horizontal lines and a smaller triangle. In the lower right, there are more horizontal lines and a triangle filled with a grid of black dots. The overall design is modern and minimalist.

# List of Publications

1. Dahy, B., Issa, S., & Saleous, N. (2023). Geo-spatial modelling of carbon stock assessment of date palm at different age stages: An integrated approach of fieldwork, remote sensing and GIS. *Ecological Modelling*, 481, 110377. <https://doi.org/10.1016/j.ecolmod-el.2023.110377>
2. Dahy, B., Issa, S., Ksiksi, T., & Saleous, N. (2020). Geospatial Technology Methods for Carbon Stock Assessment: A Comprehensive Review. *IOP Conference Series: Earth and Environmental Science*, Volume 540. Link: <https://iopscience.iop.org/article/10.1088/1755-1315/540/1/012036/meta>
3. Issa, S., Dahy, B., Ksiksi, T., & Saleous, N. (2020). Allometric equations coupled with remotely sensed variables to estimate carbon stocks in date palms. *Journal of Arid Environments*, 182, 104264. Link: <https://doi-org.uaeu.idm.oclc.org/10.1016/j.jaridenv.2020.104264>
4. Issa, S. M., Dahy, B., & Saleous, N. (2020). Accurate mapping of date palms at different age-stages for the purpose of estimating their biomass. *ISPRS Annals of Photogrammetry, Remote Sensing and Spatial Information Sciences*, V-3-2020, 461-467. Link: <https://pdfs.semanticscholar.org/1965/e4eb18f-84c12e3d0427047e7e855866ad912.pdf>
5. Issa, S., Dahy, B., Ksiksi, T., & Saleous, N. (2020). A Review of Terrestrial Carbon Assessment Methods Using Geo-Spatial Technologies with Emphasis on Arid Lands. *Remote Sensing*, 12(12), 2008. Link: <https://www.mdpi.com/2072-4292/12/12/2008>
6. Dahy, B., Issa, S., Ksiksi, T., & Saleous, N. (2019). Non-Conventional Methods as a New Alternative for the Estimation of Terrestrial Biomass and Carbon Sequestered: Mini Review. *World Journal of Agriculture and Soil Science*. Link: <https://irispublishers.com/wjass/fulltext/non-conventional-methods-as-a-new-alternative-for-the-estimation-of-terrestrial-biomass.ID.000579.php>
7. Issa, S., Dahy, B., Saleous, N., & Ksiksi, T. (2019). Carbon stock assessment of date palm using remote sensing coupled with field-based measurements in Abu Dhabi (United Arab Emirates). *International Journal of Remote Sensing*, 0(0), 1-20. Link: <https://www-tandfonline-com.uaeu.idm.oclc.org/doi/full/10.1080/01431161.2019.1602795>
8. Issa, S., Dahy, B., Ksiksi, T., & Saleous, N. (2018). Development of a new allometric equation correlated with RS variables for the assessment of date palm biomass. *Proceedings of the 39th Asian Conference on Remote Sensing (ACRS 2018)*, Kuala Lumpur, Malaysia, 15-19 October 2018. Link: <https://a-a-r-s.org/proceeding/ACRS2018/ACRS%202018%20PROCEEDING.pdf>





# List of Figures

Figure 1: Carbon pools	29
Figure 2: Textual analysis using Google Scholar	38
Figure 3: Geospatial input data used in in reviewed papers at different forests	41
Figure 4: Different RS/GIS procedures available for estimating AGB and CS	43
Figure 5: Different biophysical parameters used in RS based estimation of AGB	52
Figure 6: The use of vegetation indices and NDVI for estimating AGB	55
Figure 7: Studies on estimating AGB using RS in arid/semiarid ecosystems	57
Figure 8: Multipurpose advantages of date palms	66
Figure 9: Uprooting, partitioning, and weighing date palms	69
Figure 10: Structural field variables of date palm	73
Figure 11: Lab works, preparing samples, grinding, weighing, and drying	75
Figure 12: Allometric equation for estimating CB of DP as function of CA	79
Figure 13: Allometric equation for estimating TB of DP as function of Ht	81
Figure 14: Prediction equation of soil organic carbon as function of CA	82
Figure 15: LULC classification and mapping the date palm trees	93
Figure 16: A subset of pan-sharpened WV-2 image	94
Figure 17: Separating age classes of date palm trees	95
Figure 18: Mean signature value of LULC classes vs. Landsat-8 bands	97
Figure 19: LULC map of the study area	98
Figure 20: Vegetation bitmap of Abu Dhabi	100
Figure 21: Min., max., and mean signature value of DP versus Landsat bands	100
Figure 22: Abu Dhabi Emirate DP trees map (mature DP) using Landsat-8 OLI	101
Figure 23: Object-oriented classification of DP in Abu Dhabi	103
Figure 24: Map of DP trees showing three age stages using WV-2	103
Figure 25: The flowchart of Chapter 4 for developing and validating the RS-based biomass model	113
Figure 26: The 40 × 40 m plot design	114
Figure 27: AGB for DP in function of TCW and RDVI	123
Figure 28: Pipeline of the spatial modeler used to build the two sub-models for calculating CS in DP	125
Figure 29: The aboveground carbon (AGC) map of DP in the study area	127
Figure 30: The biomass (dry weight) of DP versus age stages	135
Figure 31: Differences in estimating DP trees areas at the same farm	142



The background features a light teal color with several abstract geometric elements. In the upper right, there is a large triangular shape filled with a grid of black dots. Below this, there are several horizontal lines and a solid grey triangle. In the lower right, there are more horizontal lines, a solid grey triangle, and a pattern of horizontal lines that tapers to a point. The text 'List of Tables' is centered in the middle of the page.

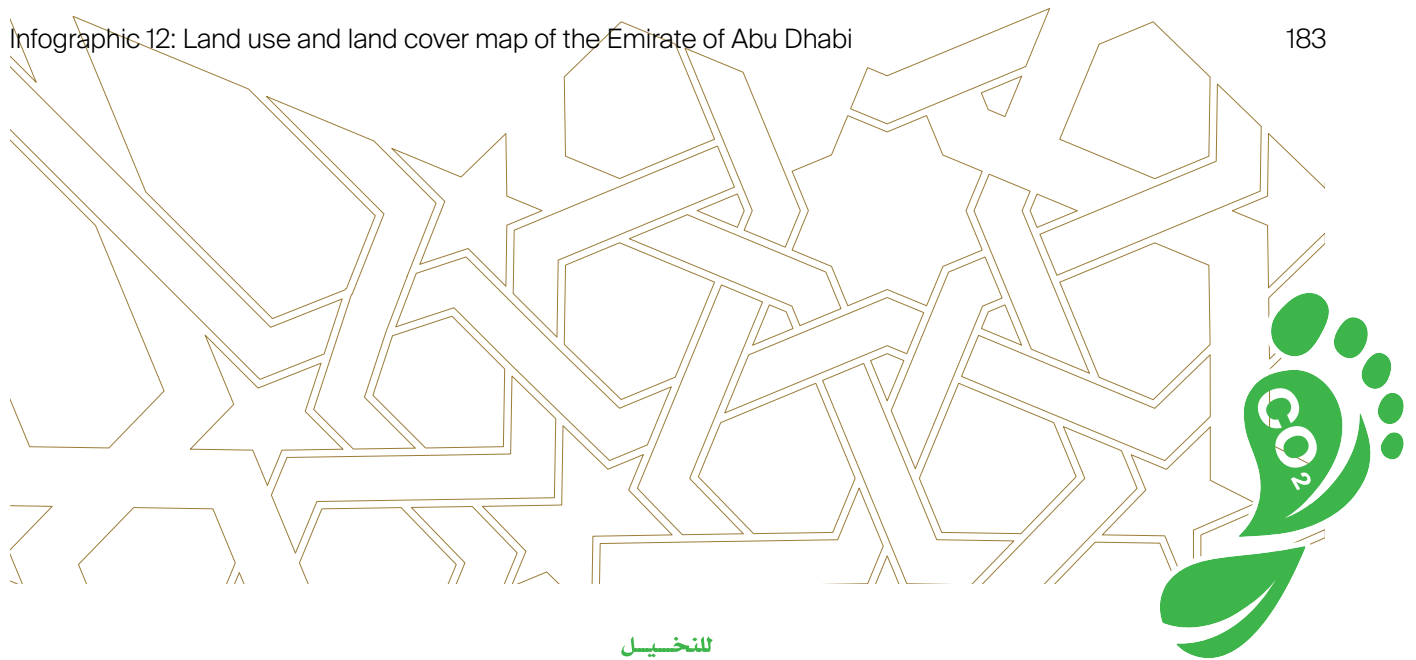
# List of Tables

Table 1: Calculation methods of CS components in terrestrial ecosystems	30
Table 2: Calculation of different date palms biomass components	70
Table 3: Calculation of OM and OC of the collected samples	71
Table 4: Formulae used to calculate the different soil parameters	71
Table 5: Average of dry to fresh weight factor for each DP component.	74
Table 6: Field variables of DP used to assess allometric equations	74
Table 7: DP component's biomass calculated as a ratio of total or AGB	77
Table 8: Best prediction equations for crown biomass estimation of DP	79
Table 9: Best prediction equations for trunk biomass estimation of DP	80
Table 10: OM and OC (Kg. palm-1) in DP components at different age stages	82
Table 11: Percent SOM and SOC for different canopy positions	83
Table 12: SOM and SOC at 10 cm depth under DP at three different age stages	83
Table 13: The area and percentage of each class LULC of Abu Dhabi	96
Table 14: Accuracy assessment of the classified maps	104
Table 15: The preliminary results of the total numbers of the DP in AD	106
Table 16: The Crown and Trunk biomass equations used for AGB (kg. palm-1) estimation of DP in study area	114
Table 17: Details of dataset used in the current research	114
Table 18: Selected Landsat 8 OLI-derived vegetation indices (VIs)	115
Table 19: Crown area (CA), trunk height (Ht), and density values of DP for each age stage	120
Table 20: The averages and ranges of AĜB (ĈB and TĤB) at each DP age stage	121
Table 21: Model(s) used for AĜB estimation (t. ha-1) for mature and non-mature date palms	124
Table 22: The total ĈS (in Mt) by DP trees in Abu Dhabi, UAE	128
Table 23: RS predictive variables used in the RS based biomass models	129



# List of Infographics

Infographic 1: Afforestation and land-use conversion to a forest (reforestation) can be used to earn carbon credits and balance carbon emissions	25
Infographic 2: Efforts to reduce its carbon footprint have not been accounted for due to a lack of tools to assess biomass and carbon sequestration in its territories	27
Infographic 3: Geospatial techniques enhance natural resource management, particularly in biomass and carbon assessment, yielding positive results	27
Infographic 4: The estimation of aboveground biomass (AGB) holds significance as it represents the most visible, dominant, dynamic, and critical component of the terrestrial ecosystem.	31
Infographic 5: The majority of biomass and carbon estimation studies have predominantly focused on boreal and tropical forests, while comparatively fewer have been undertaken in arid and semiarid regions.	33
Infographic 6: Geospatial technologies for biomass and carbon assessment offer numerous advantages over traditional methods.	37
Infographic 7: Biomass and carbon estimation studies with geospatial technologies can be grouped by methodological complexity into tiers with varying detail and accuracy.	42
Infographic 8: The comprehensive methodology flowchart and their corresponding chapters within this book.	59
Infographic 9: Summary of statistics, equations, and ratios for estimating aboveground biomass, belowground biomass, and carbon stock in date palm trees.	86
Infographic 10: Summary of statistics, equations, and ratios for estimating aboveground biomass, belowground biomass, and carbon stock in date palm trees.	87
Infographic 11: A graphic abstract illustrating the conceptual summary of the process for estimating carbon stock in date palm plantations as carbon assessment maps	116
Infographic 12: Land use and land cover map of the Emirate of Abu Dhabi	183



The background features a light teal color with several abstract geometric elements. In the upper right, there is a large triangular area filled with a grid of black dots. Below this, there are several horizontal lines and a solid dark grey triangle. To the right, there are more geometric shapes, including a triangle with a diagonal line of dots and another with a diagonal line of horizontal lines. In the lower right, there is a large triangle filled with horizontal lines, with a smaller triangle of dots at its top-left corner. The word "Appendices" is centered in a bold, black, sans-serif font.

# Appendices

**Appendix 1:** Different field variables used in allometric equations to estimate palm biomass, mostly oil palm (*Elaeis guineensis*).

Source	Output	Allometric Equations	Field Variables
(Saldarriaga et al., 1988)	AGB	$= 1.697 \times 10^{-3} \times \text{DBH}^{1.754} \times \text{H}^{2.151}$	DBH and H
(Brown, 1997)	Biomass	$= 10.0 + 6.4 \times \text{H}$ $= 4.5 + 7.7 \times \text{Ht}$	H and Ht
(H. Khalid et al., 1999a)	AGB		H
(Hughes et al., 1999)	AGB	$= 0.3060 \times \text{DBH}^{1.837} \times 1.035$	DBH
(Henson & Chang, 2003)	Biomass	$= -0.00020823\text{Age}^4 + 0.000153744\text{Age}^3 - 0.011636\text{Age}^2 + 7.3219\text{Age} - 6.3934$	Age
(Thenkabail et al., 2004)	AGB <sub>fresh</sub> AGB <sub>dry</sub>		Ht
(R. Hereward V. Corley & Tinker, 2008)	Trunk biomass Frond biomass	$= 0.1 \times \text{TD} \times \text{H} \times (\text{DBH}/2)^2$	H, TD, DBH, W, D, and Age
(Dewi et al., 2009)	AGB		H
(Goodman et al., 2013)	AGB	$= 13.59 \times \text{H} - 108.8$	H
(Goodman et al., 2013)	AGB	$= 0.0950 \times (\text{DF} \times \text{DBH}^2 \times \text{H})$	DF, DBH, and H
(Da Silva et al., 2015)	AGB	$= 0.167 \times (\text{DBH}^2 \times \text{H} \times \text{TD})^{0.883}$	DBH, H, and TD
(Prayogo et al., 2018)	AGB	$= 0.03883 \times \text{H} \times \text{DBH}^{1.2}$	DBH and H
(Zahabu et al., 2018)	AGB	$= 3.7964 \times \text{H}^{1.8130}$	H

Where DBH is diameter breast height, H is palm height, Ht is trunk height, TD is trunk density, W is frond width, D is frond depth, and DF is dry to fresh weight ratio.

الكربونية



**Appendix 2:** A summary of limitations and benefits of Optical, RADAR, and LiDAR sensors used for estimating the Above Ground Biomass (AGB) of standing forests.

Sensor Types	Approaches/ Resolutions	Limitations	Benefits
<b>Optical Sensors</b>	Coarse Resolution Spatial (>100 m)  Examples: MODIS, AVHRR, NOAA, METEOSAT and SPOT Vegetation	<ul style="list-style-type: none"> <li>- Average R value of 0.58, with average predictive of 42%</li> <li>- Saturation of spectral data at high biomass density</li> <li>- Mismatch between the size of field plots, field measurements and pixel size (mixed pixels)</li> <li>- Cloud cover</li> <li>- Limited to discriminating vegetation structure</li> </ul>	<ul style="list-style-type: none"> <li>- Availability of data with huge datasets archived</li> <li>- Estimation and mapping of AGB at continental and global scale</li> <li>- Repetitive, with high temporal frequency increasing the probability of acquiring cloud-free data</li> <li>- Provide consistent spatial data</li> </ul>
	Medium Spatial Resolution (10-100 m)  Examples: TM Landsat, ETM+, OLI and SPOT	<ul style="list-style-type: none"> <li>- Average R value of 0.68 with average predictive error of 32%</li> <li>- Single pixel can encompass many tree crown or non-crown features</li> <li>- No reliable indicators of biomass in closed canopy structure</li> <li>- Not all texture measures can effectively extract biomass information</li> </ul>	<ul style="list-style-type: none"> <li>- Provide consistent global data</li> <li>- Archived datasets back to 1972 for Landsat</li> <li>- Small to large-scale mapping</li> <li>- Cost-effective (Free)</li> </ul>
	Fine Spatial Resolution (<5 m)  Examples: Quickbird, World-View-2, and IKONOS	<ul style="list-style-type: none"> <li>- Need large data storage and processing time</li> <li>- High cost, and more costly when it applies on large areas</li> </ul>	<ul style="list-style-type: none"> <li>- Average R value of 0.75 and average predictive error (27%)</li> <li>- Estimate tree crown size</li> <li>- Validation at localized scale</li> </ul>
	Hyperspectral Many, very narrow, and contiguous spectral bands  Examples: AISA Eagle, HYDI-CE and ALOS	<ul style="list-style-type: none"> <li>- Cloud cover</li> <li>- High cost</li> <li>- Suffer from band redundancy and saturation in dense canopy</li> <li>- Computationally intensive and technically demanding</li> </ul>	<ul style="list-style-type: none"> <li>- Average R value of 0.83</li> <li>- Allows discrimination of subtler differences (species level)</li> <li>- Potential for the future of RS-based biomass estimation models</li> <li>- Integration with LiDAR can improve results.</li> </ul>

**Appendix 2:** A summary of limitations and benefits of Optical, RADAR, and LiDAR sensors used for estimating the Above Ground Biomass (AGB) of standing forests. Continued.

Sensor Types	Approaches/ Resolutions	Limitations	Benefits
<b>RADAR Sensors</b>	<p>Approaches involve the use of either backscatter values or interferometry techniques</p> <p>Examples: Microwave/radar i.e., ALOS PALSAR, ERS-1, Envisat and JERS-1.</p>	<ul style="list-style-type: none"> <li>-Not accurate in mountainous region due to spurious relation between AGB and backscatter values.</li> <li>-Signal saturation in mature forests at various wavelengths (C, L and P bands)</li> <li>-Polarization (e.g., HV and VV) problems</li> <li>-Low spatial resolution makes it inaccurate for AGB assessment at the species level.</li> <li>-Cannot be applied on any vegetation type without considering stand characteristics and ground conditions.</li> </ul>	<ul style="list-style-type: none"> <li>-Measure forest vertical structure</li> <li>-Generally free</li> <li>-Can be accurate for young and sparse forests</li> <li>-Repetitive data</li> </ul> <p>Can give an average R value of 0.74, with average predictive error of 25%. Integrating RADAR with multi source data (optical, microwave data and GIS modeling techniques) is a promising approach.</p>
<b>LiDAR Sensors</b>	<p>Using laser light</p> <p>Spatial Resolution: (0.5 cm – 5 m)</p> <p>Examples: Carbon 3-D</p>	<ul style="list-style-type: none"> <li>- Repetitive at high cost and logistics deployment</li> <li>-Requires extensive field data calibration</li> <li>-Highly expensive</li> <li>-Technically demanding</li> </ul>	<ul style="list-style-type: none"> <li>-Penetrate cloud cover and canopy</li> <li>-Among all sensors option, LiDAR is the easiest to use for the extraction of tree attributes for estimating AGB with great accuracy</li> <li>-Accurate for estimating forest biomass in all spatial variability (sparse, young or mature forests)</li> <li>- Average R value of 0.89, with average predictive error equal 14%</li> <li>-Potential for satellite-based system to estimate global forest carbon stock</li> </ul>

الكربونية



**Appendix 3:** Specifications of the RS optical sensors most commonly used for AGB estimation.

Sensor	Type	Bands	Spatial Resolution	Temporal Resolution	Swath	Cost
AVHRR	Multispectral	5 bands (Red, IR, and 3 Thermal IR)	1,100 meters	12 hours	2,500 km	Free
MODIS	Multispectral	36 bands (from Blue to Thermal IR)	250, 500 and 1,000 meters	1-2 days	2,330 km	Free
SPOT VEG	Multispectral	4 bands (Blue, red, NIR, and SWIR)	1,000 meters	1 day	2,250 km	Free
TM	Multispectral	7 bands (3 VIS, 3 IR and Thermal IR)	30 and 120 meters	16 days	185 km	Free
ETM+	Multispectral	9 bands (3 VIS, 3 IR and 2 Thermal IR and 1 PAN)	15, 30 and 60 meters	16 days	185 km	Free
SPOT	Multispectral	4 bands (2 VIS, 1 NIR, and 1 PAN)	5, 10 and 20 meters	26 days	60 km	Commercial
Landsat 8 OLI	Multispectral	11 bands (1 Ultra, 3 VIS, 3 IR, 1 Cirrus, 2 Thermal IR, and 1 PAN)	15, 30 and 100 meters	16 days	185 km	Free
LISS-III (IRS)	Multispectral	5 bands (2 VIS, 2 IR, and 1 PAN)	5.3, 23 and 50 meters	5-24 days	142 km	Commercial
Sentinel-2	Multispectral	13 bands (4 VIS, 6 NIR and 3 SWIR)	10, 20, and 60 meters	5-10 days	290 km	Free
IKONOS	Multispectral	5 bands (3 VIS, 1 IR, and 1 PAN)	1 and 4 meters	3 days	11 km	Commercial
World View2	Multispectral	9 bands (6 VIS, 2 IR, 1 PAN)	1.84 and 0.46 meter	1.1 days	16 km	Commercial
Quickbird	Multispectral	5 bands (4 bands and 1 PAN)	0.61 and 2.44 meter	3 days	16 km	Commercial
HyMap	Hyperspectral	126 bands	2-10 meters	Airborne	2.3 km and 4.6 km	Commercial
AVIRIS	Hyperspectral	224 bands (from VIS to MIR)	2.5 to 20 meters	Airborne	1.9 km and 11 km	Not Commercial

**Appendix 4:** Different cultivars and age stages from three different farms of the study area are selected to run the destructive method and to build the allometric equations.

No. Palm	Cultivar	Destruction Date	Location	Age (year)
1	LuLu	24-Apr-18	Masakin	2.5
2	Khalas	24-Apr-18	Masakin	2.5
3	Fardh	24-Apr-18	Masakin	3
4	Bumaan	24-Apr-18	Masakin	3
5	Khunaizi	24-Apr-18	Masakin	4
6	Khalas	29-Apr-18	Salamat W.	5
7	Fahel (Male)	29-Apr-18	Salamat W.	7
8	Khunaizi	29-Apr-18	Salamat W.	8
9	Fardh	29-Apr-18	Salamat W.	9
10	Bumaan	29-Apr-18	Salamat W.	10
11	Baghel	25-Apr-18	Qattara	11
12	Jabri	25-Apr-18	Qattara	14
13	Shahem	25-Apr-18	Qattara	16
14	Jash Ramli	25-Apr-18	Qattara	18
15	Neghal	25-Apr-18	Qattara	20

الكربونية

**Appendix 5:** The average amounts of date palm biomass, organic matter, organic carbon, and soil organic carbon at different age stages.

Item	Average amount (Kg palm-1)		
	Young (< 5 year)	Medium (5 - 10 years)	Mature (>10 years)
Crown Biomass (CB)	22.51	65.17	148.5
Trunk Biomass (TB)	0	29.53	135.91
AGB	22.51	94.69	284.41
BGB	7.46	87.61	141.23
Total Biomass	29.97	182.3	425.63
Organic Matter (OM)	27.39	166.56	388.94
Organic Carbon (OC)	15.88	96.62	225.58
SOC	18.09	62.59	92.91
Total Carbon Stock (CS)	33.97	159.21	318.49



**Appendix 6A:** Details of the Landsat-8 OLI Level-2 used (6 scenes)

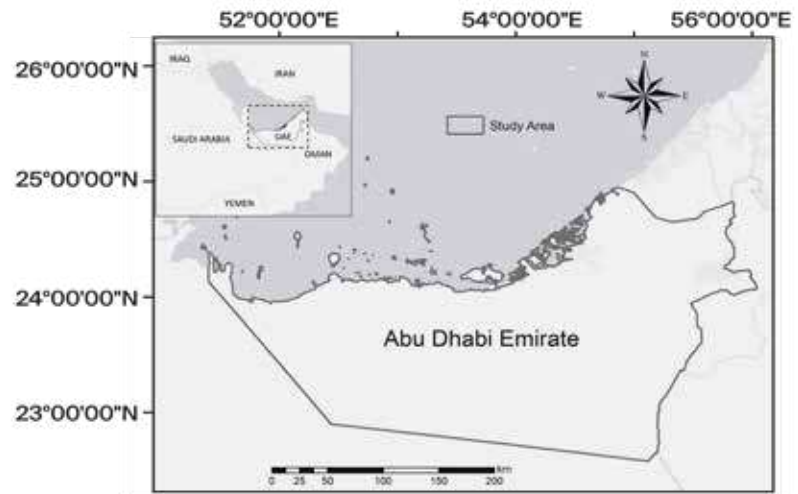
No.	Scene (Path/ Row)	Date (2017)	Bands Used ( $\mu\text{m}$ )	Resolution/ Swath
1	160/43	24 <sup>th</sup> April	Band1 (coastal): 0.433–0.453, Band2 (blue): 0.450–0.515, Band3 (green): 0.525–0.600, Band4 (red): 0.630–0.680, Band5 (NIR): 0.845–0.885, Band6 (SWIR 1): 1.560–1.660, Band7 (SWIR 2): 2.100–2.300, and Panchromatic: 0.500–0.680	30 meters for multispectral bands and 15 meters for panchromatic. Swath area is 185 km.
2	160/44	26 <sup>th</sup> May		
3	161/43	15 <sup>th</sup> April		
4	161/44	15 <sup>th</sup> April		
5	162/43	22 <sup>nd</sup> April		
6	162/44	22 <sup>nd</sup> April		

**Appendix 6B:** Details of the WorldView-2 used (829 scenes)

No.	Band	Width ( $\mu\text{m}$ )	Resolution/ Swath
1	Band 3 (Green)	0.510 - 0.580	1.85 meters for multispectral bands and 0.50 meters for panchromatic. The swath of each scene is 16 kilometers.
2	Band 5 (Red)	0.630 - 0.690	
3	Band 7 (NIR 1)	0.770 - 0.895	
4	Panchromatic	0.450 - 0.800	

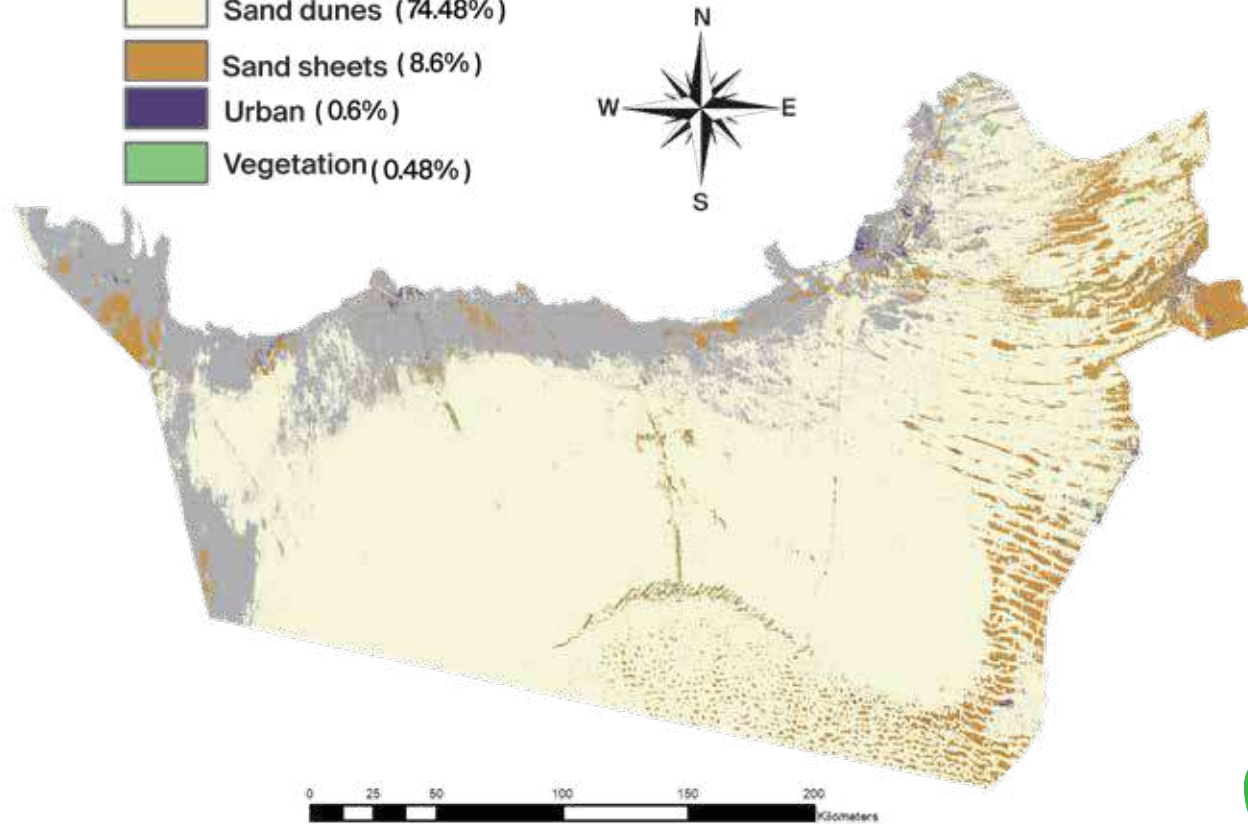
**Appendix 7:** Geographic and environmental settings of the study area

Elevation	0 - 200 m
Geomorphology	sand dunes, inter-dunal sands, coastal and inland sabkhas and exposed rocks.
Climate	The Köppen Climate subtype is "BWh" (Tropical/Subtropical Desert Climate)
Seasons	two seasons: summer (April - Sept) and winter (Oct - Mar).
Temperature	from 35° to 45 C in summer and from 10 to 24°C in winter.
Relative humidity	high in the coasts (reach 90%) and extremely dry in western and southern deserts.
Rainfall	variable among years. Occurs in winter and reaches 12 cm annually
Groundwater	low with large amount of salinity levels
Soils	sandy, sandy calcareous, gypsiferous, saline, salinegypsiferous and hard pan soils
Vegetation	~ 60% are annuals species and germinate from Feb to April, generally and the perennial species flower from Jan to early May, and some in Sept and Nov.



### Abu Dhabi LULC (%)

- Sabkha (15.51%)
- Sand dunes (74.48%)
- Sand sheets (8.6%)
- Urban (0.6%)
- Vegetation (0.48%)



The main Land cover classes of the Emirate of Abu Dhabi

Infographic 12: Land use and land cover map of the Emirate of Abu Dhabi



**Appendix 8:** Linear correlation between RS variables and AGB of date palm (mature, medium, and young). Here, 54 field plots were used covering the whole study area of Abu Dhabi (see Chapter 4).

Age Class	RS Variable	Constant	Coefficient	R2	P value	
Mature	Single Bands	B1	85.270	-0.047	0.113	0.187
		B	93.557	-0.043	0.143	0.135
		G	107.820	-0.036	0.187	0.083
		R	103.466	-0.029	0.230	0.052
		NIR	149.462	-0.026	0.086	0.255
		SWIR1	115.464	-0.021	0.302	0.022
		SWIR2	102.826	-0.023	0.290	0.026
	VI's	SR	-32.033	37696	0.545	0.0007
		RVI	131.267	-164.234	0.315	0.019
		DVI	-98.847	0.084	0.412	0.006
		NDGI	100.560	636.247	0.609	0.0002
		NDVI	-17.970	194.545	0.398	0.007
		TVI	-476.939	454.517	0.379	0.009
		GNDVI	-53.452	249.782	0.311	0.020
		RDVI	-47.289	3.911	0.418	0.005
		SAVI	-18.985	131.919	0.413	0.005
		MSAVI	-38.643	175.245	0.337	0.013
		TCB	123.051	-0.013	0.227	0.053
		TCG	0.146	0.060	0.313	0.20
		TCW	84.780	0.037	0.396	0.007

Medium	Single Bands	B1	28.817	-0.007	0.027	0.504
		B	29.653	-0.006	0.026	0.507
		G	31.553	-0.004	0.030	0.479
		R	33.809	-0.005	0.057	0.327
		NIR	24.178	-0.0002	0.0001	0.966
		SWIR1	37.538	-0.004	0.075	0.256
		SWIR2	35.052	-0.004	0.074	0.260
	VI's	SR	-7.827	17.892	0.195	0.058
		RVI	53.020	-50.018	0.159	0.091
		DVI	-3.322	0.018	0.208	0.049
		NDGI	36.484	108.230	0.128	0.132
		NDVI	6.605	64.310	0.164	0.085
		TVI	-125.108	132.281	0.131	0.128
		GNDVI	1.429	59.096	0.081	0.239
		RDVI	0.224	1.191	0.205	0.052
		SAVI	6.695	42.842	0.159	0.091
		MSAVI	3.003	50.018	0.159	0.091
		TCB	34.810	-0.002	0.041	0.407
		TCG	15.280	0.015	0.164	0.085
		TCW	34.943	0.008	0.125	0.137

**Appendix 8:** Linear correlation between RS variables and AGB ( Continued ).

Young	Single Bands	B1	1.126	0.005	0.172	0.087
		B	1.137	0.004	0.159	0.101
		G	0.260	0.003	0.157	0.103
		R	-0.217	0.002	0.154	0.107
		NIR	-7.186	0.003	0.283	0.023
		SWIR1	-1.031	0.002	0.105	0.190
		SWIR2	0.620	0.002	0.079	0.258
	VI's	SR	8.420	-1.581	0.006	0.753
		RVI	3.403	3.907	0.008	0.723
		DVI	3.091	0.003	0.044	0.404
		NDGI	9.509	23.810	0.036	0.451
		NDVI	7.367	-6.913	0.012	0.661
		TVI	18.283	-11.195	0.007	0.738
		GNDVI	9.674	-11.393	0.031	0.485
		RDVI	5.550	0.042	0.002	0.855
		SAVI	6.978	-3.095	0.006	0.767
		MSAVI	7.310	-3.907	0.008	0.723
		TCB	-2.488	0.001	0.174	0.085
		TCG	6.290	-0.001	0.004	0.802
		TCW	5.885	-0.0001	0.0002	0.951

الكربونية



The background features a light teal color with several abstract geometric patterns. In the upper right, there is a large triangular area filled with a grid of black dots. Below this, there are several horizontal lines and a smaller triangle. In the lower right, there are horizontal lines and a triangle filled with a grid of black dots. The overall design is modern and minimalist.

# List of Abbreviations

<b>AGB</b>	Aboveground Biomass	<b>NDFI</b>	Normalized Difference Fraction Index
<b>AGC</b>	Aboveground Carbon	<b>NDGI</b>	Normalized Difference Greenness Index
<b>AOAD</b>	Arab Organization for Agricultural Development	<b>NDVI</b>	Normalized Difference Vegetation Index
<b>APAR</b>	Absorbed Photosynthetically Active Radiation	<b>NN</b>	Nearest Neighborhood
<b>BGB</b>	Belowground Biomass	<b>OBC</b>	Object-Based Classification
<b>BGC</b>	Belowground Carbon	<b>OC</b>	Organic Carbon
<b>CA</b>	Crown Area	<b>OLI</b>	Operational Land Imager (landsat-8)
<b>CB</b>	Crown Biomass	<b>OM</b>	Organic Matter
<b>CD</b>	Crown Diameter	<b>OOC</b>	Object -Oriented Based Classification
<b>CS</b>	Carbon Stock	<b>PBC</b>	Pixel- Based Classification
<b>DBH</b>	Diameter at Breast Height	<b>R</b>	Coefficient of Correlation
<b>DF</b>	Dry to Fresh Factor (biomass)	<b>R2</b>	Coefficient of Determination
<b>DP</b>	Date Palm	<b>REDD+</b>	Reducing Emissions from Deforestation and Forest Degradation
<b>DTM</b>	Digital Terrain Model	<b>RMSE</b>	Root Mean Square Error
<b>DVI</b>	Difference Vegetation Index	<b>RS</b>	Remote Sensing
<b>ETM+</b>	Enhanced Thematic Mapper (landsat-7)	<b>RVI</b>	Ratio Vegetation Index
<b>EVI</b>	Enhanced Vegetation Index	<b>SAVI</b>	Soil Adjusted Vegetation Index
<b>FAO</b>	Food and Agriculture Organization of the United Nations	<b>SE</b>	Standard Error
<b>FMT</b>	Feature Model Tree	<b>SOC</b>	Soil Organic Carbon
<b>FOTO</b>	Fourier Transform Texture of Ordination	<b>SOM</b>	Soil Organic Matter
<b>#FronD</b>	Number of Palm Fronds	<b>SR</b>	Simple Ratio
<b>GEMI</b>	Global Environmental Monitoring Index	<b>SWIR</b>	Shortwave Infrared
<b>GHGs</b>	Greenhouse Gases	<b>TB</b>	Trunk Biomass
<b>GIS</b>	Geographic Information Systems	<b>TCB</b>	Tasseled Cap Index of Brightness
<b>GPS</b>	Global Positioning System	<b>TCG</b>	Tasseled Cap Index of Greenness
<b>H</b>	Palm Height	<b>TCW</b>	Tasseled Cap Index of Wetness
<b>Δheight</b>	Crown Depth	<b>TM</b>	Thematic Mapper (landsat-5)
<b>HIA</b>	Hierarchical Integrated Approach	<b>TSAVI</b>	Transformed Soil-Adjusted Vegetation Index
<b>HCM</b>	Hybrid Classification Method	<b>UAE</b>	United Arab Emirates
<b>Ht</b>	Palm Trunk Height	<b>UN</b>	United Nations
<b>IPCC</b>	Intergovernmental Panel on Climate Change	<b>UTM</b>	Universal Transverse Mercator
<b>IR</b>	Infrared	<b>VIs</b>	Vegetation Indices
<b>LAI</b>	Leaf Area Index	<b>VOB/ha</b>	Volume of the Biomass Per Hectare
<b>LiDAR</b>	Radar and Light Detection and Ranging	<b>WV-2</b>	World View 2
<b>LULC</b>	Land Use/ Land Cover	<b>YDP</b>	Young Date Palm
<b>MDP</b>	Mature Date Palm		
<b>MeDP</b>	Medium Date Palm		
<b>MSAVI</b>	Modified Soil-Adjusted Vegetation Index		



The background features a light teal color with several abstract geometric elements. In the upper right, there is a large triangular area filled with a grid of black dots. Below this, there are several horizontal lines and a smaller triangle. To the right, there are more geometric shapes, including a triangle with a grid of dots and a triangle with horizontal lines. In the lower right, there is a large triangle filled with horizontal lines, with a smaller triangle containing a grid of dots at its top-left corner. The word "Biographies" is centered in the lower half of the page in a bold, black, sans-serif font.

# Biographies

## Prof. Abdelouahhab Zaid

- Professor Zaid is an Agricultural Advisor to the United Arab Emirates Ministry of Presidential Affairs. He also serves as Secretary General of the Khalifa International Award for Date Palm and Agricultural Innovation. Throughout a distinguished career devoted to crop science, horticulture and agronomy, he has held several high-level government, academic and institutional roles and participated in biotechnology development projects aimed at increasing plant production and employment in more than 20 countries.
- Throughout a distinguished career devoted to crop science, horticulture and agronomy, he has held several high-level government, academic and institutional roles and participated in biotechnology development projects aimed at increasing plant production and employment in more than 20 countries.
- Professor Zaid has been honored with multiple awards, including a BR. Sen Award and Honorary Medal from FAO, and an Award of Excellence from AOAD. As well as an Honorary Medal from United Nations Food and Agriculture Organization (FAO) (2019), and five letters of recognition from His Majesty King Mohammed VI of the Kingdom of Morocco, "May God protect Him" (2004-2011-2015-2021- and 2022).
- Professor Zaid has also contributed significantly to the FAO Organization's credibility in various countries by preparing several development projects in Burkina Faso, The Hashemite Kingdom of Jordan, Kingdom of Saudi Arabia, Kingdom of Morocco, Niger, Nigeria, Syria, Tunisia, the United Arab Emirates, Republic of Yemen, Namibia, and Republic of South Africa.
- Professor Zaid also initiated significantly in providing technical leadership to regional and international agricultural activities.

## Dr. Basam S. Dahy

- Dr. Basam Saeed Mohammed Dahy received scholarships for his Master's and Ph.D. studies in Environmental Sciences at the UAE University in recognition of his outstanding academic achievements.
- Dr. Dahy is a specialist in geospatial technologies (remote sensing and GIS) and earth observation products (satellite imagery/aerial photographs) for scientific research. His research interests encompass carbon sequestration, remote sensing applications, geospatial modeling, arid and semi-arid regions, sustainable development, and climate change.
- Currently, Dr. Dahy is a Post-Doctoral Associate at CITIES, New York University - Abu Dhabi Campus.
- Dr. Basam Dahy's work has garnered recognition both locally and internationally. He was honored with the 'Outstanding Paper' prize at the Asian Conference on Remote Sensing in Malaysia in 2018. Additionally, he was a member of the research team that earned the UAE University's Chancellor Innovation Award in the Space Category in 2021. In 2023, he achieved the 1st place award for the best Ph.D. dissertation presented by the Association of Arab Universities (AARU).
- Basam Dahy has authored books aimed at children and youth, including "The Wise Ghaf Tree", "The Possible Spring", and "How to Establish a Speech Club." He also has experience in writing documentary film scripts and served as the president of the Abjad Toastmasters Club, the first Arabic-language Toastmasters club in Abu Dhabi.

Since its establishment in 2007, Khalifa International Award for Date Palm and Agricultural Innovation General Secretariat, has sought to work according to a clear strategic plan, through which it seeks to achieve the objectives for which it was established, and to translate the vision of the UAE's wise leadership, in supporting and developing the date palm cultivation and production sector, promoting agricultural innovation, and disseminating specialized scientific knowledge nationally, regionally, and internationally.

The success achieved by the United Arab Emirates, and the high credibility the Award gained over the past sixteen years, has been achieved with thanks to the directives of the wise leadership of H.H. Sheikh Mohamed bin Zayed Al Nahyan, President of the United Arab Emirates, and the continuous support of H.H. Sheikh Mansour bin Zayed Al Nahyan, UAE Vice President and Deputy Prime Minister, Minister of the Presidential Court, and ongoing follow-up of H.E. Sheikh Nahayan Mubarak Al Nahyan, Minister of Tolerance and Coexistence, Chairman of the Award's Board of Trustees. This reaffirms the strategic importance of the date palm cultivation and production sector in order to enhance food security, and support the national economy to achieve sustainable development.

In appreciation of this important role, the Award's General Secretariat continuously seeks to disseminate knowledge and empower its target groups, through the issuance of specialized scientific books, on various topics related to this sector. Where the "Date Palm and Carbon Footprint" book comes within this context, due to its importance in absorbing greenhouse gases and reducing global warming to limit climate change, within the framework of the Award's participation in the Climate Change conference (COP28).

**Dr. Abdelouahhab Zaid, Prof.,**

Secretary General of Khalifa Int'l Award  
for Date Palm and Agricultural Innovation